DEVELOPMENT OF A NEW PERFORMANCE CRITERIA FOR HIGHER WIRE-ELECTRICAL DISCHARGE MACHINING PERFORMANCE CONSIDERING THE ECOLOGICAL AND ECONOMICAL ASPECTS

IBRAHEM MAHER ABDELRAHEM SOLTAN

FACULTY OF ENGINEERING
UNIVERSITY OF MALAYA
KUALA LUMPUR

2016

DEVELOPMENT OF A NEW PERFORMANCE CRITERIA FOR HIGHER WIRE-ELECTRICAL DISCHARGE MACHINING PERFORMANCE CONSIDERING THE ECOLOGICAL AND ECONOMICAL ASPECTS

IBRAHEM MAHER ABDELRAHEM SOLTAN

THESIS SUBMITTED IN FULFILMENT OF THE REQUIREMENTS FOR THE DEGREE OF DOCTOR OF PHILOSOPHY

FACULTY OF ENGINEERING
UNIVERSITY OF MALAYA
KUALA LUMPUR

2016

UNIVERSITY OF MALAYA

ORIGINAL LITERARY WORK DECLARATION

Name of Candidate: **IBRAHEM MAHER SOLTAN**

Registration/Matric No: **KHA130012**

Name of Degree: **DOCTOR OF PHILOSOPHY**

Title of Project Paper/Research Report/Dissertation/Thesis ("this Work"):

Development of a new performance criteria for higher wire-electrical discharge machining performance considering the ecological and economical aspects

Field of Study: **MANUFACTURING PROCESSES**

I do solemnly and sincerely declare that:

(1) I am the sole author/writer of this Work;
(2) This Work is original;
(3) Any use of any work in which copyright exists was done by way of fair dealing and for permitted purposes and any excerpt or extract from, or reference to or reproduction of any copyright work has been disclosed expressly and sufficiently and the title of the Work and its authorship have been acknowledged in this Work;
(4) I do not have any actual knowledge nor do I ought reasonably to know that the making of this work constitutes an infringement of any copyright work;
(5) I hereby assign all and every rights in the copyright to this Work to the University of Malaya ("UM"), who henceforth shall be owner of the copyright in this Work and that any reproduction or use in any form or by any means whatsoever is prohibited without the written consent of UM having been first had and obtained;
(6) I am fully aware that if in the course of making this Work I have infringed any copyright whether intentionally or otherwise, I may be subject to legal action or any other action as may be determined by UM.

Candidate's Signature Date:

Subscribed and solemnly declared before,

Witness's Signature Date:

Name:

Designation:

ABSTRACT

Wire electrical discharge machining (WEDM) is a manufacturing process whereby a desired shape is obtained using electrical discharges (sparks). WEDM involves high cutting rates and superior quality to improve machining performance in manufacturing hard materials. The machining performance of computer-controlled WEDM is directly dependent on spark energy (pulse on time, peak current, and gap voltage), pulse frequency (pulse off time and pulse on time), and wire electrode parameters (material, wire speed, and wire tension). In the field of wire electrical discharge machining, it is necessary to develop suitable WEDM technology to facilitate the production of high quality workpiece surfaces at high cutting rates. Surface roughness and white layer thickness are the most important factors in evaluating WEDM surface quality. In order to ensure good surface quality, the surface roughness must be low and the white layer must be as thin as possible, homogeneous, crack-free, and well-bonded to the substrate material. In this study, the effect of cutting parameters is investigated on the machining performance parameters including cutting speed, surface roughness, wire rupture, and white layer thickness. The adaptive Neuro-Fuzzy Inference System (ANFIS) along with the Taguchi method is applied to determine the effects of the significant parameters on WEDM performance. Moreover, a new performance index is proposed to identify the effects of spark energy and pulse frequency simultaneously on machining performance and to identify the wire rupture limit. However, the performance index cannot be used to identify the most feasible wire electrode from ecological (energy and wire consumption) and economic (machining costs) perspectives. Therefore, a new performance criterion (production economic index) is developed to select the most feasible wire electrode considering the economic and ecological aspects along with the performance index to achieve superior machining performance at the lowest cost. This can be done by dividing the performance index by the total machining cost ((Es×DF)/Ct). In addition, a new coated-wire electrode

design with higher strength for less wire rupture and high machining performance in WEDM is proposed. The results obtained represent a technological knowledge base for the selection of optimal machining conditions along with suitable types of wire electrodes for WEDM in terms of ecological and economic aspects. By applying the proposed performance criterion (Es×DF/Ct), it appears that using lower spark and higher pulse cycle settings with a brass wire electrode can decrease the surface roughness and white layer thickness, and facilitate more economical cutting speed. This could lead to faster cutting with good surface finish and less wire rupture.

ABSTRAK

Mesin wayar nyahcas elektrik (WEDM) adalah satu proses pembuatan di mana bentuk yang diingini diperolehi menggunakan nyahcas elektrik (percikan bunga api). WEDM memerlukan kadar pemotongan yang tinggi dan berkualiti untuk meningkatkan prestasi mesin bagi pembuatan bahan yang keras sifatnya. Prestasi pemesinan komputer yang dikawal WEDM adalah secara langsung bergantung kepada parameter tenaga pencucuh (denyut pada masa, puncak arus, dan jurang voltan), kekerapan denyutan (denyut pada masa dan denyut luar masanya), dan elektrod dawai (bahan, kelajuan dawai dan ketegangan dawai). Dalam bidang pemesinan dawai nyahcas elektrik (WEDM) adalah perlu untuk membangunkan teknologi WEDM sesuai yang membolehkan untuk menghasilkan permukaan bahan kerja yang licin dengan kadar pemotongan tinggi. Kekasaran permukaan dan ketebalan lapisan putih adalah faktor yang paling penting untuk menilai kualiti permukaan dalam WEDM. Dalam usaha untuk memastikan kualiti permukaan yang baik, kekasaran permukaan mestilah kecil dan ketebalan lapisan putih mestilah senipis yang mungkin, homogen, bebas dari keretakan dan bercantum baik kepada bahan substrat. Dalam kajian ini, kesan parameter proses terhadap prestasi proses dikaji termasuk kelajuan pemotongan, kekasaran permukaan, pecah wayar dan ketebalan lapisan putih. Sistem mudah suai inferens neural-fuzi (ANFIS) bersama Taguchi digunakan untuk menentukan kesan parameter yang signifikan ke atas prestasi WEDM. Selain itu, indeks prestasi yang baru dicadangkan untuk mengenal pasti kesan-kesan tenaga percikan dan kekerapan denyutan serentak dalam prestasi pemesinan dan mengenalpasti had pecah wayar. Namun, prestasi indeks tidak boleh digunakan untuk mengenalpasti paling layak kawat electrode dari ecological (energi dan kawat dikuasakan) dan ekonomi (berhenti menatap biaya) perspectives. Terdapat untuk, kriteria prestasi yang baru telah dibangunkan untuk memilih elektrod dawai yang paling ketara mempertimbangkan aspek ekonomi dan ekologi dengan indeks prestasi tenaga wajaran

untuk mendapat prestasi yang pemesinan yang lebih tinggi dengan kos terendah. Ini boleh dilakukan dengan membahagikan indeks prestasi oleh jumlah kos pemesinan ((Es × DF) / Ct). Selain itu, reka bentuk elektrod bersalut dawai yang baru diperkenalkan dalam WEDM dengan kekuatan yang lebih tinggi untuk mengurangkan pecah wayar dan prestasi pemesinan yang tinggi. Keputusan yang diperolehi mewakili asas pengetahuan teknologi untuk pemilihan keadaan pemesinan optimum dalam bersama-sama dengan jenis yang sesuai elektrod dawai tentang aspek ekologi dan ekonomi di WEDM. Dengan menggunakan kriteria prestasi dicadangkan (Es × DF / Ct), didapati bahawa menggunakan tetapan pencucuh yang lebih rendah dan tetapan kitaran nadi yang lebih tinggi dengan elektrod dawai tembaga akan mengurangkan kekasaran permukaan dan ketebalan lapisan putih dan menghasilkan kelajuan pemotongan ekonomi yang lebih. Ini boleh membawa kepada lebih cepat memotong dengan kemasan permukaan yang baik dan kurang pecah wayar.

ACKNOWLEDGEMENTS

First of all, my gratitude and thanks to **ALLAH**, the Most Gracious and the Most Merciful.

I wish to express my sincere gratitude to **Prof. Dr. Ahmed A. D. Sarhan** for suggesting the research point, his valuable guidance, help, and encouragement, which have made this research possible and for the valuable discussions throughout the stages of this work.

I would like to express my deep and sincere gratitude to **Prof. Dr. Mohd Hamdi Bin Abd Shukor** for his support and encouragement.

Finally, thanks to everyone who has helped me with this thesis.

Ibrahem Maher, 2016

TABLE OF CONTENTS

LIST OF FIGURES

LIST OF TABLES

LIST OF SYMBOLS AND ABBREVIATIONS

WEDM	:	Wire Electrical Discharge Machining
EDM	:	Electrical Discharge Machining
MMCs	:	Metal Matrix Composites
CNC	:	Computer Numerical Control
WLT	:	White Layer Thickness
ANFIS	:	Adaptive Neuro-Fuzzy Inference System
RSM	:	Response Surface Methodology
Vo	:	DC source
Vd	:	Breakdown voltage
C	:	Capacitor
SF	:	Servo Feed
VP	:	Gap voltage
SV	:	Spark gap set voltage
Ton	:	Pulse on time
Toff	:	Pulse off time
IP	:	Peak current
WS	:	Wire speed
WT	:	Wire tension
Tc	:	pulse cycle time
Es	:	Spark Energy
F	:	pulse frequency
DF	:	Duty Factor
Ra	:	Surface Roughness
CS	:	Cutting Speed

WL	:	Wire Loss
IACS	:	International Annealed Copper Standard
HIF	:	High Falcon
HIH	:	High Hawk
HIE	:	High Eagle
HIS	:	High Sonic
HIR	:	High Real
HAZ	:	Heat Affected Zone
SEM	:	Scanning Electron Microscopy
EDX	:	Energy-Dispersive X-ray spectroscopy
WP	:	Flushing Pressure
WQ	:	Dielectric flow rate
WC	:	Water Dielectric Conductivity
d	:	Wire diameter
V	:	Main power supply voltage
DOE	:	design of experiment
HRB	:	Rockwell Hardness measured on the B scale
OM	:	Optical Microscope
OPS	:	Oxide Polishing Suspension
Lc	:	Cut off length
S/N	:	Signal to Noise Ratio
gbellmf	:	Generalized bell membership function
Ei	:	represent the percentage error for the sample number i
Tm	:	The measured value of the performance outcomes
Tp	:	The model predicted value of the performance outcomes
Eav	:	Average percentage error

VR	:	Volume Removal
MMR	:	Material Removal Rate
w	:	Kerf width
b	:	Workpiece depth
h	:	Hour
Ce	:	Energy cost
Cw	:	Wire waste cost
Ct	:	Total cost
E	:	Energy consumption
WC	:	Wire consumption
Wm	:	Wire mass per meter
T	:	Machining time

LIST OF APPENDICES

CHAPTER 1: INTRODUCTION

1.1 Introduction

Wire electrical discharge machining (WEDM) is one of the most commonly known and applied nonconventional machining processes in today's industrial practice. WEDM is an electro-thermal machining process for electrically conductive materials. Improvements to WEDM components and the control unit have rapidly been taking place.

During the WEDM process, the cutting tool (wire electrode) never touches the workpiece. Since WEDM does not involve cutting forces, it is commonly used in cases requiring low residual stresses. Any electrically conductive material can be cut using WEDM regardless of hardness, ranging from ordinary metals including copper, aluminum, tool steel, and brass, to uncommon new alloys such as tungsten carbide, wafer silicon, cast alloys, Inconel, titanium, carbide, and polycrystalline diamond. Moreover, WEDM can be used to machine high strength, highly corrosion resistant, highly wear resistant, and difficult-to-machine materials such as metal matrix composites (MMCs) and cemented carbides (Sommer & Sommer, 2013). Besides machining electrically conductive materials, some insulating ceramics and non-conductive materials have also been cut with WEDM (Kozak, Rajurkar, & Chandarana, 2004; Mohri, Fukuzawa, Tani, & Sata, 2002). WEDM also facilitates machining complicated shapes that cannot otherwise be achieved with conventional machining processes like turning, milling, and grinding (Cheng, Yang, Huang, Zheng, & Li, 2014). WEDM is additionally applied in producing fuel injector nozzles, extrusion dies, turbine blades, and aircraft engines (Huang et al., 2013; Kanlayasiri & Boonmung, 2007).

WEDM technology is in increasing demand for its higher speed and precision machining in order to yield greater productivity and superior workpiece quality. Productivity and surface quality are the most important performance parameters in

WEDM. While productivity affects the cost efficiency of a process, quality determines the overall utility of products. Productivity is expressed as cutting speed and surface quality is defined by surface parameters such as surface roughness as well as white layer thickness. These parameters have varying significance depending on the machining process applied (Maher, Ling, Sarhan, & Hamdi, 2015). In the WEDM process, surface roughness and white layer thickness have a vital role in the operational characteristics of the part (e.g., fatigue, corrosion, creep life, fracture resistance, surface friction, and coating ability). To achieve low surface roughness and white layer thickness values, the part must be machined more than once. Therefore, the target surface roughness and white layer thickness are set prior to selecting processing steps appropriate for yielding the desired quality (El-Hofy, 2005) .

Wire electrical discharge machining (WEDM) is an electro-thermal production process, in which a thin, single-strand metal wire in conjunction with deionized water (to conduct electricity) cuts through metal using heat from electrical sparks. Many process factors control the WEDM performance outcomes (cutting speed, surface roughness, white layer thickness, and wire rupture) as shown in the fishbone diagram (**Figure 1.1**). These factors can be categorized as electrical (peak current, pulse on time, pulse off time, servo feed, spark gap set voltage, and gap voltage), wire electrode related (shape, tension, material and speed), workpiece (height and material), and nonelectrical (dielectric fluid conductivity and flow rate) parameters. Any small variation in one of these parameters will affect the cutting quality, including the cutting speed and surface integrity (surface roughness and white layer thickness) (Garg, 2010).

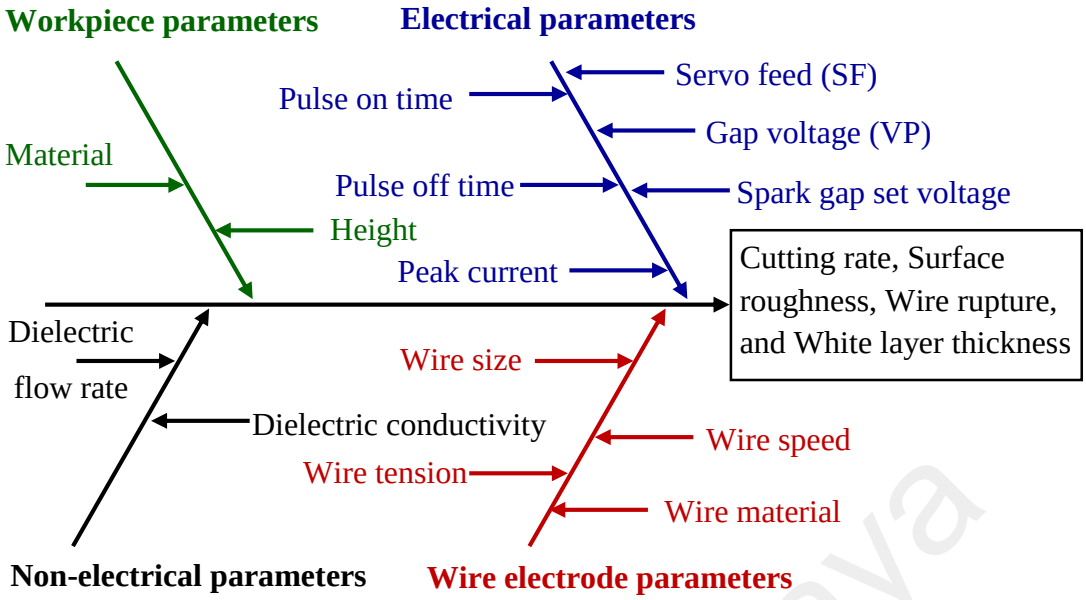

Figure 1.1: Fishbone diagram of the WEDM factors and performance measures (Garg, 2010)

Practically, productivity increases with increasing spark energy parameters (voltage, current, and pulse duration) and with stable cutting and no wire rupture. On the other hand, increasing discharge voltage, peak current, and pulse duration can effectively increase surface roughness and white layer thickness (Maher, Sarhan, Marashi, Barzani, & Hamdi, 2015, 2016; Marashi, Sarhan, Maher, Sayuti, & Hamdi, 2015; Yeh, Wu, Lee, & Yan, 2013).

In addition, machining performance depends on the electrical, mechanical, physical, and geometrical properties of the wire electrode. Besides, other WEDM factors including the mechanical theory, machine intelligence, type of pulse generator, and dielectric flushing system affect machining performance. The wire used in WEDM is important component of the machining process. Copper-zinc alloy (brass) wire electrodes are extensively employed as WEDM tools. However, along with current and continuous variations in the manufacturing applications field, there is rising demand for higher performance wire electrodes over traditional wire electrodes made of brass. High performance wires are known to possess high conductivity, tensile strength and sparking

ability. In practice, coated, porous, composite, and diffusion annealed wires are categorized under high performance wires. These wire electrodes are usually made of copper-zinc alloy or steel core with a coating of pure zinc or brass and a small proportion of chromium or high zinc concentration. Currently, WEDM users are interested in shortening the cutting time without compromising the surface quality of products (Kapoor, Singh, & Khamba, 2010).

Moreover, the dielectric is crucial as a working fluid. During cutting, the heat-molten material is ejected into the dielectric fluid. The presence of very small metal particles pollutes the dielectric fluid that is present in the spark gap between the workpiece and wire electrode, affecting the cutting speed and surface integrity. The dielectric fluid has many functions, such as cooling, cleaning of machined particles, ionization, and electrical insulation. When the voltage reaches the spark gap voltage established, the dielectric fluid ionizes and becomes an electrical conductor. When the spark terminates, the water serves as a coolant and flushes away the machined particles.

Extensive research work has been done with the aim to improve WEDM performance. Theoretical, numerical, and empirical techniques have been employed to correlate the performance parameter measures with machining parameters. In practice, spark energy (peak current, pulse on time, and pulse off time), pulse frequency (pulse on time and cycle time), and wire electrode parameters (wire tension, speed, and material) are varied in order to efficiently control the WEDM process. However, a challenge remains in studying the impact of spark energy and pulse frequency simultaneously on machining performance. Moreover, the discharge parameters should be low and the dielectric flushing rate high to yield low surface roughness and white layer thickness. Such parameter setting would consequently lower the cutting rate in WEDM. Due to this technical trade-off, one set of process parameters fails to attain a high cutting rate and the

least surface defects at the same time. As mentioned before, the WEDM process is usually modeled following either theoretical or empirical methods. Theoretical models seem to produce higher errors compared to experimental results. Moreover, the application and effectiveness of empirical models appear to be limited to certain machining procedures. The most common modeling techniques used to correlate performance parameter measures with machining parameters in WEDM are the Taguchi method and Response Surface Methodology (RSM). In addition, the correlation between input parameters and output measures has been studied with a process model developed from a feedforward neural network and Adaptive Neuro-Fuzzy Inference System (ANFIS).

Although minimizing process energy has been considered in some past literature, the consumption of total electricity of the machine tool and other consumables like the wire, filters and resins has not been considered. Wire consumption is known as one of the most important elements in WEDM machine tool utilization, as it directly affects waste generation and machine tool operation cost. The majority of efforts in past decades have been directed to increasing machining speed without reducing machining accuracy while considering various process-related constraints like wire breakage. However, these approaches do not take into account the impact of cutting conditions on energy and wire consumption, which is essential from both economic as well as ecological points of view. The ecological aspect is expressed by energy and wire consumption, while the economic aspect is defined by costs such as energy consumption and wire consumption costs. These parameters are of varying significance depending on the machining process and wire electrode type. Considering various consumables is especially important as the cost of a WEDM is small compared to the cost of the consumed wire over the machine tool life.

Following a comprehensive review of published research works in this field, a few of the works are introduced to discover changes in workpiece mechanical properties and

surface integrity involving white layer thickness. Moreover, it is still a challenge to study the impact of spark energy and pulse frequency simultaneously on machining performance. So far, very little research has been introduced that identifies the wire rupture limit. Besides, identifying the most suitable wire electrode type for higher WEDM performance considering ecological and economic aspects has not been reported yet.

Hence, the aim of this work is to obtain the best cutting parameters (pulse off time, pulse on time, peak current, wire speed, and wire tension) with the most suitable wire electrode type to enhance the WEDM process keeping in view the ecological and economic aspects.

1.2 Impact of the study

The search for performance improvement in machining processes, particularly WEDM, is always a challenge in the manufacturing industry. Performance improvement in the WEDM process greatly depends on the spark energy, pulse frequency, and wire electrode parameters. This study is important as it addresses the following aspects:

- The effect of WEDM parameters on machining performance is investigated using ANFIS modeling along with the Taguchi method.
- A new performance index is proposed to identify the effects of spark energy and pulse frequency simultaneously on machining performance and to identify the wire rupture limit in WEDM.
- A new production economic index is proposed to identify the most suitable wire electrode type for higher WEDM performance considering the ecologic and economic aspects.
- An electrode wire design is proposed for use in the WEDM process to facilitate better machining performance and cutting accuracy.

1.3 Problem statement

Based on the literature reviewed regarding WEDM of difficult-to-machine materials as well as wire electrode materials and types, there are a few gaps with respect to WEDM of difficult-to-machine materials using different wire electrodes. The gaps are as follows:

- Very little research work has been introduced regarding the study of the spark energy and pulse frequency parameters' effects simultaneously.
- Very little work has been reported on finding changes in the mechanical properties (hardness, wear) and surface integrity of WEDM materials.
- There is limited research on the wire rupture limit during WEDM. Moreover, the effects of the process parameters on wire breakage have not been considered.
- The development of an economic index to identify the most suitable wire electrode type for higher WEDM performance considering the ecological and economic aspects has not yet been reported.
- The development of economic wire electrodes with high conductivity, elongation, and strength for higher cutting rate and surface quality remains a key research area.

1.4 Research motivation

In engineering applications, high precision machining with accurate dimensions is developed using different machining processes. WEDM is usually employed when low residual stresses are required, because it does not entail high cutting forces for material removal. WEDM can machine any electrically conductive materials regardless of hardness, from common materials such as copper, aluminum, tool steel, and graphite, to unusual modern alloys including wafer silicon, Inconel, titanium, carbide, polycrystalline and diamond compacts. Besides, WEDM is also utilized to machine modern composite materials such as conductive ceramics. In WEDM, the workpiece is machined with a series of electrical sparks that are produced between the workpiece and the wire electrode.

The wire electrode discharges high frequency pulses of alternating or direct current to the workpiece through a very small spark gap with a nonconductive dielectric fluid. To acquire low surface roughness and small heat-affected zone, low discharge energy parameters with high dielectric flushing rate are required. However, such parameters decrease the material removal rate. This implies that it is difficult to attain a high cutting rate and minimum surface defects using a single parameter setting. Moreover, it is very difficult to study the effects of spark energy and pulse frequency simultaneously on machining performance. In addition, the impact of cutting conditions on energy and wire consumption, which is important for both economic as well as ecological reasons, must be considered. Considering various consumables is especially important, as the cost of wire EDM is smaller than that of the wire consumed over the machine tool lifetime. Moreover, manufacturers' guidelines for the selection of machining parameters are conservative in nature and do not lead to optimal and economically effective machine use. Finally, selecting an optimal wire for a particular application would mostly likely be a trade-off for the properties mentioned above. As an example, wires with high conductivity usually have low tensile strength. Thus, the development of an economical wire electrode with high conductivity, elongation, and strength should be developed for higher cutting rate and surface quality in view of the economic and ecological aspects.

1.5 Objectives

In order to improve WEDM process performance by applying a new coated wire electrode, this study embarks on the following objectives:

- To investigate the effect of WEDM parameters on machining performance using different wire electrodes to improve surface micro-characteristics in WEDM.
- To propose a new performance index to identify the effects of spark energy and pulse frequency simultaneously on machining performance.

- To propose a production economic index to identify the most suitable wire electrode type for higher WEDM performance considering the ecological and economic aspects.
- To propose a new coated wire electrode with higher strength for less wire rupture and high WEDM performance.

1.6 Scope of the study

First, ANFIS modeling of WEDM parameters and performance measures is introduced to achieve wire electrode productivity and good quality associated with sustainable production. Second, a new performance index is introduced to identify the effects of spark energy and pulse frequency simultaneously on machining performance. Third, a new production economic index to identify the most suitable wire electrode type for higher WEDM performance considering the ecological and economic aspects is proposed. Finally, a new coated-wire electrode with higher strength for less wire rupture and high machining performance in WEDM is developed.

1.7 Research methodology

The detailed research methodology of this work is categorized into several stages, as shown in the research flow chart in **Figure 1.2**. The initial research stage entails a literature review followed by the experimental setup and result analysis, discussed below.

(a) ***Literature review***

This stage focused on gathering information required to characterize the WEDM process. The preliminary data were collected from various sources, such as preliminary experimentation, reported publications, etc. A literature review of related research is taken into consideration for the following reasons.

- To analyze existing problems, and set the problem statement and objectives.

- To collect preliminary data, and locate the major variables and parameters.
- To use appropriate collected data for a suitable experimental setup.
- To plan all materials and specific equipment required.

(b) ***Design an experimental plan and setup***

At this stage, an appropriate experimental design was identified to ensure it was possible to carry out the experiments. Several experimentation steps were conducted by using the recommended parameters.

- Instrumentation (WEDM and wire electrodes)
- Planning materials required (Ti6Al4V and AISI 1050 carbon steel)
- Planning preparation equipment and chemicals to condition the samples for measurement, including sand paper, grinding and polishing machine, chemical reagents, and optical microscope.
- Planning measuring equipment for response evaluation, such as a balancer, surface meter, SEM, EDX, etc.

(c) ***Data collection and analysis***

All data were analyzed using various techniques including Taguchi analysis and the ANFIS approach. Moreover, appropriate data were collected from the experiments to validate the performance index. For the unfeasible results obtained, the experimentation was repeated after modifying the previous experimental process.

(d) ***Propose a new performance index***

A new performance index is introduced to study the effects of spark energy and pulse frequency simultaneously on machining performance and to identify the wire rupture limit.

(e) ***Propose a new production economic index***

A new production economic index is proposed to identify the most suitable wire electrode type for higher WEDM performance considering the ecological and economic aspects.

(f) ***Design a new coated wire electrode***

A new coated-wire electrode design is proposed to improve precision and accuracy with increased mechanical load. Manufacturing the new wire electrode will be developed in future work. The new wire electrode will be verified using a performance indicator and a comparison study between the new wire and conventional wires will be introduced in future work as well.

(g) ***Writing the thesis***

In this final stage, all information was gathered systematically and a report was written together with the details of the experimentation and confirmation tests.

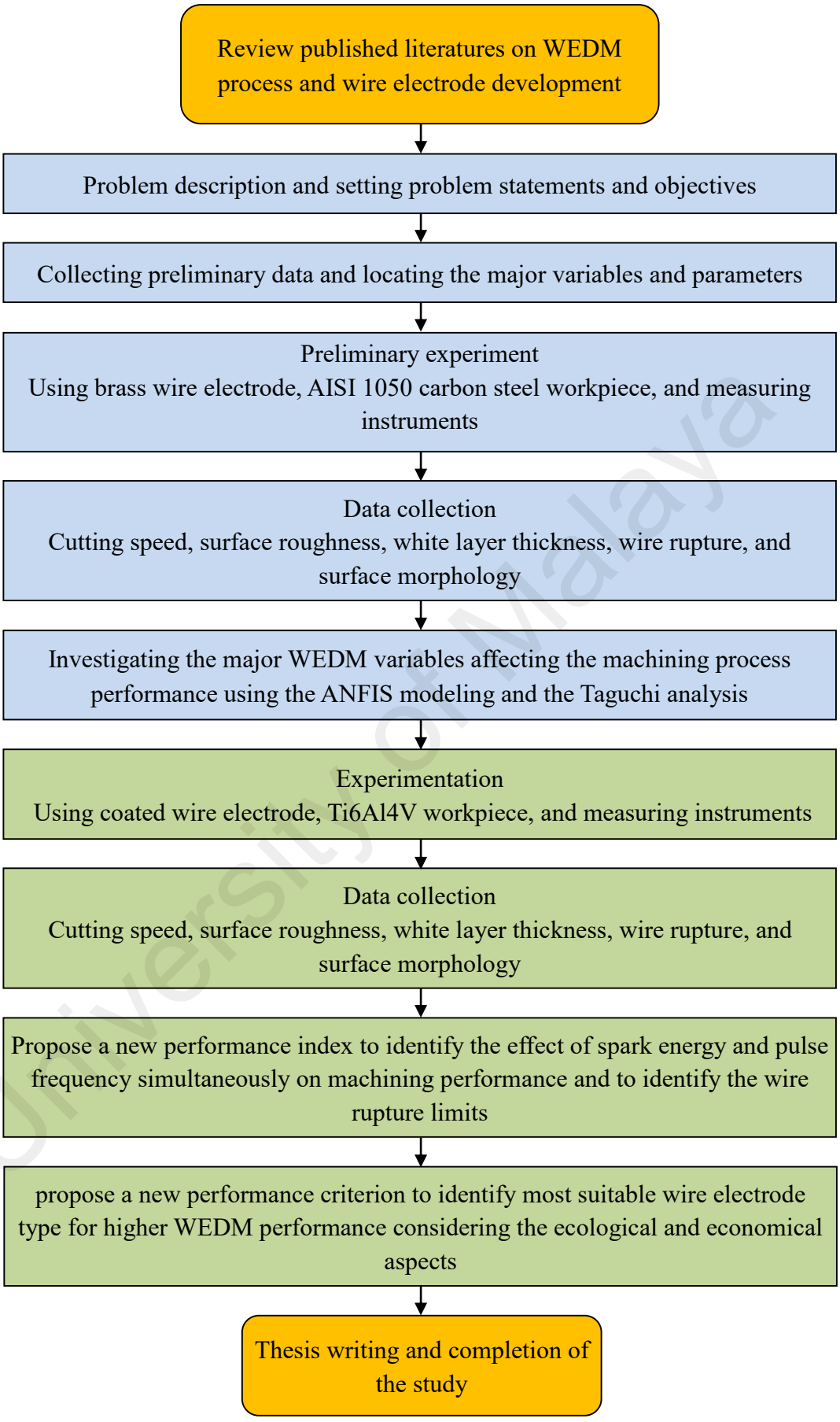

Figure 1.2: Research methodology flowchart

1.8 Arrangement of thesis content

This thesis comprises six chapters, which are organized to present a background of the study, literature review, experimental work, results, analysis, discussion, and conclusions.

The chapter details are summarized below:

Chapter 1 provides a general view of the study background and offers a scenario of problems to be investigated as the motivation of this study. Next, the current study objectives are identified. The scope is also stated and the methodology used to solve the problems is briefly presented.

Chapter 2 presents a literature review of all matters related to the WEDM process and wire electrode. The relevant and similar concepts reported by previous researchers are highlighted to help understand the subject matter presented in this work. Most importantly, the research gaps are realized to establish the problem statement, objectives, scopes and research methodology.

Chapter 3 describes the experimental work done in this study in terms of experimental design, experimental setup, procedures, materials and apparatus used to conduct the experiments and collect data. The variables, experimental procedures and data collection techniques are clearly outlined. Details of the operating parameters and specifications of all equipment are also included.

Chapter 4 exhibits the results obtained from the experiments, an analysis, and a discussion. An investigation of the effects of WEDM parameters on the machining performance of Titanium alloy grade 5 (Ti6Al4V) and AISI 1050 carbon steel using brass and coated-wire electrodes to improve surface micro-characteristics in WEDM is presented in this chapter. Moreover, a new performance index is introduced to study the

effects of spark energy and pulse frequency simultaneously on machining performance and to identify the wire rupture limit.

Chapter 5 proposes a new production economic index to identify the most suitable wire electrode type for higher WEDM performance from ecological and economic perspectives. In addition, a new coated-wire electrode design with higher strength for less wire rupture and high WEDM performance is proposed.

Chapter 6 concludes with the findings of this study. Recommendations for further considerations and future research pertaining to this project are suggested and proposed.

CHAPTER 2: LITERATURE REVIEW

2.1 Introduction

A review of past research suggests that an analysis of the wire electrical discharge machining (WEDM) process can be divided into three main basic areas:

1. WEDM process and pulse generator parameters.
2. Development of EDM wire electrodes.
3. WEDM performance outcomes and indicators

The first research area reviewed refers to the main components of the WEDM process and an analysis of the pulse generator. Here, the relationship between electrical process parameters (peak current, pulse on time, and pulse off time) is identified. The second area is mainly devoted to addressing developments in the wire electrode made from conventional brass wire to the most recent wire electrodes on the market. The third area focuses on the performance outputs and indicators including cutting speed, surface roughness, white layer thickness, and wire rupture caused by the WEDM process parameters including peak current, pulse on time, pulse off time, wire speed, and wire tension.

2.2 WEDM process and pulse generator analysis

Wire electrical discharge machining involves electrical discharges for forming desired shapes in the manufacturing process while the NC table undergoes movements in the X and Y directions (**Figure 2.1**). Due to sparks and wire burning involved, it is also termed spark eroding, wire burning or wire erosion.

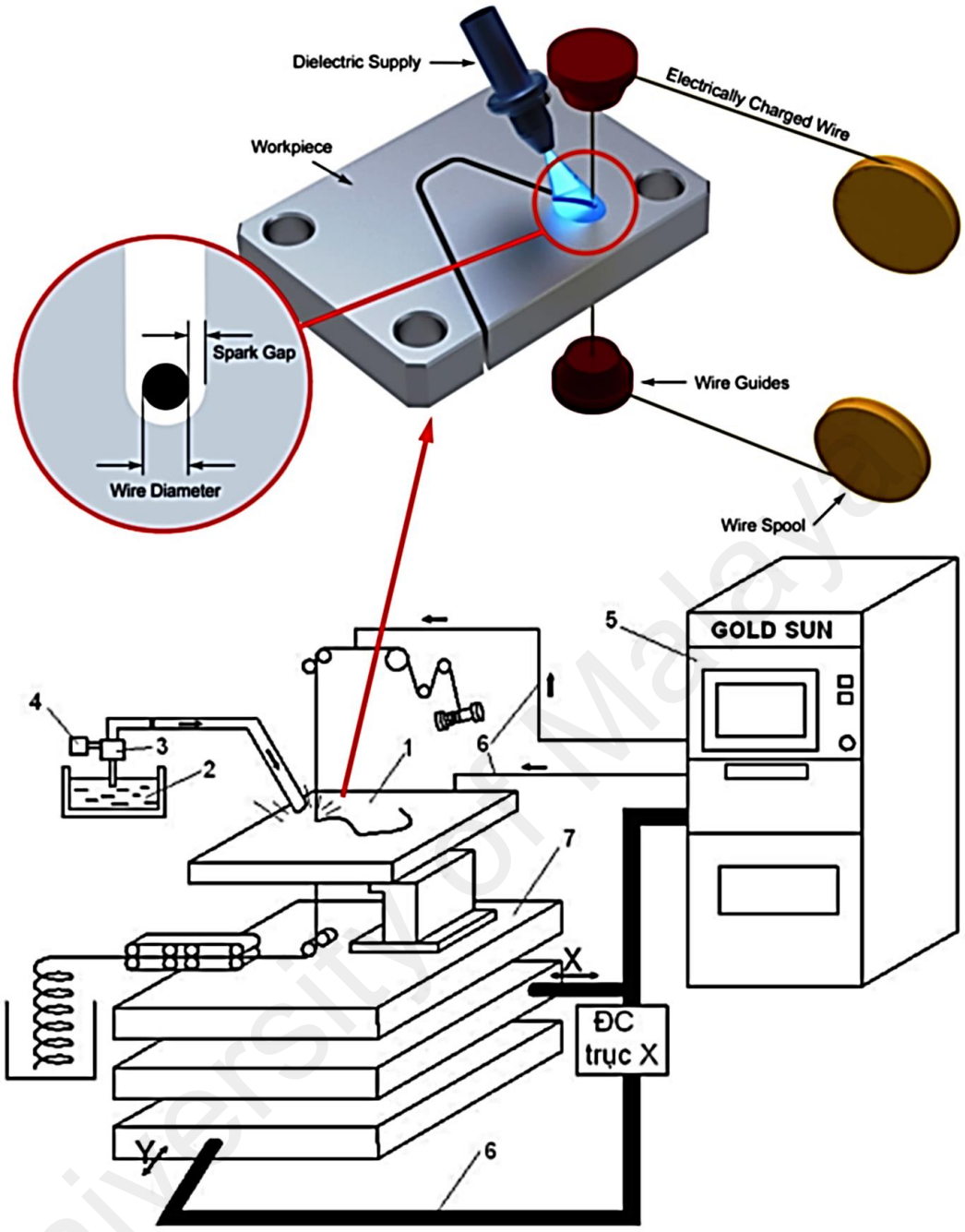

Figure 2.1: WEDM machine components (1-workpiece, 2-dielectric fluid, 3- pump, 4-pressure gaga, 5- power supply, 6- X-Y control unit, 7- machine table) (Jameson, 2001)

WEDM produces a series of electrical discharges between the workpiece and electrode to achieve workpiece machining. High frequency alternating current or direct current is discharged through a very small spark gap between the wire electrode and the workpiece with a nonconductive dielectric fluid (Jahan, 2013). The sparks due to discharge are easily seen instantaneously in the cutting zone (**Figure 2.2**) as they occur at rates of over one hundred thousand times per second (El-Hofy, 2005).

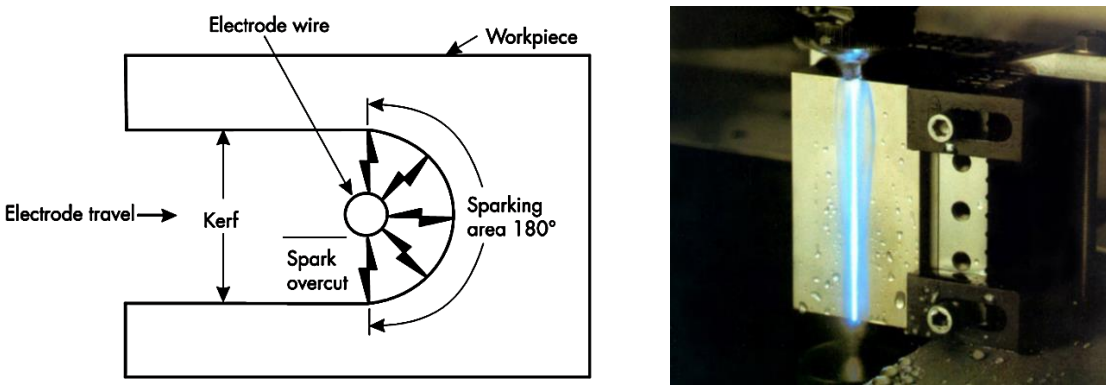

Figure 2.2: WEDM discharge sparks (Jameson, 2001)

It is possible to attain continuous machining during wire electrode operation. The spark and burning processes melt and vaporize a small amount of the workpiece and wire electrode, resulting in residuals that are contained in plasma. However, the plasma is in transient state that eventually breaks down at pulse off time. The discharged material residues in liquid and vapor states condense into solid debris in the dielectric fluid. This process repeats over nanoseconds along the length of the wire in the cutting zone (Marashi, Sarhan, Maher, & Sayuti, 2016; Moulton, 1999). **Figure 2.3** illustrates the WEDM components and a detailed description of the pulse generator used in WEDM.

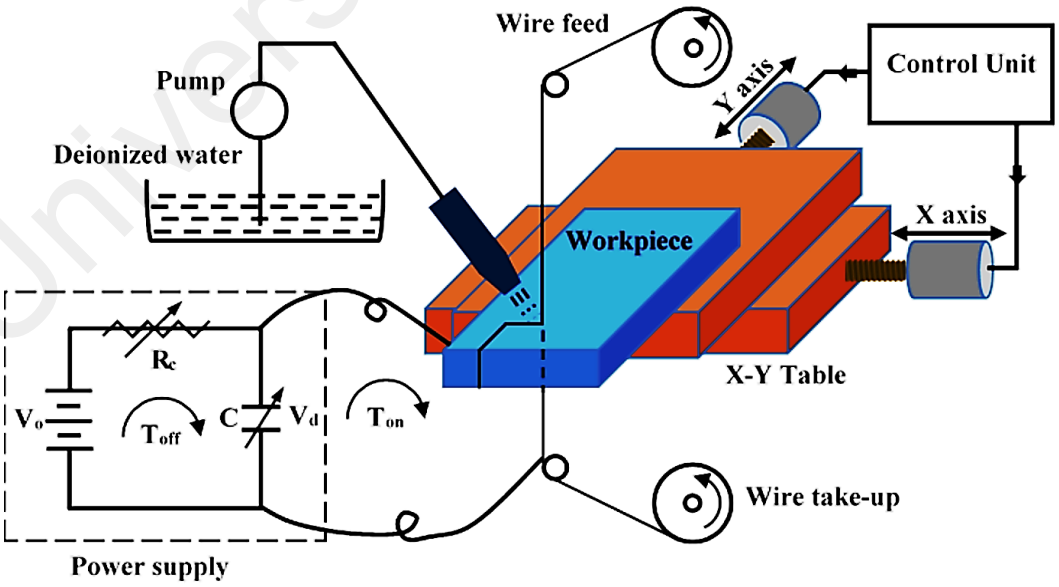

Figure 2.3: Pulse generator and components of WEDM

In a pulse generator, the capacitor is charged by a DC source (*Vo*). As long as the capacitor voltage does not reach the breakdown voltage of the dielectric medium under machining conditions (*Toff*), the capacitor (*C*) continues to charge. Once breakdown voltage (*Vd*) is reached, the capacitor starts discharging and a spark is established between the tool and workpiece, leading to machining. Such discharging continues as long as sparks can be sustained. When the voltage becomes too low (*Vd**) to sustain the sparks, the capacitor continues to charge as shown in **Figure 2.4** (El-Hofy, 2005).

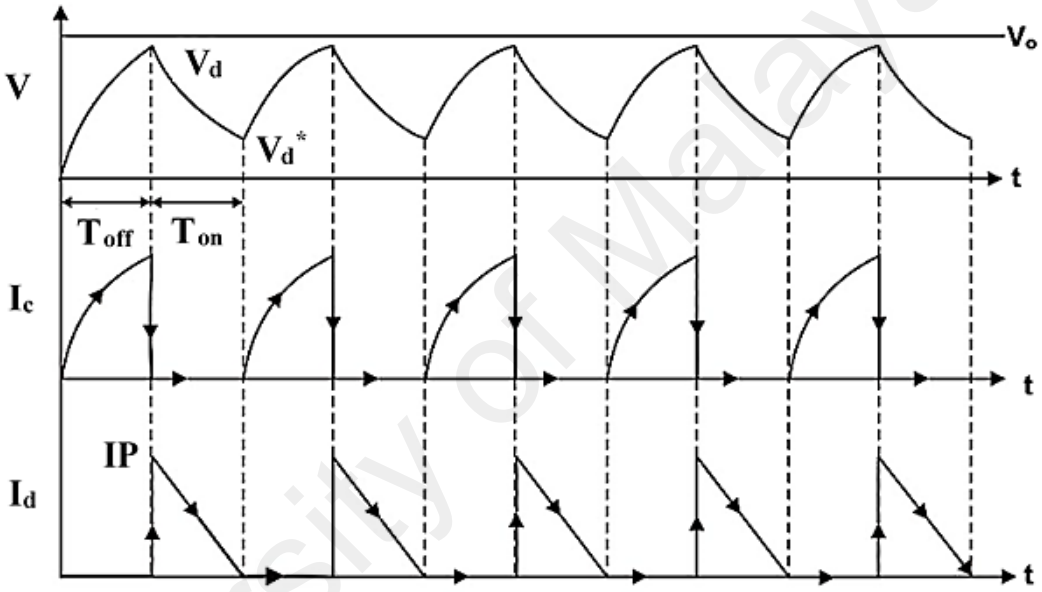

Figure 2.4: Analysis of RC type EDM Generator (El-Hofy, 2005)

An electrical discharge involves time-varying voltage and current impulses. The following variables are used to determine electric impulses: discharge voltage (*Vd*), pulse off time (*Toff*), pulse duration (*Ton*), peak current (*IP*), pulse cycle time (*Tc*), pulse frequency (*F*), and duty factor (*DF*). The most important WEDM parameters are spark energy and duty factor. Spark energy is defined by the electrical energy in each spark, which can be expressed by **Equation (2.1)**.

$$Es = Vd \times IP \times Ton \qquad 2.1$$

According to Equation (1), spark energy is proportional to three variables: discharge current, discharge voltage, and pulse duration. The discharge voltage is dependent on the properties of the wire electrode and workpiece pair (Ferreira, 2007). The spark intensity develops as a result of discharge current and pulse duration (**Figure 2.5**). The spark energy determines the spark size and hence, the chip size. High spark intensity leads to long sparks, thus increasing the cutting speed and chip size but deteriorating the surface finish as shown in **Figure 2.5a** (Portt, 1992).

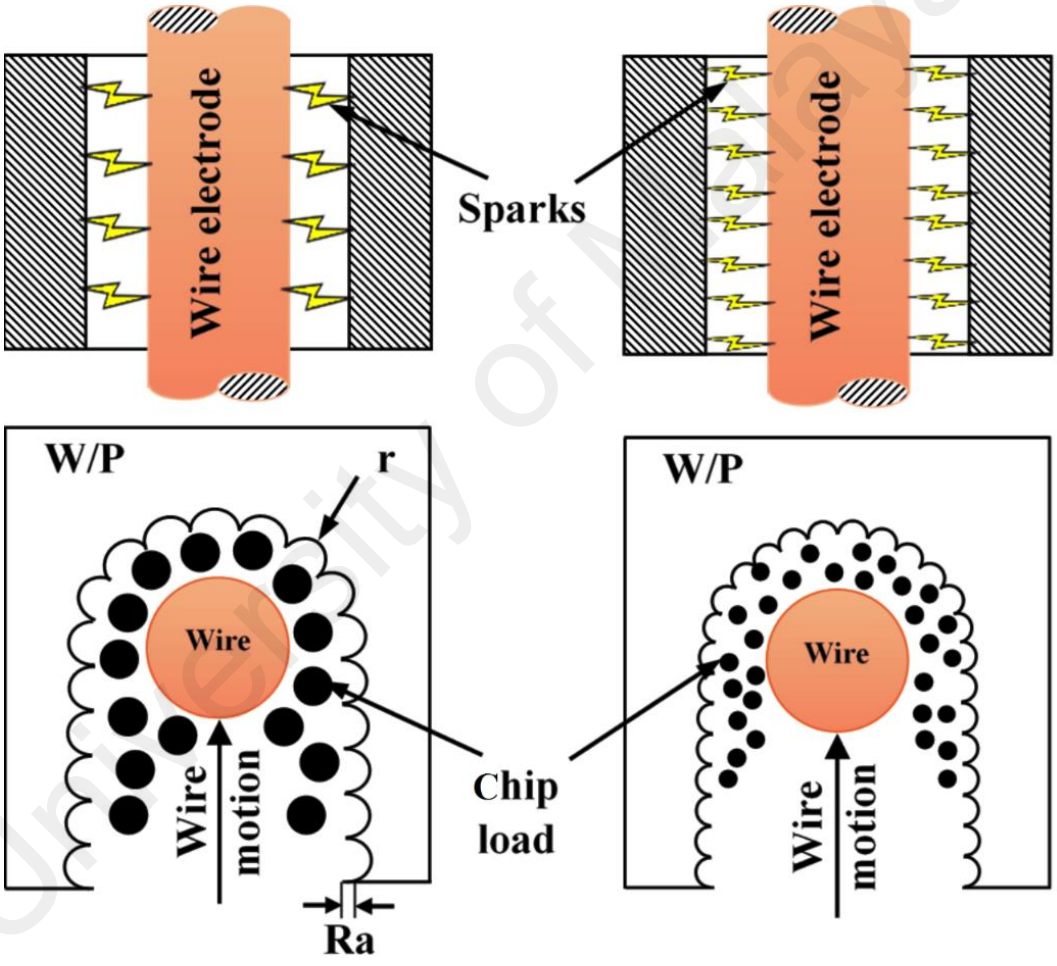

Figure 2.5: Chip size and load at different spark energy and pulse frequency (a) High spark energy with low pulse frequency (b) Low spark energy with high pulse frequency

The other very important electrical parameter with significant influence on WEDM performance is the pulse frequency (*F*), or duty factor (*DF*). The duty factor determines the weight and number of pulses (**Equations 2.2** and **2.3**) and it is the percentage of pulse duration over the total cycle time. In machines with duty factor settings, the pulse interval is set indirectly by setting the pulse duration and duty factor. Pulse frequency is used to set the pulse interval on some machines and to determine the number of chips per second.

$$\boldsymbol{F = \frac{1}{T_{on}+T_{off}}} \qquad \textbf{2.2}$$

$$\boldsymbol{DF = \frac{T_{on}}{T_{on}+T_{off}} = T_{on} \times F} \qquad \textbf{2.3}$$

Selecting a spark microsecond cycle time depends on the workpiece thickness, flushing condition, and required surface quality. High pulse frequency leads to short sparks, hence decreasing the chip size (**Figure 2.5b**). This condition is consequently recommended to improve surface finish. Low pulse frequency leads to long sparks and thus greater chip size (**Figure 2.5a**), so it is recommended for increasing cutting speed (Jameson, 2001).

2.3 EDM wire electrode types and functionality

The wire electrode is the central component of a WEDM system for the process of producing steady electrical discharge. Therefore, WEDM performance is largely affected by the wire electrode (Aoyama, 2001). Wire rupture is a critical phenomenon that affects quality and productivity in the WEDM process. It requires some prior knowledge about the wire electrode and workpiece characteristics in the cutting process in order to avoid such ruptures for continuous process operation (Dauw & Beltrami, 1994). The parameters that define these characteristics are wire tension, thermal load, electrical discharge impact, and flushing rate. Wire rupture is likely to occur when the developed stress exceeds the wire's strength. The effect of the developed stress is determined by factors such as cross-section reduction and increase in wire temperature. High process temperatures and varying workpiece thickness, both of which eventually lead to wire rupture, directly affect the wire strength.

In the early 1970s, pure copper wire electrodes were used to compromise between machining accuracy and strength. By the mid-1970s, brass wires started replacing copper wire electrodes. Following these developments, wire electrodes made of copper and coated with zinc appeared in machining applications in 1980. In the following years, brass wire electrodes coated with zinc replaced these, and brass wire electrodes were developed containing aluminum or chromium. Since 1990, brass wire electrodes have been developed with different compositions to achieve a range of processing goals. To ensure quality for high precision cutting, the brass wire electrode is coated with zinc, and high-speed cutting is achieved for productivity using Cu-50%Zn coating. Subsequently, for higher productivity or cutting speed, wire electrodes made with higher zinc proportions have been found to be effective. In cutting thick materials, the heat resistance is enhanced by applying brass wire electrodes containing titanium and aluminum (Paul, Kumar, Bhargava, & Kukreja, 2013). Moreover, other special wire electrodes have been tailored

to meet conditions desirable for cutting and workpiece characteristics, such as steel, tungsten, molybdenum, abrasive-assisted and porous-wire electrodes (Ho, Newman, Rahimifard, & Allen, 2004).

2.3.1 Wire electrode properties

In practice, the cutting efficiency in the WEDM process reply on a complex consideration of mechanical, electrical, geometrical, and physical, properties of the wire electrode. However, the overall cutting performance is controlled by several WEDM process factors such as the mechanical effect, machine intelligence, pulse generator improvements, and the dielectric flushing methods. The following section discusses EDM wires in terms of their physical properties and their relationships with practical cutting processes (Aoyama et al., 1999; Dauw & Albert, 1992).

(a) ***Conductivity***

Conductivity determines the transfer of power from the feed source to the target point of cutting. It enables the EDM wire to transfer energy over the distance, and thus serves as a key property of the wire. When the cutting process involves open guide to clear a workpiece obstruction, the distance for power transfer can be considerable. A low conductivity is responsible for a considerable voltage drop over the distance between the power source and cutting target, which eventually results in power loss at the cutting point. This loss can be significant as the modern power supplies usually produce electric currents over 100 amps. The conductivity value of metals and alloys is determined relative to that of the standard annealed copper based on IACS (International Annealed Copper Standard). Conductivity is expressed as a percentage of IACS which is 100% for the standard copper wire (Davis, 1998).

(b) ***Tensile strength***

Tensile strength is a mechanical property of the wire, which refers to its ability to withstand the applied tension in a cutting procedure aiming a vertically straight cut (M.-T. Yan & Huang, 2004). EDM wires with tensile strengths of 900 MPa or above are categorized as "hard", whereas "half-hard" wires possess tensile strengths around 490 MPa, and "soft" wires are with tensile strengths below 440 MPa. In practice, hard wires are used for most of the cutting processes. However, in taper cutting, hard wire will resist bending at the guide pivot resulting in faulty taper cutting. In this case, half-hard and soft wires are primary choices where the taper angle is greater than five degrees. In general, half-hard and soft wires are not appropriate for automatic threading unless the machine is tailored to work with such wires (Roger Kern, 2013).

(c) ***Elongation***

Elongation defines the amount of deformation the wire produces prior to the breaking down. This is a key property of the wire, which is commonly subjected to high-tension load and countless sparks during the cutting process. The percentage of gauge length is used to estimate the elongation in a given test. Elongation also determines if a type of wire is brittle than the other. Hard wires possess relative much less elongation than half-hard wires. Therefore, a brittle wire is more likely to break down early due to an overload condition, while a more ductile wire may survive in a temporary overload.

(d) ***Melting point***

Melting point is not listed as a specification parameter for a given wire; however, it plays a significant role during the spark erosion process of the WEDM. In addition, the wire electrode should possess certain resistance to the rapid melting caused by the sparks.

(e) ***Straightness***

Straightness is rarely specified for EDM wires, however it plays an important role in successful auto threading and cutting thicker workpieces.

(f) ***Flushability***

Flushability indicates the quality of the cut in the WEDM process. Although it is not a specified item for a given wire, a better flushability refers to a faster cut by the wire (Cut, Masuzawa, & Taniguchi, 1993). It depends on the metallurgical property of the alloy components of the wire.

(g) ***Cleanliness***

Cleanliness is also not found in the specification of EDM wires. This refers to the quality of the wire being clean from the contamination. The contamination may appear as dirt by residual metal powder from the drawing process, drawing lubricant, or due to added paraffin prior to spooling. These chemical and metallic contaminants can accumulate over time and eventually clog guides and power feeds, or slipping belts or rollers.

(h) ***Geometrical Properties***

Geometrical Properties specify the diameter, shape, and coating and layer structure of the given EDM wires. In general, WEDM involves wires with diameter between the ranges of 0.02 mm to 0.36 mm. A larger diameter yields an increased supply of pulse energy to the working gap, which improves the overall material removal rate (Gedeon, 2011; P. Lin & Liao, 2009). In contrast, micro-WEDM involves ultra-fine wires less than 30 microns in diameter to handle predominantly small pulse energies (Uhlmann & Roehner, 2008). Considering the application and process conditions, many patents are available proposing a number of other wire electrode shapes (Gonnissen & Van Vooren, 2001; Groos, 1988; Walder & Balleys, 1999).

Meanwhile, the high manufacturing cost of modified cylindrical wires limit their usage in practical applications. An improved heat transfer in wire electrodes has been found to yield 15-20% increase in the cutting rate. Wire electrodes with twisted groves have been patented to resist sparks occurring at the same point (Inoue, 1985). Regarding their patents, several inventors have disclosed that the change in the direction of wire's rectangular cross-section played a vital role to move the generated sparks very near to the workpiece and to prevent hot spots on the wire electrodes during the WEDM process (Groos, Barthel, Noethe, & Dietrich, 2004b; K. Seong, 1999). **Figure 2.6** illustrates several wire shapes that are patented to improve the material removal rate (Inoue, 1983, 1985).

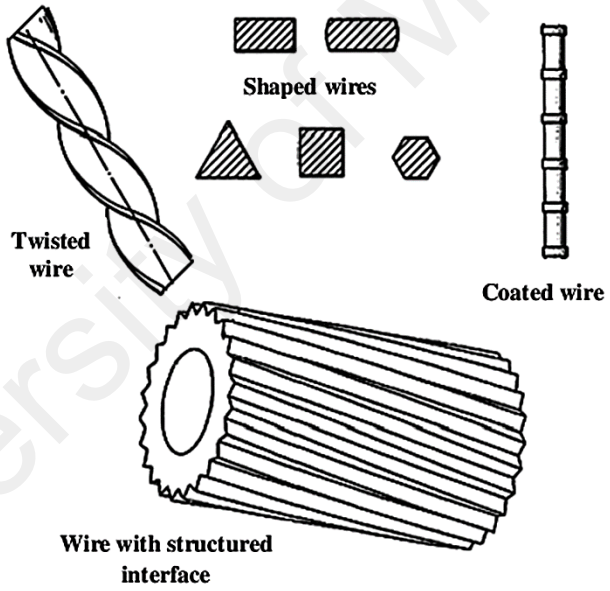

Figure 2.6: Customized wire shapes (Inoue, 1983, 1985).

In 1969, the maximum possible cutting rate was achieved by a 0.15 mm diameter wire, which was later increased to 0.36 mm. **Figure 2.7** depicts how the wire diameter is increased every time to facilitate an improved wire electrode for the WEDM process (Kaneko & Onoue, 1984). The effect of several important force factors such as electromagnetic, electrostatic, wire traction, dielectric flushing, wire feed have been analyzed on the application of the smaller diameter wire electrode (0.03 mm) (Herreroa

et al., 2008; Makino, Obara, Ohsumi, & Niwa, 1995). Prior works have been conducted to enhance the power supply and transportation system suitable for fine wires of diameter less than 80 microns (Ezaki, Hasegawa, & Seto, 1991; Uhlmann & Roehner, 2008). To achieve a successful operation, selecting the suitable wire electrode is a very challenging task in WEDM (Roger Kern, 2008). This demands the study of a variety of wire electrodes to yield the optimal result for this process.

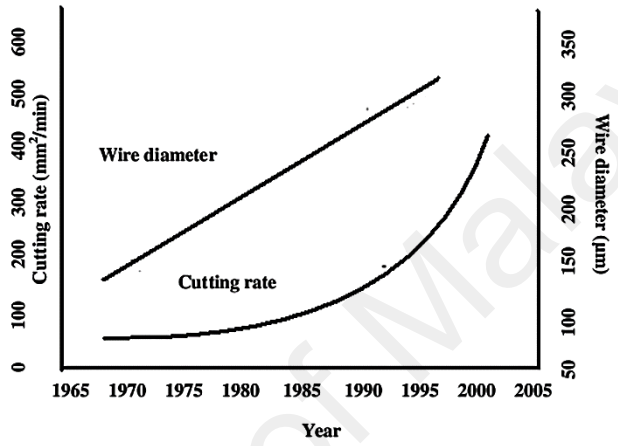

Figure 2.7: Cutting rate improvement in relation to wire diameters (Jatinder Kapoor, S. Singh, & J. S. Khamba, 2012)**.**

2.3.2 Development of EDM wire electrodes

The cutting machines in the early 70s had an extremely low yield with cutting rates of about 21mm^2/min. By early 80s, cutting rates went up to 64 mm^2/min, while the current machines are able to cut at a speed more than 20 times higher than the earliest machines. **Figure 2.8** shows the advancement rate of WEDM with brass wire and performance wire electrodes, since its development (Kaneko & Onoue, 1984; Sánchez & Ortega, 2009; Sommer & Sommer, 2005; Weng & Her, 2002).

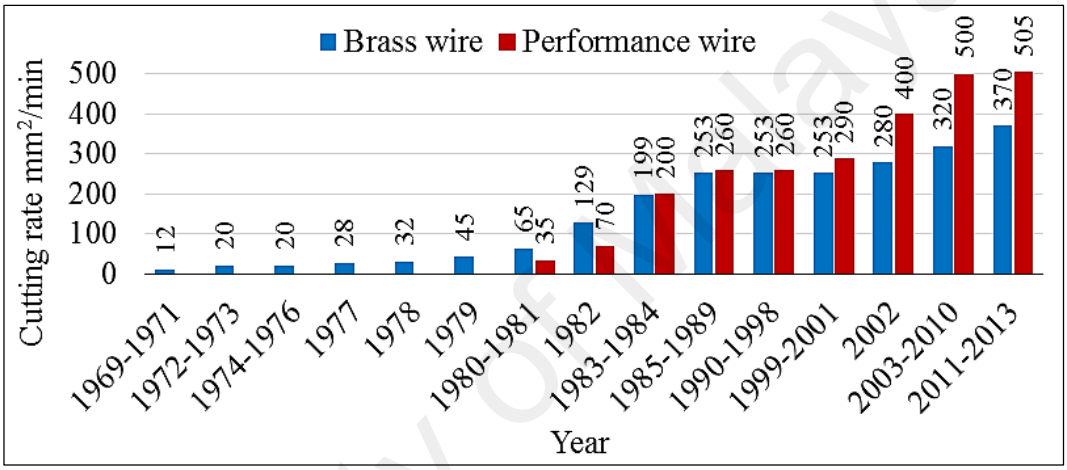

Figure 2.8: Advancement rate of the WEDM, since its development(B. Schacht, 2004)

The existing brass coated wires are found in one of the following categories: HIF (high falcon), HIH (high hawk), HIE (high eagle), HIS (high sonic), and HIR (high real) (Aoyama, 2001). HIS and HIR wire electrodes are suitable for high cutting speed and have been commonly used in applications involving mass production such as electronic and metal molds for IC lead frames. On the other hand, HIE and HIH wire electrodes were used for high precision machining and being utilized for precise applications such as biomedical and aerospace products. **Figure 2.9** shows different wire electrodes produced to offer fasted cutting speed with improved surface finish and flatness (Aoyama, Kuroda, Seya, Kimura, & Sato, 2008).

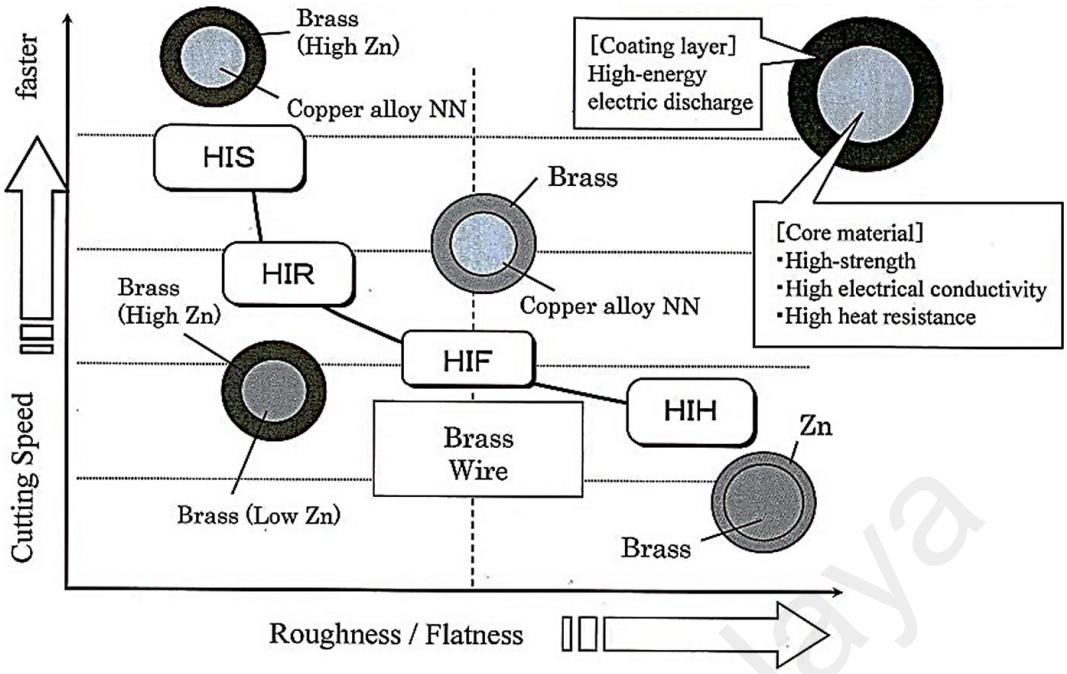

Figure 2.9: Characterization of electrical discharge wire electrode (Aoyama et al., 2008)

Electrical discharge property can be regulated by adding zinc to the wire electrode, which consequently helps to enhance the machining performance. Properties like clarification and heat release can be controlled by alloying conductive elements to the core surface of wire electrodes (Haruki Obara, Ohsumi, Masahashi, Miyanishi, & Hatano, 2002). Several inventors have considered these properties as the primary control parameters to improve the wire electrode performance (Kuroda, Aoyama, Kimura, Sawahata, & Sato, 2003; Otsuka et al., 2001). Prior studies involving plain, alloyed, or coated (zinc-coated, diffusion annealed, etc.) wire electrodes report a significant enhancement in the WEDM performance (Yamauchi, Okada, Morita, Shimizu, & Uno, 2005). Due to stable discharge, brass wires are the most popular electrodes in machining, but they suffer from low electrical conductivity. The electrical conductivity and heat resistance of the core or coating of the wire have been commonly considered in developing many wire electrodes. Fracture toughness is one of the properties that control the WEDM performance. Fracture toughness is referred to the ability of the wire electrode

to resist break down and withstand the formation of craters on its surface (Haruki Obara, 1989; Haruki Obara, Abe, & Ohsumi, 1997). Wires with high tensile strength are likely to break during the machining process. The issues associated with fracture and electrical conductivity has been addressed using composite materials with the steel core wire electrode. Under the applied preload tension, a discharge may cause a flaw greater than a critical flaw level that sets off a catastrophic failure. This event may break an EDM wire as shown in **Figure 2.10** (Hatvki Obara, Yamada, Ohsumi, & Hatano, 2002). High strength materials used in EDM wire manufacturing are vulnerable to small flaws, as they tend to fail because of their low fracture toughness. Each discharge in the WEDM process results in a flaw in the form of a crater in both the wire and workpiece. These flaws gradually grow larger with the deteriorating flushing conditions and eventually lead to catastrophic wire failure (Luo, 1999; Rajurkar, Wang, & Lindsay, 1991).

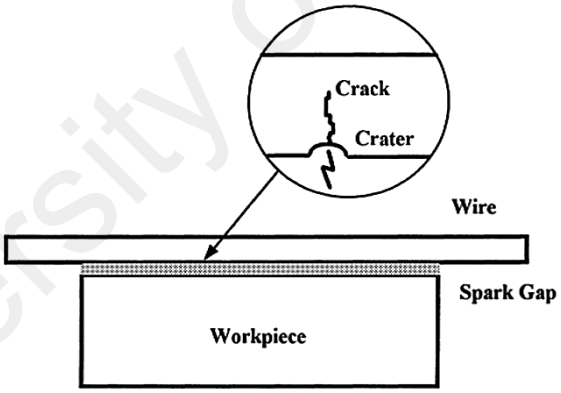

Figure 2.10: Defect and fracture in the wire EDM process (Luo, 1999)

2.3.3 Plain EDM wires

The manufacturing of brass wire starts with a continuously cast rod of 20 mm diameter. The rod is made about 6 mm round or in hexagonal cross-section following either cold rolled or cold drawn procedure. The wire is then shaped around 0.9 mm through annealing and drawing by a series of dies. This state is usually termed as a redraw wire. Prior to forming the final size, the redraw wire is drawn through another series of diamond dies. In the final stage, the wire is resistively annealed or thermally tempered in an inert

atmosphere, cleaned, and then spooled (Roger Kern, 2013; Schuler, 1998; Wright, 2010). According to the convention, the term plain simply refers to the wire that consists of a single homogeneous component without involving coating or alloying of other materials (Roger Kern, 2013).

2.3.3.1 Copper wire

There was a common notion that the high electric conductivity of copper wire would make it an ideal EDM wire. Unfortunately, copper wire suffers from low tensile strength, high melting point and low vapor pressure rating (Intech, 1995). This became evident at the advent of the 2nd generation of pulse power supplies; hence, brass wire had to take over copper wires in WEDM process. However, copper wire is occasionally found in applications where the Zinc contaminant, either contained in brass or coated wires, is not acceptable (Roger Kern, 2013; Wang & Ravani, 2003).

2.3.3.2 Brass wire

There have been numerous efforts to enhance the performance of wire electrodes. Brass wire is an alloy of copper and zinc with compositions and in the range of 63–65% Cu and 35–37% Zn. It has been reported that increasing the proportion of zinc enhances cutting speed and performance (Prohaszka, Mamalis, & Vaxevanidis, 1997). The zinc in the brass wire evaporates during the cutting process, provides more energy yield by cooling the wire. Adding zinc provides significantly higher tensile strength and greater vapor pressure rating, which compensates its loss in conductivity. In addition, the dielectric fluid may not be able to clean some zinc particles which will stay between the workpiece and wire electrode gap to facilitate necessary ionization and cutting process (Kaneko & Onoue, 1984). These qualities make brass one of the most popular choice of materials for WEDM electrodes. However, the addition of zinc to any extent significantly reduces the conductivity of the electrode. For example, hard brass wire possesses only

20% of the conductivity of copper wire. Because of the improved flushability with zinc wire, currently a high-zinc brass is available composed of Cu60%Zn40%. This additional zinc content speeds up the cutting process up to 5% in some optimized applications (Antar, Soo, Aspinwall, Jones, & Perez, 2011). However, zinc proportion more than 40% is not practical to cold-draw wire. The change in the grain structure of wire may turn the wire too brittle to process into fine diameter required for WEDM. In several cases, there can be significant amount of brass deposit on the workpiece after the cutting process, which has been found harder to remove. These findings have encouraged the formation of coated wires (Altpeter & Perez, 2004; Kapoor et al., 2010; S. Singh, Maheshwari, & Pandey, 2004).

2.3.3.3 Aluminum-brass wire

A special type of alloy wire is made by alloying a small amount of aluminum with the brass wire. The tensile strength of the wire can be improved by such alloying process, which can raise the tensile strength as high as 1200 MPa without deteriorating the elongation. These alloyed wires are less prone to damage than the wires made of plain brass (Roger Kern, 2013).

2.3.4 Coated EDM wires

US Patent No. US1896613-1933 refers to one of the earliest patents on zinc-coated wires aimed to enhance the cutting performance of EDM wires (Fowle, 1933). Since there is a limitation to raise the zinc content beyond 40%, zinc is alternatively used to coat the core wire material to enhance the quality of the wire (Groos, Barthel, Noethe, & Dietrich, 2004a). Coated wires are developed by plating or hot dipping redrawn wire, and then drawing it to the final size. This process is challenging since the zinc surface has to withstand the final drawing process. Currently, the coating is not deposited on the final shape of the EDM wire. The existing wires usually consist of a core made of either brass

or cupper to facilitate conductivity and tensile strength. In addition, to enhance the spark formation and flush characteristics pure or diffused zinc is electroplated as the coating on the wire surface (Jatinder Kapoor, Sehijpal Singh, & Jaimal Singh Khamba, 2012; Kuriakose & Shunmugam, 2004; Akira Okada, Yamauchi, Arizono, Shimizu, & Uno, 2008; Akira Okada, Yamauchi, Arizono, & Uno, 2008; Akira Okada, Yamauchi, Higashi, Shimizu, & Uno, 2009; Akira Okada, Yamauchi, Nakazawa, Shimizu, & Uno, 2011).

2.3.4.1 Single-layer coated wires

One of the earliest strategy to add zinc to the wire surface is the development of Zinc-coated brass wire. One of the standard EDM brass alloy wires consists of zinc coating over the core as thin as 5 microns (**Figure 2.11**). The zinc-coated brass wire yields significant rise in the cutting speed over the plain brass wire without compromising with any other important properties (Nourbakhsh, Rajurkar, Malshe, & Cao, 2013). The wire can provide an excellent surface finish in cutting tungsten carbide and this wire is commonly used to cut Polycrystalline Diamond and Graphite. This wire is also utilized in certain cases where the brass wire creates undesirable plating of brass on the workpiece.

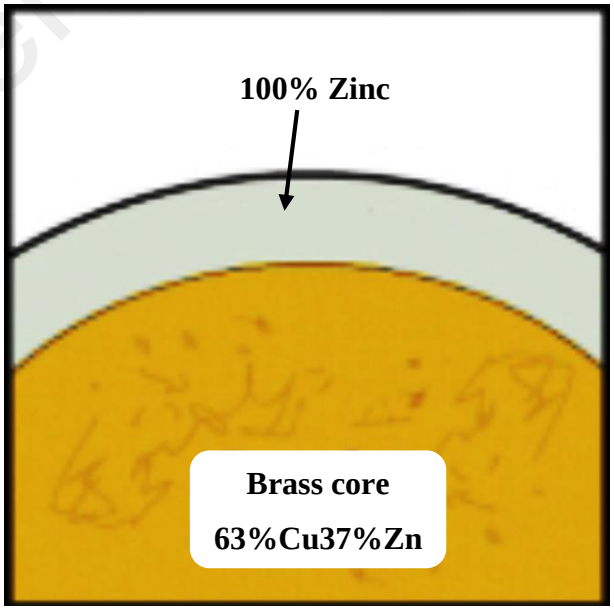

Figure 2.11: Zinc coated brass wire (Roger Kern, 2013).

In order to attain the benefits of the conductivity of a copper and flushability of zinc together, zinc-coated copper wire was one of the earliest attempts in the wire development. It does not currently exist in application since the spark penetrates the thin zinc coating and the copper core inside slows down the cutting process (Pérez Delgado et al., 2013; M. T. Yan, Fang, Liu, & Li, 2013).

US patent no. US4287404 revealed that electrode wires coated with metals of low vaporization temperature, such as bismuth, tin, zinc, lead, cadmium, antimony, or alloys that prevent the core from the thermal stress from the electrical discharge. Additionally, it allows to increase the frequency of electrical discharge without causing damage to the wire (Convers, Balleys, & Pfau, 1981). Patent No. US6300587 is for a wire electrode containing a core, and coating layer formed on the outer periphery of the core contains copper. The coating layer comprises an alloy of 55.5 to 75 wt% copper and at least one element selected from the group consisting of Zn, Cs, Se, Te, and Mg. The coating layer does not have an oxide film thereon other than a natural oxide film (Nakai, Yamada, et al., 2001). Patent No. US6348667 refers to a wire electrode that prevents the corrosion, particularly of the non-eroded surfaces of the hard metal block. This purpose is attained by selecting a wire electrode for the spark-erosive cutting of hard metals, the outer coat of which consists of a metal or metal alloy and which is not nobler than the binder contained in the hard metal. Thus, small metal particles of the outer coat come loose during cutting due to wear of the outer wire electrode coat, and they remain in the dielectric. However, since these small metal particles are not nobler than the metal contained in the hard metal, electrochemical corrosion, namely pitting of the hard metal, can therefore not occur as soon as the small metal particles come into contact with the hard metal block. Consequently, the pitting phenomena in the hard metal block are avoided. As a rule, the hard metal block contains cobalt, aluminum, magnesium, zinc, or iron (Baumann & Barthel, 2002).

2.3.4.2 Double-layer coated wires

The wire electrode referred by US patent no. US4968867 has a core with a higher thermal conductivity, an inner coating made of a low-boiling point material, and an outermost layer of brass offering high mechanical strength. The core of such wires is made of a single metal such as copper, silver, aluminum, or alloys (**Figure 2.12**). Such wires are found to increase the cutting speed due to having several properties such as the vibration dumping, heat transfer, and resistance to breakage.

Figure 2.12a shows a cross-sectional view of the first embodiment of the wire electrode invented. A core wire (6) is covered by a coating layer (7). In this embodiment, brass containing 35 % Zn is used for the core wire coating layer, and a Cu-Sn alloy including 0.15 % Sn balanced by Cu is used for the core wire. Besides brass, a Cu alloy containing Cu as the main component and less than 50 % Mg and/or Cd may be used for the core wire coating layer. As the second embodiment of the present invention, a wire electrode in composite form is obtainable by determining the coating layer thickness so that the cross-sectional area of the coating layer to the entire cross-sectional area of the wire electrode of the first embodiment is in the range of 50–90 %. In this embodiment, tensile strength is large, as the coating layer thickness is large too. The cross-sectional area of the coating layer to the total cross-sectional area of the wire electrode is about 69 %. In the third embodiment, the core wire (6) is covered by a layer (7) which is in turn covered by a layer (8), as shown in **Figure 2.12b**. For the wire electrode, the outermost layer is formed by a metallic material including Zn, Cd, or Mg as the major component, which has a low boiling point. Accordingly, machining speed can be improved.

Figure 2.12c shows a cross-sectional view of the fourth embodiment. The outermost layer (9) is an oxide film onto coating layer (7). Unnecessary electric discharges at the lateral side of the wire electrode can be reduced because an oxide layer forms on the wire

electrode surface. This realizes narrow machined groove width. In the fifth embodiment, the wire electrode constitutes a core wire (6) of a Cu alloy having high thermal conductivity, a layer (10) that is formed by twisting thin wires of brass with high mechanical strength, and an outermost layer (11) formed by Zn or Zn alloy (**Figure 2.12d**). It was confirmed that the electric discharge characteristic can be increased to thereby realize uniform electric discharge so that the surface roughness of a workpiece can be improved. This is because the coating layer, as an intermediate layer with high mechanical strength, is covered by a low boiling point material.

Figure 2.12e shows a cross-sectional view of the sixth embodiment. The wire electrode comprises a core wire coating layer (12) on the circumferential surface of the core wire by plating a material of Zn and an outermost layer (13) formed by brass. A linear material made of a Cu alloy including 0.15 % Sn balanced by Cu is subjected to zinc plating to obtain the core wire (6). **Figure 2.12f** presents a cross-sectional view of the seventh embodiment, where brass with 35 % Zn is used for the coating layer and a Cu alloy including 0.15 % Sn balanced by Cu is used for the core wire. At least one piano wire may be incorporated in the twisted linear elements to improve the mechanical strength of the core wire so that the performance of the electrode can be further improved (Banzai & Shibata, 1990).

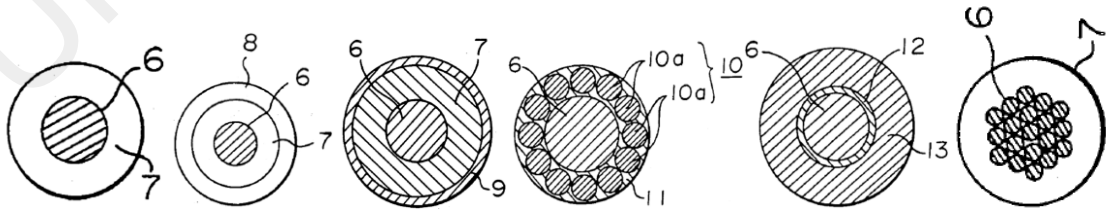

Figure 2.12: Construction of wire electrodes (Banzai & Shibata, 1990).

Patent No. US4977303 disclosed a method of forming an EDM wire electrode by coating a copper wire core with zinc and then heating the coated wire in an oxidizing

atmosphere to simultaneously provide a copper-zinc alloy layer over the copper core and a zinc oxide surface over the alloy layer. The resulting electrode wire permits for greater current density and traction force to be employed, yielding a significantly greater machining speed in the EDM process than achieved with earlier electrode wires (J. Briffod, 1990).

2.3.4.3 Multi-layer coated wires

The main object of Patent No. US4341939 is to provide an increase in machining speed by eliminating the short circuits that cause a decrease in machining efficiency, more exactly by rapidly affecting the transformation of non-erosive short circuited electrical discharges into electro-erosive effective discharges. The electrode is characterized by a structure comprising a wire coated with at least one layer of a second material, provided in turn with a thin film of non-metallic material; the thin film has a thickness sufficient to provide a semi-conductive effect when the film is in contact with the electrode workpiece and when a few volts are applied between the electrode wire and electrode workpiece, the film completely becomes a conductor by electrical and/or thermal breakdown when the voltage thus applied rises between a few volts to about 100 V. The wire coated with at least one layer of metal has low vaporization temperature and a metal oxide film coating the metal layer. The metallic coating is preferably made of zinc and is subjected to an oxidizing thermal or electrolytic treatment such that on the surface of the metallic layer a thin film of zinc oxide would form.

Figure 2.13a illustrates a schematic of a section through an electrode wire having a core (1) of copper and a superficial copper core coating of a copper-zinc alloy film (2) coated in turn with a thin film (3) of zinc oxide. Other materials, such as brass or steel may be used as the wire core (1) as long as they satisfy the requirements of good electrical conductivity, good mechanical strength, and resistance to rupture. Good results have been

achieved with a coating of metal such as magnesium, cadmium, tin, lead, antimony, bismuth, or alloys thereof. Tests have shown that favorable machining results are not only limited to zinc oxide but also other metallic oxides may be used. It has been found practical to coat the top of the zinc coating with a film a few microns thick of another metal that can be easily oxidized by heating in the presence of oxygen. Other oxides also known for being semi-conductors have been used, for instance CuO, Cu_2O, CdO, In_2O_3, PbO, TiO_2, MnO_2, MgO, and NiO. Nonetheless, dielectric oxides such as $A1_3O_3$ can also be employed. The films adhering to the metallic layer surface may consist of other non-metallic materials too, such as carbides, borides, silicides, sulfides, and nitrides of various metals.

Figure 2.13b illustrates a cross section through a wire having a copper core (1) provided with two, copper-zinc superimposed coatings (2) and (4) each covered with a zinc oxide film as shown in (3) and (5), respectively. Instead of a single, 8-micron thin zinc coating, a first coating (2) of 2 to 4 microns has been affected followed by a first heat treatment under the conditions disclosed previously to form a thin film (3) of ZnO. A second zinc coating (4) of about 4 microns is subsequently applied on the surface of the thin oxide film (3), followed by a second heat treatment similar to the first, providing a thin film (5) of ZnO onto the surface of the second zinc coating (4). With the structure in **Figure 2.13b**, the same phenomena of copper diffusion into zinc and vice versa have been observed, together with coating porosity resulting in outer surface irregularities and roughness (J.-P. Briffod, Martin, Pfau, Bommeli, & Schnellmann, 1982).

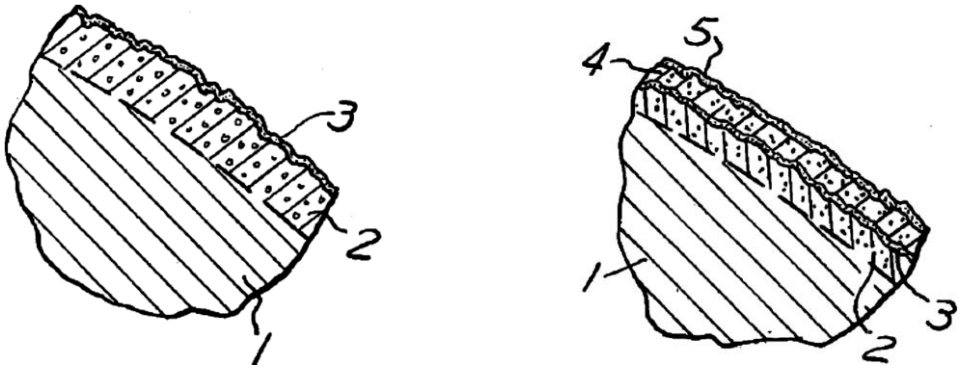

(a) **(b)**

Figure 2.13: Schematic section of wire electrodes (J.-P. Briffod et al., 1982).

An electrode wire with multi-coated layers for EDM that is capable of rapidly and precisely machining a workpiece into a desired shape without changing the electrode wire was disclosed in US Patent 20080245773 (J.-C. Lee, 2008). The wire has at least two coating layers including an outer layer made of zinc for precision machining and a lower layer made of zinc alloy for fast machining, thereby machining a workpiece continuously without change thereof (**Figure 2.14**). Moreover, the electrode wire can be manufactured at a relatively low cost. Also, when discharging for machining a workpiece, no debris separates from the core wire so the machining work is not interrupted by the electrode wire.

Figure 2.14 shows the multi-coated electrode wire with a core (22) made of copper or brass. The lower layer of coating (26) is made of zinc alloy (CuZn80 to CuZn95), which has a higher sublimation point required for fast machining. The upper layer (28) made of zinc alloy (CuZn90 to CuZnl00) has a lower sublimation point for precise machining and is formed onto the lower layer (26). Therefore, this wire electrode provides fast and precise machining without interrupting the EDM process.

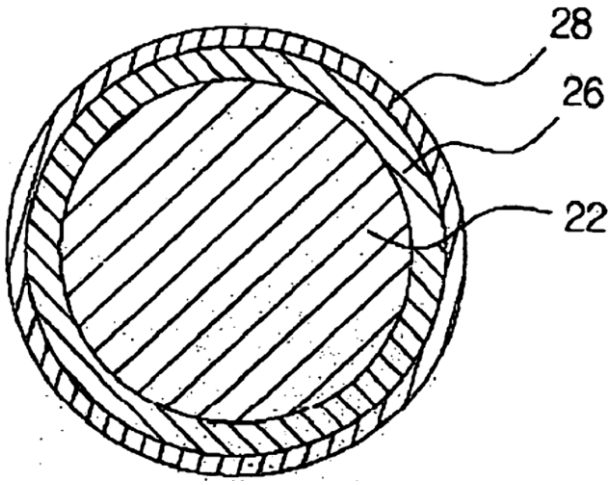

Figure 2.14: Cross section of wire electrodes (J.-C. Lee, 2008).

US Patent No. US5196665-93 was another attempt to improve the mechanical strength of electrodes while maintaining benefits such as heat shield effect and the elimination of short circuits. The core is covered with a film of multiple, fine layers. The layers are characterized by high electrical conductivity and low melting and vaporization temperatures in an alternating fashion. The alternating wire electrode layers may diffuse into one another in order to produce alloys of desired structure and composition. The core, which is a metal selected from the group consisting of copper, brass, steel, or copper clad steel, is covered with superimposed alternate layers of copper and a metal selected from the group consisting of zinc and zinc alloys containing 30 to 60 % zinc content with thickness less than 0.5 microns (J.-P. Briffod, 1993a).

Patent No. US5721414 produced an electrode wire having a thicker surface layer of diffused copper zinc alloy by thermal diffusion method, such that spark erosion machining was accelerated (Lacourcelle, 1998). The surface of the wire obtained in accordance with the invention is just rough enough for spark erosion, thus requiring no mechanical surface treatment apart from sizing. The wire electrode (16) is characterized as comprising a core (17) of copper or copper alloy made up of a central core (19) covered with an upper layer (18) of copper or copper alloy that itself covers the surface layer (20)

of diffused copper and zinc alloy or copper alloy. Surface layer (20) has a slightly granular surface (21) as shown diagrammatically in **Figure 2.15**.

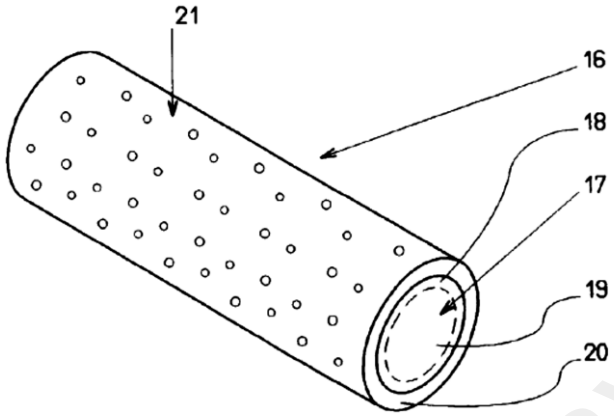

Figure 2.15: Diagram of wire electrode (Lacourcelle, 1998).

2.3.5 Diffusion-annealed coated wires

In theory, a pure zinc coating would produce the perfect wire with superb flushability. However, in practice, the thin layer of zinc on the core surface is blasted off by electric discharge intensity because of its low melting point. Therefore, zinc hardly gets chance to provide its full potential (Hermanni, 1990). Therefore, the coating should contain high zinc content with materials of relatively higher melting point to ensure better adhesion to the core wire. A heat-treating process known as diffusion annealing can obtain this better adhesion. In a diffusion process, atoms transfer from higher to lower concentration regions. The zinc atoms with higher concentration diffuse into the brass, and the copper atoms from the brass diffuse into the zinc. This diffusion process between the core and coating materials eventually produces a zinc-brass alloy which is rich in zinc, but possesses a relatively higher melting point, and is metallurgically bonded to the core material (Tominaga, Takayama, Ogura, & Yamaguchi, 1987).

2.3.5.1 Alpha phase wires

The brass alloy phases commonly applicable to EDM wires are alpha phase, beta phase, gamma phase, and epsilon phase, as shown in **Figure 2.16** (Baker, 1992). Alpha

phase has the highest melting point (approximately 910 °C at its highest commercially feasible zinc content of 35–39 wt%); beta phase has the next highest melting point (approximately 890 °C in a diffusion-annealed coating with a typical 40–53 wt% zinc content); gamma phase has the next melting point (approximately 800 °C in a diffusion-annealed coating with a typical 57–70 wt% zinc content); and epsilon phase has the lowest melting point (approximately 550 °C in a diffusion-annealed coating with a typical 85 wt% zinc content) (Brandes, Brook, & Smithells, 1998).

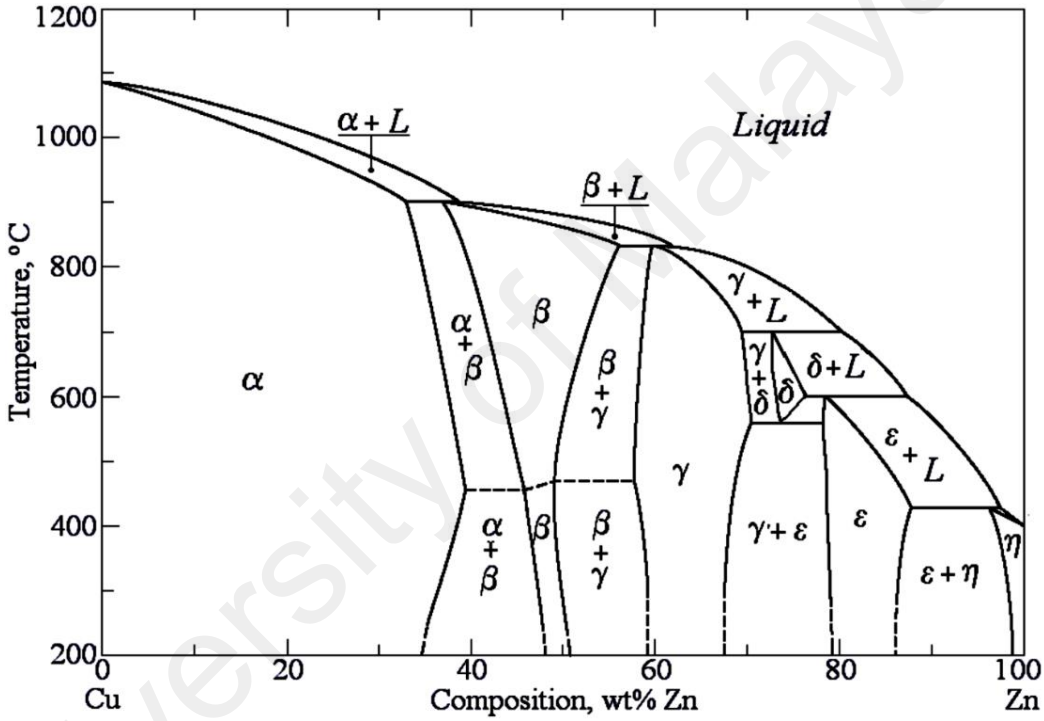

Figure 2.16: Cu-Zn phase diagram (Baker, 1992).

2.3.5.2 Beta phase wires

The X-type wire was the earliest type of diffusion-annealed wire usually termed as SWX, Bronco Cut-X, Beta Cut-X, X-Kut, A beta brass is coated over a pure copper core of such type of wire as shown in **Figure 2.17a**. It combines the advantages from the high conductivity of copper and coherent zinc-rich coating. However, it comes with limitations such as 50% drop in tensile strength, poor straightness, and higher cost when compared

to solid brass wires. However, it has a significant yields in aerospace applications offering alloys like Inconel and Titanium (J. P. Briffod, 1999).

Figure 2.17b shows the D-type wire, which is the second diffusion-annealed wire typically, termed as Cobra Cut-D, D-Kut. The wire has a copper core alloyed with 20% zinc and a beta brass coating. Its advantages include enhanced conductivity of the 80% Zn to 20% copper core, a coherent zinc-rich coating, and a relatively high tensile strength (800 N/mm2). High production cost is its major shortcoming. This wire yields a significantly high productivity in a good number of different machines (Roger Kern, 2013).

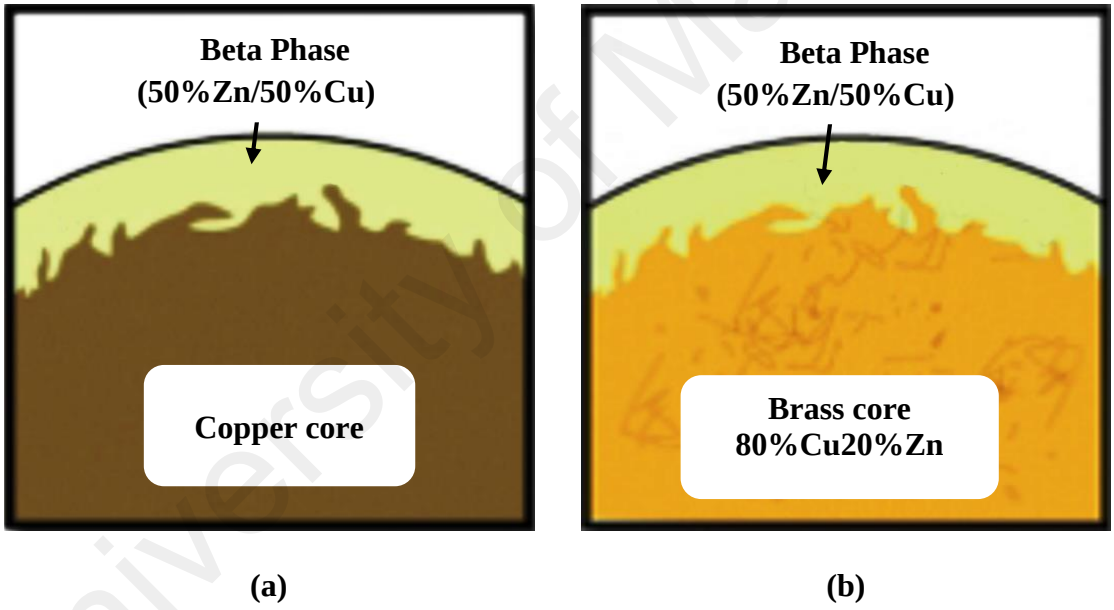

Figure 2.17: X and D types wire electrodes (Roger Kern, 2013).

Patent no. US4935594-90 presents a wire electrode that has an erosive wear resistant outer coating the common eroding electrode. Referring to **Figure 2.18**, making an eroding electrode according to the invention, a core (2) of 0.1- to 0.6-mm diameter can be used as an initial material. Onto the core, an original material coat (3) (**Figure 2.18a**) is applied, consisting of zinc, cadmium, bismuth, antimony, or an alloy of these metals. Such a wire

(1) is annealed at 700–850 °C most advantageously while passing through a protective gas and is subsequently cooled off to less than 80 °C again using a protective gas.

In this manner, an altered coating (3') (**Figure 2.18b**) with the aforementioned advantageous characteristics is produced. The core (2) of the wire (1') consists favorably of electrolytic copper having more than 99 wt% copper and very low oxygen content. A copper-zinc-alloy with 79.5–80.5 wt% Cu, the remainder being Zn, can also beneficially be used. The altered coating (3') includes layers of a mixed structure of metallic phases, and its content of low volatilization temperature metal decreases as the altered coating (3') extends from its outer surface to the core (2). The metallic phase layers include alpha-beta phases and beta-gamma phases (Groos & Hermanni, 1990).

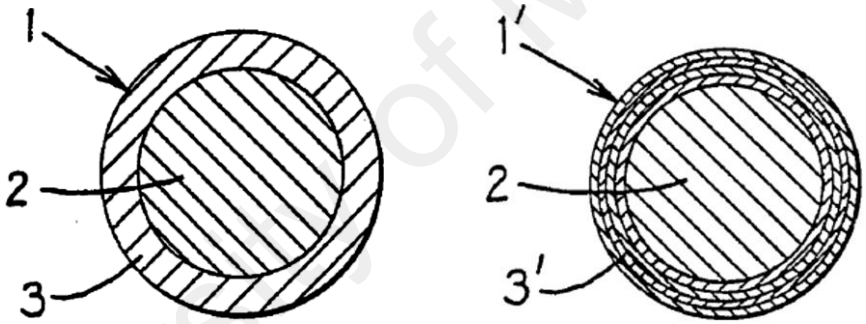

Figure 2.18: Cross section of wire prior and after the process (Groos & Hermanni, 1990)

European Patent No. EP0526361A1 introduced an electrode to obtain high-stability electric discharge while machining an object. A layer of Zn is formed on a copper or copper alloy wire. The wire is heat-treated at a temperature below the beta prime-beta transition temperature of the binary alloy CuZn until an outer layer (31) consisting of a homogeneous beta prime phase is formed. Then, the wire is drawn at a drawing ratio greater than 100 % in order to obtain an electrode (1) as shown in **Figure 2.19**. Electrodes for electro-erosion have an outer metal layer (3) made of Cu-Zn alloy in the homogeneous

beta prime phase free of oxide inclusions with a junction (32) of low thickness. The wire (20) is made of copper or copper alloy doped with one or more elements selected from Fe, Co, Ti, P, Mg, Cr, Zr, Si, at a global content between 0.1 and 1 wt% or with one or more elements selected from Al, Sn, Ni up to 4 wt% overall. The outer metal layer (3) has a Zn weight concentration in the region of 46.5 % +/−1, substantially constant throughout its thickness (Negrerie, Leterrible, & Voirin, 1993).

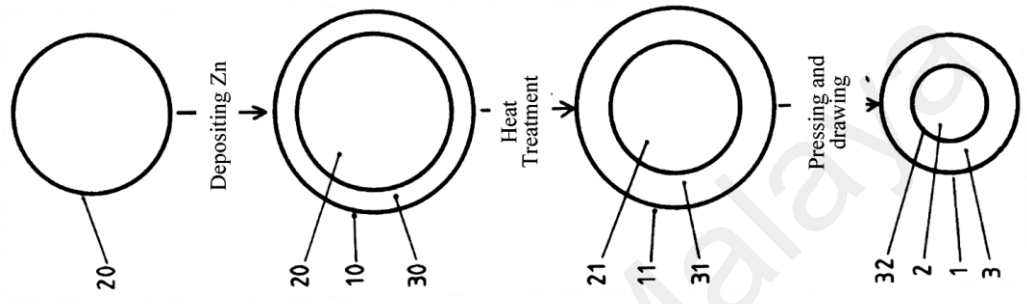

Figure 2.19: Different processing steps of the wire electrode (Negrerie et al., 1993)

In Patent No. US5858136, copper wire coated with a layer of zinc is heated to 750 °C, sufficient for the formation of a brass beta phase. The temperature is maintained until zinc completely diffuses, as shown in **Figure 2.20a**. The wire is then heated to a temperature of 950 °C, which is necessary for the formation of a brass phase, and the central copper part of the wire transforms into a brass alpha phase (**Figure 2.20b**). It has the advantage of both high conductivity and relatively high tensile strength (J. P. Briffod, 1999).

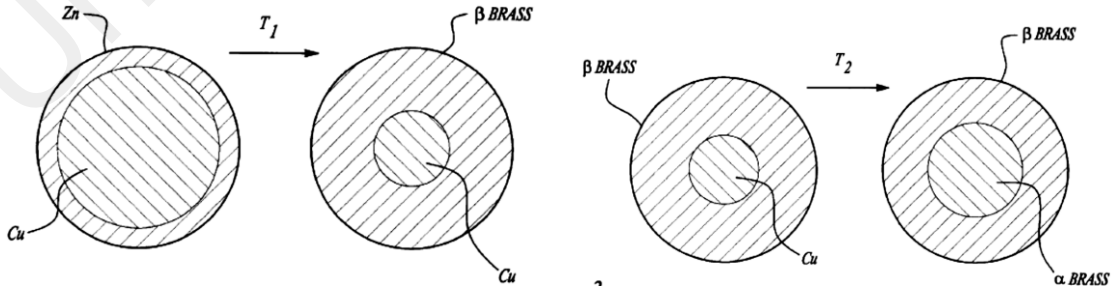

(a) **(b)**

Figure 2.20: Wires with different coating thickness (J. P. Briffod, 1999)

Patent no. US7687738 refers to an electrode wire with a single copper core with a diffused zinc alloy coating. The thickness of the coating is more than 10% of the wire diameter. A surface contact film is optionally formed on this coating layer using one of the following elements: Zn, Cu, Ni, Si or Au. In any of these cases, the spark erosion rate increases by about 30% when compared to a brass or zinc-plated brass wire of the same diameter. The effect of overall conductivity of the wire on spark erosion performance is another key aspect of this patent. Considering the conductivity property, it is assumed that higher conductivity of the design wire can lead to higher machining rate as more electrical energy can be supplied from generators that are more powerful.

It has been found that such electrode wire has an overall conductivity within the range from 65% IACS to 75% IACS. Conductivity below 65% IACS is considered inadequate to attain optimum spark erosion cutting performance. At low electrical conductivity, the wire is more prone to breakage due to the impact of heating in the sparking area. This is resulted due to the Joule effect following the reduced cooling related to lower thermal conductivity. The conductivity above 75% IACS cannot be obtained for this type of electrode wire, because it would then restrict the thickness of the diffused layer to below 10% of the electrode wire diameter. If this procedure is failed, the wire is formed too rigid and brittle and must not be drawn during the fabrication. The most recommended overall electrical conductivity of the electrode wire is in the order of 69% IACS which is for a 0.33 mm electrode wire with 35 μm thick diffused layer (relative thickness approximately 11%). This combination of relative thickness (11%) and overall electrical conductivity (69% IACS) yields good machining performance for wires ranging in diameter from approximately 0.20 mm to 0.35 mm (Ly, 2010).

2.3.5.3 Gamma phase wires

Gamma phase brass is made of higher zinc content than beta phase brass. The brittleness of gamma phase brass typically limits the gamma coating thickness to less than 5 microns. A thicker coating will fracture and strip off in the final drawing process. The brittleness of the gamma phase brass causes discontinuity on the surface as fractures during the final drawing process. This coarse surface improves flushing as the wire passes through the cut enhancing water flow and scouring debris from the gap, which eventually increases the machining speed. However, the discontinuity in the surface may result in a slightly dirtier surface than other zinc-coated wires (J.-C. Lee, 2008). The gamma brass type wire consists of a brass core coated with a gamma phase brass outer layer, and it usually has trade names such as Z-Kut, Topaz, Gamma-Z, Delta Cut. A gamma phase brass coating replaces the pure zinc coating of the zinc-coated brass wire as shown in **Figure 2.21a**. This construction usually yields 10 to 25% faster cutting performance than pure zinc-coated wires (Roger Kern, 2013).

Patent no. US6566622B1 features the wire electrode core made of copper (X-type wire) or copper alloy (D-type wire). Such electrode is first diffusion heat-treated to yield a beta phase and then a stabilization treatment is conducted to obtain an outer layer of the gamma phase (**Figure 2.21b** and **c**) (Barthel & Neuser, 2003). The application of such electrodes can be similar as traditional X and D wire types, but it improves the machining performance by approximately 10% (Barthel, Groos, Hermanni, & Tauber, 1998). The diffusion-annealed beta phase brass has a high melting point and is composed of zinc in the range of 45%–50%, which provides an excellent tenacity. Gamma wire offers a low cost method of plating the gamma phase layer over the wire electrode surface. These wires offer an increased removal rate to reduce the cost of rough cuts, which enables them to decrease the cycle time (J.-p. Briffod, 1993b).

The upgrade in technology suggested by various inventors have led to numerous efforts to improve gamma-coated wires by employing low temperature diffusion annealing (Banzai & Shibata, 1990; Nakai, Yamada, et al., 2001). A number of inventors attempted to coat the conductive core with multiple layers of film. The alloys of desired structure and composition is obtained by forming alternating coating layers on the core, where the layers are diffused into one another. These layers offer properties of high conductivity and low melting and vaporization in an alternating fashion (Nakai, Kishida, et al., 2001). The gamma coating phase is subjected to cladding surface passivation in order to build resistance against corrosion (Chiriotti, Pinaya, & Fluekiger, 2002).

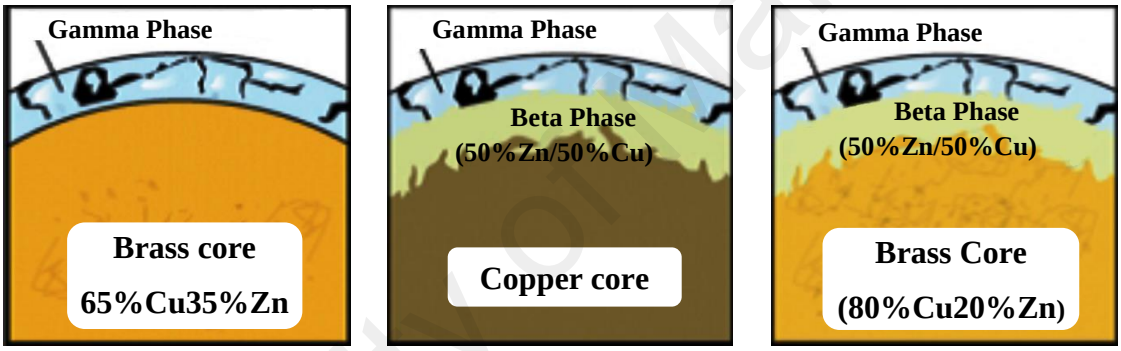

Figure 2.21: Gamma phase wire electrodes (Roger Kern, 2013).

Patent No. US5945010-97 revealed an electrode wire with a coating of a copper-zinc gamma phase alloy or a nickel-zinc alloy. The core of the wire usually contains any one of the following metals: copper, copper clad steel, or brass. The second coating is formed of a metal such as Zn, Mg, and Al by employing low temperature diffusion anneals. The resulting EDM wire offers a faster cutting rate and a surface finish better than traditional wire electrodes. Other pros of the US Patent no. 5945010-99 is achieved by the higher zinc content in the coating compared to the earlier US Patent no. 5945010-97. This results in significantly lower volumetric heat of sublimation for the coating, which leads to more efficient flushing of wire ensuring sufficient tenacity to survive the EDM erosion process. The tensile strength rises very rapidly with the appearance of the beta phase. At 32 % zinc

content, the tensile strength of brass reaches a maximum when alpha and beta phases are present in approximately equal proportion (D. S. Tomalin, 1999). Keeping the above aspect in view, the present invention, Patent No. EP0799665A1 and Patent No. US5808262, is meant to produce a spark erosion electrode, the core of which is of comparatively low zinc alpha brass with a top layer of highly rich zinc beta and gamma brass to facilitate better flushability of the electro-erosion process and also to achieve comparatively higher tensile strength of the electrode core material (Mukherjee, 1998).

Patent No. US2011/0290531A1 relates to a wire electrode (1,1') for electric discharge cutting processes. The wire electrode (1,1') has a core (2) containing a metal or metal alloy, and a coating (3, 4; 3, 4, 5), at least one (3) of which contains a phase mixture of beta brass or beta prime brass and gamma brass as shown in **Figure 2.22**. The beta phase or beta prime phase and the gamma phase are arranged next to each other in a fine-grained structure in which the mean size of the beta brass or beta prime brass grains and the gamma brass grains amounts to a maximum of 5 microns relative to the cross section of the wire electrode (1, 1').

In the preferred embodiment according to **Figure 2.22b**, a core (2) is formed from CuZn20%; the covering layer (4) which adjoins the core is formed predominantly from beta or beta prime brass having a zinc content of about 45 wt%; the covering layer (3) is formed principally from a phase mixture of beta or beta prime brass and gamma brass having a mean zinc content of about 53 wt%; the top layer (5) consists primarily of zinc oxide. The wire electrode (1') has a tensile strength of about 750 N/mm^2 and electrical conductivity of about 17 $m/\Omega mm^2$ (Baumann & Nöthe, 2011).

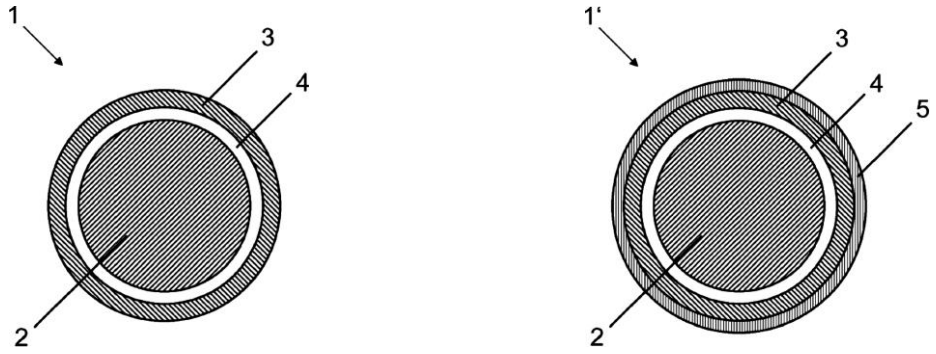

(a) **(b)**

Figure 2.22: Cross-section of electrode wire (Baumann & Nöthe, 2011)

Patent No. US8338735 comprises a brass core (1) covered with a gamma phase brass coating (2) having a structure fragmented into blocks (2a) between which the core (1) is exposed. The blocks (2a) have a thickness E2 with a narrow distribution and cover the core (1) according to a coverage rate greater than 50 % as shown in **Figure 2.23**. This produces regular fragmentation of the coating, which improves the finish state of the machined parts (Ly & Sanchez, 2012).

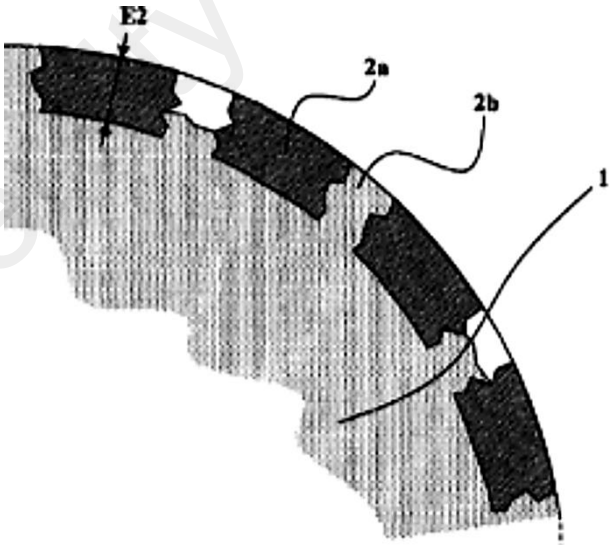

Figure 2.23: Large scale diagrammatic view of cross sectioned wire (Ly & Sanchez, 2012)

US Patent No. 5762726-98 is recognized for higher zinc content phases in the copper-zinc system, specifically the gamma phase, which would be more desirable for EDM wire electrodes. It has even better cutting capacity than a wire electrode with a sheath layer

consisting of a pure beta phase. The choice of a pure gamma phase, to which hard inert materials are added where appropriate, has proved even more advantageous than the beta phase in terms of cutting behavior. With conventional processes, that is to say longtime diffusion, it is scarcely possible to produce such a gamma phase in pure form. As a rule, a mixed structure with fractions of alpha, beta, and/or gamma phases is obtained. **Figure 2.24a** represents the starting material, which consists of a core of alpha brass and a sheath layer of zinc (eta zinc). After heating has taken place and following the shortest possible holding time, an epsilon zinc layer forms in the region between the core and sheath layer (**Figure 2.24b**), the eta zinc layer transforms into an epsilon zinc layer during increasing annealing time and therefore diffusion increases (**Figure 2.24c**). It is possible to see in **Figure 2.24c** that a narrow layer, especially a gamma brass layer, forms in the transitional region between the core and epsilon zinc layer while annealing time continues. The gamma brass layer expands so that the epsilon zinc layer is transformed into a gamma brass layer as a result of the diffusion processes (**Figure 2.24d**). A narrow beta brass layer forms at a substantially lower growth rate in the transitional region between the gamma brass layer and the alpha brass core (**Figure 2.24e**). **Figure 2.24f** illustrates the moment at which the sheath layer transforms into a gamma brass layer with the beta brass sheath layer growing only slightly larger in the transitional region between the core and gamma brass sheath layer with respect to the stage represented in **Figure 2.24e**. Finally, **Figure 2.24f** illustrates the end of the time sequence in which the eta zinc layer is largely decomposed and beta crystals expand to form a thin layer around the core. But the inability to cope with the brittleness of these phases limits the commercial feasibility of manufacturing such wire (Barthel, Groos, & Hermanni, 1998).

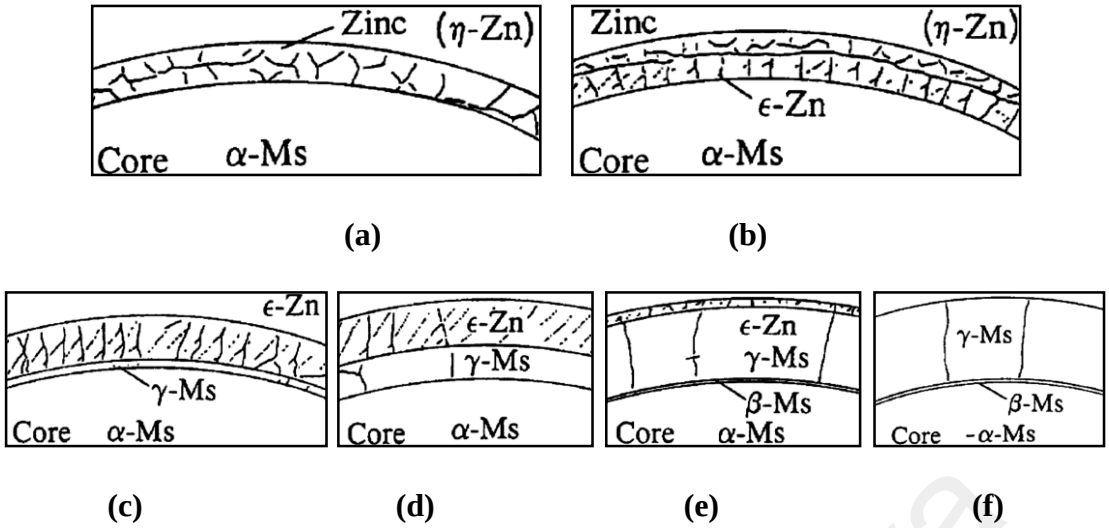

Figure 2.24: An enlarged representation of the detail of the sheath layer and the core (Barthel, Groos, & Hermanni, 1998).

There is still a need to machine as quickly as possible for a given machining current and also to be able to use the highest possible machining current for a given wire diameter. It is surprising that with respect to Patent No. US8378247, with an EDM wire (1) having a metal core covered with a layer of alloy, appreciably enhanced EDM performance can still be obtained by providing a core (2) made of copper or brass with a coating layer that combines a fractured gamma brass surface layer (4) and a beta brass sub-layer (3) (**Figure 2.25**). As an advantageous embodiment, beta brass at least partially fills the fractures (5a) in the gamma brass surface layer (5). The beta brass sub-layer may favorably be continuous, affording better results than a discontinuous sub-layer. Better results, combining both a higher EDM rate and good surface finish of the machined workpiece are obtained by giving the fractured gamma brass surface layer a thickness of less than 5 % of the wire diameter (Blanc, Ly, & Sanchez, 2013).

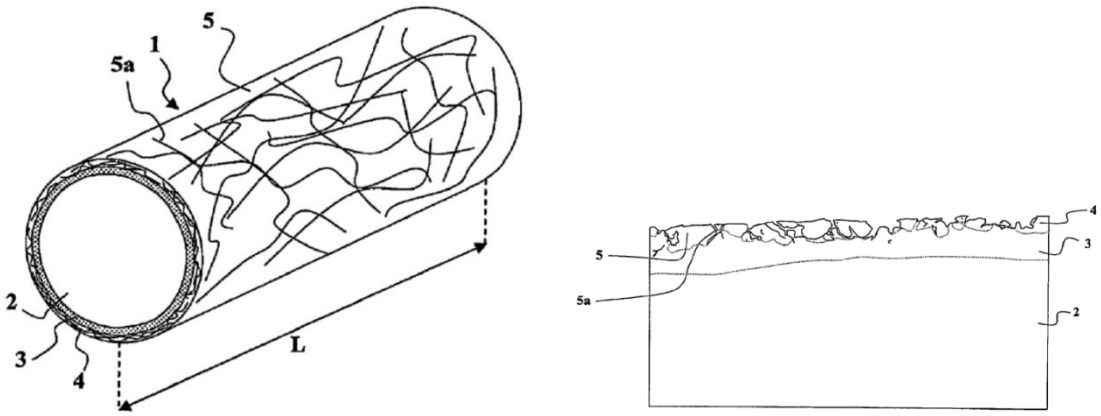

Figure 2.25: Schematic perspective view and a longitudinal section through an EDM Wire (Blanc et al., 2013).

2.3.5.4 Epsilon phase wires

The lower melting point of the epsilon phase is considered a disadvantage of epsilon phase coatings compared to beta or gamma phase. However, the limitation is compensated by the higher zinc content in the epsilon phase, which matches the epsilon phase coating performance with that of beta phase coatings while being competitive with gamma phase coating performance. Therefore, epsilon phase coatings provide similar cutting performance but at a lower manufacturing cost than either beta or gamma phase (Kapoor et al., 2010). US patent no. 20070295695 reveals an EDM wire with copper core, which is layered with continuous coating of porous epsilon phase brass. Graphite particles are used to fill out the porous coating in order to enhance the performance of epsilon phase coating (D. S. Tomalin, 2007).

Patent No. US8067689 provided an EDM wire containing an outer coating of gamma phase brass with an over layer of continuous unalloyed zinc or ductile epsilon phase brass entrapping the gamma phase, thereby filling in any discontinuities and thus presenting a workpiece surface with homogeneous electrical properties (**Figure 2.26**). For rough cuts where speed is of utmost interest and accuracy is of lesser importance, any zinc or epsilon phase brass covering the underlying gamma phase brass alloy particles will quickly be

consumed because, it will be proportionately thinner than that filling the gaps between the gamma particles, thereby giving evidence of high-performance gamma coating.

Referring to **Figure 2.26a,** a high brass core (12) is covered with a zinc coating (15) with an initial thickness of 10 pm. After heat treatment at 1,700 °C for 6 h in a nitrogen atmosphere, the wire is depicted in **Figure 2.26b**, with a gamma phase brass coating (18) on the high brass core (12). Since a non-oxidizing atmosphere of nitrogen gas was employed during the heat treatment, the wire can be electroplated again with a zinc coating (15) 10 pm thick as depicted in **Figure 2.26c**. Cold drawing the composite wire to its final diameter of 0.25 mm causes the brittle gamma phase to fracture and form discrete particles (19) as portrayed in **Figure 2.26d**. However, the zinc coating (16) is sufficiently ductile to flow around these particles and encapsulate them on the high brass core (12). According to the invention, the core substrate preferably includes copper at or near its outer surface. Thus, a variety of substrate materials are contemplated for the present invention, including, but not limited to, pure copper, brass, brass on copper, copper clad steel, brass on copper clad steel, brass clad steel, and brass on brass (e.g., high zinc content brass on lower zinc content brass) (D. Tomalin, 2011).

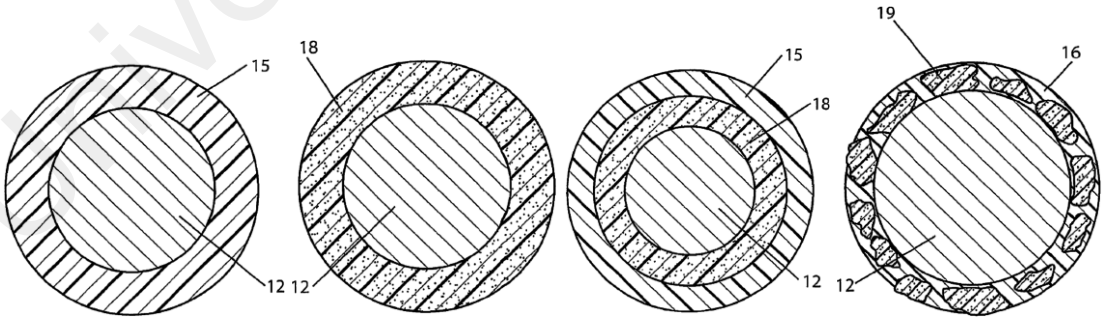

Figure 2.26: Cross sectional view of wire (D. Tomalin, 2011).

2.3.6 High tensile strength wires

The electric discharge during the machining process creates electrostatic and electromagnetic forces on the wire electrode. The machined area of the wire electrode is

also subjected to a force opposite to direction of the machining process. During the machining process, all these force factors including the wire vibration can deviate the wire position from its programmed position. This affects the quality and precision of the machining process (Cut, Masuzawa, & Fujino, 1991; A. Okada, Uno, Nakazawa, & Yamauchi, 2010; Puri & Bhattacharyya, 2003; Tomura & Kunieda, 2009).

The deviation of the wire position yields round corners instead of the desired sharp corners (Iwata, Obara, Ohsumi, & Matsuda, 1995). As a result, plain Molybdenum or Tungsten wires can form because of high tensile strength (>1900 MPa) (Akira Okada et al., 2007; Uhlmann & Roehner, 2008). In order to address the high cost and poor flushability of wires, an improved wire type is developed that is made of a high strength pearlite steel wire with over 0.06% carbon content and a layer of copper-free zinc or zinc alloy coating. This yields a better precision and accuracy even under a higher mechanical load (Kapoor et al., 2010; J.-C. Lee, 2008).

2.3.6.1 Molybdenum wire

Molybdenum wire is found in very specific applications. In order to achieve a decent load carrying capacity in a thin wire, it requires a very high tensile strength. Moly wire is an excellent candidate in this regard, as it offers both high tensile strength and high melting point at a diameter of 0.1 mm and under. Unfortunately, this wire suffers from low electrical conductivity and poor flushability. Furthermore, Moly wire is found to be very abrasive to power feeds and wire guides, very hard to auto thread, as well as very expensive to produce (Ezaki et al., 1991; Roger Kern, 2013).

2.3.6.2 Tungsten wire

Tungsten wire is often chosen as a cost effective option over Moly wires for a diameter of 0.05 mm or smaller. In addition, it offers a higher melting point and tensile strength than those of Moly wire. Therefore, high precision machining prefers tungsten wire over

Moly wire, as it requires smaller inner radii within the range of 0.025-0.1 mm. These materials are preferable in high load carrying capacity requirements, which are not feasible using brass and coated wires at such smaller diameter. However, tungsten and Moly wires are not suitable for thick work, because of their numerous shortcomings such as high melting point, limited conductivity, low vapor pressure rating, and slow cutting tendency (Ezaki et al., 1991; Kondo & Nishimoto, 1985).

2.3.6.3 MolyCarb wire

For small diameter wire requirement, a composite wire known as MolyCarb competitive advantages. The flushability of Moly wire is improved in this type of wire by coating graphite and Molybdenum oxide mixture (Roger Kern, 2013; Mujahid & Conrad, 1991).

2.3.6.4 Steel Core wires

The steel core wire uses a steel core and typically known by trade names such as Compeed, MicroCut, MacroCut. The steel core provides an excellent tensile strength and ductility, and the intermediate copper layer provides conductivity besides a beta phase brass outer layer (**Figure 2.27**). Steel core wire shows significant resistance to interrupted cuts, breakage for tall workpieces, and poor flushing conditions without compromising with an exceptional machining performance. However, the steel core has several drawbacks such as straightness issues, high cost, possible damage to scrap choppers, and auto-threadability (Blanc et al., 2013; Roger Kern, 2013; Kruth, Lauwers, Schacht, & van Humbeeck, 2004).

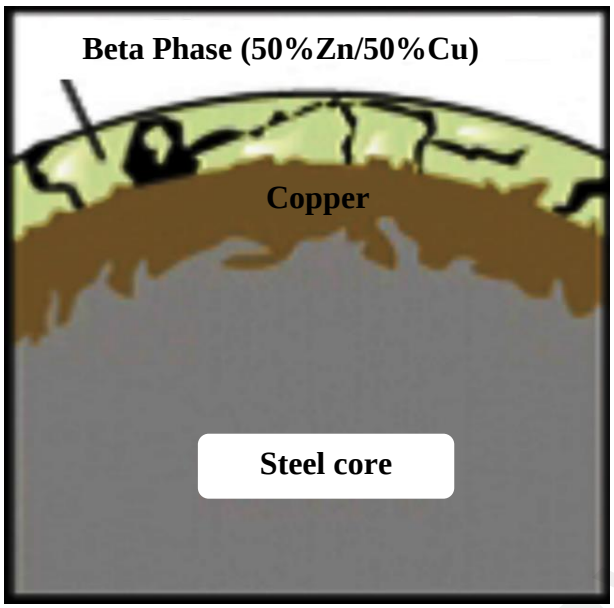

Figure 2.27: Steel core wire (Roger Kern, 2013).

US Patent 4287404-1981 was designed to make the steel core wire effective in machining process (Convers et al., 1981). This invention includes steel core wire with a first copper coating and then a coating of a material such as zinc, cadmium, tin, lead, antimony, bismuth, or alloys. This electrode offers a good triggering of electrical discharge and reduces the probability of any short circuit. The outcome of this wire electrode is a machining speed higher than that of other conventional electrodes. In addition, Korean patent no. 10-1-0009194 and US patent no. US20080245773 offer a wire electrode for electrical discharge machining. These inventions include a steel core coated with copper or a copper-zinc alloy layer of CuZn10-CuZn50 (J.-C. Lee, 2008).

US Patent No. US4686153-87 provides an electrode wire with a core including a steel wire coated with copper or another conductive material as well as a surface coating layer of zinc or the like. The average concentration of zinc in the copper-zinc alloy layer should preferably be less than 50 wt% but not less than 10 wt%. Referring to **Figure 2.28**, an electrode wire (10) comprises a copper clad steel wire (13) including a steel core wire (11) covered with a copper coating layer (12) of uniform thickness and a copper-zinc alloy layer (14) of generally uniform thickness ranging from 0.1 to 15 microns (Tominaga

et al., 1987). The wire electrode of US patent no. 4998552-91 includes a steel core wire with two layers: an inner layer of pure copper and an upper brass layer composed of 50 wt% zinc. The steel core is covered by pure or alloyed copper, which results in a higher mechanical strength through a multi-layer structure (Kapoor et al., 2010).

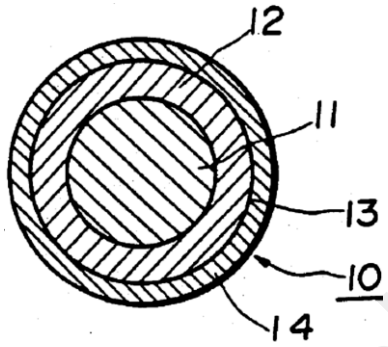

Figure 2.28: Sectional view of electrode wire (Tominaga et al., 1987).

US patent no. 6875943-2005 refers to a high strength pearlitic steel wire (10) characterized by more than 0.6% carbon and higher than 3000 MPa tensile strength. The steel core (12) of the electrode is layered by copper-free zinc or zinc alloy coating (14). The electrode is found effective in applications requiring high precision machining. Alternatively, a steel strip can be used as shown in **Figure 2.29b**. The wire of circular cross-section, as shown in **Figure 2.29a**, should preferably have a diameter lower than 0.35 mm and can be as low as 0.1, 0.07 or 0.03 mm.

Wires with considerably low thickness such as 0.1 mm, 0.05 mm or 0.02 mm are used as flat wires (40). The pearlitic steel core (42) contributes high strength, whereas the zinc or zinc alloy (Zn-Al alloy) coating (46) offers qualities like heat dissipation and machining functions. The coating with zinc-aluminum alloy consists of between 2% and 10% Al. A rare earth element such as La and/or Ce can be mixed between the proportion of 0.1 and 0.4%. An intermediate layer (44), made of aluminum or silver or alloy or a nickel or nickel alloy, can be placed between the steel core and zinc or zinc alloy coating. This intermediate layer improves the electrical conductivity of the electrode. In one

embodiment of the present invention, an additional layer is formed on the zinc or zinc alloy coating and one of the following materials is used to form this additional layer: graphite, metal oxides like, ZnO, TiO2, A12O3, Cr2O3, ZrO2 or Ag (Gonnissen & Vooren, 2005).

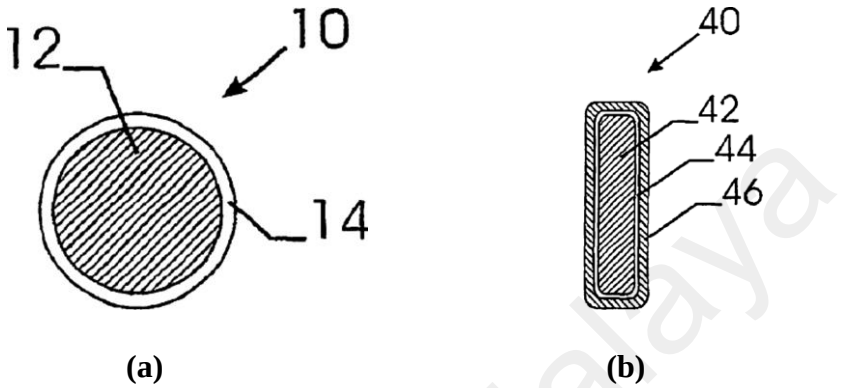

Figure 2.29: Round and flat EDM wires (Gonnissen & Vooren, 2005).

2.3.7 Special wires

2.3.7.1 Abrasive assisted wire

The EDM wire research currently focuses on achieving higher machining speed and surface integrity. In this regard, US20100012628A1 patent presents a hybrid wire embedded with electrically non-conducting abrasives as shown in **Figure 2.30**. In this process, two-body abrasion is used to improve material removal through electrical erosion. This results in a remarkable improvement in removal rate and ensures better recast surface layer when compared to an equivalent WEDM process.

There had been a negligible recast material present on the machined surfaces. A majority of this process are dedicated to machining steel. However, it may be useful in machining metal matrix composites such as Polycrystalline Diamond, which are usually hard to process by WEDM. The abrasion can negatively affect the machining performance, which make such process suitable for roughing sequences. Therefore, it is usually developed in a twin-wire machine tool. Although diamond wire can be effective in such work, wire with aluminum oxide abrasives can provide better performance at a lower cost (Koshy & Menzies, 2010; Menzies & Koshy, 2008).

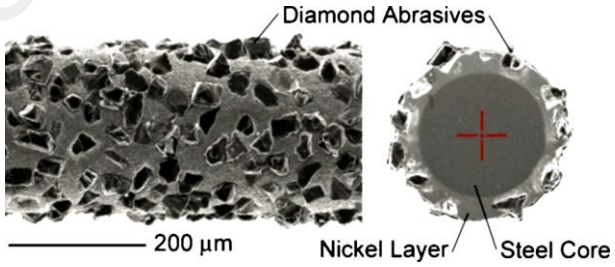

Figure 2.30: Surface and section of abrasive assisted wire (Koshy & Menzies, 2010; Menzies & Koshy, 2008)**.**

2.3.7.2 Hot dip galvanized wire

There are special cases when diffusion annealed wires have been found less efficient because of the non-uniform composition of zinc and alloy (Ghodsiyeh, Golshan, & Shirvanehdeh, 2013). This led to the invention of US patent no. 20060138091, which involves the hot dip galvanization method. This method has been found effective in developing uniform zinc coating on the wire surface (Cheremisinoff, 1996). Firstly, the wire is subjected to a surface-forming process followed by a pre-coating process. Then, the wire is subjected to a main-coating process, after which it is exposed to a second surface-forming process. Finally, the wire is subjected to a homogeneously heat-treating process. Environmental contamination problems by harmful gas and waste water generated from conventional methods can be prevented with this type of wire. Further, increasing the thickness and adhesion of a zinc-coated layer leads to diminished generation of waste powder, thus improving all functions of the electrode wire (J.-C. Lee, 2006).

2.3.7.3 Porous electrode wire

Prior studies revealed that the discharge property of diffusion annealed wire electrodes are improved because of their porous surface infiltrated with graphite (D. S. Tomalin, 2007). Continuous coating is maintained when the heat-treated wire is cold drawn. Also, the wire improves machining speed by at least 15 % compared with a conventional zinc-coated wire, thanks to an increased cooling ability of the wire with a cooling liquid. This is due to the enlarged surface area of the wire that has a porous surface morphology (D. S. Tomalin, 1999).

Patent No. US6482535 relates to a porous electrode wire for use in EDM, as shown in **Figure 2.31**. The purpose of the invention is to provide a coated wire for EDM with improved machining speed by increasing the surface area and inner part of the wire. The

inner part will be in contact with a cooling liquid so as to increase the wire's cooling ability. Therefore, the steps to achieve the above-mentioned purposes are as follows: provide a wire with an initial diameter made of a first metal; hot dip galvanize the wire by passing it for a desirable amount of time through a molten second metal with lower vaporization temperature than the first metal; form an alloy layer by the diffusion reaction between the first and second metals, the second metal has higher hardness and less elongation than the first metal and a coating layer made of the second metal; finally, draw the wire with the alloy and coating layers to form a second diameter, thereby forming cracks in the alloy and coating layers due to the high hardness and low elongation of the alloy layer. At this time, copper or brass having 63 – 67 wt% copper and 33–37 wt% zinc may be added to the first metal. Furthermore, zinc, aluminum, or tin may be used in the second metal. The porous nature of the wire arises from the cracks in the alloy and coating layers during the drawing step (K. C. Seong, 2002).

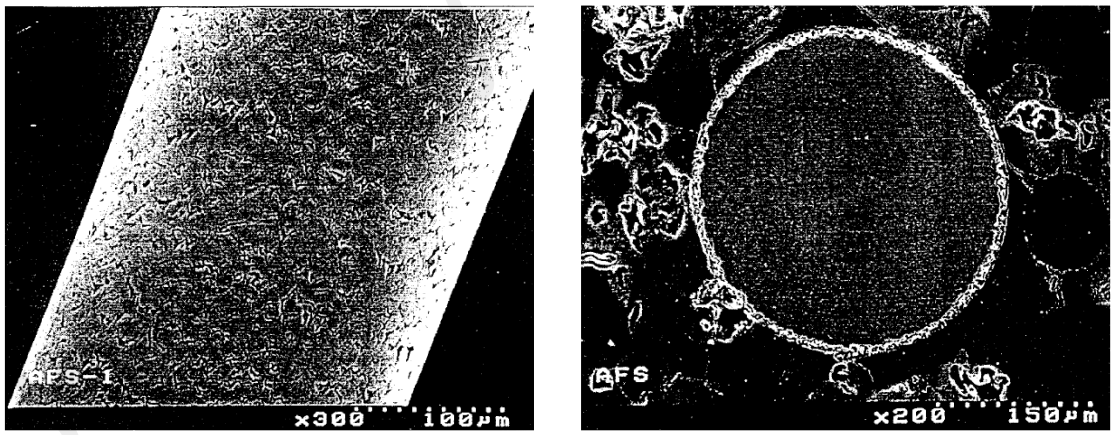

Figure 2.31: illustration of the cross section and surface of porous coated wire (K. C. Seong, 2002).

Similar to many other engineering practices, the selection of an optimal wire for a particular application would mostly likely make trade-off with the properties mentioned above. As an example, wires with high conductivity are usually low in tensile strength.

2.4 WEDM performance outcomes and indicators

The demand for machining at high cutting rates and superior quality is continually increasing for WEDM technology in order to achieve productivity with low wire rupture and superior workpiece surface quality. Productivity and surface quality are the most important performance parameters in WEDM. While productivity affects the cost-efficiency of a process, quality determines the overall utility of products. Productivity is expressed as cutting speed with low wire breakage, while surface quality is defined by surface parameters such as surface roughness and white layer thickness. The importance of these performance parameters is relative and mainly dependent on spark energy and pulse frequency parameters (Maher, Ling, et al., 2015). Productivity practically increases with increasing spark energy (voltage, current, and pulse duration). On the other hand, surface roughness and white layer thickness increase with increasing discharge voltage, current, and pulse width (Yeh et al., 2013). Therefore, this section introduces an analysis of performance parameters, including cutting speed, surface roughness, white layer thickness, and wire rupture.

2.4.1 Cutting speed

In WEDM, the molten crater can be assumed to have hemispherical shape with a radius r that forms due to a single spark (**Figure 2.5**). Hence, volume removal (VR) in a single spark can be expressed as (El-Hofy, 2005):

$$VR = 2\pi r^3/3 \qquad 2.4$$

Material removal in a single spark is proportional to spark energy. Thus:

$$VR \; \alpha \; Es \qquad 2.5$$

The material removal rate is the ratio of material removed in a single spark to cycle time. Thus

$$MRR = VR/Tc \quad (2.6)$$

$$Tc = Ton + Toff \quad (2.7)$$

$$MRR \alpha Es/(Ton + Toff)$$

$$MRR = CS \times w \times b \quad (2.8)$$

where CS is the cutting speed, w is the kerf width, and b is the workpiece depth.

$$CS = MRR/w \times b$$

$$CS \alpha Es / (Ton + Toff) \quad (2.9)$$

From **Equations (2.1)** and **(5.23)**, we get:

$$CS \alpha Es \times F \quad (2.10)$$

2.4.2 Surface roughness

Surface roughness is defined as a set of asperities of the real surface, which are conventionally described as deviations of the measured profile from a reference line within the limits of a length along which waviness is not taken into account (Maher, 2008). Surface roughness is one of the key factors for evaluating surface quality during the finishing process. Surface quality affects the functional characteristics of the workpiece such as fatigue and fracture resistance, and surface friction. Furthermore, surface roughness in addition to tolerance imposes a critical constraint for cutting parameter selection in manufacturing process planning (Barzani, Sarhan, Singh, Maher, & Farahany, 2015).

The three-dimensional surface structure contains surface asperities, or peaks and valleys. These asperities are described by parameters of roughness and waviness, as well

as flaws in the geometrical surface structure as shown in **Figure 2.32** (Burakowski & Wierzchoń, 1999). Therefore, the asperities should be described in all three dimensions. However, practical difficulties with their measurement causes the problem to be reduced to a two-dimensional plane on which a roughness profile is traced.

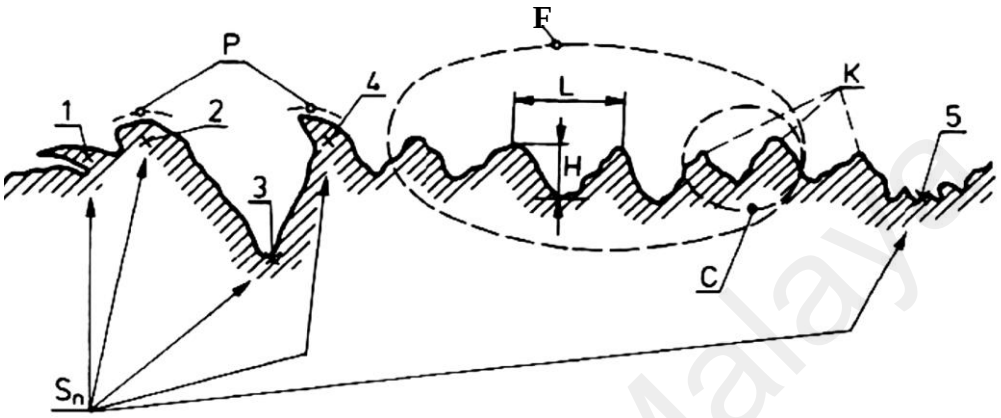

Figure 2.32: Profile of asperities on surface of a solid: H - peak to valley height; L - peak to peak distance; F - waviness; C - roughness; P - adhesion; K-orientation of asperities; Sn - asperity flaws; 1 - flaking; 2 - folding; 3 - scratch; 4 - burr; 5 - pit

The terms surface finish and surface roughness are used very widely in industry and generally serve to quantify surface finish smoothness. Many of the concepts of surface metrology and terminology are given in **Table 2.1**. The most common measures of primary roughness are the arithmetic averages (Ra) and the total roughness (Rt), or the vertical distance from the deepest valley to the highest peak, which describe the surface roughness deviations from a mean line or center line **Figure 2.33** and are defined by **Equations (2.11)** and **(2.12)**.

Table 2.1: Surface profile parameters

Parameter	Name	Standards	Related
Height Parameters			
Ra	Roughness Average (Ra)	ASME B46.1-1995	Pa, Wa
Rq	Root Mean Square (RMS) Roughness	ASME B46.1-1995	Pq, Wq
Rt	Maximum Height of the Profile	ASME B46.1-1995	Pt, Wt
Rv, Rm	Maximum Profile Valley Depth	ASME B46.1-1995	Pv, Wv
Rp	Maximum Profile Peak Height	ASME B46.1-1995	Pp, Wp
Rpm	Average Maximum Profile Peak Height	ASME B46.1-1995	
Rz	Average Maximum Height of the Profile	ASME B46.1-1995	Pz, Wz, Rtm
Rmax	Maximum Roughness Depth	ASME B46.1-1995	Ry, Rymax, Rti,Rz
Rc	Mean Height of Profile Irregularities	ISO 4287/1-1997	Pc, Wc
Rz(iso)	Roughness Height	ISO 4287/1-1997	
Ry	Maximum Height of the Profile	ISO 4287/1-1997	
Wt, W	Waviness Height	ASME B46.1-1995	Rt,Pt
Spacing Parameters			
S	Mean Spacing of Local Peaks of the Profile	ISO 4287/1-1997	
Sm, RSm	Mean Spacing of Profile Irregularities	ASME B46.1-1995	PSm, WSm
D	Profile Peak Density	ISO 4287/1-1997	Sm
Pc	Peak Count (Peak Density)	ASME B46.1-1995	
HSC	Hight Spot Count		
λa	Average Wavelength of the Profile	ISO 4287/1-1997	
λ q	Root Mean Square Wavelength of the Profile	ISO 4287/1-1997	
Hybrid Parameters			
Δa	Average Absolute Slope	ASME B46.1-1995	P Δ a, W Δ a
Δ q	Root Mean Square (RMS) Slope	ASME B46.1-1995	P Δ q, W Δ q
Lo	Developed Profile Length	ISO 4287/1-1997	lr
lr	Profile Length Ratio	ISO 4287/1-1997	Lo
ADF and BAC Parameters			
Rsk,Sk	Skewness	ASME B46.1-1995	Psk, Wsk
Rku	Kurtosis	ASME B46.1-1995	Pku, Wku
tp, Rmr(c)	Profile Bearing Length Ratio (Material Ratio of the Profile)	ASME B46.1-1995	Pmr(c), Wmr(c), Pmr, Rmr, Wmr
Htp, Rδc	Profile Section Height Difference	ASME B46.1-1995	
H	Swedish Height		Htp, Rt
Rk	Core Roughness Depth	ISO 13565-1996	
Rpk	Reduced Peak Height	ISO 13565-1996	Rpk*
Rvk	Reduced Valley Depth	ISO 13565-1996	Rvk*
Mr1	Material Portion	ISO 13565-1996	Rmr(c), tp
Mr2	Material Portion	ISO 13565-1996	Rmr(c), tp
Vo	"Oil-Retention" Volume		
Rpq, Rvq, Rmq	Material Probability Curve Parameters		

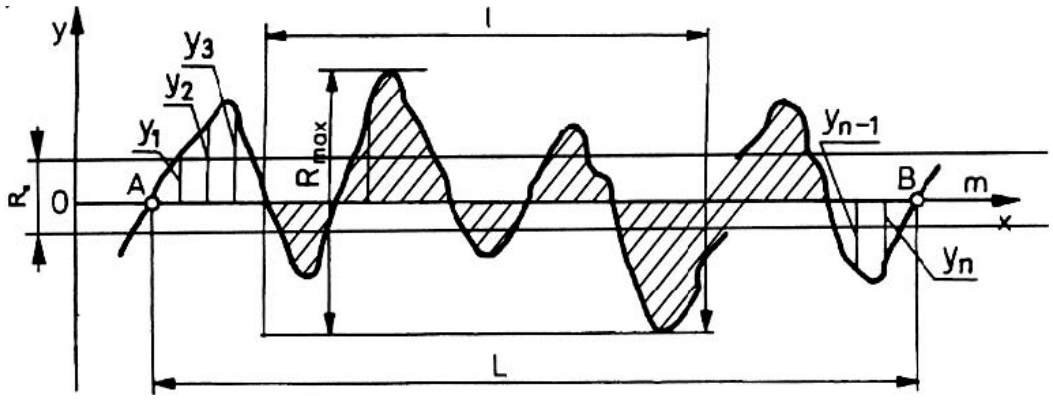

Figure 2.33: Evaluation of surface roughness average (Ra).

$$Ra = \frac{1}{L}\int_0^L |y(x)|dx \qquad \textbf{2.11}$$

$$Rt = Rmax \qquad \textbf{2.12}$$

where L is the sampling length and y represents the deviation from the mean line at a location along the x direction.

Surface roughness (Ra) is the most well-known product quality concern in WEDM. In WEDM, no two sparks can take place side-by-side. They occur completely randomly, so that over time, uniform average material removal occurs over the entire wire electrode's contact length. For the sake of simplicity, it is assumed that sparks occur side-by-side as shown in **Figure 2.5**. Thus,

$$Ra \propto r \qquad \textbf{2.13}$$

From **Equations (2.4)** and **(2.5)**

$$r = (3VR/2\pi)^{1/3} = (3KEs/2\pi)^{1/3} \qquad \textbf{2.14}$$

$$Ra \propto (Es)^{1/3} \qquad \textbf{2.15}$$

It is noted from **Equation (2.15)** that surface roughness increases with increasing spark energy (El-Hofy, 2005). Moreover, pulse frequency has considerable effect on surface roughness (**Figure 2.5**).

2.4.3 White layer and heat affected zone

During WEDM, the discharge temperature can reach up to 12,000°C, and metallurgical changes happen in some of the workpiece surface layers. This way, the zone below the machined surface can be annealed. Moreover, some molten material remains out of the dielectric fluid and chills quickly, mainly by heat conduction throughout most of the workpiece, resulting in a hard surface. The annealed layer depth is generally proportional to the spark energy used in the cutting process. It is around 50 µm for finish cutting to approximately 200 µm for high cutting rates (**Figure 2.34**) (El-Hofy, 2005; McGeough, 1988).

Levy and Maggi (Levy & Maggi, 1990) reported the formation of a thin heat-affected region of 1 µm at 5 µJ spark energy, which increased to 25 µm at high spark energy. A recast layer appeared in different spark erosion conditions and contained many pockmarks, globules, cracks, and micro-cracks. Three types of recast layer were reported. Type 1 represents a single layer less than 10µm thick without any distinct features. Type 2 is an etchable, single layer 10 to 20µm thick. Type 3 consists of overlapping multiple hard layers 20µm thick or more (Tomlinson & Adkin, 1992).

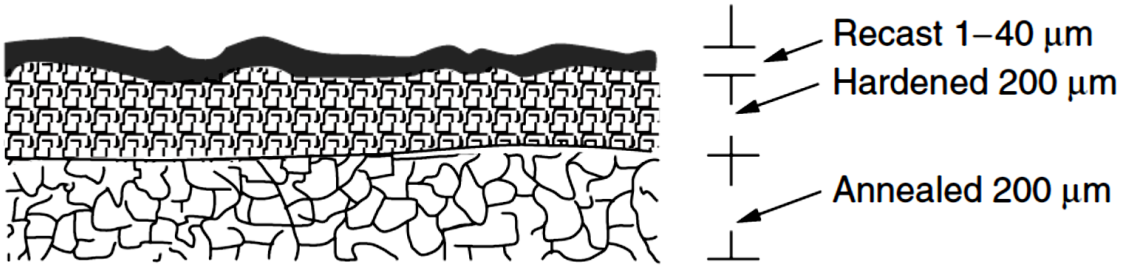

Figure 2.34: EDM machined surface heat affected zone (El-Hofy, 2005).

Researchers have carried out several investigations and noted the presence of this layer under all machining conditions, even when water is used as dielectric fluid (Jangra, Grover, & Aggarwal, 2011; Kruth, Van Humbeeck, & Stevens, 1995; Ramasawmy, Blunt, & Rajurkar, 2005). The white layer is heavily contaminated with carbon, which gives it a structure that is very different from the base material. The WEDM process expels the hydrocarbons from the electrode, and the dielectric fluid breaks down and creates extensive carbon particles that generate a molten white layer **Figure 2.35**. **Figure 2.35** shows the heat-stressed regions of AISI1050 carbon steel (**Figure 2.35a**) and titanium alloy grade 5 (Ti6Al4V) material (**Figure 2.35b**). According to **Figure 2.35,** the heat stressed regions consist of a white layer and thermally-affected zone (Maher, Sarhan, & Marashi, 2016).

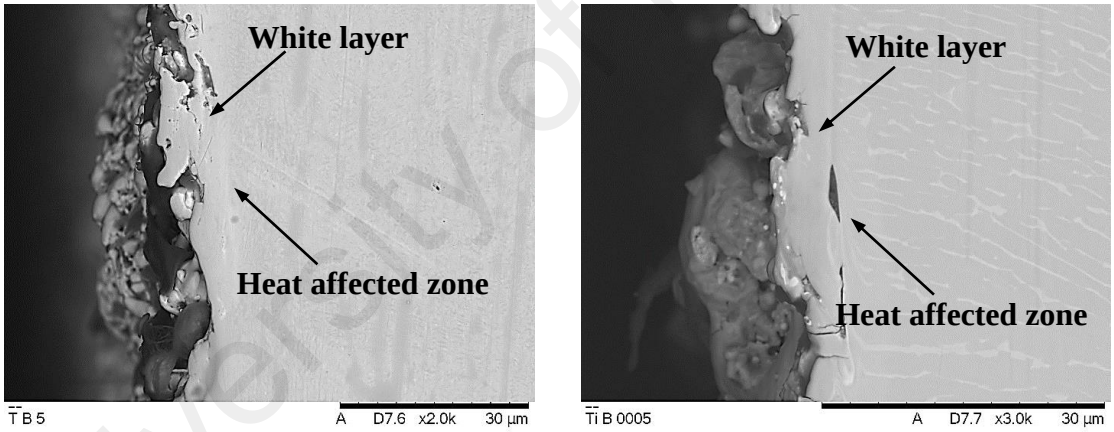

(a) **(b)**

Figure 2.35: Thermally affected zone of (a) AISI 1050 carbon steel and (b) titanium alloy grade 5 (Maher, Sarhan, & Marashi, 2016)

The microstructure, topography, and composition of AISI 1050 carbon steel were analyzed by scanning electron microscopy (SEM) coupled with energy-dispersive X-ray spectroscopy (EDX) as displayed in **Figure 2.36**. **Table 2.2** represents a comparative breakdown of the elements present in the AISI 1050 carbon steel base material prior to WEDM and after white layer formation due to WEDM. It is evident there is a significantly

high presence of carbon content after the WEDM process compared to the base material before WEDM. The heat-affected region lies beneath the white layer. Since this layer is thermally treated at a temperature below the melting point, it is impacted minimally due to the carbon infiltrating the white layer. This heat treatment below the melting point is rather absorbed by the heat-affected region without causing any alteration in the metallurgical structure of the parent material. Therefore, the WEDM process does not affect the parent material below the heat affected region (Maher, Sarhan, & Marashi, 2016).

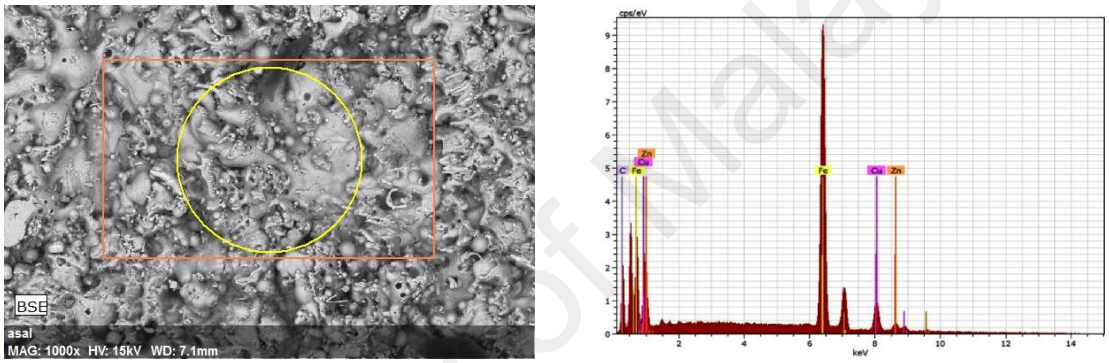

Figure 2.36: EDX analysis of AISI 1050 carbon steel surface (Maher, Sarhan, & Marashi, 2016)

Table 2.2: Elemental analysis of AISI 1050 carbon steel surface before and after WEDM'ed

Element	C	Mn	P	S	Fe	Cu	Zn
Before	0.54	0.69	0.03	0.04	98.7	-	-
After WEDM'ed	14.8	-	-	-	63.5	15.8	5.9

Figure 2.37 indicates very high prevalence of micro-cracks in the white layer. Micro-cracks may cause early material failure in case the white layer becomes too thick or is not cleaned through fine finishing or polishing. Furthermore, micro-cracks are responsible for reduced corrosion and fatigue resistance of the product. Surface integrity is a major concern in WEDM performance evaluation, and hence the WEDM process should be aimed at eliminating the formation of such white layer.

Micro-cracks form due to the heat stress in the pulse-on-time phase of the WEDM cycle. The micro-crack intensity is partially determined by the WEDM process, and the white layer thickness increases proportionately with the spark energy. The number and size of micro-cracks present in the cavity also increase on account of this process. The surface integrity affected by the WEDM process can be controlled using recent power supply technologies. The power supply parameters that control surface integrity are voltage, peak current, pulse on time, pulse off time, and pulse frequency. Efficient and balanced control of these power parameters can help optimize WEDM performance and maintain surface integrity throughout the stages from roughing to final finish (Maher, Sarhan, & Marashi, 2016).

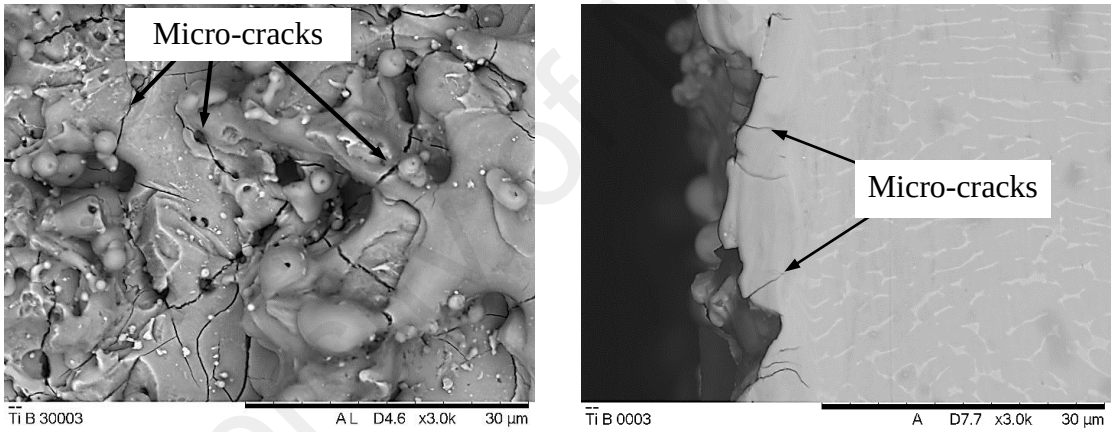

(a) **(b)**

Figure 2.37: SEM analysis of (a) Ti6Al4V surface and (b) cross section illustrating micro-cracks in the white layer (Maher, Sarhan, & Marashi, 2016).

It is speculated that the intensity of spark energy during WEDM discharge directly determines the white layer thickness and micro-crack depth. The spark energy gradually lowers from the roughing to the finishing states to reduce the white layer depth and crack formation.

2.4.4 Wire rupture

The wire electrode is the core of the WEDM process and is used to attain stable electrical discharge. Therefore, the wire electrode is among the most important factors contributing to the overall WEDM performance (Aoyama, 2001). Wire rupture is a serious problem associated with the WEDM process and the wire electrode. This problem affects surface finish quality and accuracy, limits cutting speed and increases machining time (R. Kern, 2007). In fact, wire breakage poses a constant threat to WEDM productivity, but WEDM operators can avoid wire breakage and maintain operations running smoothly and efficiently with some knowledge about the WEDM process, wire rupture causes, and the behavior of the wire and workpiece materials subjected to the process (Dauw & Beltrami, 1994).

Different factors lead to wire breakage, such as high wire tension, thermal load, electrical discharge impact, and poor flushing. When the developed stresses in the wire are greater than the wire strength, the wire will rupture. The stresses developing in the wire increase with changing wire properties and characteristics, reducing the cross section and increasing the wire temperature. High temperature, varying workpiece thickness, and process parameters influence the wire strength and consequently, wire rupture (Luo, 1999).

Lin et al. (C.-T. Lin, Chung, & Huang, 2001) developed a control strategy based on fuzzy logic to improve the machining accuracy and concentrate the sparking in the corner areas without affecting the cutting feed rates. During WEDM of pure titanium, wire breakage occurs when the wire encounters non-conducting particles. Patil and Brahmankar (N. G. Patil & Brahmankar, 2009) revealed that wire breakage appears to pose limitations on the material removal rate in the machining of MMCs. Many research works have been done on WEDM in contrast to very few investigations on the wire

breakage frequency of pure titanium. Kinoshita et al. (Kinoshita, Fukui, & Gamo, 1982) analyzed the various types of wire breakage. To prevent wire breakage, they developed a control system with a means of monitoring the pulse frequency.

Since the introduction of WEDM on the market in the early 1970s, the overall performance of WEDM has undergone tremendous evolution. Moreover, the possibility of controlling the upper and lower wire guides independently enables the generation of all kinds of edge profiles (van Luttervelt, 1989). The Russian Lazarenko couple was the first to design an electro-discharge machine in 1955 (Motoki & summer, 1978). A computer-based, numerically controllable component (CNC) wire-cut machine was developed 10 years later. A machine for mass commercial production was constructed in 1969. However, by 1972, the WEDM machine was able to yield corners with smaller radii. In the early 1970s, the WEDM machine yield was limited to cutting around 13 cm^2/hr., which gradually reached 40 cm2/hr. by the early 1980s (Sommer & Sommer, 2013). CNC components played a major role in improving the majority of wire electric discharge controllers for WEDM.

The discharge parameters need to be low and the dielectric flushing rate high to yield low surface roughness and thin white layers. This parameter setting ultimately lowers the cutting rate in WEDM. Due to this technical trade-off, one set of process parameters fails to achieve a high cutting rate and the least surface defects at the same time. Manufacturers should have access to mathematical, numerical, and empirical models of the input parameters and output performance characteristics for effective machining throughput. Hence, many works with the aim of enhancing process performance based on electro-thermal concepts have been introduced, including theoretical (Liao & Yu, 2004; A. Singh & Ghosh, 1999), numerical (Izquierdo, Sánchez, Plaza, Pombo, & Ortega, 2009; Salah, Ghanem, & Atig, 2006), and empirical (Dekeyser, Snoeys, & Jennes, 1988; C.-S. Lee,

Heo, Kim, Choi, & Kim, 2015; N. Patil & Brahmankar, 2010) involving performance parameters and guesstimate results associated with the machining process.

Theoretical models seem to produce higher errors compared to experimental results. The application and effectiveness of empirical models are limited to certain machining procedures. The relationship between a set of input parameters and output responses is commonly determined using the Taguchi method and Response Surface Methodology (RSM) (Hewidy, El-Taweel, & El-Safty, 2005; Myers & Anderson-Cook, 2009). The correlation between input parameters and output measures was studied using a process model developed with a feedforward neural network (Tarng, Ma, & Chung, 1995). Moreover, machine performance can be estimated with an Adaptive Neuro-Fuzzy Inference System (ANFIS)-based model of the machining process (Çaydaş, Hasçalık, & Ekici, 2009; Maher, Eltaib, Sarhan, & El-Zahry, 2015).

In the absence of proper mathematical models, soft computing techniques appear efficient. In contrast to traditional computing, these techniques suffer from approximation, partial truth, met heuristics, uncertainty, and inaccuracy. The relationships between input and output parameters can be modeled by soft computing techniques like ANFIS (Maher, Eltaib, Sarhan, & El-Zahry, 2014; Maher, Sarhan, Barzani, & Hamdi, 2015), which uses an adaptive neural network to develop a fuzzy inference system. ANFIS can build an input-output mapping model based on both human knowledges as fuzzy if-then rules and known input-output data pairs to train neural networks in a hybrid learning procedure. It offers fuzzy models a way to learn the known dataset, which estimates membership function parameters that facilitate detection from given input-output data (Jang, Sun, & Mizutani, 1997; Maher, Eltaib, & El-Zahry, 2006). Hence, the first objective of this work is to study the effect of cutting parameters on

machining performance to enhance the WEDM process using ANFIS modeling along with the Taguchi approach.

As mentioned earlier, the generation and distribution of spark energy within the discharge zone determine the WEDM efficiency (Gostimirovic, Kovac, Sekulic, & Skoric, 2012; Salonitis, Stournaras, Stavropoulos, & Chryssolouris, 2009). In practice, spark energy (peak current, pulse on time, and pulse off time) and pulse frequency parameters (pulse on time and cycle time) are varied to achieve efficient WEDM process control. However, there is still a challenge in studying the impact of spark energy and pulse frequency simultaneously on machining performance. Therefore, it is difficult to attain a high cutting rate with minimum surface defects using a single parameter setting. Hence, the second objective of this research work is to propose a new performance index to study the effects of spark energy and pulse frequency simultaneously on machining performance measures to enhance the WEDM process.

2.5 Economic and ecological aspects in WEDM

Economic and ecological aspects are known to be the most important factors in any production process especially in WEDM, which they directly affect machining cost and quality. The economic aspect can be expressed as the total machining costs while the ecological aspect can be expressed as the energy and wire consumption in WEDM (Dhanik, Xirouchakis, & Perez, 2011).

Besides investigating WEDM process parameters, a number of researchers have introduced and analyzed ecological (energy and wire consumption), economic (machining costs), and environmental (electrophysical and electrochemical) impacts of WEDM. Tonshoff et al. (Tönshoff, Egger, & Klocke, 1996) reported on the electrophysical and electrochemical, environmental and safety aspects of EDM processes. Heavy metals may be carried by the dielectric and the sludge. Since a great number of

hazardous substances are generated during the EDM process, it is very important to carefully treat and dispose of the waste.

Yeo et al. (Yeo, Tan, & New, 1998) introduced a method of identifying the environmental impact of waste streams from EDM and transforming each of the three mass flows (electrode waste, part chip, and dielectric waste streams) into a weighted mass flow considering the three hazard factors (toxicity, flammability, and mass flow magnitude) of each mass flow. The proposed method allows ranking from an environmental impact point of view as alternative electrode-dielectric fluid combinations for the EDM process. (Deiss, 2009) found that a significant part of energy consumption is due to water cooling, spark generator, and water injection systems. Subsequently, different operation modes were studied with variations in part height, wire diameter, part material, wire material and cutting rates. According to results, changing the cutting conditions may yield higher energy efficiency. Machine, wire consumption and energy costs were further studied for a range of process parameters. From these numerical examples it was determined that wire consumption costs are three to five times higher than energy consumption costs. It can be concluded that although various efforts have been oriented towards environmental impact reduction, the following gaps can be identified. First, the relationship between WEDM parameters and machine tool energy consumption has not been modeled. Second, the electrode, filter, and deionized resin consumables have not been considered.

Although machine tools are equipped with cutting condition tables for each wire, it is still difficult to decide which wires are feasible for a particular operation according to technical limitations and what the most suitable wire among them is. It is daunting to select an appropriate wire that adheres to the machining requirements as well as minimizes machine tool energy and consumable utilization. Hence, a system is required

that can help the process planner rank the different choices according to predefined performance criteria. Therefore, the third objective of this research is to propose a new production economic index to identify the most suitable type of wire electrode for higher WEDM performance keeping in view the ecological and economic aspects. The last objective is to propose a new electrode wire design for use in the WEDM process in order to facilitate superior machining performance and cutting accuracy.

2.6 Conclusion

The following conclusions are reached after a comprehensive review of published research works in this field. A few studies introduced refer to discovering changes in the mechanical properties and surface integrity of the workpiece. Therefore, numerous options in this field remain open to exploration in future research (L. Li, Guo, Wei, & Li, 2013; Newton, Melkote, Watkins, Trejo, & Reister, 2009). A limited number of studies involve white layer thickness prediction models (Maher, Sarhan, & Hamdi, 2015). Furthermore, there remains a practical challenge in controlling all factors necessary to yield reproducible results due to many machining parameters. Moreover, studying the impact of spark energy and pulse frequency simultaneously on machining performance is a complex matter. Very little research work introduced has identified the wire rupture limit. Also, developing a performance criterion to identify the most suitable wire electrode type for higher WEDM performance considering both ecological and economic aspects has not been reported yet.

Hence, the first aim of this work is to obtain the best parameters (pulse off time, pulse on time, peak current, wire speed, and wire tension) to enhance the WEDM process using ANFIS modeling along with the Taguchi approach. In this case, titanium alloy grade 5 (Ti6Al4V) and AISI 1050 carbon steel work materials were cut using brass and coated-wire electrodes in the WEDM process. The second goal is to propose a new performance index to identify the effect of spark energy and pulse frequency simultaneously on machining performance and to identify the wire rupture limit. The next aim is to propose a production economic index to identify the most suitable wire electrode type for superior WEDM performance keeping in view the ecological and economic aspects. The last objective is to propose a new, stronger coated-wire electrode for less wire rupturing and higher WEDM performance.

CHAPTER 3: METHODOLOGY

3.1 Introduction

Overall plan of this experimental work is illustrated in **Figure 3.1**. This research plan was designed to achieve the current study objectives. In this work, the WEDM process was utilized to improve machining performance with minimum cost and wire consumption for sustainable production. The workpiece materials were selected from the hard and difficult-to machine categories of metals commonly used in industrial practice. The cutting speed, surface roughness, white layer thickness, and wire loss were measured using appropriate equipment. Then further analysis and discussions were carried out to introduce a technological knowledge base for machining parameter selection to achieve high productivity with the highest possible surface quality considering the ecological and economic aspects.

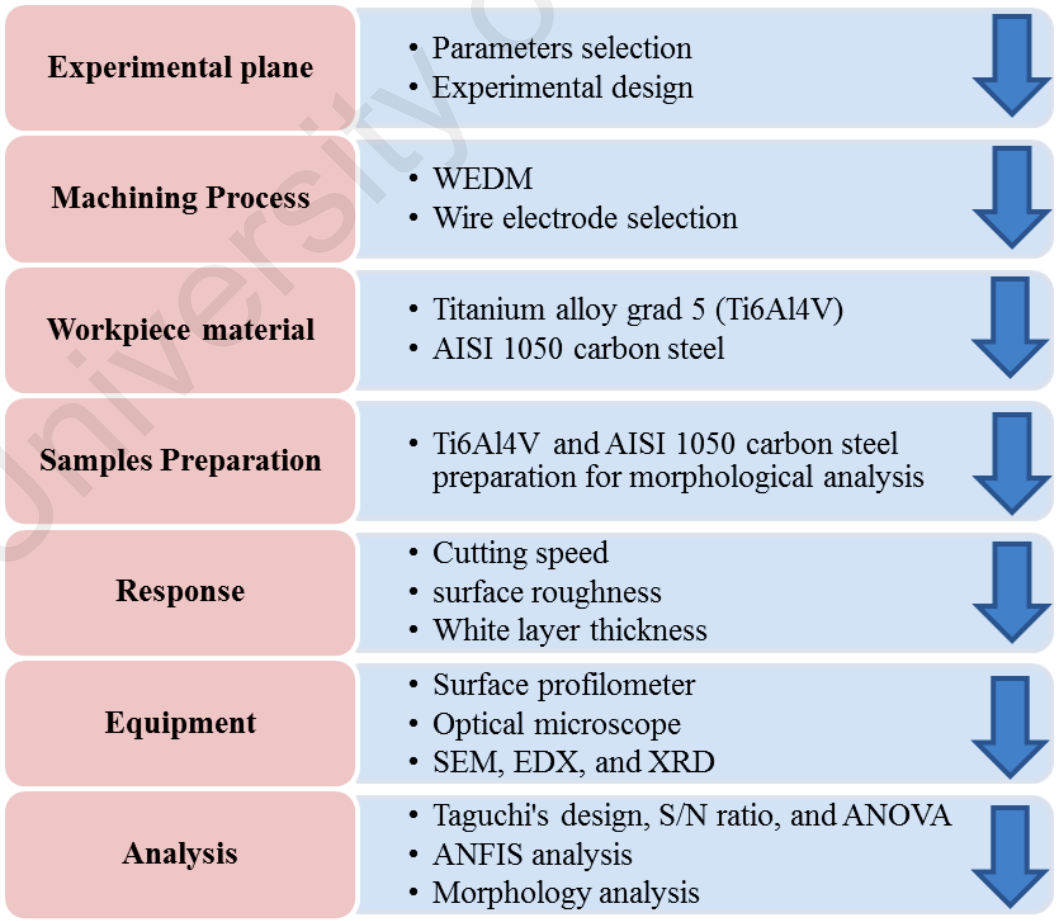

Figure 3.1: Overall plan of this experimental work

3.2 Machining parameters selection

The effects of machining parameters related to power supply, wire electrode, dielectric fluid, and workpiece were investigated on cutting speed (*CS*), surface roughness (*Ra*), white layer thickness (*WLT*), and wire loss (*WL*). The parameters were peak current (*IP*), pulse on time (*Ton*), pulse off time (*Toff*), wire speed (*WS*), and wire tension (*WT*). The machining parameter levels (**Table 3.1**) were selected from prior studies, with the working range and WEDM process parameter levels following the one-factor-at-a-time method. Two different wire electrode materials (brass and the most recent coated wire) were chosen to cut two different workpiece materials: a very hard metal (Titanium alloy grade 5) and a soft metal (AISI 1050 carbon steel), using a WEDM tool.

Table 3.1: Levels of machining parameters

Machining parameter	Symbol	Units	Levels		
			1	2	3
Peak current	*IP*	A	16	17	-
Pulse on time	*Ton*	µs	0.2	0.3	0.4
Pulse off time	*Toff*	µs	0.5	0.9	1.3
Wire speed	*WS*	m/min	3	7	11
Wire tension	*WT*	N	3.5	6	10.5

The other machining parameters were kept constant (**Table 3.2**) during the experiments in order to optimize the process. The machining parameters were selected based on the literature review, experience, and machine maker's recommendations.

Table 3.2: Constant machining parameters

Machining parameter	Symbol	Units	Value
Spark gap set voltage	SV	V	20
Flushing pressure	WP	kgf/cm^2	12
Dielectric flow rate	WQ	l/min	6
Dielectric conductivity (Water)	WC	Ω.cm	1/(5×104)
Wire diameter	d	mm	0.2
Main power supply voltage	V	V	100

3.3 Experimental design

The design of experiment (DOE) is one of the most powerful tools for experimental planning. It can serve as great leverage to reduce experimental design changes and design cost as well as increase design process speed by using statistical methods. The Taguchi method is the most important DOE that is a simple, systematic, and efficient approach to determine the optimum process parameters. In the Taguchi method, an orthogonal array design of experiments is applied and a large number of control factors with a reduced number of experiments is selected. In this array, the control factor matrix ensures a balanced contrast between the levels and independent distribution among parameters. DOE is effective for studying the influence of many variables on performance as well as studying the influence of individual parameters to determine which variable is more influential on the performance measure (Roy, 2001).

The Taguchi L18 orthogonal array was selected because of the four machining variables with three levels each and one machining variable with two levels, as shown in **Table 3.1**. These parameter levels were selected within the limit range of a machine working without wire breakage based on the initial investigation. The Taguchi L18 standard orthogonal array is displayed in **Table 3.3**.

Table 3.3: Table Taguchi's L18 Standard Orthogonal Array

Column No.	***IP***	***Ton***	***Toff***	***WS***	***WT***
1	1	1	1	1	1
2	1	1	2	2	2
3	1	1	3	3	3
4	1	2	1	1	2
5	1	2	2	2	3
6	1	2	3	3	1
7	1	3	1	2	1
8	1	3	2	3	2
9	1	3	3	1	3
10	2	1	1	3	3
11	2	1	2	1	1
12	2	1	3	2	2
13	2	2	1	2	3
14	2	2	2	3	1
15	2	2	3	1	2
16	2	3	1	3	2
17	2	3	2	1	3
18	2	3	3	2	1

3.4 WEDM machine tool

The experiments were performed using a computer numerical control (CNC) Sodick A500W WEDM machine tool. The machine consists of four systems that are shown in **Figure 3.2**. A worktable motion system provides the table motion to generate the required shapes. A dielectric fluid circulation system provides the required fluid pressure and flow rate to assist the sparking process and remove debris. A wire feeding system provides a continuous fresh wire electrode to the cutting zone, while a control system monitors the electrical parameters and is used to write the program codes.

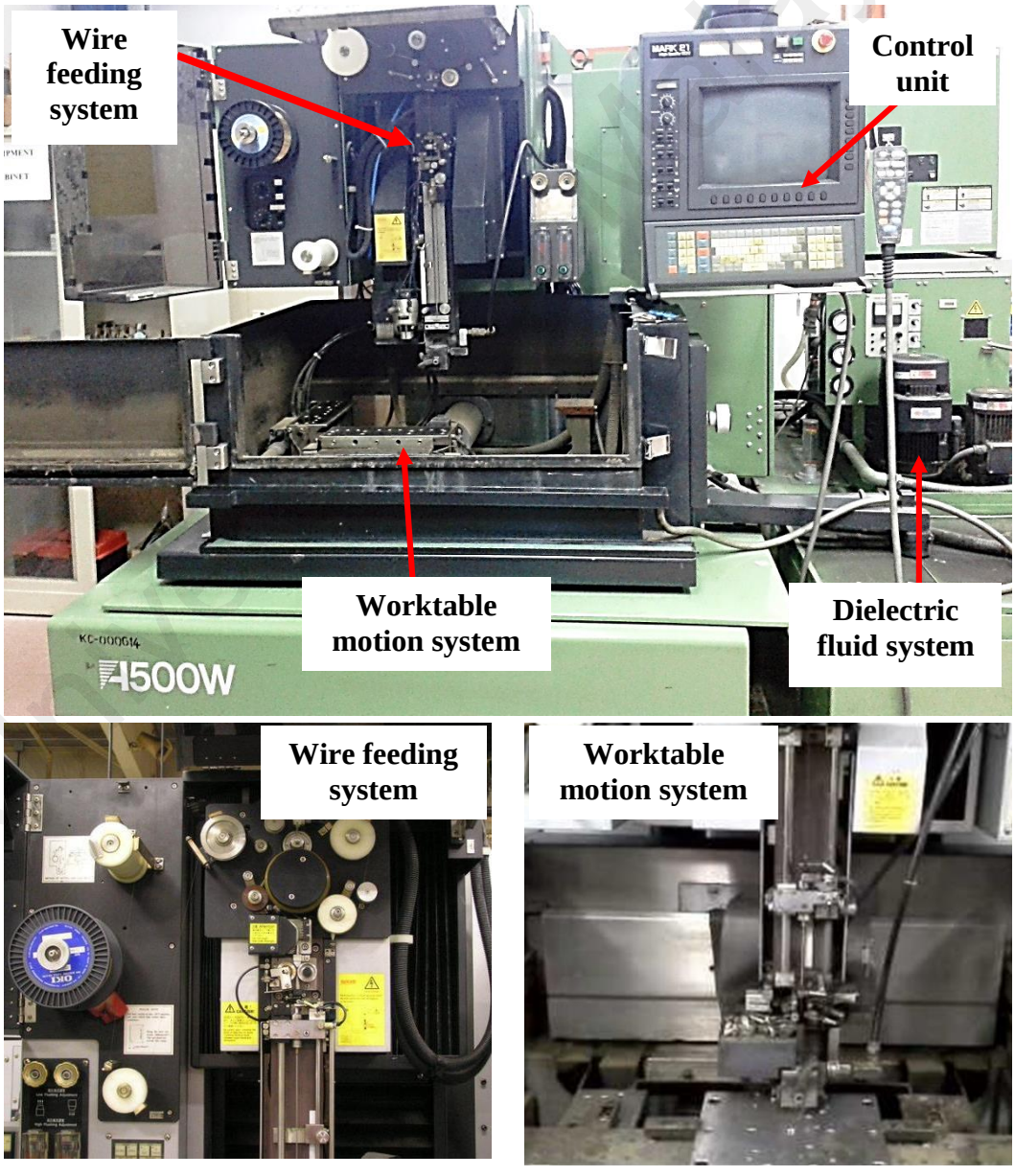

Figure 3.2: WEDM machine

3.5 Wire electrode materials

Two different wire electrodes were employed: a hard brass wire and a coated brass wire. The hard brass wire was developed with a high zinc concentration (60%Cu 40%Zn by weight) in order to achieve higher quality and cutting speed in WEDM. The coated brass wire has a core of 65%Cu 35%Zn coated with a layer with high Zinc concentration (40%Cu 60%Zn by weight). The high zinc concentration in the coating layer enhances cutting speed and surface finish. The properties of the two wire electrodes are introduced in **Table 3.4**.

Table 3.4: Wire electrodes properties

Wire	Material composition	Tensile strength	Elongation	Electric conductivity
Brass	60%Cu40%Zn	1000 N/mm2	1.5%	22% IACS
Coated	Core: 65Cu35Zn Coating: 40Cu60Zn	875 N/mm2	2%	20% IACS

3.6 Workpiece materials

Two different workpiece materials were selected with different electrical resistivity and thermal conductivity. Their effects on surface quality and productivity under different machining conditions were investigated. The workpiece materials used are titanium alloy grade 5 (Ti6Al4V) and AISI 1050 carbon steel. Titanium is a metal with high strength-to-weight ratio that is maintained at elevated temperatures because titanium is a very strong and light metal. It is stronger than aluminum and as strong as steel. In addition, it is 45% lighter than steel and only 60% heavier than aluminum. Besides, titanium is an attractive metal as it has high corrosion resistance and high durability, and is long lasting. Some of the properties of titanium are tensile strength of 241 GPa, hardness of HRB 70 to 74 and density of 4.50 Mg/m^3. Titanium and its alloys are used in many industries, such as biomedical, automobile, aerospace, chemical, electronic, gas and food industry applications.

AISI 1050 steel is a medium carbon steel. This grade steel is used for manufacturing forged shafts and gears and for a wide range of applications owing to its good combination of mechanical properties. The chemical composition of titanium alloy was achieved by EDX machine as shown in **Table 3.5** and AISI 1050 carbon steel as shown in **Table 3.6**. The electrical resistivity and thermal conductivity of titanium alloy were 17.8x10-5 Ω·cm and 6.7 W/(m·K) respectively and 1.63x10-5 Ω·cm and 49.8 W/(m·K) respectively for AISI 1050 carbon steel.

Table 3.5: Chemical compositions of Titanium alloy (Grade 5)

Element	Al	V	Fe	O	C	Ti
Weight, wt (%)	5.65	3.93	0.13	0.11	0.08	90.1

Table 3.6: Chemical compositions of AISI 1050 carbon steel

Element	C	Mn	P	S	Fe
Weight, wt (%)	0.54	0.69	0.03	0.04	98.7

3.7 Machined samples preparation for morphological characterization

A workpiece plate 100 x 100 x 20 mm was mounted on the Sodick A500W WEDM machine tool and machined into 5 x 5 x 20 mm specimens. A set of cut specimens is illustrated in **Figure 3.3**.

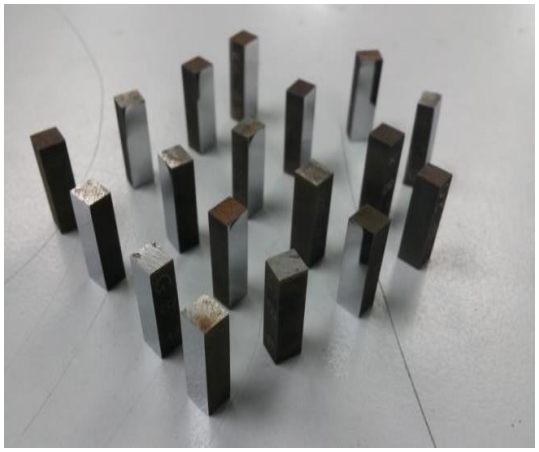

Figure 3.3: Set of 18 samples after cutting with WEDM

3.7.1 Titanium alloy grad 5 (Ti6Al4V) preparation

The samples were ground using grinding and polishing machine, P240 (30 second), P320 (40 seconds), P400 (60 seconds), P600 (90 seconds), P800 (120 seconds), P1200 (180 seconds), P2500 (210 seconds), grit silicon carbide paper with pressure of around 9N, counter rotation of 400 rpm, and plenty of coolant water. Then the samples cleaned using ultrasonic agitator between the steps in ethanol at 30°C for 15 minutes. Then the samples polished using 9, 6, 3, and 1 µm diamond suspension liquid with pressure 6N, 7 minutes' counter rotation of 400 rpm. Repeated until surface is smooth (checked with optical microscope (OM), interference contrast mode).

After polishing, 50 ml of oxide polishing suspension (OPS) with 10 ml H2O2 were used for final polishing with 400 rpm counter rotation for five minutes. Repeated until microstructure is nicely visible, typically 2 or 3 times (checked with OM). Then the samples surface washed with water and dishwashing liquid, wash with water, flush with ethanol, dry with hair dryer. Finally, the samples etched with Kroll's reagent 5 – 10s. The samples were then cleaned in an ultrasonic agitator in acetone at 30°C for 15 minutes, carefully rinsed and cleaned in distilled water, and dried to remove contamination to acquire a uniform surface.

3.7.2 AISI 1050 carbon steel preparation

The samples were ground using 120 SiC abrasives for stock removal requirements. Once planarity and the area of interest are obtained, one of the standard procedures such as P220 (30 second), P360 (30 seconds), P800 (30 seconds), P1200 (60 seconds), P2400 (90 seconds), P4000 (120 seconds) is applied involving grit silicon carbide paper with pressure of around 10 N, counter rotation of 400 rpm, and plenty of coolant water. Then the samples were cleaned in ethanol at 30°C for 15 minutes using an ultrasonic agitator between the steps. Then the samples were roughly polished using 6 and 3µm diamond suspension liquid with pressure 6 N, five minutes of counter rotation in 400 rpm. It is

repeated until surface is smooth (checked with optical microscope (OM) in interference contrast mode).

Finally, 0.05µm alumina suspension liquid with pressure 5 N, were used for the final polishing with 400 rpm counter rotation for five minutes. It was repeated until microstructure was nicely visible (checked with optical microscope, interference contrast mode). Then the samples surface was washed with distilled water, flushed with ethanol, dried with a hair dryer. The samples were then cleaned in an ultrasonic agitator in acetone at 30°C for 15 minutes. Then the samples carefully rinsed and cleaned in ethanol, and dried to remove contaminants to acquire a uniform surface. After samples preparation, all samples (Titanium and steel) sealed with parafilm and saved in dry place until used for measurements.

3.8 Performance parameters measurement

The WEDM output responses including cutting speed, surface roughness, white layer thickness, and wire rupture were investigated in this study. The response factors are described in the following subsections.

3.8.1 Cutting speed

This is a measure of cutting rate and material removal rate of the workpiece. Cutting speed is measured by cutting straight into the workpiece. If cutting speed is high, the productivity is high, which is a desirable characteristic in WEDM. When the wire has made approximately 50% of the cut, the cutting speed was recorded directly on the WEDM machine tool monitor. The average cutting speed was calculated from three data recorded under the same conditions.

3.8.2 Surface roughness

Surface roughness is often a good predictor of machine or wire performance and it is used in this research work. Roughness is a measure of the texture of a surface. It is quantified by the vertical deviations of a real surface from its ideal form. If deviation is large, the surface is rough but if it is small, the surface is smooth. The parameter most frequently used for general surface roughness is Ra. It measures average roughness by comparing all the peaks and valleys with the mean line and then averaging them all over the entire cut-off length. Cut-off length is the length that the stylus is dragged across the surface; a longer cut-off length will give an average value, and a shorter cut-off length may give a less accurate result over a shorter stretch of the surface. The surface roughness was measured with a stylus-based profilometer (Mitutoyo SJ-201, 99.6% accuracy). The average surface roughness was calculated for three different measurements under the same conditions with a roughness width cutoff of Lc = 0.8 mm based on standard ISO 4287:1997.

3.8.3 White layer thickness

A recast layer appears in different spark erosion conditions and contains many pockmarks, globules, cracks, and micro-cracks. White layer thickness is the measure of the recast layer thickness. If the white layer is thick, the surface is susceptible to fatigue failure. A scanning electron microscope (SEM) equipped with energy-dispersive X-ray spectroscopy (EDS) (Hitachi tabletop microscope TM3030) was used to examine the microstructural and topographical surface characteristics and white layer thickness of the machined part. The average white layer thickness was calculated from three measurements using an image processing program (ImageJ).

3.8.4 Wire rupture

In WEDM, the wire mass loss per meter can be used to calculate the wire rupture. The wire mass loss per meter was calculated by weighting 10 meters of the wire electrode before and after the cutting process using a precise balancer. Then the difference in wire mass was divided by ten meters to get the mass loss per meter.

CHAPTER 4: RESULTS, ANALYSIS, AND DISSCUSION

4.1 Introduction

This section describes the experimental results and the effects of the process parameters on machining performance. The entire set of experiments was carried out to ensure improvement in WEDM process performance. The result analysis and discussion focus on optimizing the process parameters and developing a new performance index to identify the effects of spark energy and pulse frequency simultaneously on machining performance and to identify the wire rupture limit. The results, data analysis, and discussion are organized in the following phases:

- Investigating the effect of the process parameters on WEDM process performance for sustainable production using the Adaptive Neuro-Fuzzy Inference System (ANFIS) along with the Taguchi approach.
- Proposing a new performance index to identify the effects of spark energy and pulse frequency simultaneously on machining performance and to identify the wire rupture limit in WEDM.

4.2 Experimental results

The results are divided into 4 groups, with each group containing a set of eighteen experiments based on the design of experiments for every combination of wire electrode and workpiece material type. In these groups, the measured cutting speed (CS), surface roughness (Ra), white layer thickness (WLT), and wire rupture (WL) are introduced. **Figure 4.1 - 4.5** show samples of the surface morphology, surface roughness, white layer thickness, and wire rupture results, respectively.

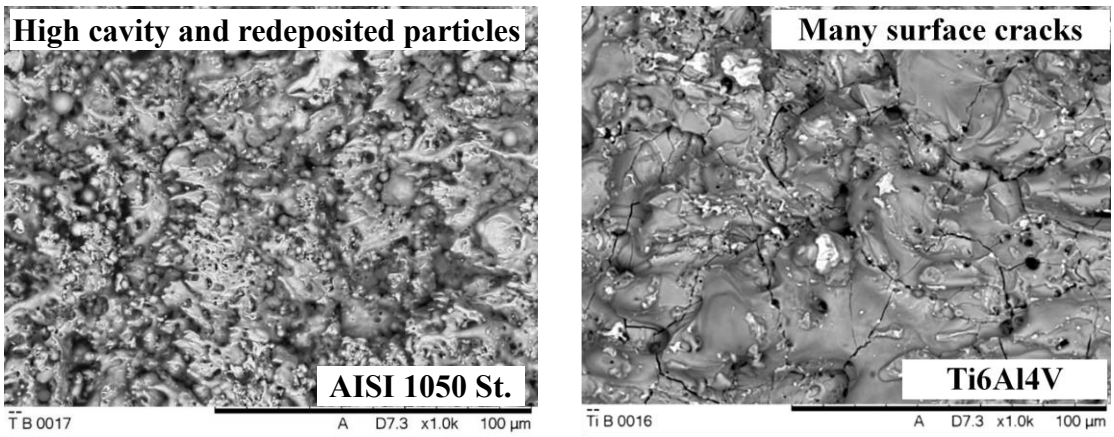

(a) **(b)**

Figure 4.1: Sample of SEM surface morphology of (a) AISI 105 carbon steel (b) Ti6Al4V

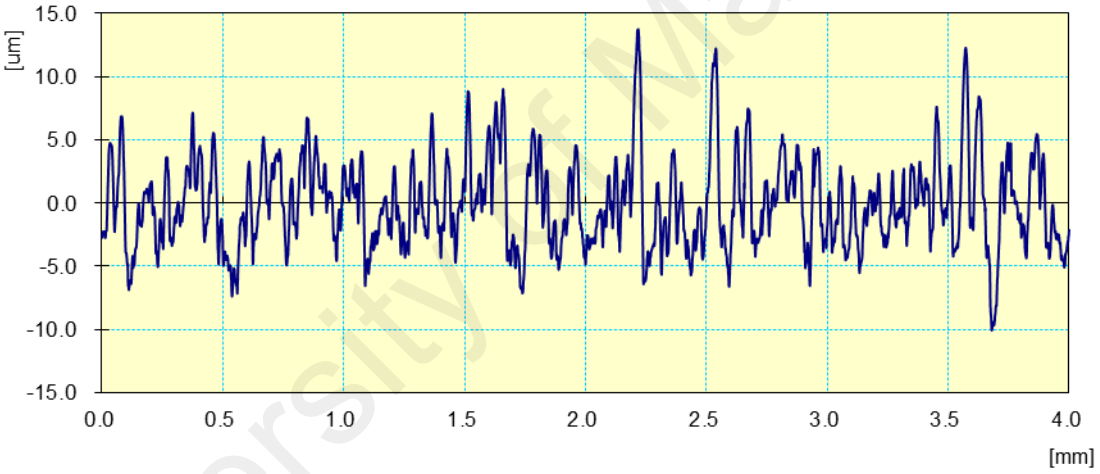

Figure 4.2: Sample of surface roughness measurement

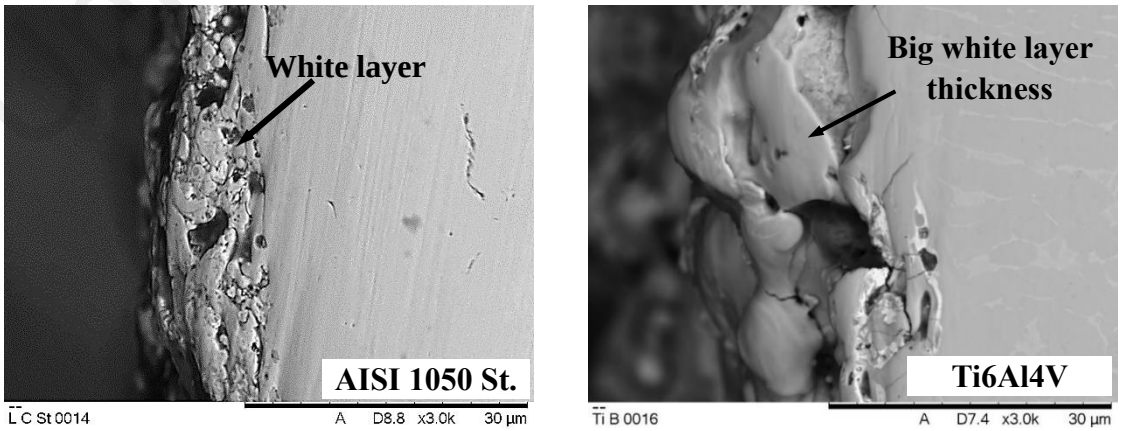

(a) **(b)**

Figure 4.3: Sample of thermally affected zone (a) AISI 1050 carbon steel (b) Ti6Al4V

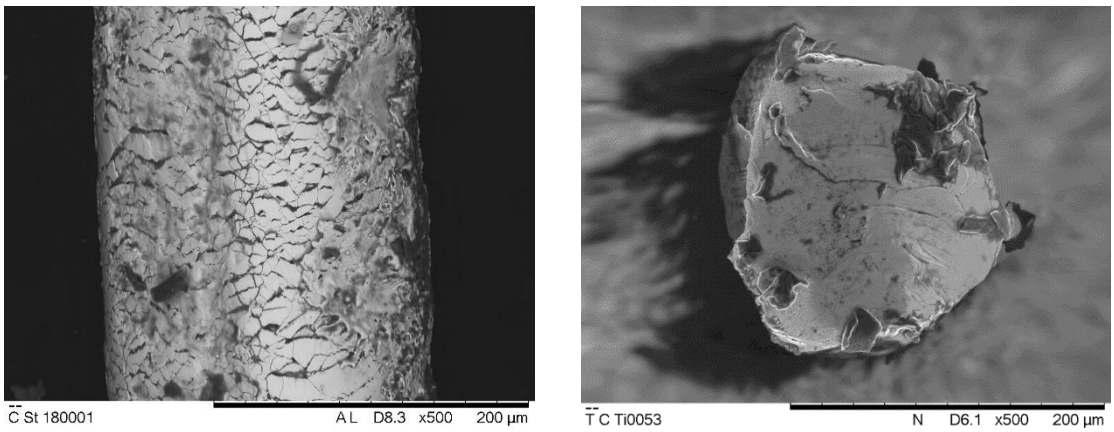

(a) **(b)**

Figure 4.4: SEM sample of wire rupture (a) coated wire after machining (b) cross section of the wire after machining

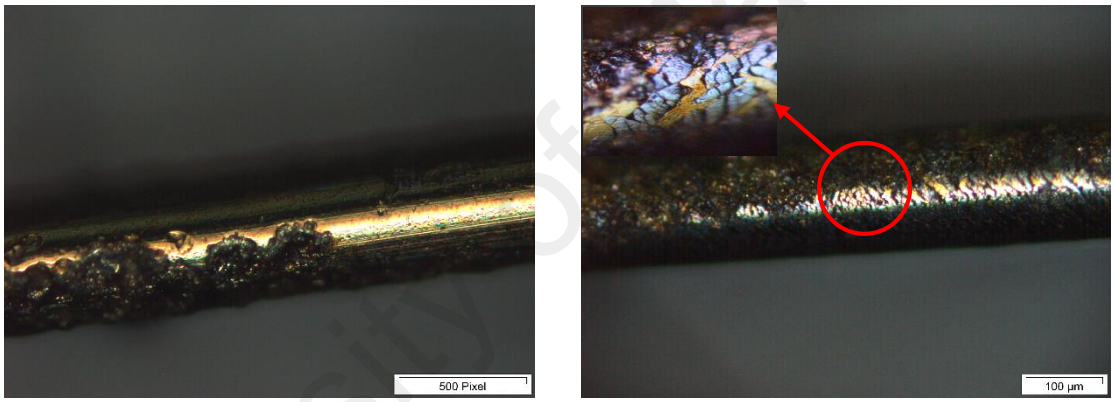

(a) **(b)**

Figure 4.5: Optical microscope sample of wire rupture after machining for (a) Brass wire (b) Coated wire

The average CS, Ra, WLT, and WL were calculated from three data recorded under the same conditions, as summarized in the following tables.

- From the first group, a brass wire electrode was used to cut an AISI 1050 carbon steel workpiece (**Table 4.1**).
- From the second group, a brass wire electrode was used to cut a Titanium alloy grade 5 (Ti6Al4V) workpiece (**Table 4.2**).

- From the third group, a coated-wire electrode was used to cut an AISI 1050 carbon steel workpiece (**Table 4.3**).
- From the fourth group, a coated-wire electrode was used to cut a Titanium alloy grade 5 (Ti6Al4V) workpiece (**Table 4.4**).

Table 4.1: Measured CS, Ra, WLT, and WL at different machining conditions for Brass wire with AISI 1050 carbon steel

No.	Machining parameters					Performance outcomes															
	IP (A)	Ton (µs)	Toff (µs)	WS (m/min)	WT (N)	CS (mm/min)				Ra (µm)				WLT (µm)				WL (mg/m)			
						1	2	3	Avg.	1	2	3	Avg.	1	2	3	Avg.	1	2	3	Avg.
1	16	0.2	0.5	3	3.5	0.45	0.46	0.45	0.45	1.76	1.68	2.01	1.82	8.53	11.96	11.43	10.64	3.78	2.20	0.95	2.31
2			0.9	7	6	0.74	0.82	0.75	0.77	2.53	2.04	2.39	2.32	11.52	7.03	8.62	9.06	0.95	1.89	2.20	1.68
3			1.3	11	10.5	0.67	0.54	0.61	0.61	2.23	2.16	2.12	2.17	5.89	4.84	5.45	5.39	1.26	2.83	1.26	1.78
4		0.3	0.5	7	3.5	0.8	0.83	0.74	0.79	2.64	2.58	2.51	2.58	8.53	8.71	7.65	8.30	2.20	1.57	1.89	1.89
5			0.9	11	6	1.44	1.46	1.45	1.45	3.2	3.18	3.16	3.18	12.84	12.13	12.84	12.60	6.30	5.67	5.04	5.67
6			1.3	3	10.5	0.83	0.82	0.82	0.82	3.09	2.88	2.94	2.97	9.23	8.62	6.86	8.24	5.35	10.07	5.67	7.03
7		0.4	0.5	3	6	0.62	1.29	0.8	0.90	3.26	2.96	3.08	3.10	16.09	12.84	13.28	14.07	5.04	6.93	5.98	5.98
8			0.9	7	10.5	2	2.1	2.08	2.06	3.34	3.34	3.35	3.34	12.75	8.97	8.26	9.99	11.33	10.07	9.13	10.18
9			1.3	11	3.5	1.26	1.19	1.17	1.21	3.31	3.21	2.92	3.15	12.92	16.53	15.47	14.97	6.30	6.30	6.30	6.30
10	17	0.2	0.5	11	10.5	0.46	0.78	0.57	0.60	2.45	2.35	2.28	2.36	9.58	8.79	9.58	9.32	2.20	1.89	2.20	2.10
11			0.9	3	3.5	0.67	0.99	0.8	0.82	2.92	2.2	2.72	2.61	16.35	14.07	14.15	14.86	3.46	3.78	2.83	3.36
12			1.3	7	6	0.72	0.77	0.7	0.73	2.54	2.23	2.2	2.32	9.14	11.17	14.15	11.49	1.89	1.57	0.32	1.26
13		0.3	0.5	11	6	1.04	2.4	1.64	1.69	3.47	4.01	2.71	3.40	11.16	10.99	10.81	10.99	9.44	7.56	8.18	8.39
14			0.9	3	10.5	1.8	1.76	1.77	1.78	2.88	2.82	3.33	3.01	16.35	17.05	16.62	16.67	12.59	10.70	10.70	11.33
15			1.3	7	3.5	1.02	1.09	1.15	1.09	2.91	3	3.18	3.03	16.53	16.97	16.97	16.82	4.09	7.87	4.72	5.56
16		0.4	0.5	7	10.5	2.06	2.47	3.2	2.58	3.79	3.58	3.97	3.78	16.62	15.82	13.63	15.36	13.85	12.91	13.85	13.54
17			0.9	11	3.5	2.22	2.38	2.43	2.34	4.03	3.42	3.25	3.57	17.41	16.35	15.74	16.50	11.65	11.02	12.28	11.65
18			1.3	3	6	2.14	2.3	2.2	2.21	2.76	3.06	3.49	3.10	14.77	12.84	18.11	15.24	24.55	25.50	25.81	25.29

Table 4.2: Measured CS, Ra, WLT, and WL at different machining conditions for Brass wire with Ti6Al4V

No.	Machining parameters					Performance outcomes															
	IP (A)	Ton (µs)	Toff (µs)	WS (m/min)	WT (N)	CS (mm/min)				Ra (µm)				WLT (µm)				WL (mg/m)			
						1	2	3	Avg.	1	2	3	Avg.	1	2	3	Avg.	1	2	3	Avg.
1	16	0.2	0.5	3	3.5	1.34	1.39	1.42	1.38	2.82	2.64	2.27	2.58	11.96	12.18	11.04	11.73	2.49	2.57	2.5	2.52
2			0.9	7	6	1.07	1.15	1.1	1.11	2.5	2.39	2.31	2.40	9.88	9.38	10.12	9.79	2.88	2.93	3.07	2.96
3			1.3	11	10.5	0.77	0.82	0.96	0.85	2.62	2.28	2.14	2.35	8.25	7.89	8.14	8.09	2.47	2.48	2.51	2.49
4		0.3	0.5	7	3.5	1.62	1.64	1.62	1.63	2.59	2.72	2.64	2.65	17.31	18.14	17.23	17.56	3.78	3.74	4.01	3.84
5			0.9	11	6	1.23	1.45	1.44	1.37	2.64	2.41	2.45	2.50	14.74	13.56	14.47	14.26	3.77	3.66	3.69	3.71
6			1.3	3	10.5	1.07	1.15	1.07	1.10	2.53	2.39	2.39	2.44	11.11	10.51	10.58	10.73	3.91	3.8	3.8	4.84
7		0.4	0.5	3	6	2.13	2.02	1.96	2.04	2.89	2.86	2.91	2.89	23.36	23.94	22.71	23.34	5.72	5.67	5.58	5.66
8			0.9	7	10.5	1.83	1.73	1.75	1.77	2.65	2.83	2.96	2.81	19.07	21.41	18.78	19.75	4.18	4.25	4.22	4.22
9			1.3	11	3.5	1.52	1.57	1.49	1.53	2.6	2.78	2.6	2.66	15.16	16.88	16.17	16.07	5.28	5.1	5.18	5.19
10	17	0.2	0.5	11	10.5	1.39	1.48	1.51	1.46	2.6	2.59	2.43	2.54	16.34	16.05	14.53	15.64	5.02	5.06	4.83	4.97
11			0.9	3	3.5	1.18	1.31	0.99	1.16	2.33	2.54	2.45	2.44	12.27	12.57	13.02	12.62	5.36	5.44	5.42	5.41
12			1.3	7	6	0.91	1.01	0.77	0.90	2.13	2.3	2.45	2.29	9.5	10.72	9.72	9.98	3.72	3.8	3.82	3.78
13		0.3	0.5	11	6	1.7	1.89	1.63	1.74	2.72	2.6	2.73	2.68	21.27	20.04	19.39	20.23	6.41	6.39	6.27	6.36
14			0.9	3	10.5	1.36	1.73	1.52	1.54	2.4	2.84	2.51	2.58	17.79	18.32	16.68	17.60	8.31	8.25	8.37	8.31
15			1.3	7	3.5	1.25	1.31	1.31	1.29	2.74	2.38	2.53	2.55	16.75	14.93	15.14	15.61	5.12	4.98	5.01	5.04
16		0.4	0.5	7	10.5	2.25	2.17	2.12	2.18	2.89	3.11	3.21	3.07	27.14	26.53	25.28	26.32	18.31	18.57	18.48	18.45
17			0.9	11	3.5	1.85	2	1.77	1.87	3.14	3.24	2.59	2.99	22.93	21.51	20.24	21.56	5.71	5.78	5.89	5.79
18			1.3	3	6	1.79	1.61	1.71	1.70	3.04	2.66	3.07	2.92	19.84	18.78	17.37	18.66	8.74	8.88	8.82	8.81

Table 4.3: Measured CS, Ra, WLT, and WL at different machining conditions for Coated wire with AISI 1050 carbon steel

No.	Machining parameters					Performance outcomes															
	IP (A)	Ton (µs)	Toff (µs)	WS (m/min)	WT (N)	CS (mm/min)				Ra (µm)				WLT (µm)				WL (mg/m)			
						1	2	3	Avg.	1	2	3	Avg.	1	2	3	Avg.	1	2	3	Avg.
1	16	0.2	0.5	3	3.5	1.04	1	1.13	1.06	2.31	2.25	2.13	2.23	5.72	5.1	5.67	5.50	5.59	6.85	7.79	6.74
2			0.9	7	6	1.44	1.56	1.58	1.53	3.02	2.82	2.94	2.93	7.93	8.39	14.01	10.11	5.59	7.79	4.33	5.90
3			1.3	11	10.5	0.96	0.94	0.88	0.93	2.61	2.59	2.66	2.62	8.34	6.95	9.47	8.25	6.53	6.85	7.16	6.85
4		0.3	0.5	7	3.5	3.42	3.33	3.32	3.36	3.4	3.26	3.32	3.33	13.67	14.91	17.93	15.50	9.05	9.05	9.05	9.05
5			0.9	11	6	2.05	1.98	2.06	2.03	3.13	2.99	3.12	3.08	18.79	15.88	12.84	15.84	9.68	10.63	10.31	10.21
6			1.3	3	10.5	1.31	1.25	1.33	1.30	3.35	3.23	3.32	3.30	10.72	11.58	10.79	11.03	10.94	10.94	9.05	10.31
7		0.4	0.5	3	6	3.34	3.34	3.49	3.39	4	3.48	3.67	3.72	10.32	11.91	12.18	11.47	15.66	16.61	17.24	16.50
8			0.9	7	10.5	2.83	2.77	2.85	2.82	3.29	3.15	3.77	3.40	19.15	18.79	21.18	19.71	11.89	12.51	12.51	12.31
9			1.3	11	3.5	1.73	1.77	1.74	1.75	3.61	3.03	2.98	3.21	20.47	18.53	15.53	18.18	8.74	8.74	10.00	9.16
10	17	0.2	0.5	11	10.5	2.85	2.58	2.94	2.79	3.22	3.01	2.69	2.97	12.88	12	12.27	12.38	9.05	10.63	12.51	10.73
11			0.9	3	3.5	1.79	1.7	1.76	1.75	3.22	3.1	3.15	3.16	13.68	12.88	9.97	12.18	11.89	11.57	10.94	11.47
12			1.3	7	6	1.15	1.04	1.13	1.11	2.89	2.84	2.52	2.75	11.74	12.53	14.03	12.77	6.53	7.16	7.16	6.95
13		0.3	0.5	11	6	3.99	3.36	3.73	3.69	3.54	3.09	3.41	3.35	13.59	12.26	12.79	12.88	14.09	16.92	13.77	14.93
14			0.9	3	10.5	2.38	2.43	2.48	2.43	3.08	3.03	3.6	3.24	14.82	14.38	15.79	15.00	12.83	18.81	15.03	15.56
15			1.3	7	3.5	1.55	1.65	1.55	1.58	3.08	2.99	3.36	3.14	9.62	9.53	13.24	10.80	10.00	10.31	9.68	10.00
16		0.4	0.5	7	10.5	2.6	2.4	3.5	2.83	3.69	2.71	3.22	3.21	13.32	14.65	14.82	14.26	14.40	14.72	14.72	14.61
17			0.9	11	3.5	3.24	3.24	3.21	3.23	3.53	3.91	3.8	3.75	16.24	19.15	16.59	17.33	13.77	14.72	15.35	14.61
18			1.3	3	6	2	1.97	2.05	2.01	4.05	3.67	3.49	3.74	19.24	19.68	17.82	18.91	16.29	14.40	15.35	15.35

Table 4.4: Measured CS, Ra, WLT, and WL at different machining conditions for Coated wire with Ti6Al4V

No.	Machining parameters					Performance outcomes															
	IP (A)	Ton (µs)	Toff (µs)	WS (m/min)	WT (N)	CS (mm/min)				Ra (µm)				WLT (µm)				WL (mg/m)			
						1	2	3	Avg.	1	2	3	Avg.	1	2	3	Avg.	1	2	3	Avg.
1	16	0.2	0.5	3	3.5	1.4	1.35	1.5	1.42	2.2	2.2	2.29	2.23	6.16	4.75	6.07	5.66	2.98	2.97	3.09	3.01
2			0.9	7	6	1.37	1.3	1.4	1.36	2.2	2.11	2.15	2.15	6.28	5.23	3.38	4.96	2.28	2.3	2.16	2.25
3			1.3	11	10.5	1.33	1.18	1.2	1.24	2.19	2.11	1.98	2.09	5.27	3.52	4.25	4.35	2.23	2.09	2.06	2.13
4		0.3	0.5	7	3.5	2.21	2.15	2.38	2.25	2.63	2.74	2.69	2.69	9.93	11.78	8.56	10.09	2.38	2.34	2.42	2.38
5			0.9	11	6	1.82	1.92	1.53	1.76	2.55	2.41	2.51	2.49	7.02	8	7.56	7.53	2.58	2.7	2.79	2.69
6			1.3	3	10.5	1.37	1.57	1.69	1.54	2.38	2.31	2.28	2.32	6.02	5.58	6.77	6.12	4	4.01	4.22	4.08
7		0.4	0.5	3	6	3.41	3.28	3.6	3.43	2.98	3.21	2.99	3.06	16.6	16.19	16.25	16.35	4.81	4.75	4.57	4.71
8			0.9	7	10.5	2.73	2.92	2.9	2.85	2.89	2.84	2.85	2.86	12.25	12.32	13.37	12.65	3.76	3.85	3.89	3.83
9			1.3	11	3.5	2.33	2.59	2.52	2.48	2.76	2.59	2.71	2.69	11.1	10.65	11.44	11.06	3.46	3.55	3.52	3.51
10	17	0.2	0.5	11	10.5	1.67	1.57	1.69	1.64	2.33	2.28	2.32	2.31	7.73	6.08	5.98	6.60	2.73	2.84	2.89	2.82
11			0.9	3	3.5	1.46	1.37	1.5	1.44	2.29	2.18	2.2	2.22	6.43	5.32	5.37	5.71	2.92	3.08	3.03	3.01
12			1.3	7	6	1.36	1.45	1.4	1.40	2.32	2.09	2.09	2.17	5.56	5.07	4.96	5.20	2.66	2.53	2.35	2.51
13		0.3	0.5	11	6	2.6	2.54	2.5	2.55	2.86	2.82	2.78	2.82	11.09	12.68	10.68	11.48	2.09	2.25	2.23	2.19
14			0.9	3	10.5	2.22	2.39	2.31	2.31	2.7	2.63	2.66	2.66	10.33	11.72	9.78	10.61	4.31	4.16	4.25	4.24
15			1.3	7	3.5	1.97	1.9	1.98	1.95	2.4	2.45	2.52	2.46	8.73	9.32	7.85	8.63	3.62	3.69	3.79	3.70
16		0.4	0.5	7	10.5	3.73	3.92	3.9	3.85	3.34	3.14	3.27	3.25	20.57	19.38	19.86	19.94	8.64	8.49	8.61	8.58
17			0.9	11	3.5	3.29	3.1	3.33	3.24	2.99	2.89	2.89	2.92	14	17.58	15.47	15.68	7.99	7.83	7.94	7.92
18			1.3	3	6	2.71	2.59	2.68	2.66	2.69	2.78	2.75	2.74	13.48	13.01	11.65	12.71	11.77	11.86	12.01	11.88

4.3 Investigating the effect of WEDM parameters on machining performance using ANFIS modeling along with the Taguchi method

Because WEDM involves multi-performance characteristics, the main objective of this section is to find a combination of WEDM parameters that achieves rapid cutting speed, low surface roughness, and small white layer thickness to meet the demand of increasing wire electrode productivity and product quality associated with sustainable production and low energy consumption. For this purpose, the effects of the machining parameters including peak current, pulse on time, pulse off time, wire speed, and wire preloading were investigated using an adaptive neuro-fuzzy inference system (ANFIS) and the Taguchi method. Moreover, an ANFIS model was used to predict the required performance levels to boost productivity and the highest possible level of product quality for sustainable production.

4.3.1 Taguchi approach

Taguchi's parameter design is a powerful tool for determining near optimum design parameters for performance, quality, and cost. Orthogonal arrays, one of the major tools used in Taguchi design which study a large number of design variables with a small numbers of experiments. The second important tool used in Taguchi design is signal to noise (S/N) ratio, which used as a measurable value instead of standard deviations and mean. Taguchi introduces a two stage optimization technique, which produces a parameter level combination with minimum standard deviation while maintaining the mean on target (Su, 2013). Taguchi's approach is completely based on design of experiments (DOE), which optimize the process design and economically solving the problem. DOE is effective in studying the effects of many variables on performance as well as studying the influence of individual parameters to determine which variable has more influence on the performance measure (Roy, 2001).

The Taguchi design (L18) was selected with four machining variables with three levels and one machining variable with two levels, as shown in **Table 3.1**. The machining parameters, including peak current (*IP*), pulse width (*Ton*), pulse off time (*Toff*), wire speed (*WS*), and wire tension (*WT*) were selected for this study to investigate the effect on machining performance, i.e., cutting speed (*CS*), surface roughness (*Ra*), white layer thickness (*WLT*), and wire rupture (*WL*). Taguchi's L18 standard orthogonal array of the parameter levels shown in **Table 3.3**. These parameter levels were selected within the limit range of a machine working with no wire breakage based on the initial investigation. The goal of the experiment is to optimize the WEDM variables to obtain high cutting speed values using the larger-is-better characteristic criteria (**Equation 4.1**), and low surface roughness, white layer thickness, and wire loss values using the smaller-is-better characteristic criteria (**Equation 4.2**).

$$\mathbf{S/N = -10\ log(1/n(\sum(1/y^2)))} \qquad \mathbf{4.1}$$

$$\mathbf{S/N = -10\ log(1/n(\sum y^2))} \qquad \mathbf{4.2}$$

where n is the number of experiments, and y is the observed data.

Table 4.1 - 4.4 introduce the real data which used to perform this approach. **Tables A.1** and **A.2** in **Appendix A**, show signal to noise ratios of cutting speed, surface roughness, white layer thickness, and wire loss. **Tables A.3** to **A.6** in **Appendix A**, present the mean S/N ratios for each level of cutting speed, surface roughness, white layer thickness, and wire loss using brass and coated wire electrodes, respectively. These data were plotted as shown in **Figure 4.6** to **4.21**, respectively. **Table** to **4.10** and **Figure 4.6** to **4.21** indicate that peak current, pulse width, and pulse of time are more significant to the mean S/N ratios for cutting speed, surface roughness, and white layer thickness but they are less significant to the wire rupture.

Moreover, these Tables and Figures depict that wire tension and wire speed do not affect cutting speed or the white layer thickness. In addition, wire speed and tension are significant on the average S/N response for surface roughness and wire rupture.

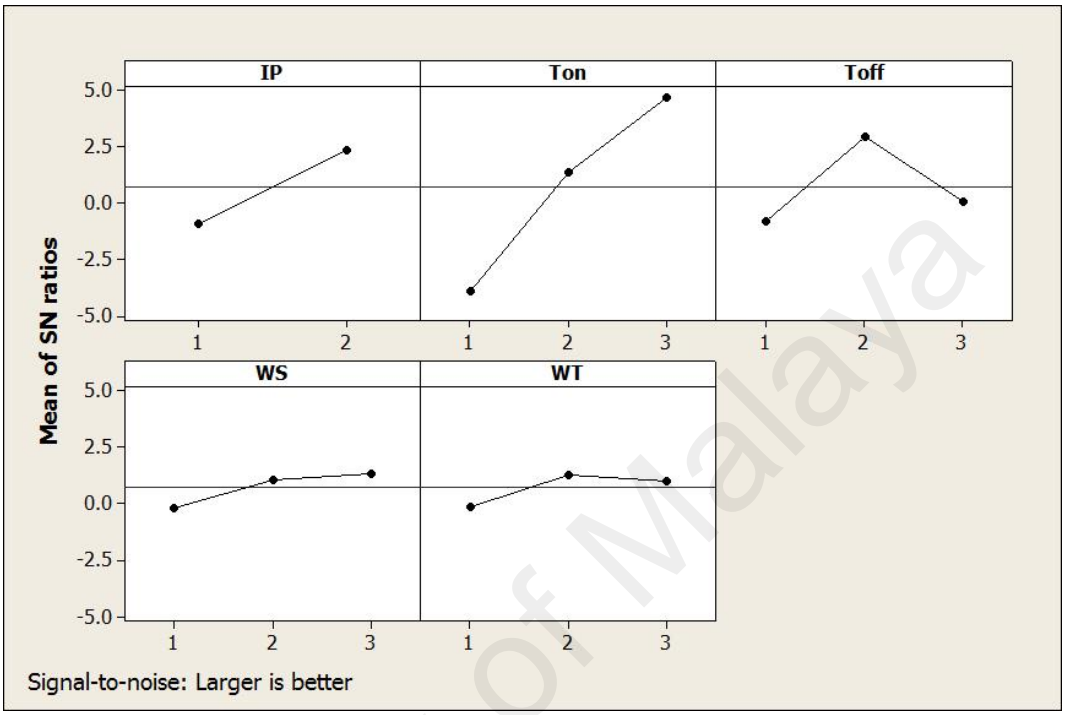

Figure 4.6: Effect of process parameters on CS using brass wire with AISI 1050 steel

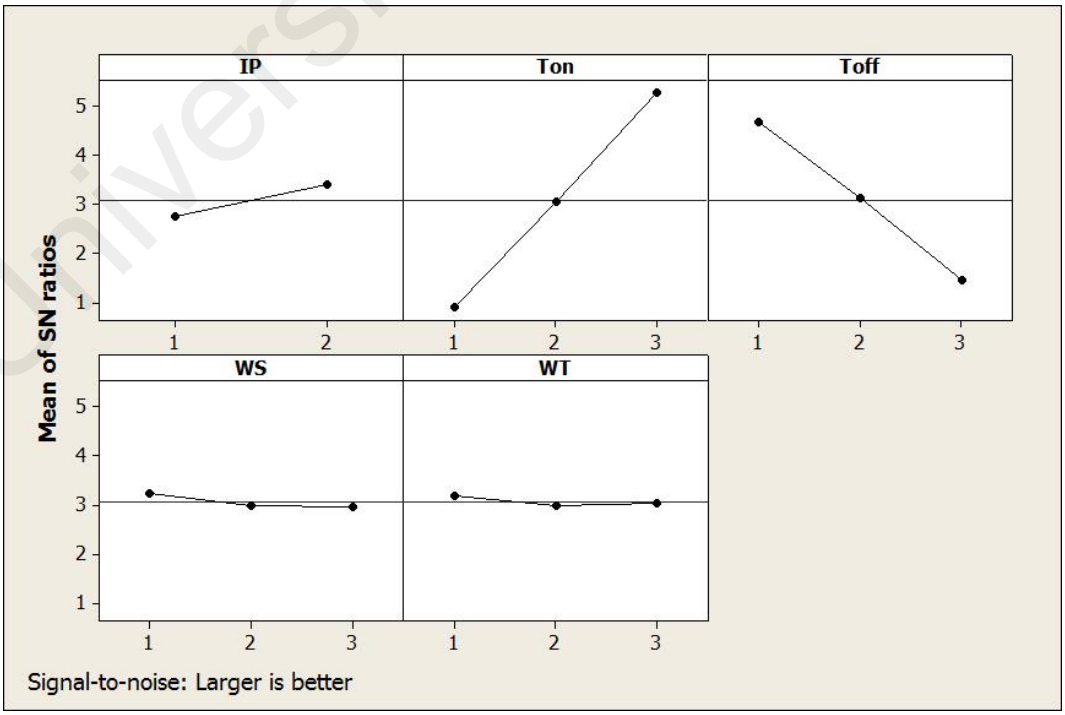

Figure 4.7: Effect of process parameters on CS using brass wire with Ti6Al4V

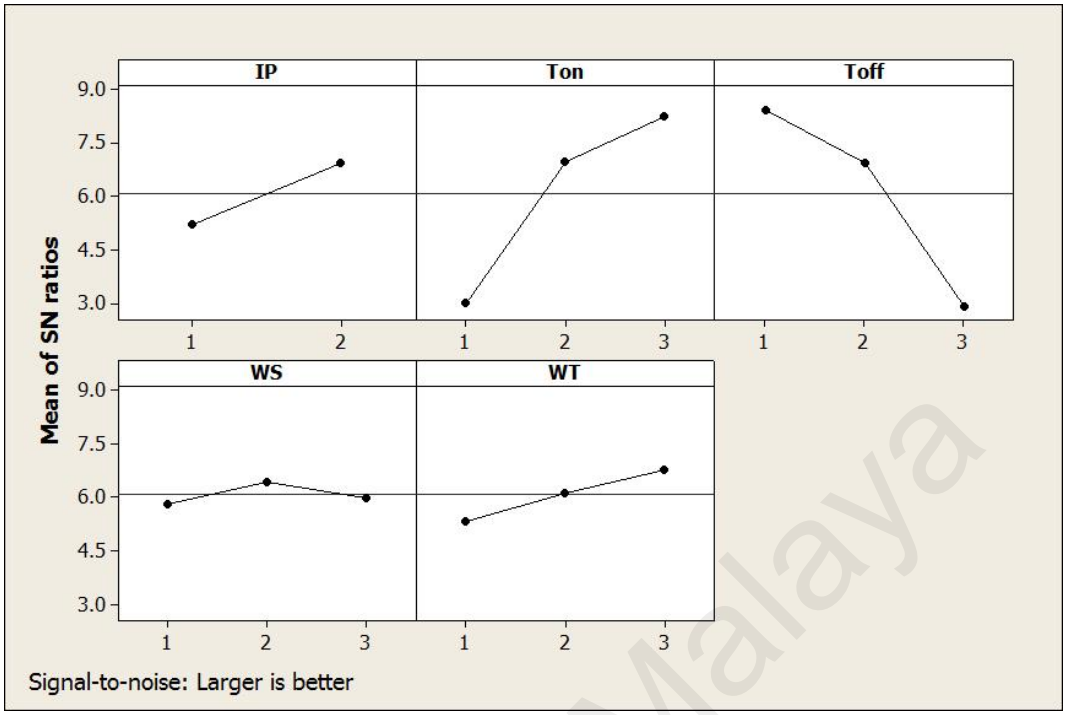

Figure 4.8: Effect of process parameters on CS using coated wire with AISI 1050 steel

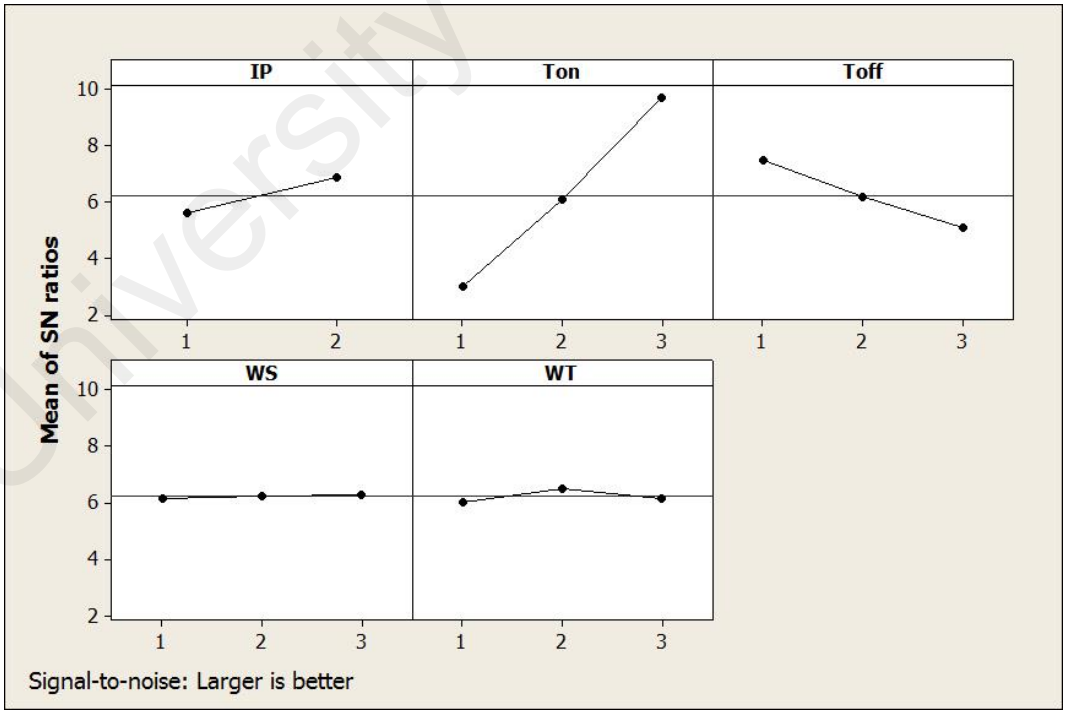

Figure 4.9: Effect of process parameters on CS using coated wire with Ti6Al4V

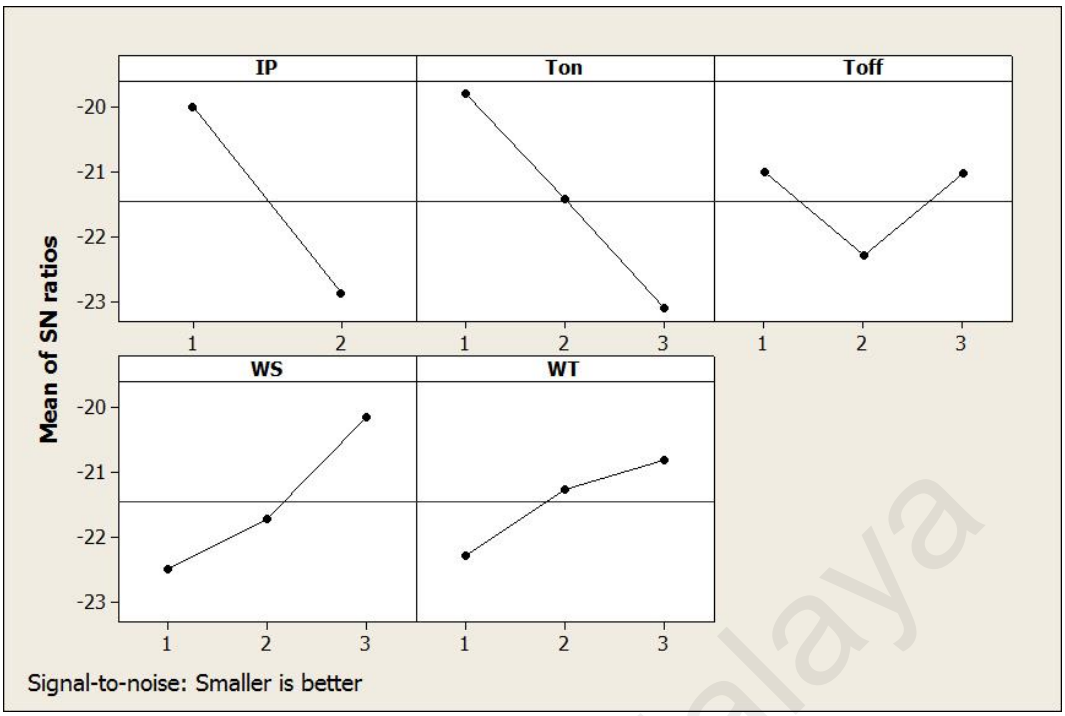

Figure 4.10: Effect of process parameters on Ra using brass wire with AISI 1050 steel

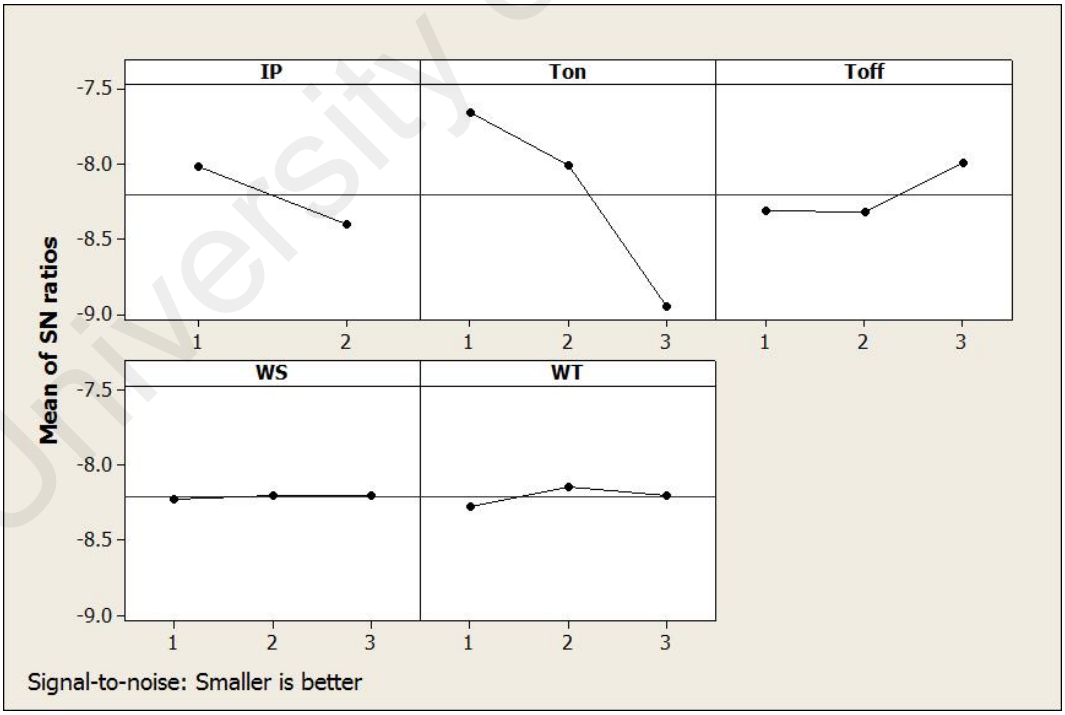

Figure 4.11: Effect of process parameters on Ra using brass wire with Ti6Al4V

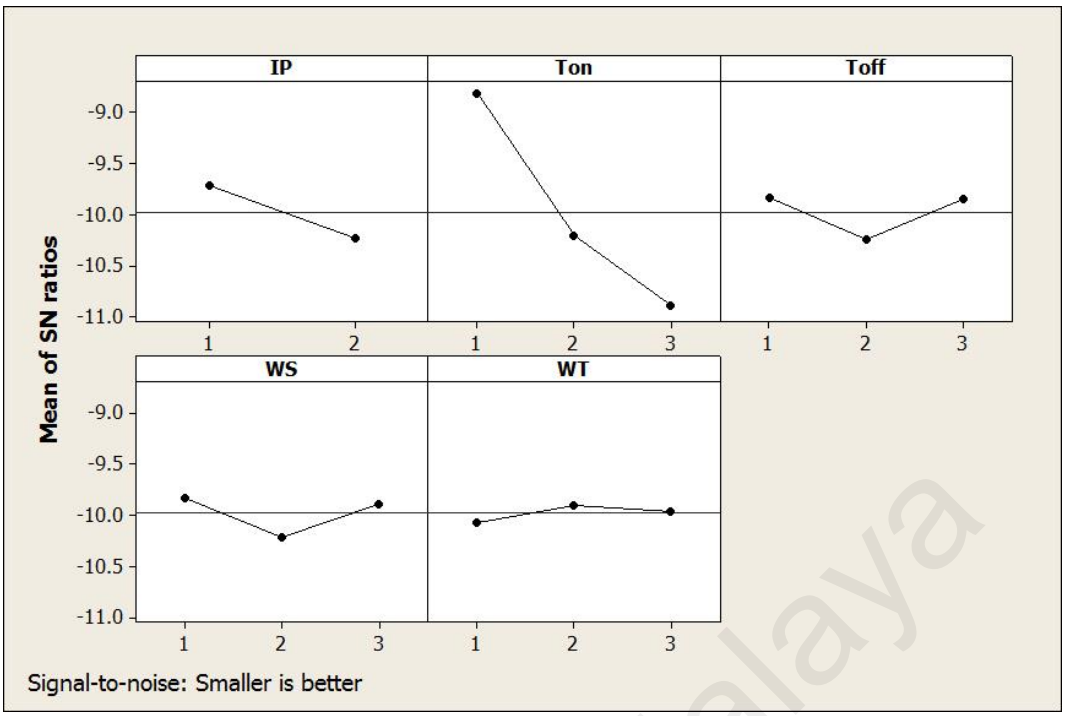

Figure 4.12: Effect of process parameters on Ra coated wire with AISI 1050 steel

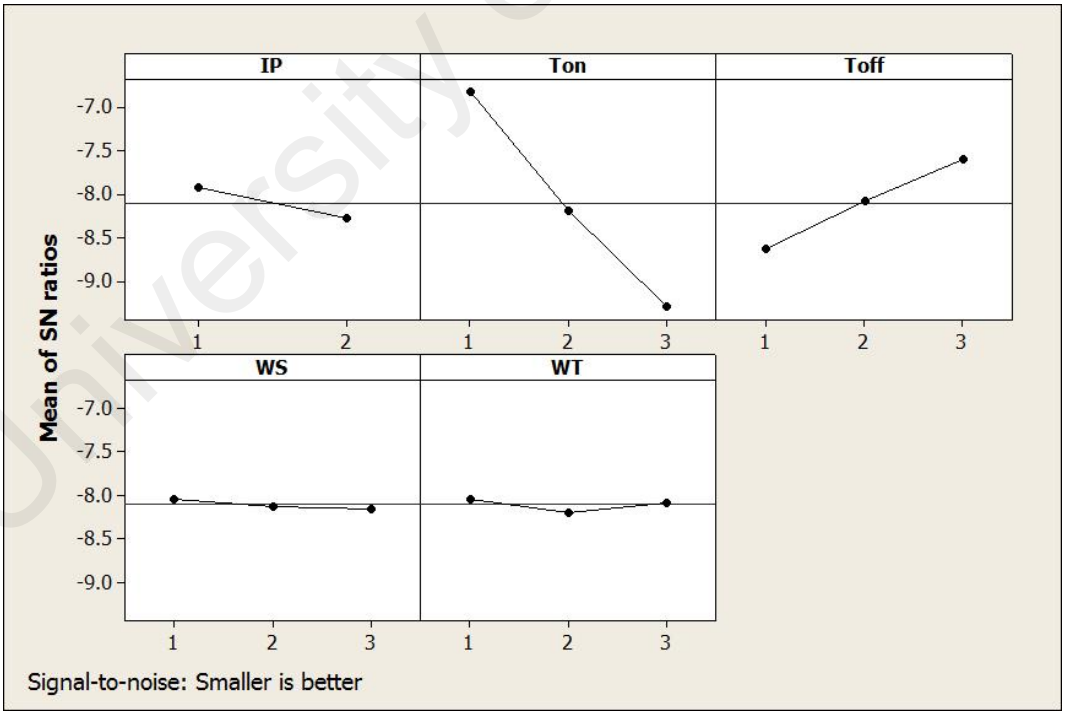

Figure 4.13: Effect of process parameters on Ra using coated wire with Ti6Al4V

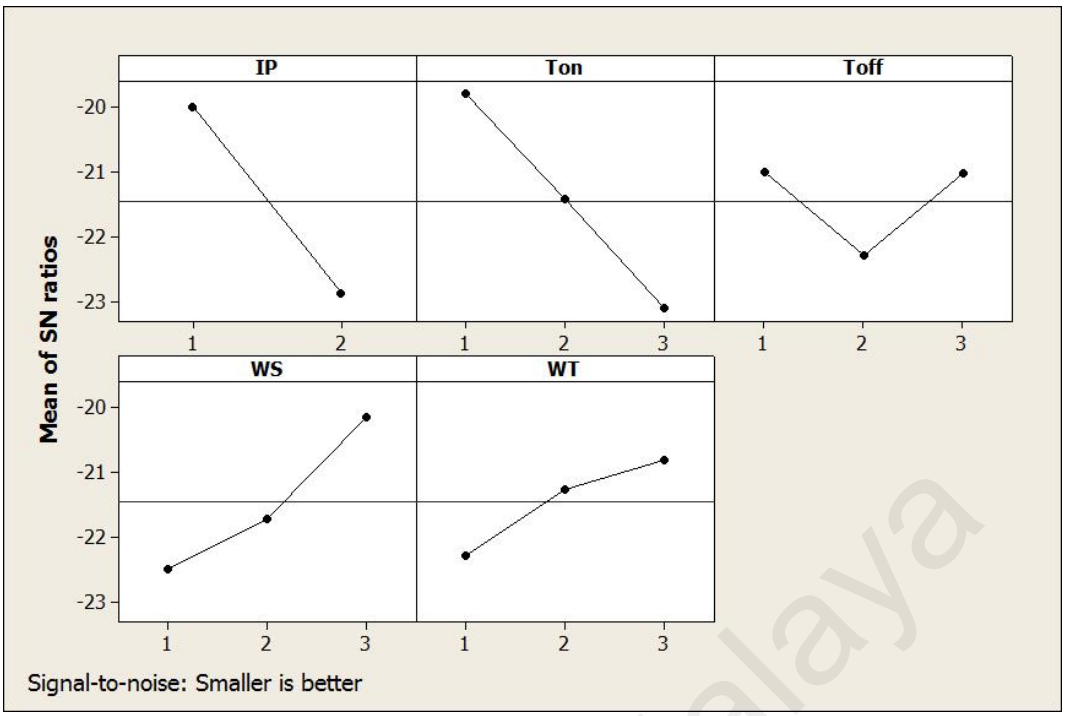

Figure 4.14: Effect of process parameters on WLT using brass wire with AISI 1050 steel

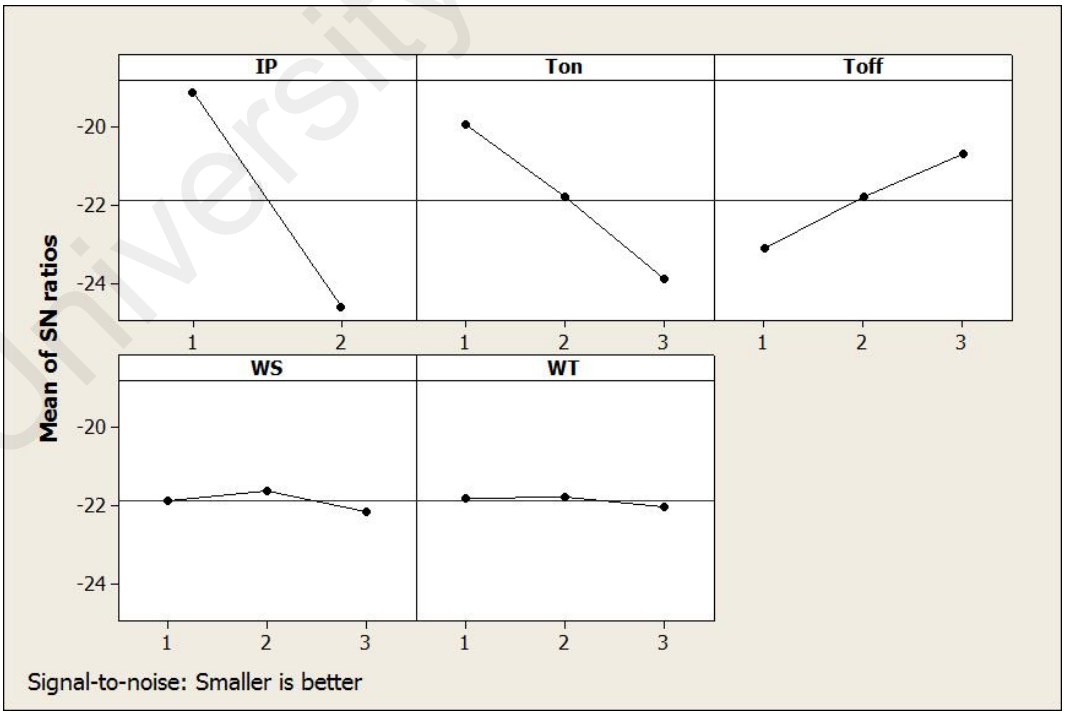

Figure 4.15: Effect of process parameters on WLT using brass wire with Ti6Al4V

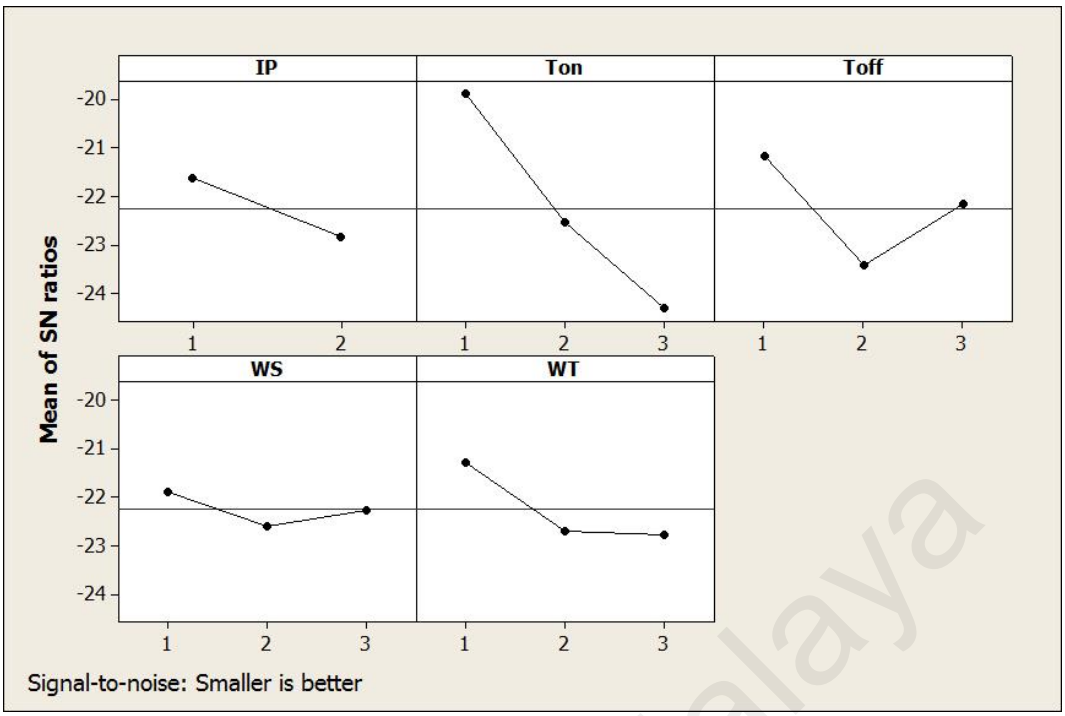

Figure 4.16: Effect of process parameters on WLT using coated wire with AISI 1050 steel

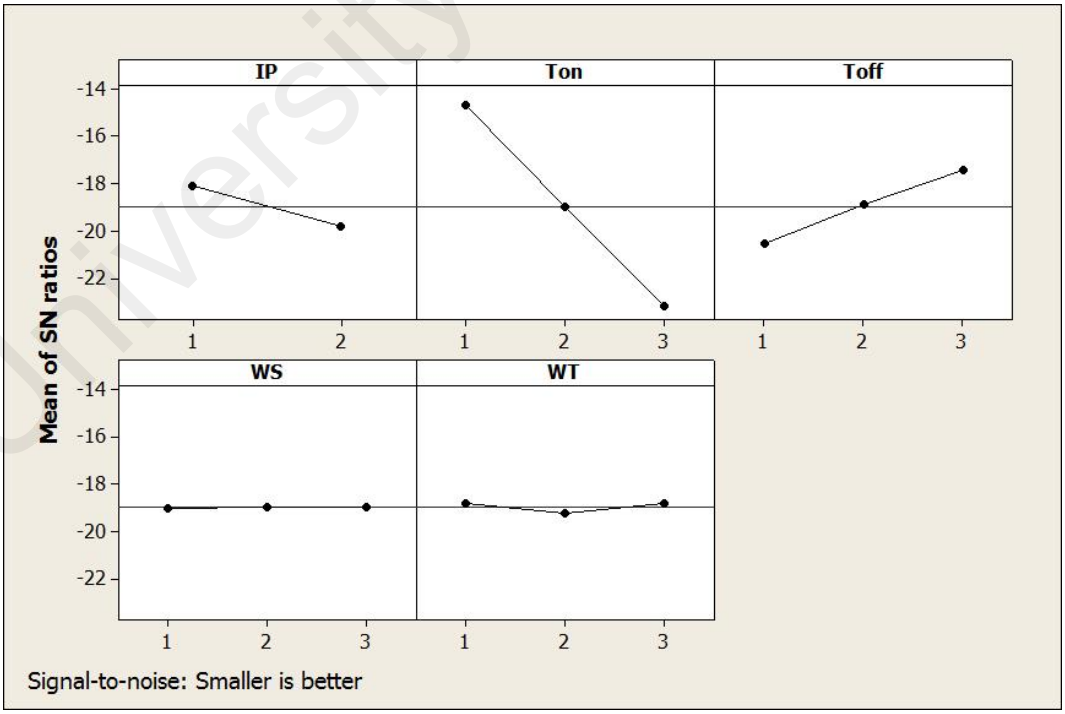

Figure 4.17: Effect of process parameters on WLT using coated wire with Ti6Al4V

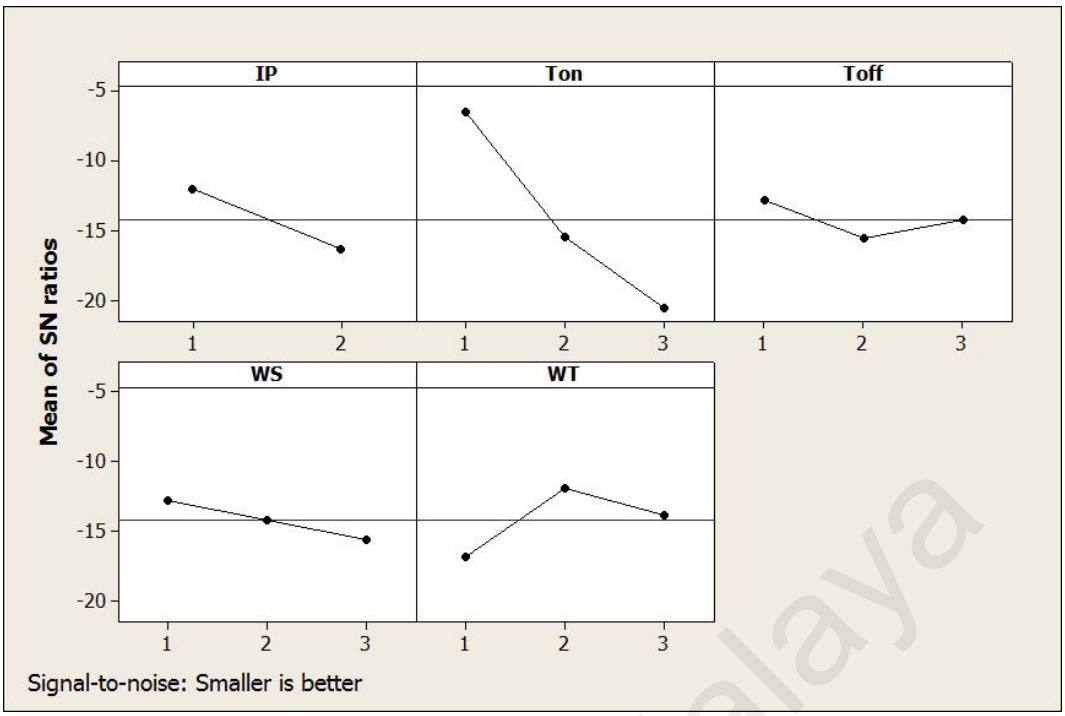

Figure 4.18: Effect of process parameters on WL using brass wire with AISI 1050 steel

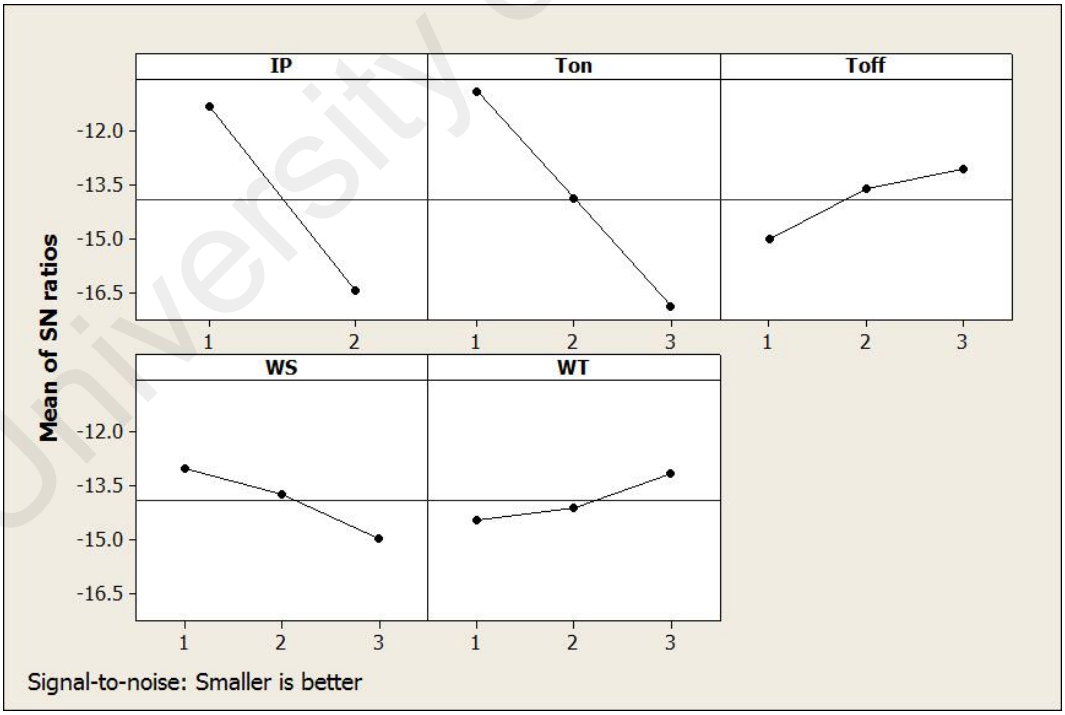

Figure 4.19: Effect of process parameters on WL using brass wire with Ti6Al4V

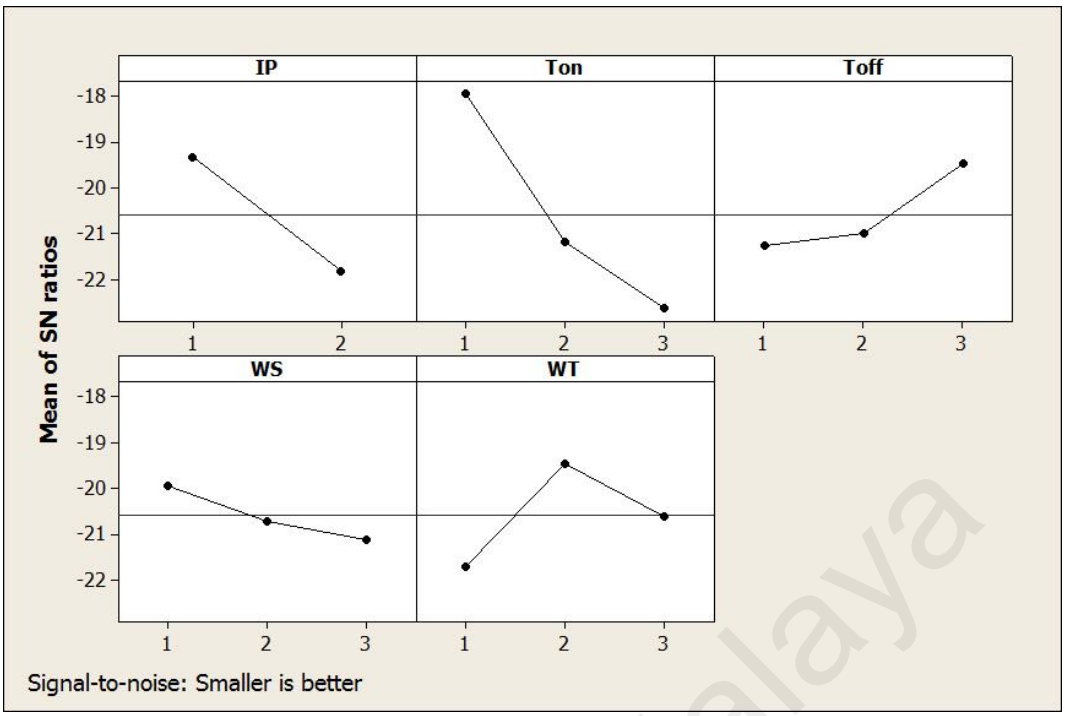

Figure 4.20: Effect of process parameters on WL using coated wire with AISI 1050 steel

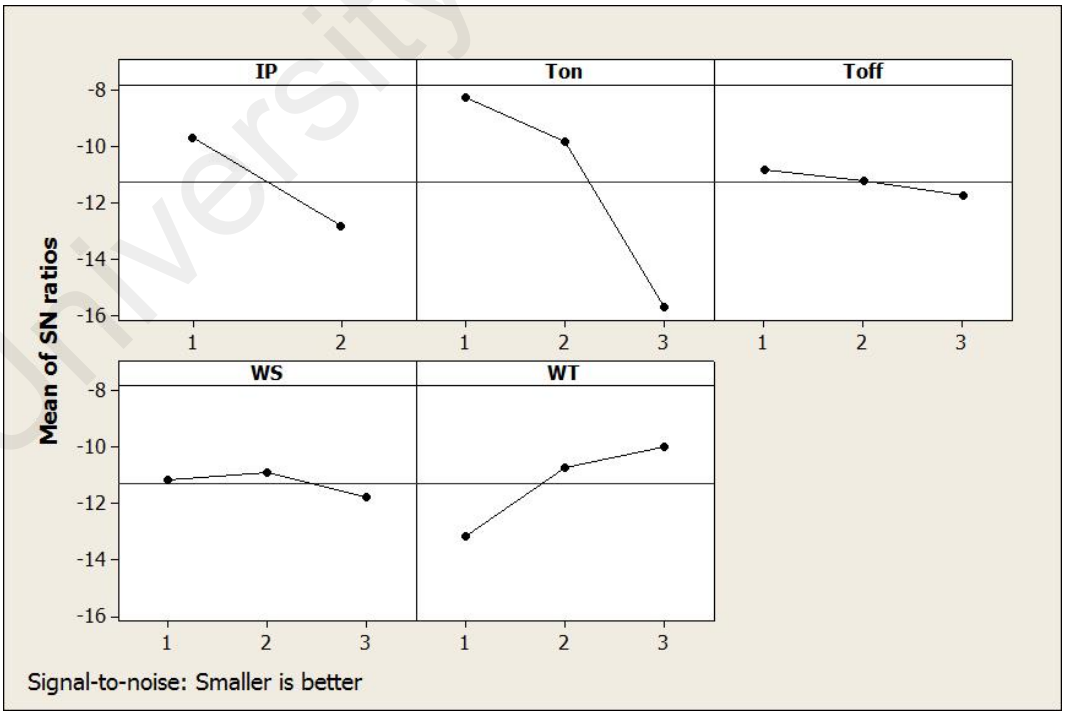

Figure 4.21: Effect of process parameters on WL using coated wire with Ti6Al4V

4.3.2 ANFIS model

ANFIS is a neuro-fuzzy approach, in which a fuzzy inference system employed in the framework of an adaptive neural network. ANFIS can be used to build an input-output mapping based on fuzzy if-then rules as well as preset input-output data pairs for neural network. The membership function parameters were computed by the ANFIS modelling to track the known experimental input-output data (Jang et al., 1997; Zalnezhad, Sarhan, & Hamdi, 2013).

Neuro fuzzy system gathers the benefits of fuzzy systems, which offers an explicit and understandable representation of knowledge. On the other hand, the neural network involves implicit knowledge that is obtained through learning. The fusion of the concepts of fuzzy logic and neural networks may be able to deal with cognitive uncertainties similar to humans. The computational steps involved in the fuzzy neural system are as follows. At first, it builds a fuzzy neuron based on the concept of biological neuronal morphologies, and then it applies a learning mechanism as shown in **Figure 4.22**. This results in three steps in a fuzzy neural process as follows (Fuller, 1995; H. Li, Chen, C. L. P., Huang, H. P., 2001).

- Biological neuron inspired construction of fuzzy neural models,
- The fuzziness introduced in neural network using synaptic connection models,
- Development of learning algorithms (algorithm to update the synaptic weights).

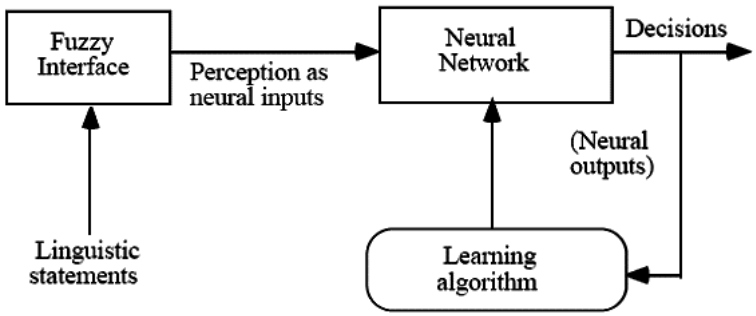

Figure 4.22: Fuzzy-neural system model (Fuller, 1995)

ANFIS was constructed on MATLAB platform, and the training data set had 18 readings for each combination of wire electrode and workpiece as listed in **Table 4.1** to **Table 4.4**. ANFIS was trained using different membership functions. For each wire electrode and workpiece, the ANFIS model was created using two membership functions for the peak current and three membership functions for other parameters (pulse on time, pulse off time, wire speed, and wire tension) as shown in **Figure 4.23**. The generalized bell membership function (gbellmf) yields the minimum training error, which is chosen for training the ANFIS model in this study. The fuzzy rule architecture of the ANFIS involves 18 fuzzy rules produced by the input-output data set following the Sugeno fuzzy model.

ANFIS uses five layers in the network to conduct several steps for fuzzy inference: (1) input parameters, (2) fuzzy set database layer, (3) fuzzy rule base construction, (4) decision-making, and (5) output defuzzification. For a simple interpretation of each input variable, we considered two rules and two linguistic values as shown in **Figure 4.23**.

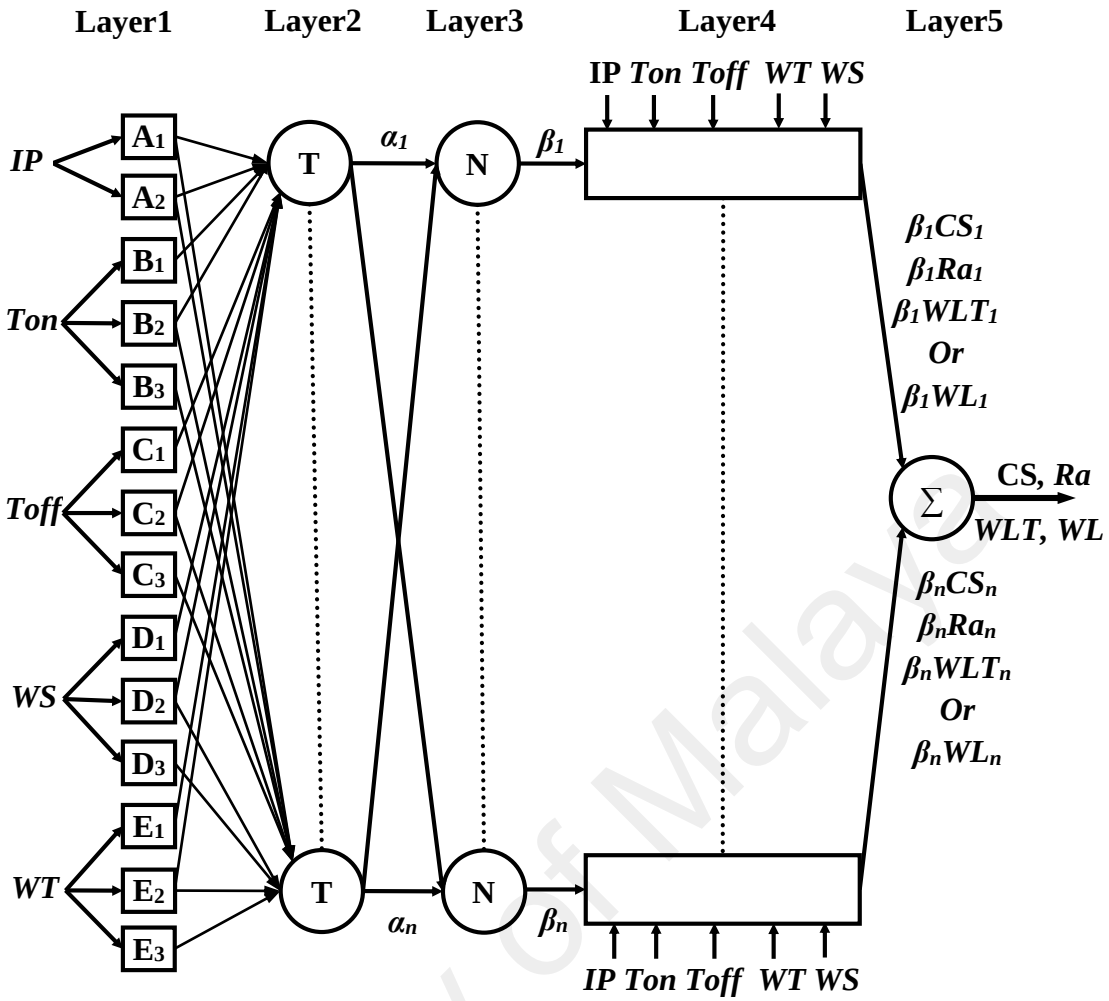

Figure 4.23: ANFIS architecture for a two-input Sugeno fuzzy model.

Layer 1: This layer outputs the degree to which the given input conforms with the linguistic label associated to the node. The linguistic terms are represented using generalized bell-shaped membership functions (gbellmf) because of the non-linear relationship between the cutting parameters and machining performance. Three parameters (***a, b, c***) as shown in **Equations 4.3** to **4.7** specify a generalized bell membership function. Here, the parameter ***b*** is usually positive and used to control the slop of the crossover point. Moreover, parameters ***a*** and ***c*** control the center and width of the membership function.

$$A_i(IP) = \frac{1}{1+\left|\frac{IP-c_{i1}}{a_{i1}}\right|^{2b_{i1}}}, \qquad i = 1, 2 \qquad \textbf{4.3}$$

$$B_i(Ton) = \frac{1}{1+\left|\frac{Ton-c_{i2}}{a_{i2}}\right|^{2b_{i2}}}, \quad i = 1, 2, 3 \qquad 4.4$$

$$C_i(Toff) = \frac{1}{1+\left|\frac{Toff-c_{i3}}{a_{i3}}\right|^{2b_{i3}}}, \quad i = 1, 2, 3 \qquad 4.5$$

$$D_i(WS) = \frac{1}{1+\left|\frac{WS-c_{i4}}{a_{i4}}\right|^{2b_{i4}}}, \quad i = 1, 2, 3 \qquad 4.6$$

$$E_i(WT) = \frac{1}{1+\left|\frac{WT-c_{i5}}{a_{i5}}\right|^{2b_{i5}}}, \quad i = 1, 2, 3 \qquad 4.7$$

Here (a_{i1} - a_{i5}, b_{i1} - b_{i5}, c_{i1} - c_{i5}) are the model parameters.

With the change in the parameter values, the bell-shaped functions differ consequently (**Figure 4.24- 4.28**). **Figure 4.24– 4.28** show the initial and final membership function of peak current, pulse on time, pulse off time, wire speed, and wire tension respectively for the WL using coated wire electrode and Ti6Al4V. This results in multiple forms of membership functions on linguistic labels A_i, B_i, C_i, D_i, and E_i. The parameters of this layer are known as principal parameters.

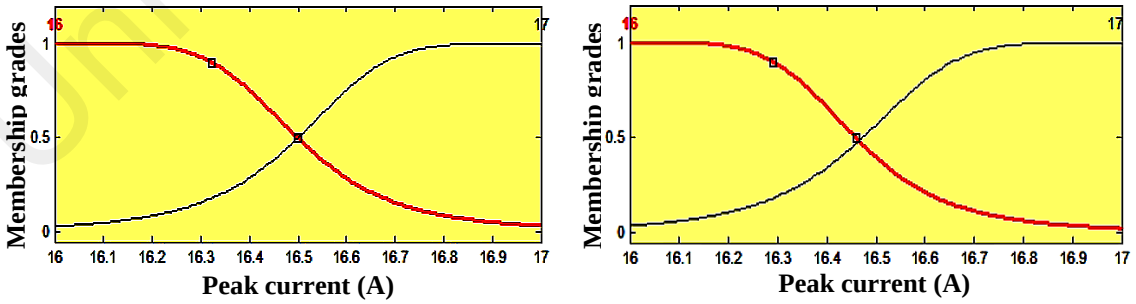

(a) **(b)**

Figure 4.24: (a) Initial and (b) final membership function of peak current

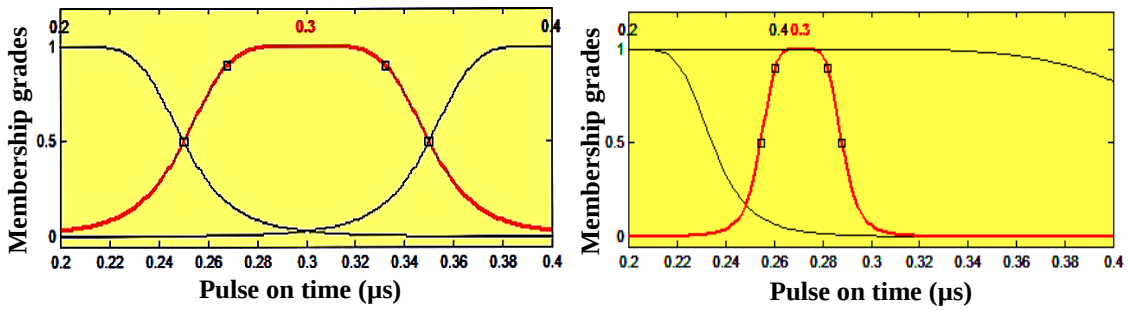

(a) **(b)**

Figure 4.25: (a) Initial and (b) final membership function of pulse on time

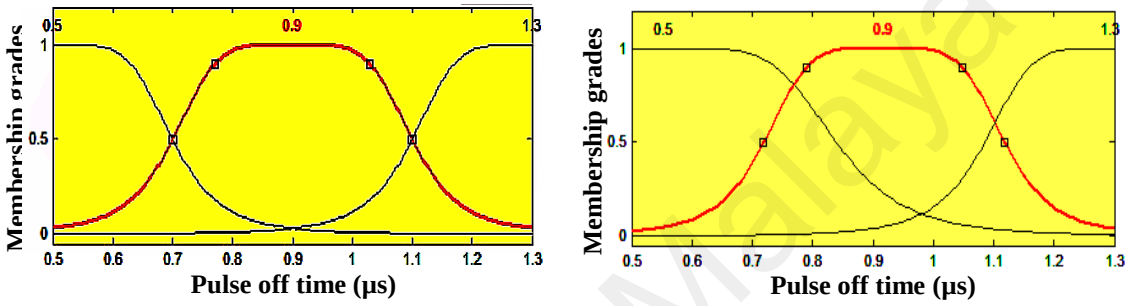

(a) **(b)**

Figure 4.26: (a) Initial and (b) final membership function of pulse off time

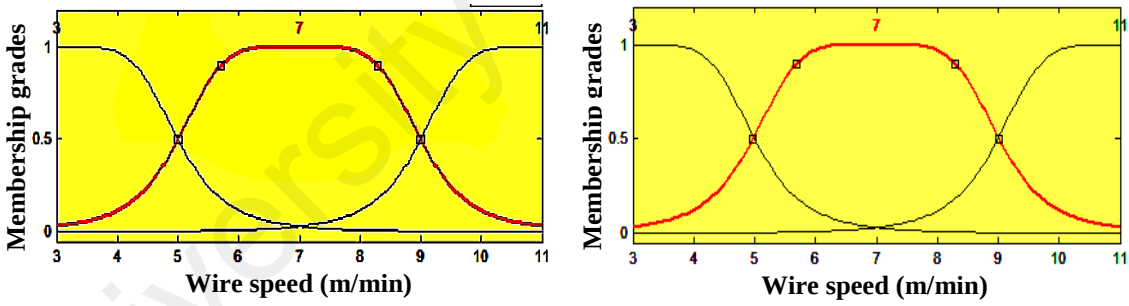

(a) **(b)**

Figure 4.27: (a) Initial and (b) final membership function of wire speed

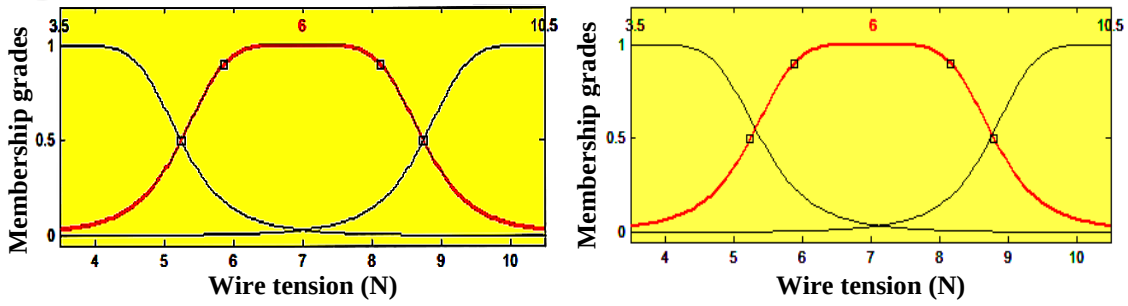

(a) **(b)**

Figure 4.28: (a) Initial and (b) final membership function of wire tension

Layer 2: Each neuron in layer 2 estimates the strength of firing or activating the associated rule. The outputs from the top and bottom nodes are as follows:

$$\begin{cases} \alpha_1 = A_1(IP) \times B_1(Ton) \times C_1(Toff) \times D_1(WS) \times E_1(WT) \\ \alpha_2 = A_1(IP) \times B_1(Ton) \times C_1(Toff) \times D_2(WS) \times E_2(WT) \\ \vdots \\ \alpha_{18} = A_2(IP) \times B_3(Ton) \times C_3(Toff) \times D_2(WS) \times E_1(WT) \end{cases} \quad \textbf{4.8}$$

The two nodes of this layer are labeled by T, because other t-norms are selected to model the logical and operator. These nodes are termed as rule nodes.

Layer 3: Individual neuron of this layer estimates the normalization of the firing levels with respect to the sum of firing levels. The output of the top and bottom neurons are the normalized firing level of the first and second roles respectively.

$$\begin{cases} \beta_1 = \frac{\alpha_1}{\alpha_1+\alpha_2+\cdots+\alpha_{18}} \\ \beta_2 = \frac{\alpha_2}{\alpha_1+\alpha_2+\cdots+\alpha_{18}} \\ \vdots \\ \beta_{18} = \frac{\alpha_{18}}{\alpha_1+\alpha_2+\cdots+\alpha_{18}} \end{cases} \quad \textbf{4.9}$$

Layer 4: Each neuron of this layer estimates the product of the normalized firing levels with the outputs of individual associated rule.

$$\begin{cases} \beta_1 CS_1 = \beta_1(a_1 IP + b_1 Ton + c_1 Toff + d_1 WS + e_1 WT) \\ \beta_2 CS_2 = \beta_2(a_2 IP + b_2 Ton + c_2 Toff + d_2 WS + e_2 WT) \\ \vdots \\ \beta_n CS_n = \beta_n(a_n IP + b_n Ton + c_n Toff + d_n WS + e_n WT) \end{cases} \quad \textbf{4.10}$$

Layer 5: neuron in this layer estimates the total system output by adding all incoming values.

$$CS = \beta_1 CS_1 + \beta_2 CS_2 + \ldots + \beta_n CS_n \quad \textbf{4.11}$$

If a crisp training set ($(IP^k, Ton^k, Toff^k, WS^k, WT^k), k = 1, \ldots, K$) is known, descent type methods can be used to train the parameters of the hybrid neural net. The error function for pattern **k** is given by:

$$E_k = (O^k - Z^k)^2 \qquad \textbf{4.12}$$

where O^k is the desired output and Z^k is the estimated output by the neural network.

The training entails 30 cycles of learning using 18 performance measure values. The learning was conducted with an average error as shown in **Table 4.5.** The small values of the training error indicate that the ANFIS can be used to model the relationship between the machining parameters and the performance outcomes in WEDM.

Table 4.5: Average training error of ANFIS models

Wire and workpiece types	Performance outcomes	Training Error
Brass wire & AISI 1050 carbon steel	CS	1.42×10^{-6}
	Ra	2.69×10^{-6}
	WLT	1.26×10^{-5}
	WL	9.05×10^{-6}
Brass wire & Ti6Al4V	CS	1.51×10^{-6}
	Ra	2.57×10^{-6}
	WLT	1.40×10^{-5}
	WL	6.52×10^{-6}
Coated wire & AISI 1050 carbon steel	CS	2.32×10^{-6}
	Ra	3.87×10^{-6}
	WLT	1.39×10^{-5}
	WL	1.12×10^{-5}
Coated wire & Ti6Al4V	CS	2.30×10^{-6}
	Ra	2.58×10^{-6}
	WLT	1.06×10^{-5}
	WL	4.65×10^{-6}

4.3.3 ANFIS models verification

Four random readings were considered in the testing data set for each wire electrode with different workpiece. The measured *CS*, *Ra*, *WLT*, and *WL* values versus predicted values from the ANFIS model using brass and coated wire electrodes are listed in **Table 4.6** and **4.7** respectively. The plot of four measured values versus predicted values from the ANFIS models are presented in **Figure 4.29 – 4.32**. These figures present a comparison of the measured and predicted performance outcomes of AISI 1050 carbon steel and Ti6Al4V using brass and coated wire electrodes respectively. There are also proper agreements between the experimental and model predicted values. This close agreement clearly shows that the ANFIS models is useful in predicting and optimizing the output performance measures under consideration.

Table 4.6: Comparison of measured *CS*, *Ra*, *WLT*, and *WL* values versus predicted values using brass wire

	AISI 1050 steel					Ti6Al4V			
Machining parameters	**Test No.**	**1**	**2**	**3**	**4**	**1**	**2**	**3**	**4**
	IP (A)	16	16	17	17	16	16	17	17
	Ton (µs)	0.25	0.35	0.25	0.35	0.25	0.35	0.25	0.35
	Toff (µs)	1.1	0.7	1.1	0.7	1.1	0.7	1.1	0.7
	WS (m/min)	5	9	5	9	5	9	5	9
	WT (N)	5	8	5	8	5	8	5	8
CS (mm/min)	**Measured**	1.17	2.13	1.27	2.41	1.38	1.69	1.42	1.28
	Predicted	1.18	2.05	1.34	2.54	1.37	1.78	1.35	2.15
	Error (%)	0.85	3.76	5.51	5.39	0.72	5.33	4.93	5.70
	Average Error (%)				3.88	**Average Error (%)**			4.17
Ra (µs)	**Measured**	2.87	3.51	3.19	3.97	2.54	2.87	2.71	3.04
	Predicted	2.98	3.33	3.03	3.73	2.42	2.76	2.56	2.87
	Error (%)	3.83	5.13	5.02	6.05	4.72	3.83	5.54	5.59
	Average Error (%)				5.01	**Average Error (%)**			4.92
WLT (µs)	**Measured**	12.74	9.88	16.55	14.22	13.01	11.91	15.97	25.13
	Predicted	13.50	10.40	16.40	14.90	12.20	12.30	16.30	26
	Error (%)	5.97	5.26	0.91	4.78	6.23	3.27	2.07	3.46
	Average Error (%)				4.23	Average Error (%)			3.76
WL (mg/m)	**Measured**	10.01	9.81	16.65	13.01	6.23	4.33	8.01	15.32
	Predicted	10.10	10.10	17.60	13.30	5.98	4.20	7.53	15.40
	Error (%)	0.90	2.96	6.99	2.23	4.01	3.00	5.99	0.52
	Average Error (%)				3.27	**Average Error (%)**			3.38

Table 4.7: Comparison of measured CS, Ra, WLT, and WL values versus predicted values using coated wire

		AISI 1050 steel				Ti6Al4V			
Machining parameters	**Test No.**	**1**	**2**	**3**	**4**	**1**	**2**	**3**	**4**
	IP (A)	16	16	17	17	16	16	17	17
	Ton (µs)	0.25	0.35	0.25	0.35	0.25	0.35	0.25	0.35
	Toff (µs)	1.1	0.7	1.1	0.7	1.1	0.7	1.1	0.7
	WS (m/min)	5	9	5	9	5	9	5	9
	WT (N)	5	8	5	8	5	8	5	8
CS (mm/min)	**Measured**	1.74	2.67	1.69	3.11	1.92	2.97	2.15	3.69
	Predicted	1.85	2.74	1.60	2.93	1.93	2.85	2.02	3.78
	Error (%)	6.32	2.62	5.33	5.79	0.52	4.04	6.05	2.44
	Average Error (%)				5.01	**Average Error (%)**			3.26
Ra (µs)	**Measured**	3.01	3.22	3.29	3.41	2.32	2.97	2.45	3.33
	Predicted	3.19	3.37	3.15	3.23	2.20	2.82	2.33	3.18
	Error (%)	5.98	4.66	4.26	5.28	5.17	5.05	4.90	4.50
	Average Error (%)				5.04	**Average Error (%)**			4.91
WLT (µs)	**Measured**	12.47	18.33	11.10	15.00	8.11	13.34	9.03	20.31
	Predicted	12.30	19.40	11.20	14.40	8.53	12.80	9.07	19.50
	Error (%)	1.36	5.84	0.9	4.00	5.18	4.05	0.44	3.99
	Average Error (%)				3.03	**Average Error (%)**			3.41
WL (mg/m)	**Measured**	10.25	13.20	10.66	14.98	5.16	4.11	9.42	8.95
	Predicted	10.30	12.30	10.50	14.60	5.02	4.27	9.57	8.54
	Error (%)	0.49	6.82	1.50	2.54	2.71	3.89	1.59	4.58
	Average Error (%)				2.84	**Average Error (%)**			3.19

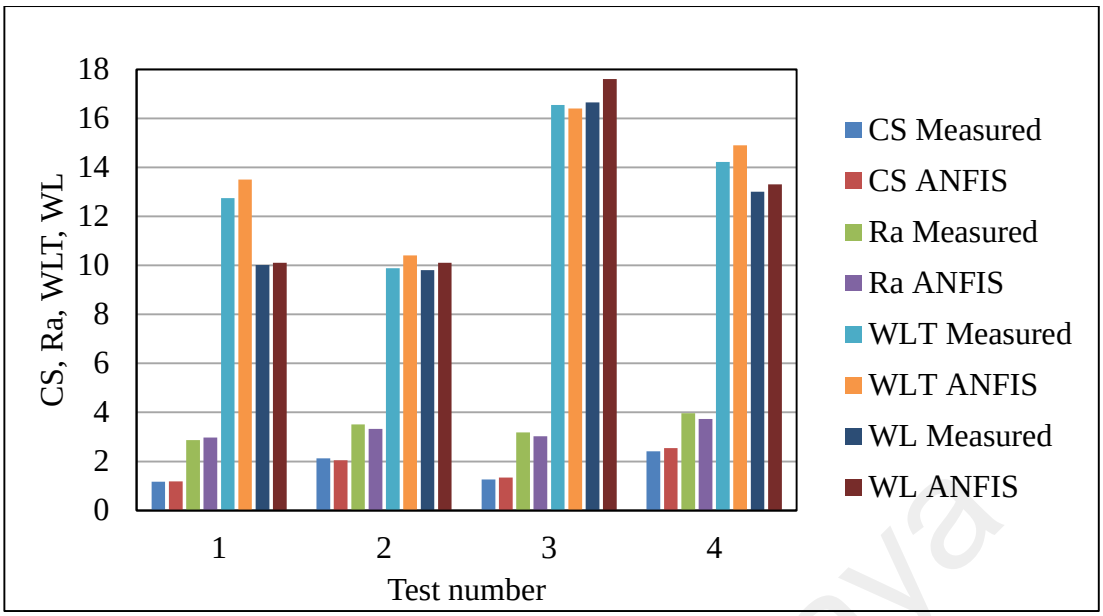

Figure 4.29: Measurement versus predicted CS, Ra, WLT, and WL for AISI 1050 carbon steel using brass wire electrode

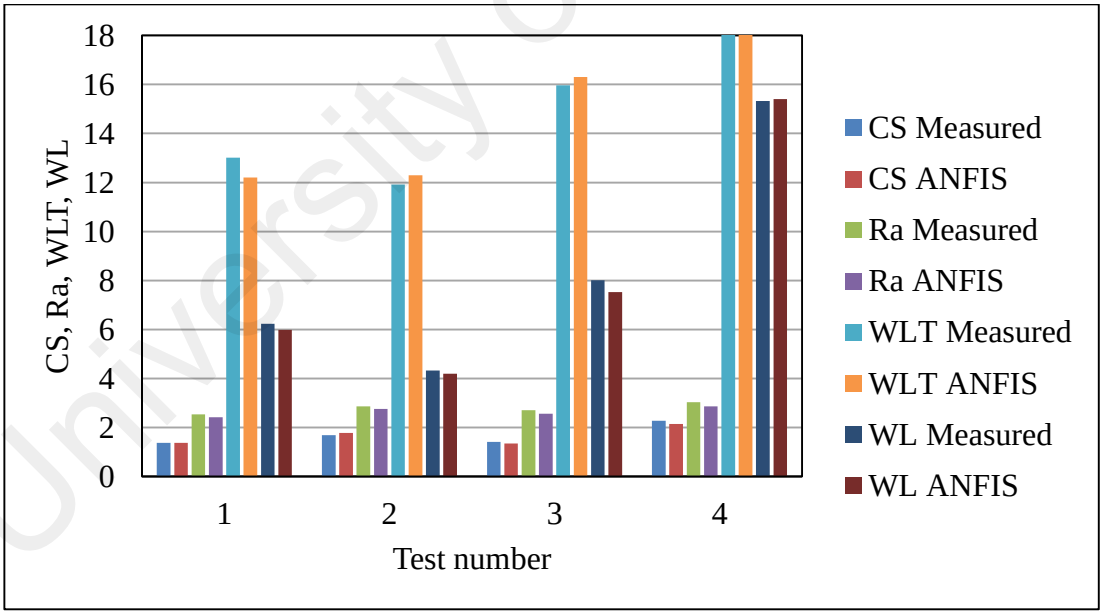

Figure 4.30: Measurement versus predicted CS, Ra, WLT, and WL for Ti6Al4V using brass wire electrode

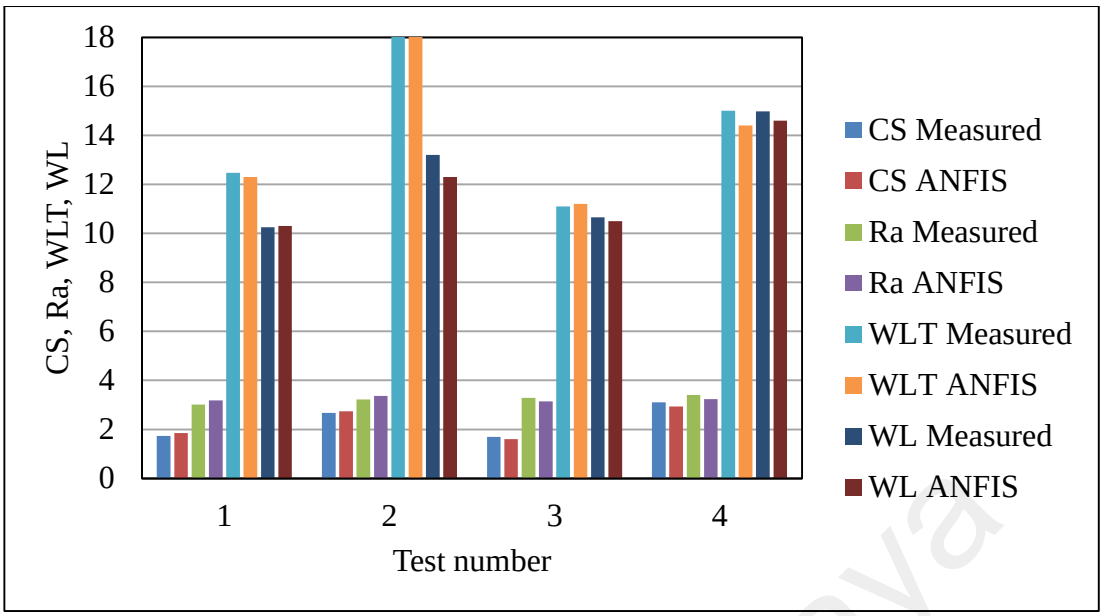

Figure 4.31: Measurement versus predicted CS, Ra, WLT, and WL for AISI 1050 carbon steel using coated wire electrode

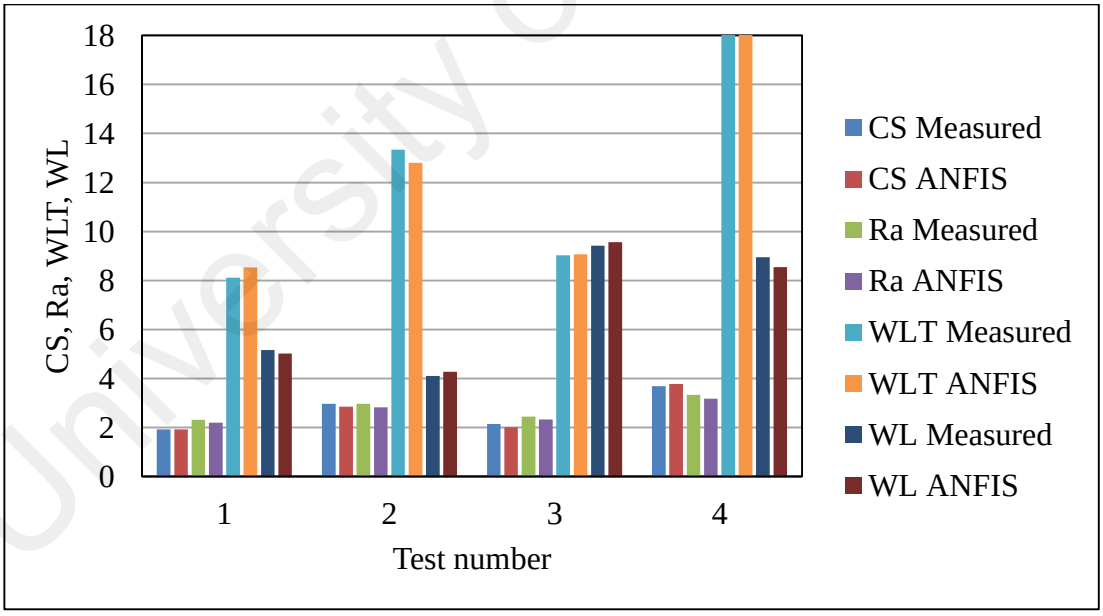

Figure 4.32: Measurement versus predicted CS, Ra, WLT, and WL for Ti6Al4V using coated wire electrode

To evaluate the Fuzzy model, the percentage error E_i and average percentage error E_{av} defined in **Equations (5.13)** and **(5.14)**, respectively, were used.

$$E_i = \frac{|T_m - T_p|}{T_m} \times 100 \qquad \textbf{4.13}$$

$$E_{av} = \frac{1}{m}\sum_{i=1}^{m} E_i \qquad \textbf{4.14}$$

Here E_i represent the percentage error for the sample number i; T_m is the measured value; T_p is the predicted value; i =1,2,3 denotes the sample number; and E_{av} represent the average percentage error of **m** sample data.

The obtained average percentage error for brass and coated wires are introduced in **Table 4.6** and **4.7**. Moreover, **Figure 4.33 – 4.36** show the error value of the testing data. These low error values indicate that the ANFIS predicted performance outcome results are almost similar to the actual measurements from the experiment. The error values suggest that the proposed model can predict and optimize the performance outcomes satisfactorily.

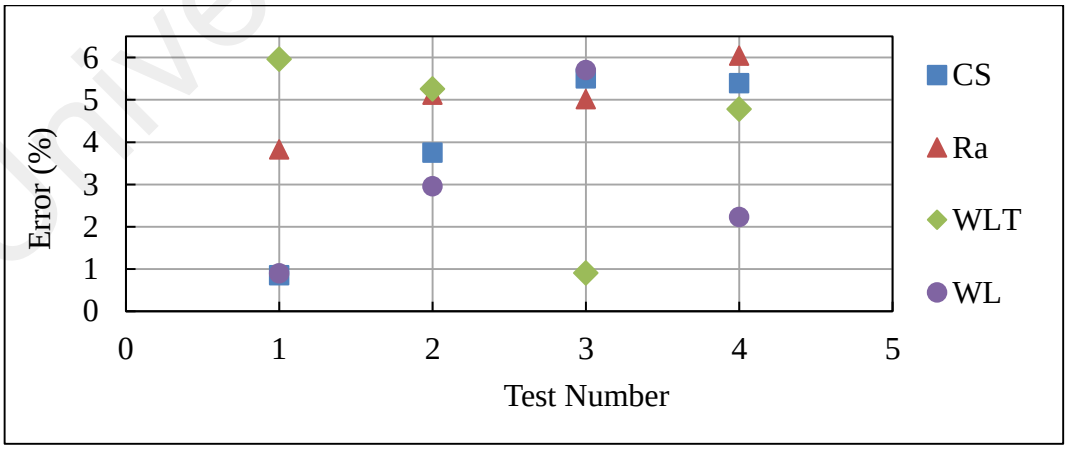

Figure 4.33: The Error percentage of CS, Ra, WLT, and WL for AISI 1050 carbon steel using brass wire electrode

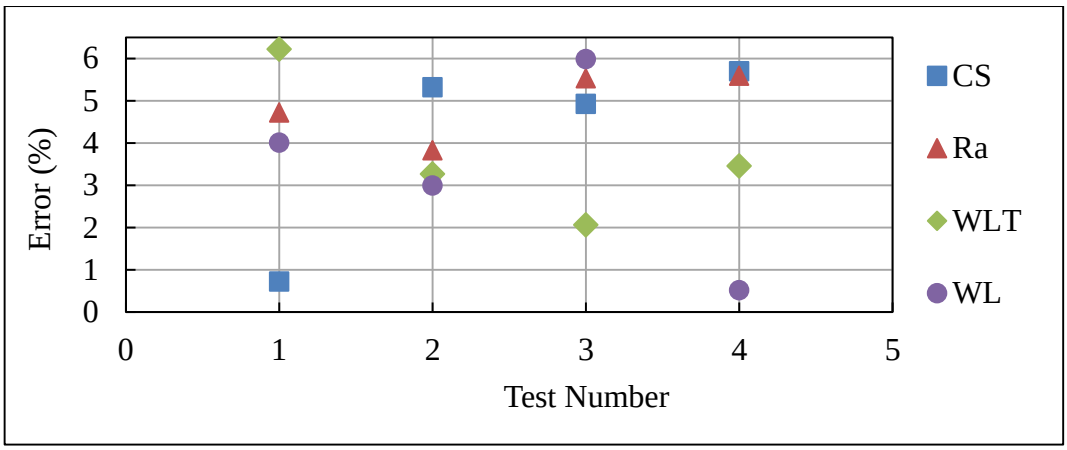

Figure 4.34: The Error percentage of CS, Ra, WLT, and WL for Ti6Al4V using brass wire electrode

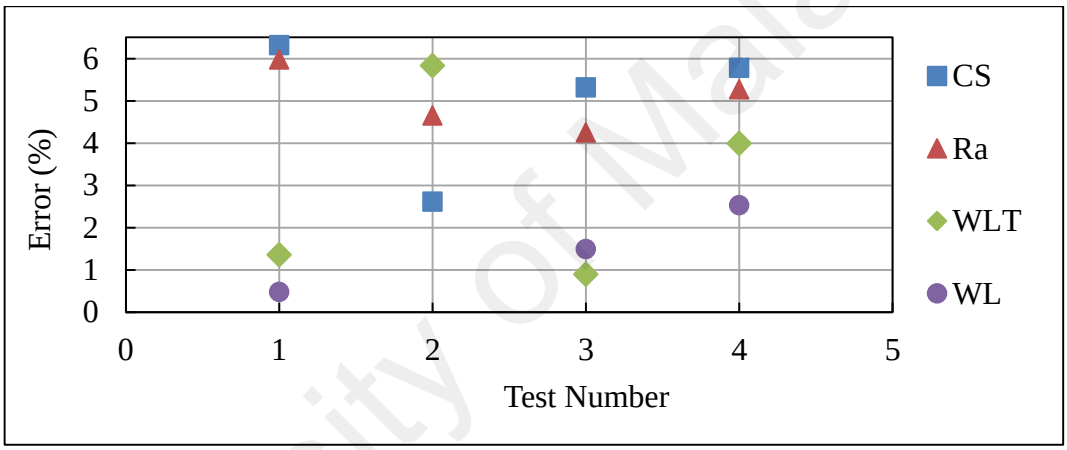

Figure 4.35: The Error percentage of CS, Ra, WLT, and WL for AISI 1050 carbon steel using coated wire electrode

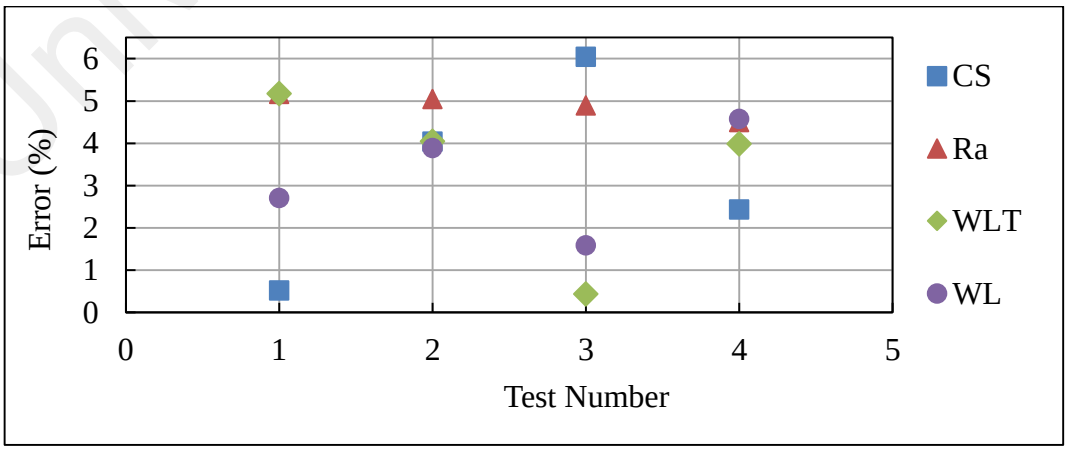

Figure 4.36: The Error percentage of CS, Ra, WLT, and WL for Ti6Al4V using coated wire electrode

4.3.4 ANFIS modeling results and discussion

This section introduces the effects of electrical parameters (pulse on time, peak current, and pulse off time) on the machining performance outcomes (cutting speed, surface roughness, white layer thickness, and wire loss) of AISI 1050 carbon steel and titanium alloy grade 5 using brass and coated-wire electrodes, respectively.

4.3.4.1 Effects of machining parameters on cutting speed

Figure 4.37 – 4.42 introduce the effects of the cutting parameters (*IP, Ton, Toff, WS,* and *WT*) on the cutting speed (*CS*) based on the ANFIS models. **Figure 4.37 – 4.40** show that the cutting speed increased with increasing peak current and pulse on time but decreased with increasing pulse off time for both wire electrodes and workpieces. Moreover, wire speed and tension had a minor effect on cutting speed as shown in **Figure 4.41** and **4.42**. **Figure 4.6 – 4.9** suggest that peak current, pulse width, and pulse off time are more significant for cutting speed. Wire tension and wire speed are not significant to the average S/N ratio for cutting speed. The highest peak current, pulse width and lowest pulse off time appear to be the best choice to obtain a high cutting speed value, thus making the process robust to peak current, pulse width, and pulse off time in particular.

The same conclusions can be drawn from **Figure 4.37 – 4.42,** where pulse width, peak current, and pulse off time had considerable effect on cutting speed, while an increase in both pulse width and/or peak current led to an increase in cutting speed. However, wire tension and wire speed had a minor effect on cutting speed, the same as (Maher, Ling, et al., 2015) obtained. Increasing pulse width and peak current values is recommended for higher productivity. The ANFIS model shows that maximum cutting speed was achieved at the highest peak current and pulse width levels. That is because the combination of pulse width and peak current determines the spark energy (**Equation (4.15))** and hence the quantity of heat required to remove a definite volume of material. By increasing the

pulse width and peak current, a large crater must be cut per spark, as seen in **Figure 4.43 (a)** and **(b)** and in the SEM micrograph (**Figure 4.44 (a)** and **(b)**). **Figure 4.44** displays SEM micrographs of the crater density and depth at extreme peak current and pulse on time levels, which would consequently increase the heat energy, leading to higher cutting speed as seen in **Equation (4.16)** (El-Hofy, 2005).

$$Es = IP \times V \times Ton \qquad \textbf{4.15}$$

$$CS \; \alpha \; Es / (Ton + Toff) \qquad \textbf{4.16}$$

Where ***V*** is the spark gab set voltage

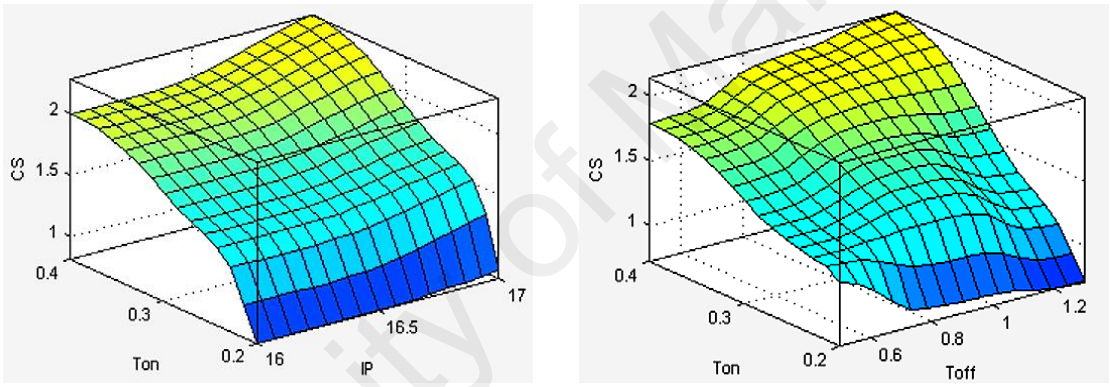

(a) **(b)**

Figure 4.37: ANFIS model of CS in relation to change of (a) *IP*, *Ton*, and (b) Ton, *Toff* for AISI 1050 carbon steel using brass wire electrode

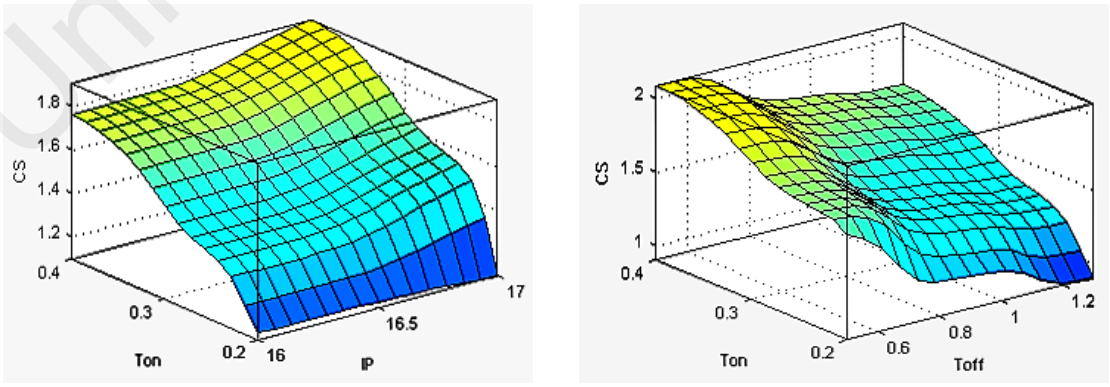

(a) **(b)**

Figure 4.38: ANFIS model of CS in relation to change of (a) *IP*, *Ton*, and (b) Ton, *Toff* for Ti6Al4V using brass wire electrode

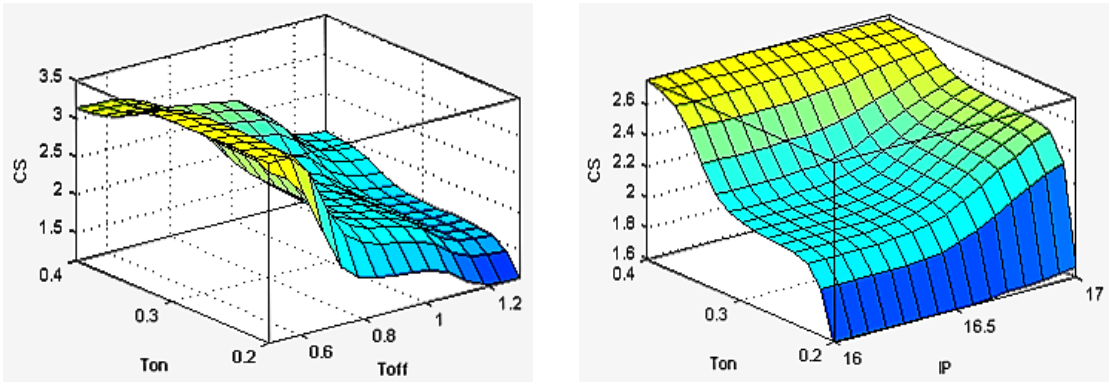

(a) **(b)**

Figure 4.39: ANFIS model of CS in relation to change of (a) *Ton*, *Toff*, and (b) Ton, *IP* for AISI 1050 carbon steel using coated wire electrode

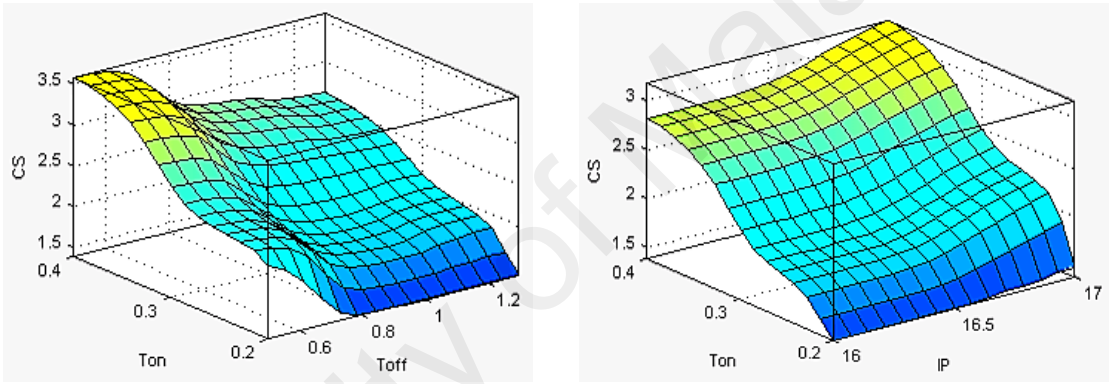

(a) **(b)**

Figure 4.40: ANFIS model of CS in relation to change of (a) *Ton*, *Toff*, and (b) *Ton*, *IP* for Ti6Al4V using coated wire electrode

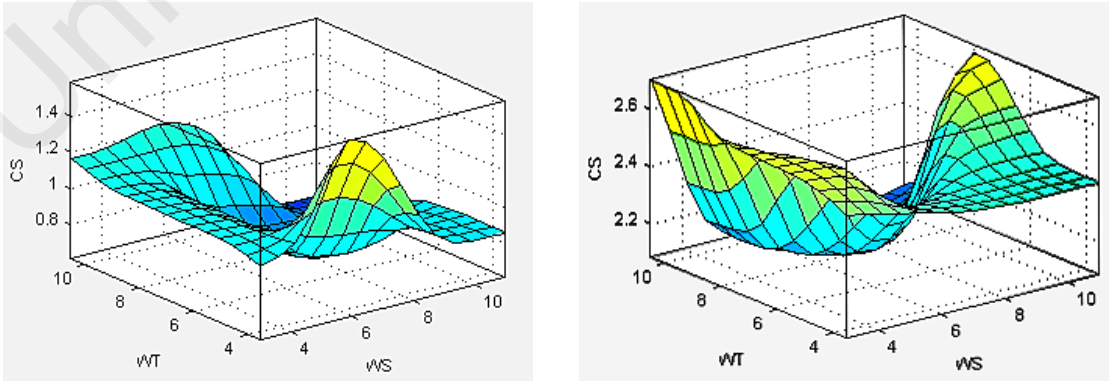

(a) **(b)**

Figure 4.41: ANFIS model of CS in relation to change of *WS* and *WT* for AISI 1050 carbon steel using (a) brass wire (b) coated wire

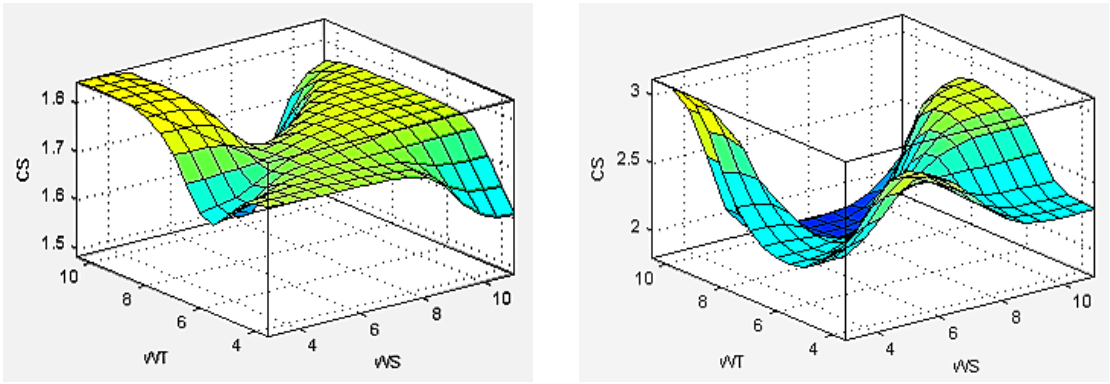

(a) **(b)**

Figure 4.42: ANFIS model of CS in relation to change of *WS* and *WT* for Ti6Al4V using (a) brass wire (b) coated wire

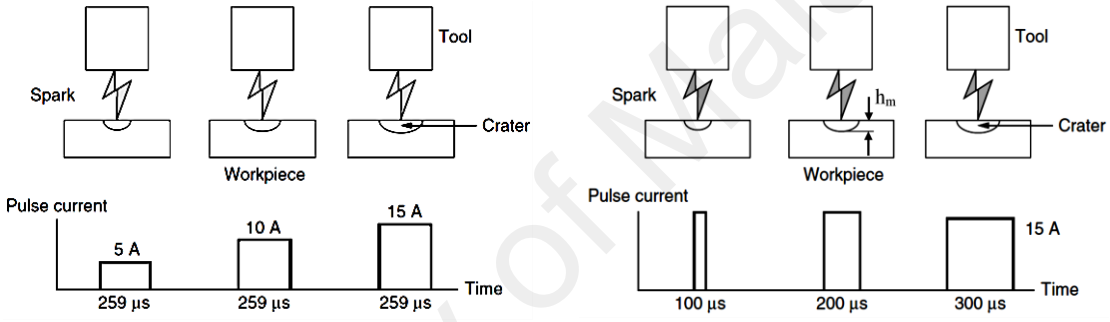

(a) **(b)**

Figure 4.43: Removal rate and surface roughness in relation to change of (a) peak current (b) pulse on time

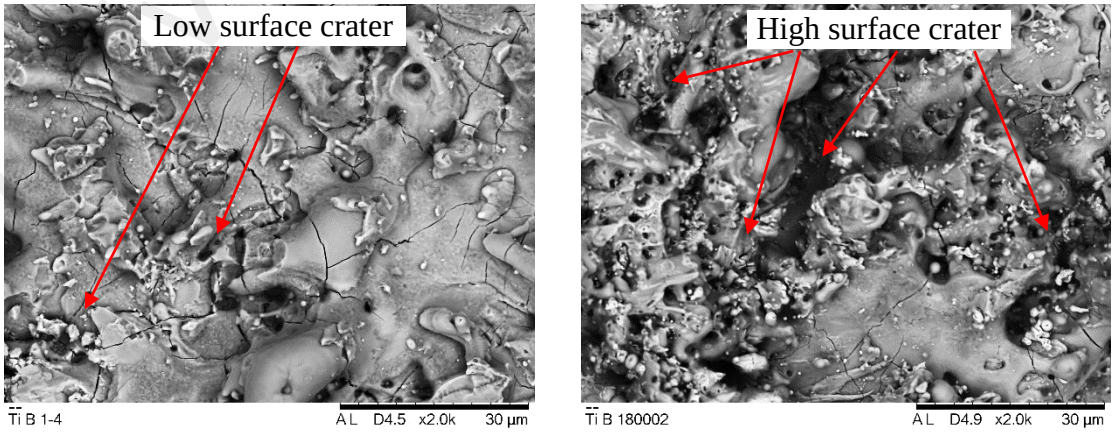

(a) **(b)**

Figure 4.44: SEM micrograph of the surface at different levels of spark energy (a) at the lowest levels of IP and Ton (b) at the highest levels of IP and Ton

4.3.4.2 Effects of machining parameters on surface roughness

Figure 4.45 – 4.50 introduce the effects of the cutting parameters on the surface roughness of AISI 1050 carbon steel and Ti6Al4V based on the ANFIS models of brass and coated-wire electrodes. **Figure 4.45 – 4.48** demonstrate that peak current, pulse on time, and pulse off time greatly affected surface roughness, which increased with increasing pulse on time and peak current but decreased with increasing pulse off time. Moreover, wire speed and wire tension had a small effect on surface roughness, as shown in **Figure 4.49** and **4.50**.

Figure 4.10 – 4.13 indicate the same findings that pulse width and peak current were more significant, followed by pulse off time, to the average S/N ratio for surface roughness; however, there were minor changes as wire speed and wire tension increased. The lowest pulse width and peak current values and the highest pulse off time value are the best choices for attaining low surface roughness. SEM micrographs of the machined surfaces at 3000X magnification with the lowest and highest levels of peak current and pulse width are illustrated in **Figure 4.51 (a) and (b)** respectively. According to the SEM micrographs, the cavity and redeposited particles with the highest peak current and pulse width were higher than the lowest peak current and pulse width. This is because the discharge energy increased with peak current and pulse width. Hence, larger craters were produced, leading to greater workpiece surface roughness (Kumar & Agarwal, 2012). This is proven by the theory displayed in **Figure 4.43 (a)** and **(b)** and **Equation (4.17)** (El-Hofy, 2005).

$$h_m \, \alpha \, (Es)^{1/3} \qquad \textbf{4.17}$$

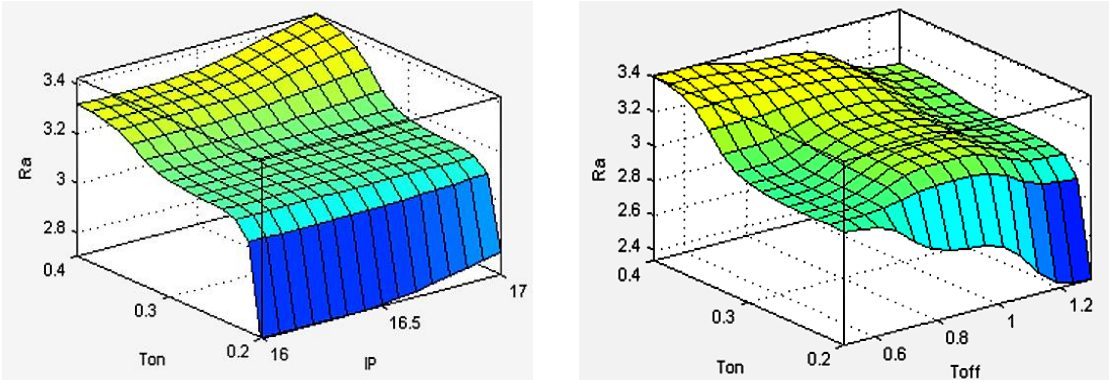

(a) **(b)**

Figure 4.45: ANFIS model of Ra in relation to change of (a) Ton, IP, and (b) Ton, Toff using brass wire electrode with AISI 1050 carbon steel

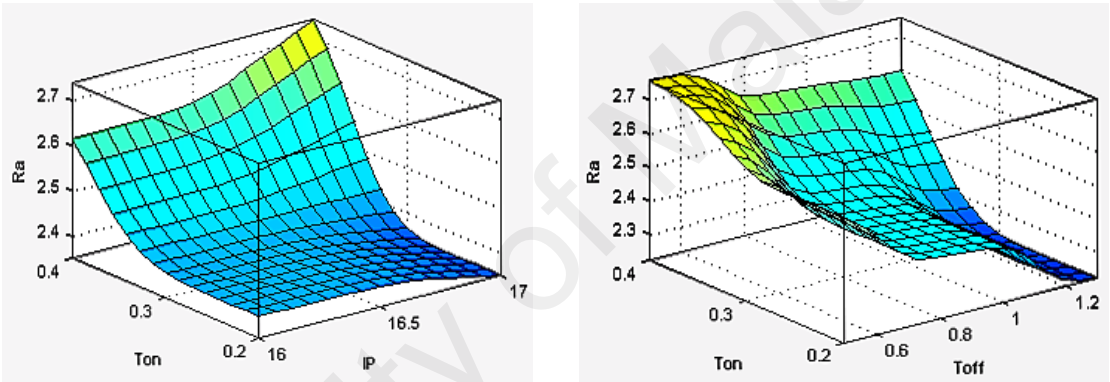

(a) **(b)**

Figure 4.46: ANFIS model of Ra in relation to change of (a) Ton, IP, and (b) Ton, Toff using brass wire electrode with Ti6Al4V

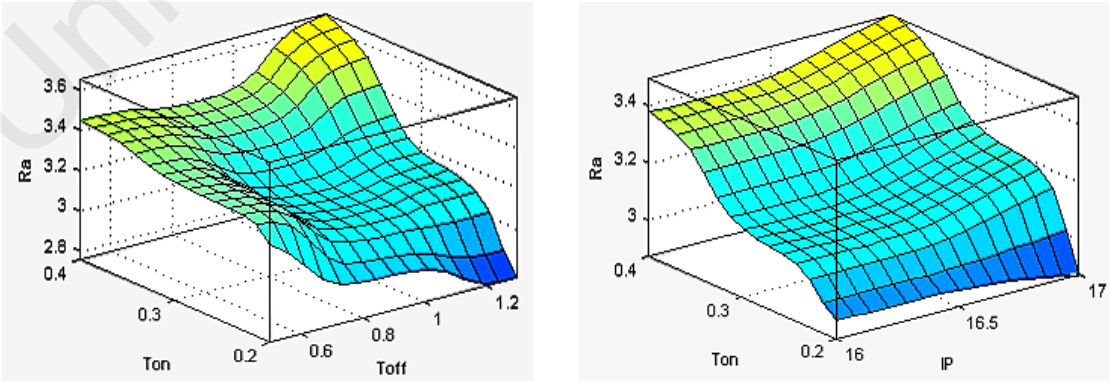

(a) **(b)**

Figure 4.47: ANFIS model of Ra in relation to change of (a) Ton, Toff, and (b) Ton, IP using coated wire electrode with AISI 1050 carbon steel

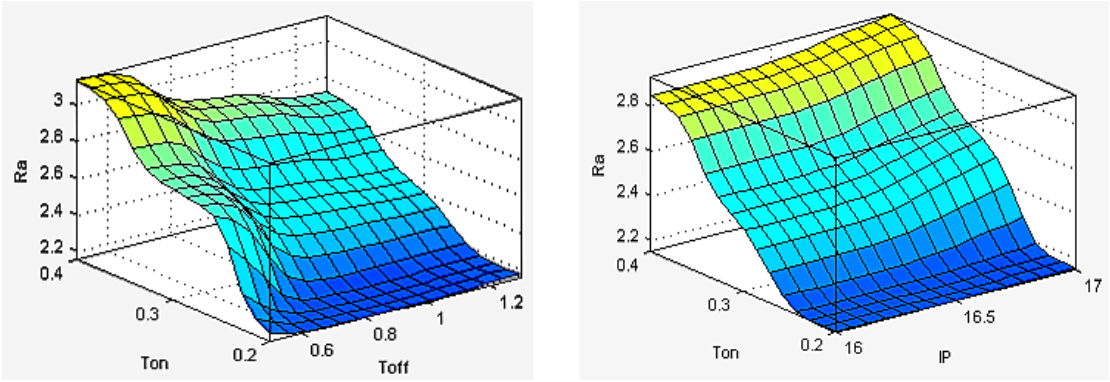

(a) **(b)**

Figure 4.48: ANFIS model of Ra in relation to change of (a) Ton, Toff, and (b) Ton, IP using coated wire electrode with Ti6Al4V

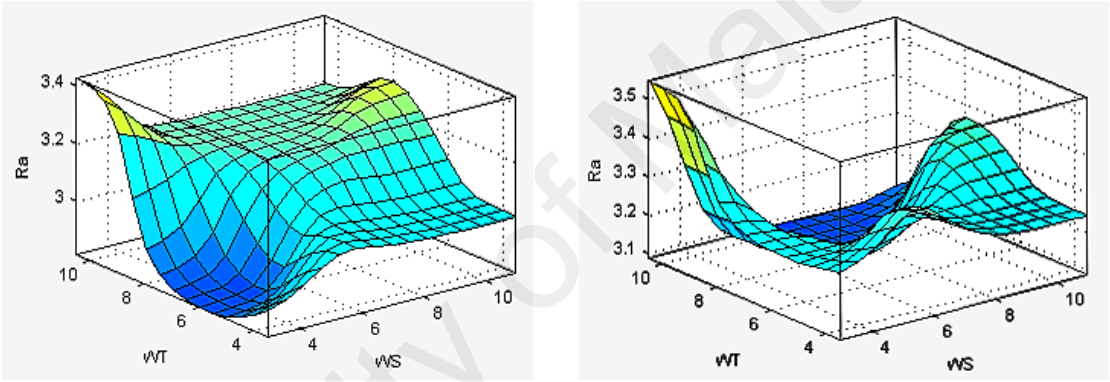

(a) **(b)**

Figure 4.49: ANFIS model of Ra in relation to change of *WS* and *WT* for AISI 1050 carbon steel using (a) brass wire (b) coated wire

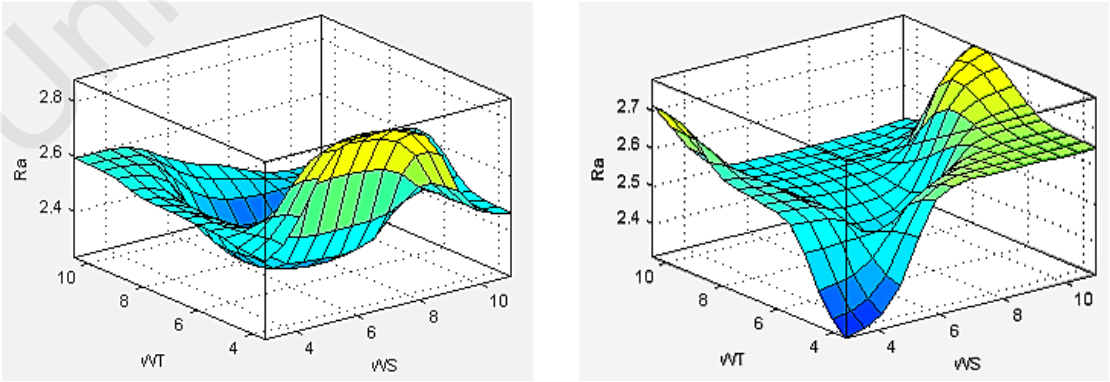

(a) **(b)**

Figure 4.50: ANFIS model of Ra in relation to change of *WS* and *WT* for Ti6Al4V using (a) brass wire (b) coated wire

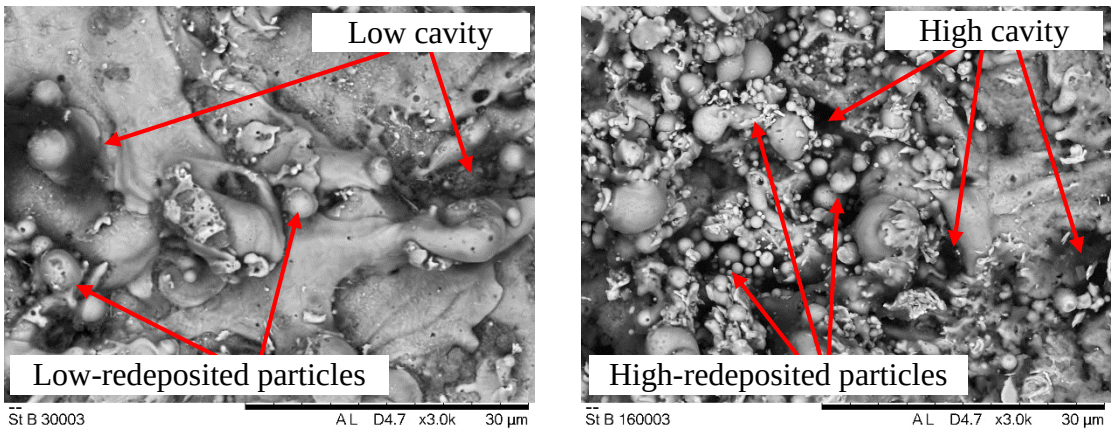

(a) **(b)**

Figure 4.51: SEM micrograph of the surface at different levels of spark energy (a) at the lowest levels of peak current (IP=16A) and pulse on time (Ton=0.2µs) (b) at the highest levels of peak current (IP=17A) and pulse on time (Ton=0.4µs)

4.3.4.3 Effects of machining parameters on white layer thickness

Based on ANFIS models (**Figure 4.52 – 4.57**), pulse on time, pulse off time, and peak current greatly affected white layer thickness but wire speed and wire tension had a minor effect. An increase in both pulse on time and/or peak current led to an increase in white layer thickness. However, the increase in pulse off time led to a decrease in white layer thickness (**Figure 4.52 – 4.55**). In addition, a study of **Figure 4.14 – 4.17** suggests that pulse width, pulse off time, and peak current were more significant, and wire speed and wire tension were insignificant to the average S/N response of white layer thickness. The smallest peak current and pulse width values and the largest pulse off time value appeared to be the best choices for obtaining a thinner white layer.

The same conclusion is obtained from the experimental work represented in **Figure 4.58 (a) and (b)**. **Figure 4.58 (a) and (b)** which introduce SEM micrographs of the white layer thickness at different spark energy levels. These micrographs verify that the maximum width of the white layer thickness was obtained at the highest peak current and pulse width values and the smallest white layer thickness was achieved at the lowest pulse

width and peak current values. This is because the heat energy increased with peak current and pulse width. Hence, more heat was produced on the machined surface that led to a thicker white layer on the workpiece (Saha, Singha, Pal, & Saha, 2008).

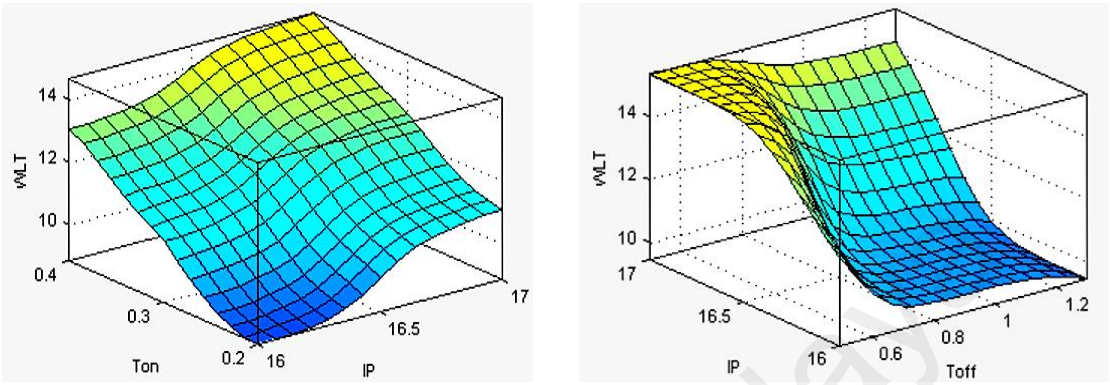

(a) **(b)**

Figure 4.52: ANFIS model of WLT in relation to change of (a) IP, Ton, and (b) IP, Toff using brass wire electrode with AISI 1050 carbon steel

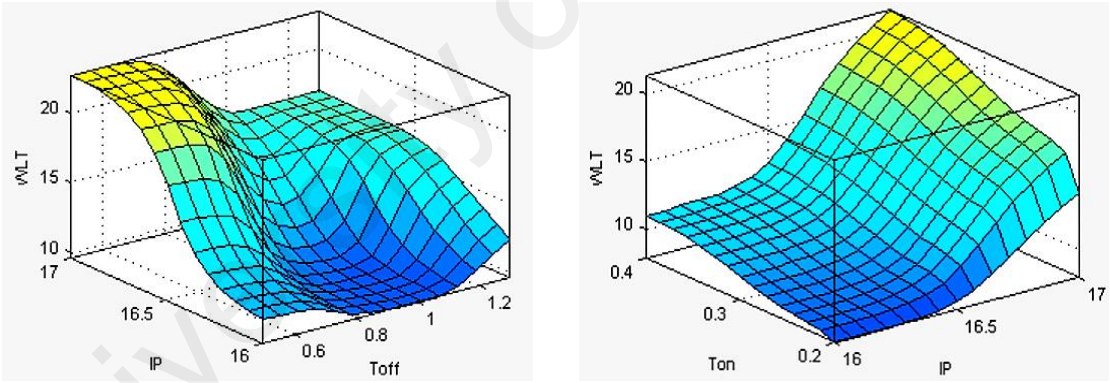

(a) **(b)**

Figure 4.53: ANFIS model of WLT in relation to change of (a) IP, Toff, and (b) Ton, IP using brass wire electrode with Ti6Al4V

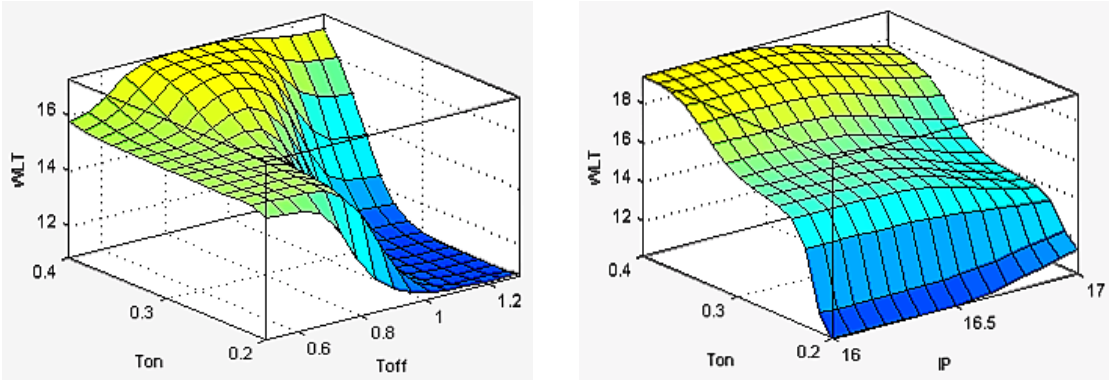

(a) **(b)**

Figure 4.54: ANFIS model of WLT in relation to change of (a) Ton, Toff, and (b) Ton, IP using coated wire electrode with AISI 1050 carbon steel

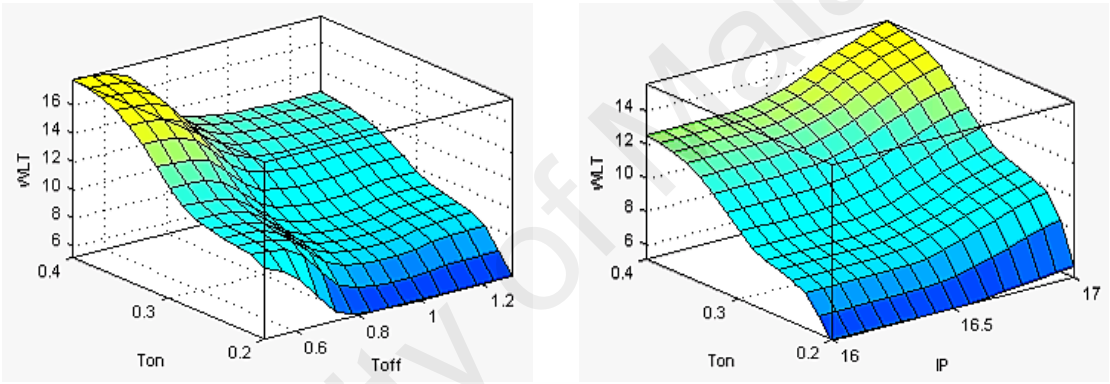

(a) **(b)**

Figure 4.55: ANFIS model of WLT in relation to change of (a) Ton, Toff, and (b) Ton, IP using coated wire electrode with Ti6Al4V

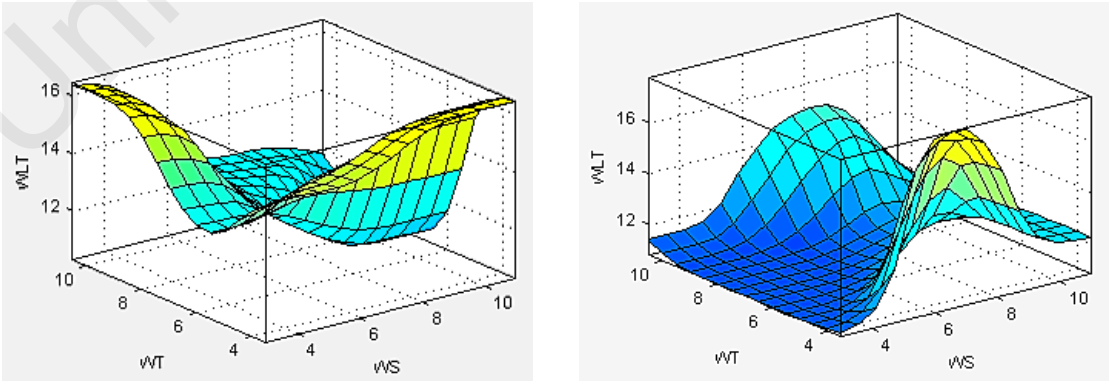

(a) **(b)**

Figure 4.56: ANFIS model of WLT in relation to change of *WS* and *WT* for AISI 1050 carbon steel using (a) brass wire (b) coated wire

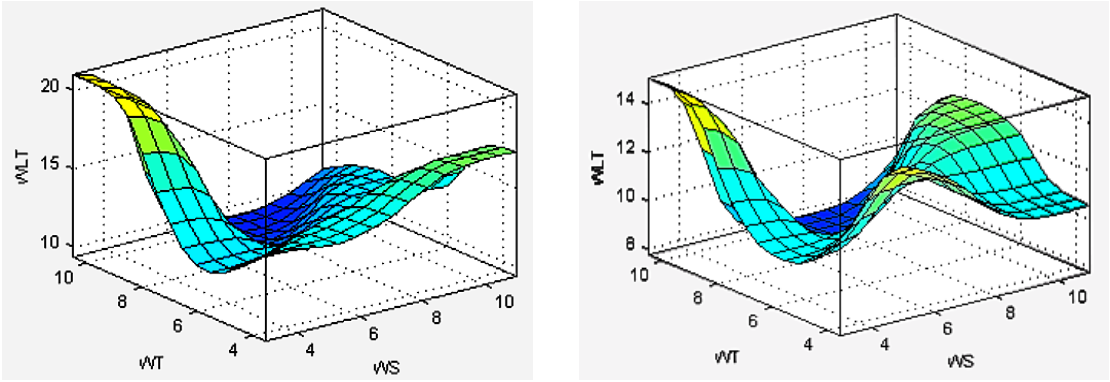

(a) **(b)**

Figure 4.57: ANFIS model of WLT in relation to change of *WS* and *WT* for Ti6Al4V using (a) brass wire (b) coated wire

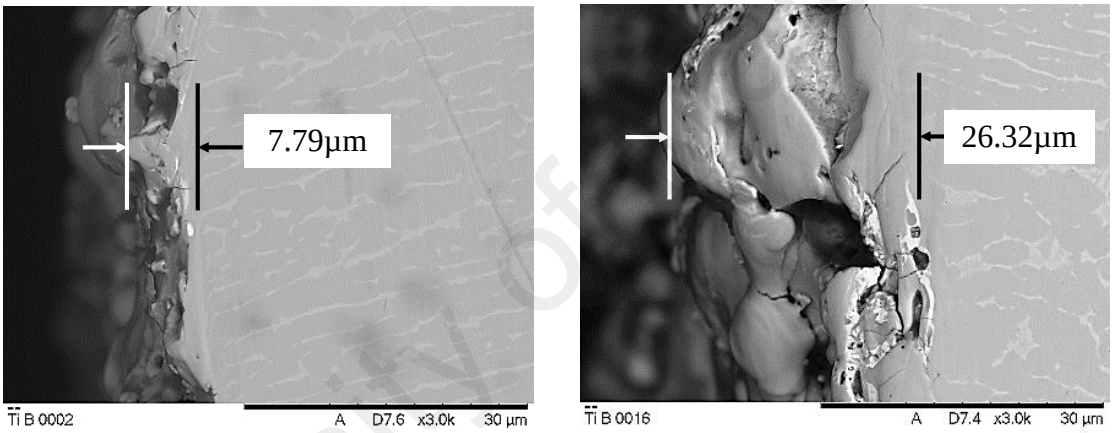

(a) **(b)**

Figure 4.58: SEM micrograph of the WLT at different levels of spark energy (a) at the lowest levels of peak current (IP=16A) and pulse on time (Ton=0.2µs) (b) at the highest levels of peak current (IP=17A) and pulse on time (Ton=0.4µs)

Moreover, the type of wire electrode had a considerable impact on maintaining surface integrity. **Figure 4.59 (a)** and **(b)** show surface micrographs of using brass and coated-wire electrodes respectively, at the same machining parameters. In addition, **Figure 4.60 (a)** and **(b)** display the WLT of using brass and coated-wire electrodes respectively, at the same machining parameters. It is evident from **Figure 4.59** that the surface finish achieved using a coated wire is better than using a brass wire electrode. Moreover, the WLT obtained using the coated wire (**Figure 4.60 (b)**) is smaller than that using a brass wire (**Figure 4.60 (a)**).

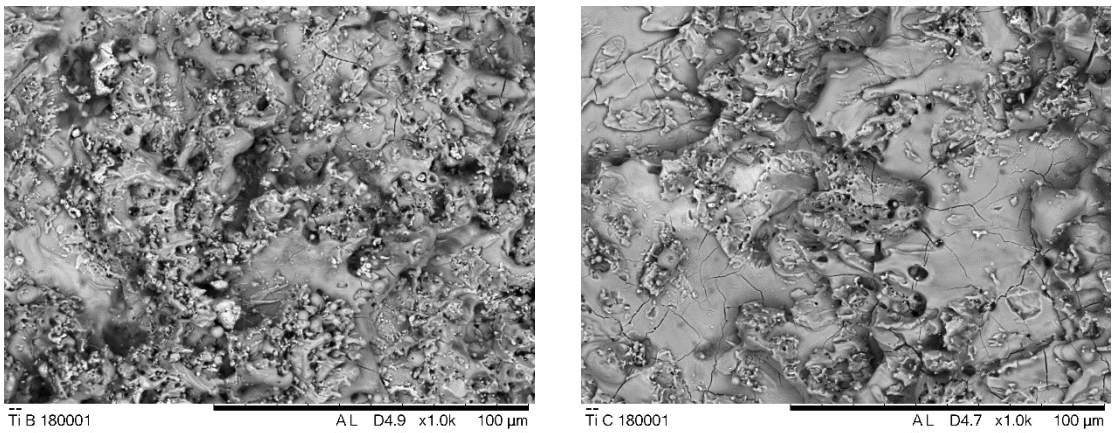

(a) **(b)**

Figure 4.59: SEM micrograph of Ti6Al4V surface using (a) brass wire (b) coated wire

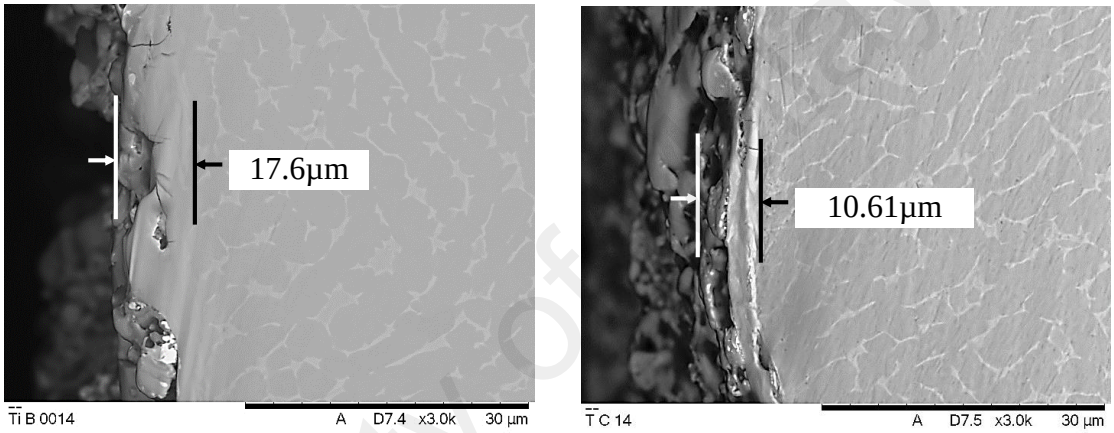

(a) **(b)**

Figure 4.60: SEM micrograph of Ti6Al4V WLT using (a) brass wire electrode (b) coated wire electrode

The thermal conductivity of the work metal has a vital role in the surface integrity achieved with WEDM. Metals with high thermal conductivity usually yield thinner white layers and less micro-cracking than lower conductivity materials. This is owing to more energy dissipation over the surface of higher conductivity materials. In the experimental work, AISI 1050 carbon steel had a thinner white layer with fewer cracks due to its high thermal conductivity and ductile nature compared to titanium alloy grade 5 (Ti6Al4V) as shown in **Figure 4.61 and 4.62**. **Figure 4.61 (a)** and **(b)** present SEM micrographs of the white layer of Ti6Al4V and AISI 1050 carbon steel respectively, at the same machining conditions (IP=17 A, Ton= 0.3 µs, Toff=1.3 µs, WS=7 m/min, WT=3.5 N) using a brass

wire electrode. The WLT of Ti6Al4V workpiece was 15.61µm and of AISI 1050 carbon steel 10.73 µm. **Figure 4.62 (a)** and **(b)** introduce the SEM micrographs of Ti6Al4V and AISI 1050 carbon steel surfaces respectively at the same machining conditions (IP=16A, Ton= 0.2µs, Toff=0.5µs, WS= 3m/min, WT=3.5N) using a brass wire electrode. There are many more Ti6Al4V surface cracks than AISI 1050 carbon steel. In contrast, a material with low thermal conductivity cannot act fast enough to dissipate energy to neighboring areas as shown in **Figure 4.61 and 4.62**. This allows the spark energy to stay for a longer time, resulting in a thicker white layer with more crack formation.

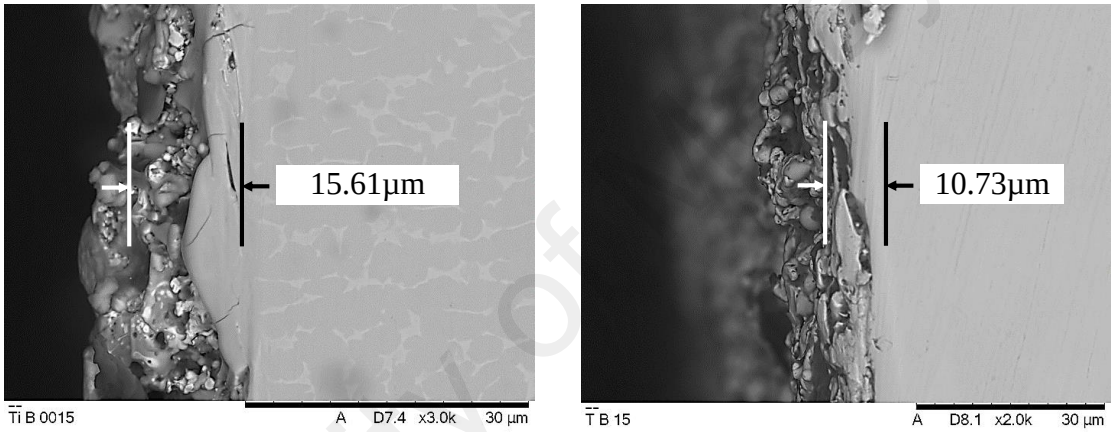

(a) **(b)**

Figure 4.61: SEM micrograph of cross section illustrating the thickness and micro-cracks of the white layer for (a) Ti6Al4V (b) AISI 1050 carbon steel.

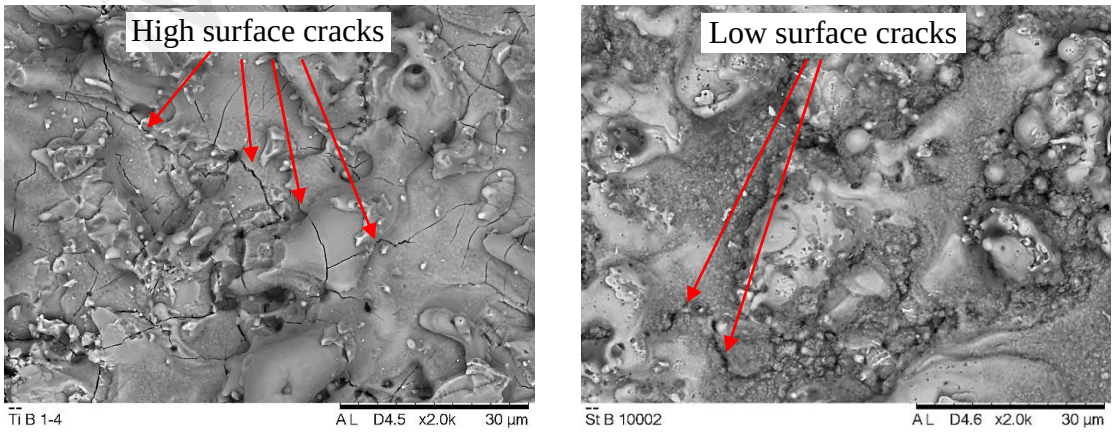

(a) **(b)**

Figure 4.62: SEM micrograph illustrating the surface finish and micro-cracks of the white layer for (a) Ti6Al4V (b) AISI 1050 carbon steel.

4.3.4.4 Effects of machining parameters on wire rupture

Figure 4.63 – 4.68 introduce the effects of the machining parameters on *WL* based on the ANFIS models of AISI 1050 carbon steel and Ti6Al4V using brass and coated-wire electrodes. **Figure 4.63 – 4.68** indicate that peak current, pulse on time, and pulse off time significantly affected wire loss, which increased with increasing peak current and pulse on time but decreased with increasing pulse off time. Moreover, wire speed and wire tension had a considerable effect on wire loss, which increased with increasing wire tension and decreasing wire speed. The reason is that the combination of pulse width and peak current determined the spark energy and hence the quantity of heat required to remove a definite volume of material. By increasing the pulse width and peak current, a large crater must be cut per spark from the wire electrode, as shown in **Figure 4.43 (a)** and **(b)** and in the SEM micrograph (**Figure 4.69** and **(4.70)**). **Figure 4.69** and **(4.70)** show SEM micrographs of the crater density and depth at extreme levels of peak current and pulse on time for brass and coated-wire electrodes respectively.

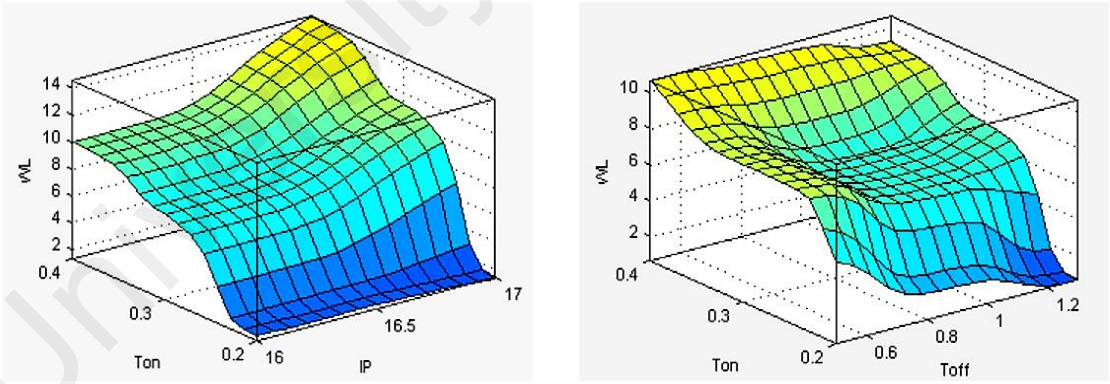

(a) **(b)**

Figure 4.63: ANFIS model of WL in relation to change of (a) IP, Ton, and (b) Ton, Toff using brass wire electrode with AISI 1050 carbon steel

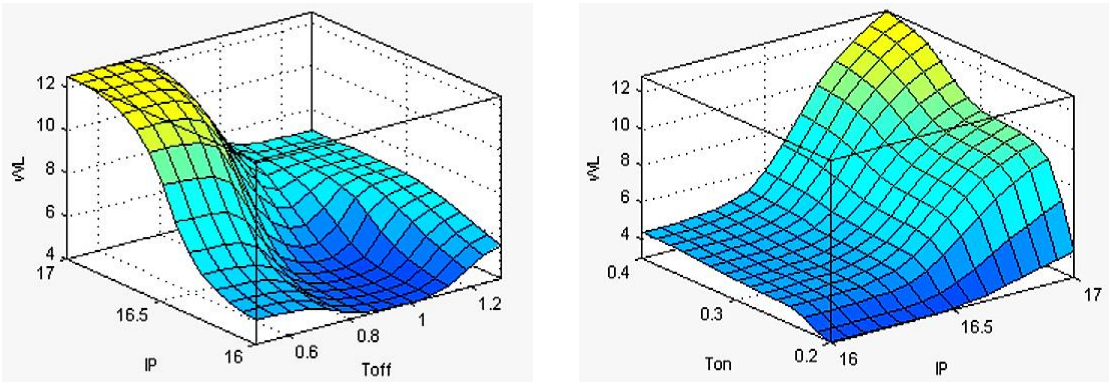

(a) **(b)**

Figure 4.64: ANFIS model of WL in relation to change of (a) IP, Toff, and (b) Ton, IP using brass wire electrode with Ti6Al4V

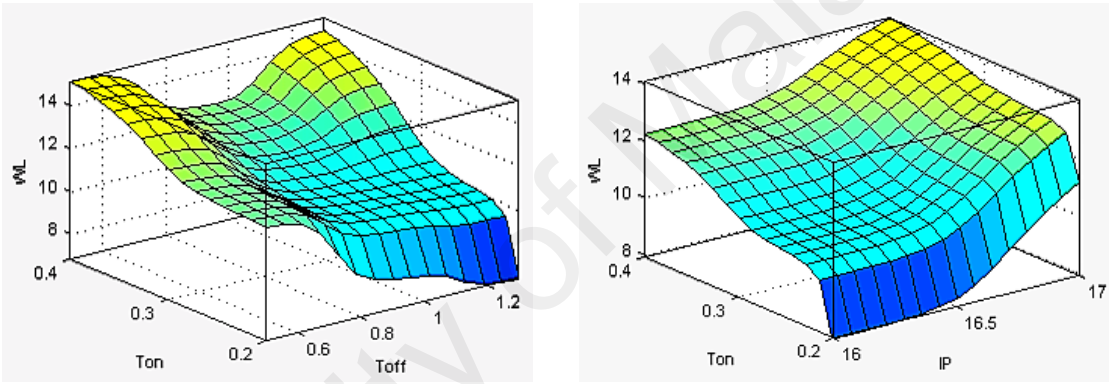

(a) **(b)**

Figure 4.65: ANFIS model of WL in relation to change of (a) Ton, Toff, and (b) Ton, IP using coated wire electrode with AISI 1050 carbon steel

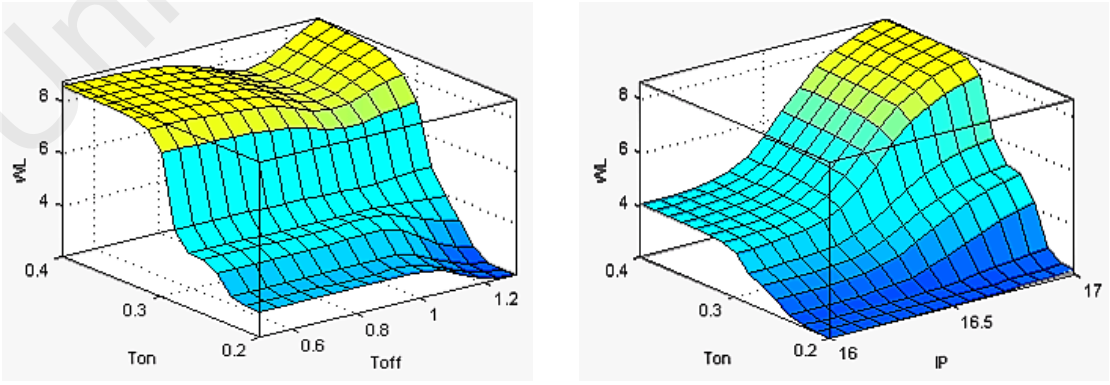

(a) **(b)**

Figure 4.66: ANFIS model of WL in relation to change of (a) Ton, Toff, and (b) Ton, IP using coated wire electrode with Ti6Al4V

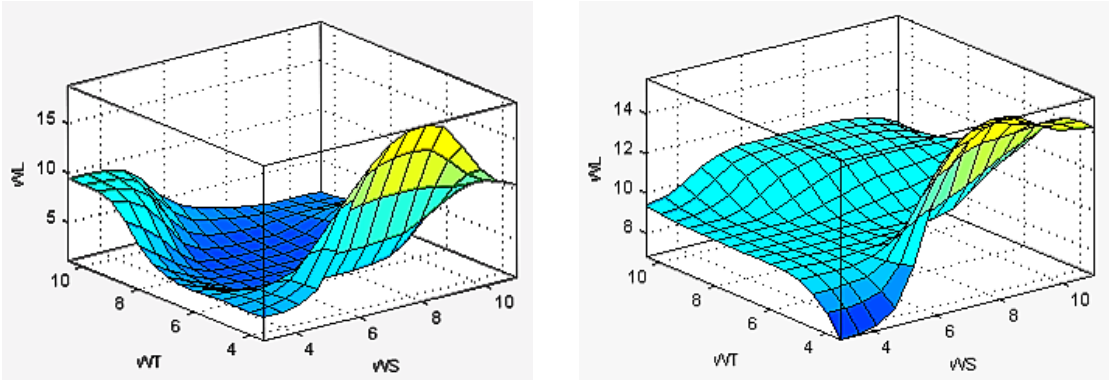

(a) **(b)**

Figure 4.67: ANFIS model of Ra in relation to change of *WS* and *WT* for AISI 1050 carbon steel using (a) brass wire (b) coated wire

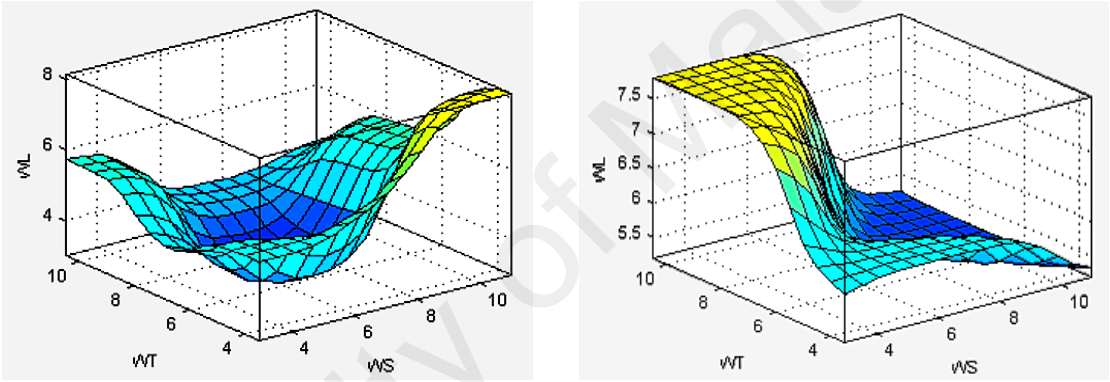

(a) **(b)**

Figure 4.68: ANFIS model of WLT in relation to change of *WS* and *WT* for Ti6Al4V using (a) brass wire (b) coated wire

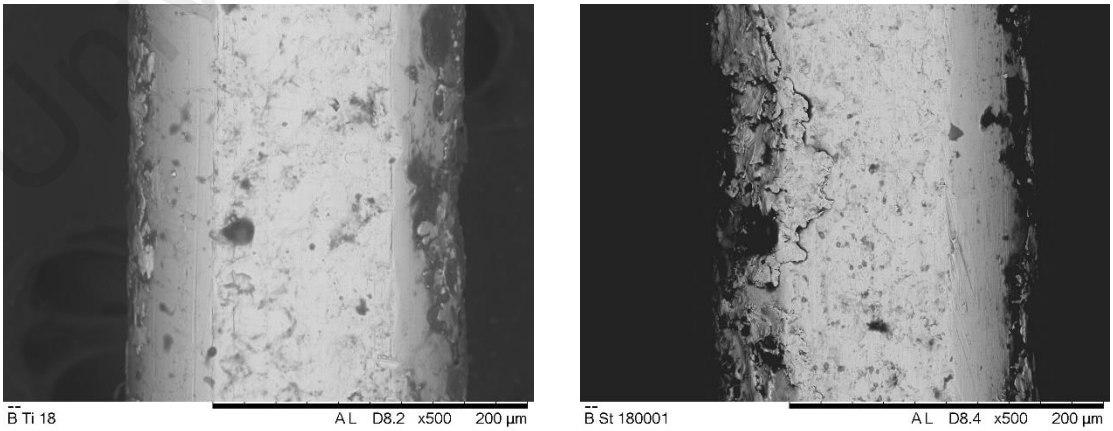

(a) **(b)**

Figure 4.69: SEM micrograph of brass wire surface at different levels of spark energy (a) at low levels of *IP* and *Ton* (b) at high levels of *IP* and *Ton*

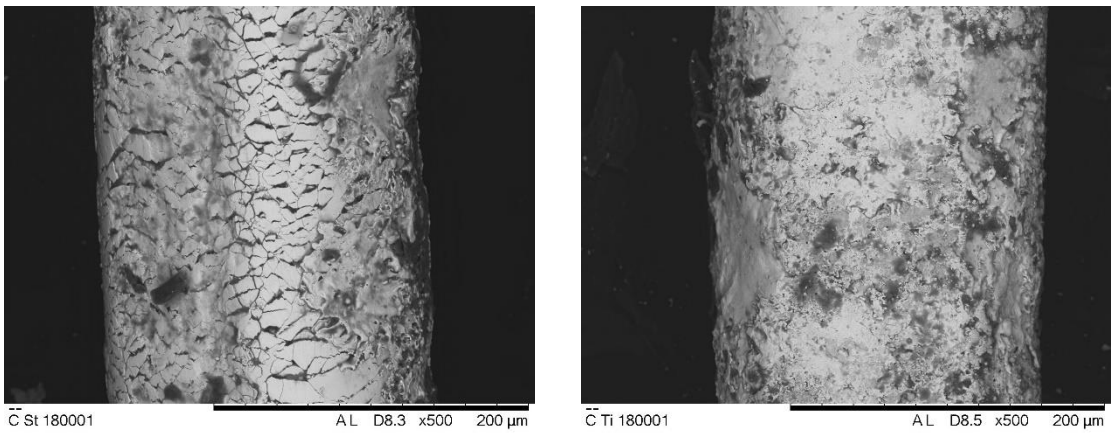

(a) **(b)**

Figure 4.70: SEM micrograph of coated wire surface at different levels of spark energy (a) at low levels of *IP* and *Ton* (b) at high levels of *IP* and *Ton*

4.4 Propose a new performance index to identify the effects of spark energy and pulse frequency simultaneously on machining performance and to determine the wire rupture limit

As previously mentioned, WEDM efficiency mostly depends on the generation and distribution of spark energy within the discharge zone. In practice, efficient WEDM control implies varying the spark energy and pulse frequency parameters. However, it is very difficult to study the effects of spark energy and pulse frequency simultaneously on machining performance. This suggests that a high cutting rate with minimum surface defects is difficult to attain using a single parameter setting. For this reason, a new, simple performance index is proposed in this section to study the effects of spark energy in conjunction with pulse frequency at different duty factors on machining characteristics in achieving high WEDM performance.

4.4.1 Selected experimental parameters and results

In this study, the brass and coated wire electrode were employed for machining titanium alloy grade 5 (Ti6Al4V). The machining parameters, including peak current (*IP*), pulse width (*Ton*), and charging time (*Toff*) were selected for this study based on **Equations (2.1), (2.2),** and **(2.3)** to investigate the effect of spark energy and pulse frequency parameters on machining performance, i.e., cutting speed (*CS*), surface roughness (*Ra*) and white layer thickness (*WLT*) and to identify the wire rupture limit.

A total of 18 sets of data were selected to study the effect of spark energy parameters and pulse frequency on machining performance, as demonstrated in **Table 4.8**. As analyzed in the WEDM pulse generator, WEDM machining performance mainly depends on spark energy and pulse frequency, which can be controlled by peak current, pulse on time, and pulse off time.

Table 4.8: Measured *CS (mm/min), Ra (µm), and WLT (µm)* at different machining conditions

Machining parameters			**Performance factors**			**Performance outcomes**					
						Coated wire			**Brass wire**		
IP (A)	T_{on} *(µs)*	T_{off} *(µs)*	E_s *(µJ)*	*DF (%)*	E_sDF *Index*	*CS (mm/min)*	*Ra (µm)*	*WLT (µm)*	*CS (mm/min)*	*Ra (µm)*	*WLT (µm)*
16	0.2	0.5	64	28.6	1829	1.42	2.23	5.66	1.38	2.58	11.73
		0.9	64	18.2	1164	1.36	2.15	4.96	1.11	2.40	9.79
		1.3	64	13.3	853	1.24	2.09	4.35	0.85	2.35	8.09
	0.3	0.5	96	37.5	3600	2.25	2.69	10.09	1.63	2.65	17.56
		0.9	96	25.0	2400	1.76	2.49	7.53	1.37	2.50	14.26
		1.3	96	18.8	1800	1.54	2.32	6.12	1.10	2.44	10.73
	0.4	0.5	128	44.4	5689	3.43	3.06	16.35	2.04	2.89	23.34
		0.9	128	30.8	3938	2.85	2.86	12.65	1.77	2.81	19.75
		1.3	128	23.5	3012	2.48	2.69	11.06	1.53	2.66	16.07
17	0.2	0.5	68	28.6	1943	1.64	2.31	6.60	1.46	2.54	15.64
		0.9	68	18.2	1236	1.44	2.22	5.71	1.16	2.44	12.62
		1.3	68	13.3	907	1.40	2.17	5.20	0.90	2.29	9.98
	0.3	0.5	102	37.5	3825	2.55	2.82	11.48	1.74	2.68	20.23
		0.9	102	25.0	2550	2.31	2.66	10.61	1.54	2.58	17.60
		1.3	102	18.8	1913	1.95	2.46	8.63	1.29	2.55	15.61
	0.4	0.5	136	44.4	6044	3.85	3.25	19.94	2.18	3.07	26.32
		0.9	136	30.8	4185	3.24	2.92	15.68	1.87	2.99	21.56
		1.3	136	23.5	3200	2.66	2.74	12.71	1.70	2.92	18.66

4.4.2 Analysis and discussion

4.4.2.1 Cutting speed analysis

Figure 4.71 and **4.72** represents the effect of the spark energy parameters (*IP, Ton,* and *Toff*) on cutting speed using coated and brass wire electrodes respectively. As **Figure 4.71** and **4.72** indicates, an increase of peak current and pulse duration leads to higher cutting speed. The same conclusion can be drawn from the cutting speed **Equation (2.10)**. The spark discharge energy obtained from **Equation (2.1)** increases with the increase of discharge current and pulse duration. However, at the same spark energy level (constant energy line represented by a dashed line in **Figure 4.71** and **4.72**), the cutting speed decreases with increasing pulse off time. Increasing pulse off time leads to decreasing pulse frequency at the same energy levels, hence the cutting speed decreases as shown in **Figure 4.73** and **4.74**. **Figure 4.73** and **4.74** introduce the effect of pulse frequency on the cutting speed of Ti6Al4V using coated and brass wire electrodes respectively.

From **Equations (2.1), (2.2)** and **Figure 4.71 - 4.74**, both the pulse frequency and spark energy affect the cutting speed. However, it is very difficult to study the effect of each one individually on cutting speed. Therefore, a new performance index is proposed in this study to merge the effect of pulse frequency with spark energy. This can be done by normalizing the spark energy parameters by multiplying the spark energy with the duty factor ($Es \times DF$).

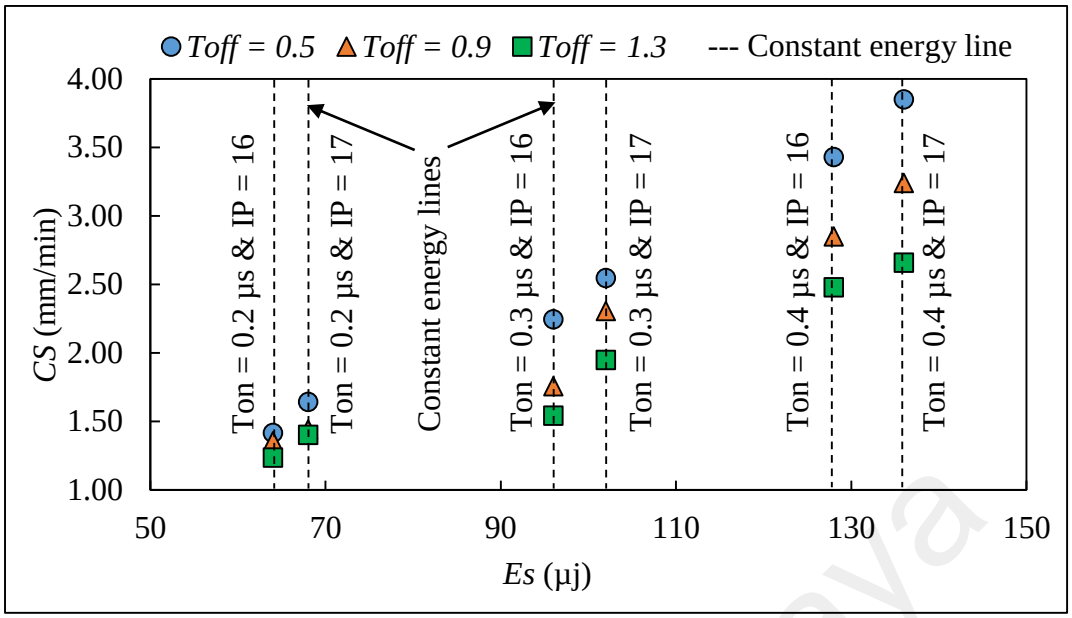

Figure 4.71: Influence of spark energy parameters on cutting speed using coated wire

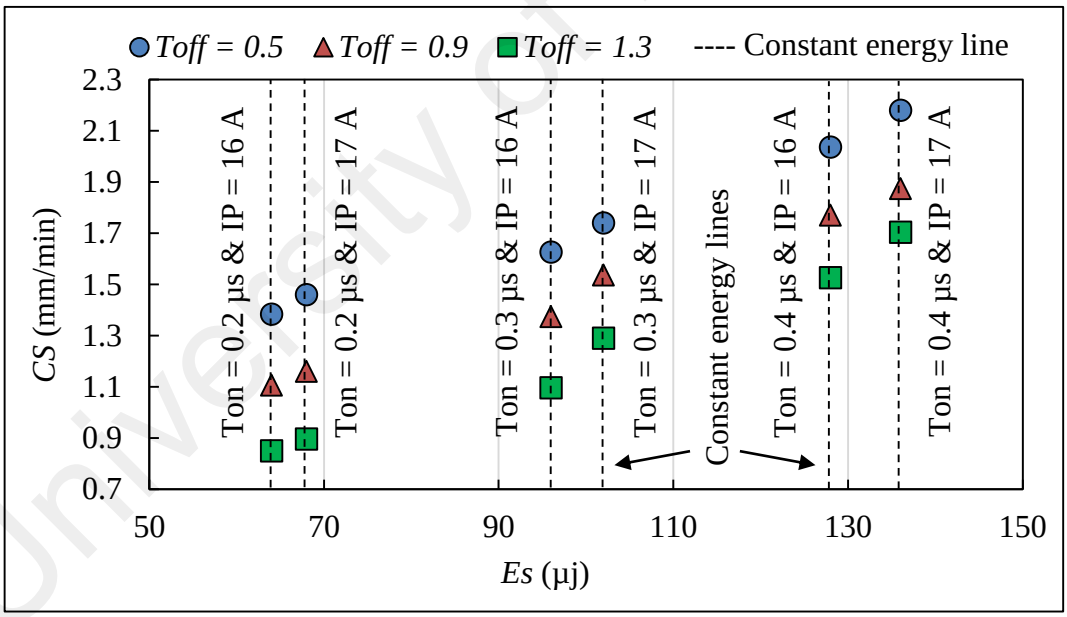

Figure 4.72: Influence of spark energy parameters on cutting speed using brass wire

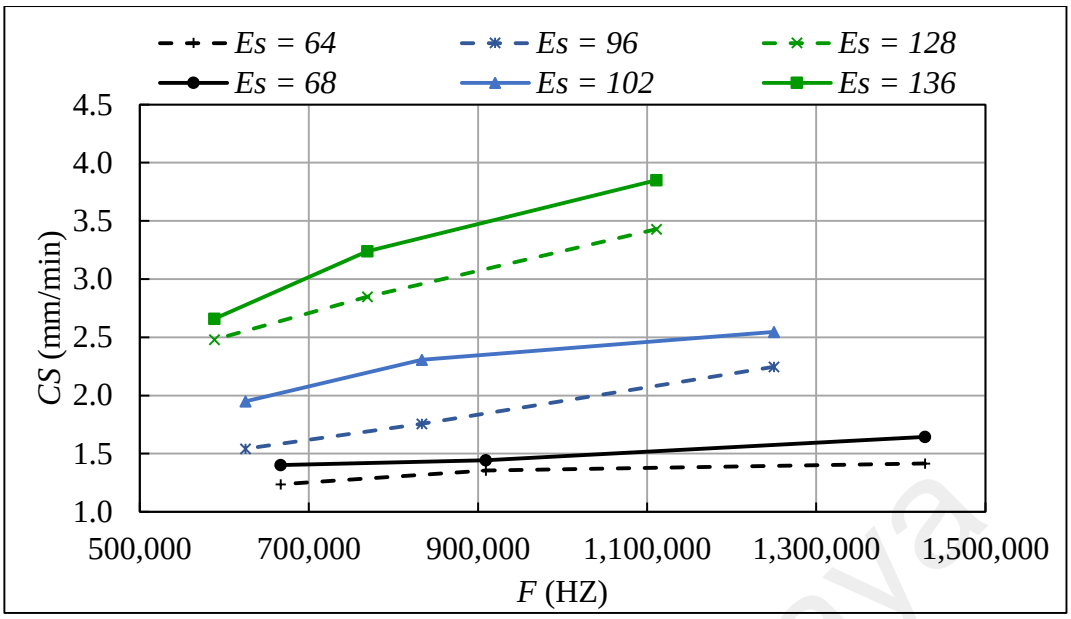

Figure 4.73: Influence of cycle frequency on cutting speed using coated wire

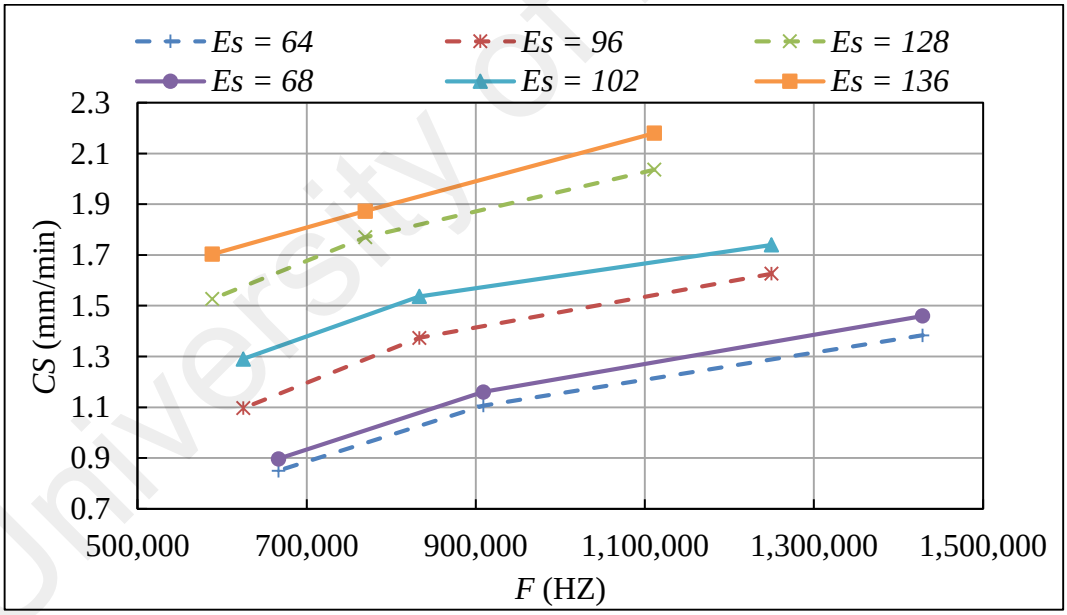

Figure 4.74: Influence of cycle frequency on cutting speed using brass wire

Figure 4.75 and **4.76** display the change in cutting speed at different performance index levels of Ti6Al4V workpiece using coated and brass wire electrodes respectively. According to **Figure 4.75** and **4.76** cutting speed increases linearly with the increase in the new performance index. When the discharge energy parameters (*Vd, IP*, and/or *Ton*) and/or the duty factor change, the new performance index changes accordingly. **Figure**

4.75 and **4.76** also show the wire rupture limit based on the new performance index. It is clear that the wire rupture phenomenon happens at the same performance index level. Moreover, the cutting speed using coated wire is better than using brass wire electrode, hence the coated wire is more feasible than brass wire electrode.

Table 4.9 and **4.10** represents the statistical analysis and effects of performance index on cutting speed. According to ANOVA, at 95% confidence level ($p < 0.05$) when p is less than 0.05, the performance index significantly affects cutting speed. A regression technique was employed to understand the effect of the performance index on cutting speed. The empirical equations of cutting speed using coated and brass wire is presented as in **Equations 4.18** and **4.19** respectively.

$$\boldsymbol{CS = 0.8056 + 0.0005\ (Es \times DF)} \quad \text{Using coated wire} \quad \textbf{4.18}$$

$$\boldsymbol{CS = 0.829 + 0.000233\ (Es \times DF)} \quad \text{Using brass wire} \quad \textbf{4.19}$$

Equations 4.18 and **4.19** indicate that cutting speed increases with increasing performance index for both wire electrodes. The analytical relationship between cutting speed and the new performance index has a high coefficient of determination ($R^2 = 0.93$ using coated wire and $R^2 = 0.92$ using brass wire). The coefficient of determination is a measure of how well an analytical model is likely to predict future outcomes. This correlation coefficient is calculated by dividing the covariance of two variables by their standard deviations. The predicted R^2 value (93.2% using coated wire and 92.4% using brass wire) and adjusted R^2 value (92.7% using coated wire and 91.9% using brass wire) match the experimental results. The adjusted R^2 determines the amount of deviation about the mean that is described by the model (Montgomery & Runger, 2003).

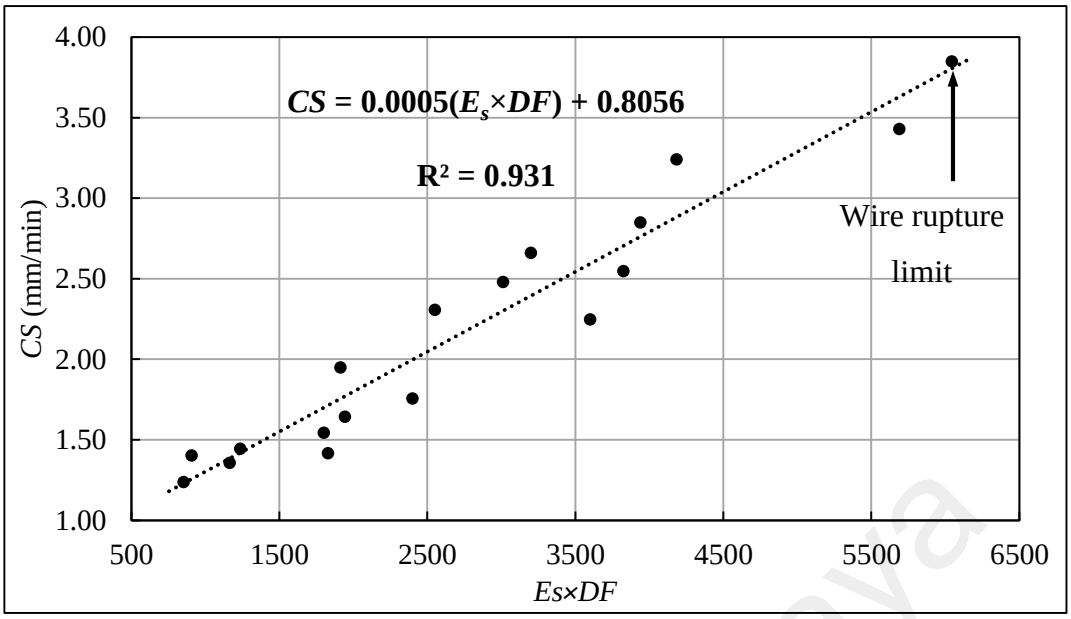

Figure 4.75: Experimental influence of weighted spark energy on the cutting speed using coated wire

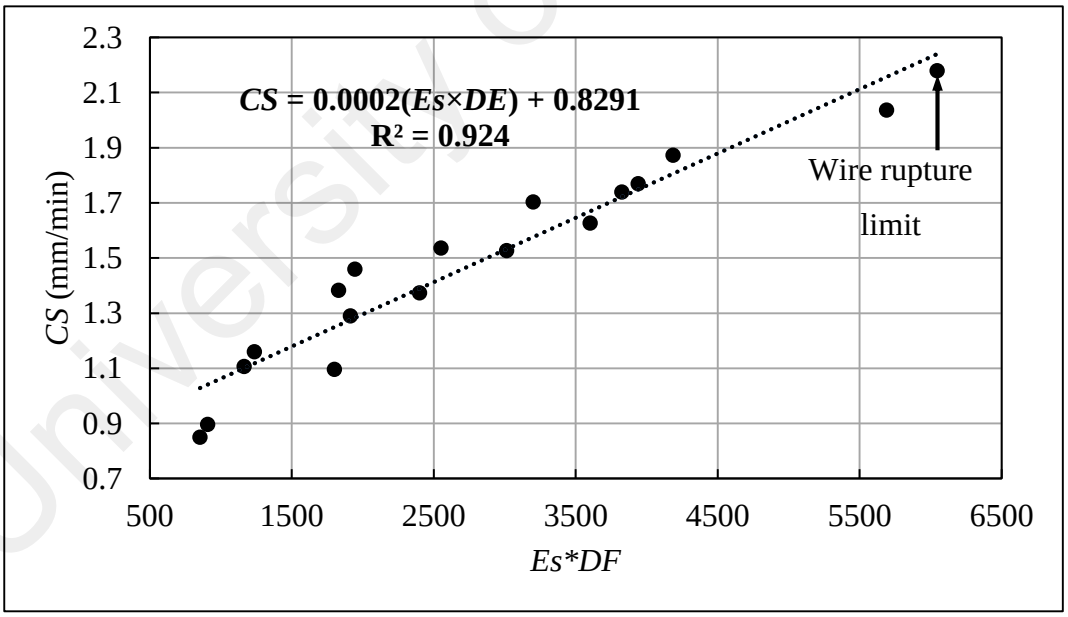

Figure 4.76: Experimental influence of weighted spark energy on the cutting speed using brass wire

Table 4.9: ANOVA table for cutting speed using coated wire

Source	DF	Sum of Squares	Mean Square	F-ratio	P-value
Es×DF	1	9.8929	9.8929	217.63	0.000
Residual error	16	0.7273	0.0455		
Total	17	10.6202			

Table 4.10: ANOVA table for cutting speed using brass wire

Source	DF	Sum of Squares	Mean Square	F-ratio	P-value
Es×DF	1	2.1862	2.1862	194.42	0.000
Residual error	16	0.1799	0.0112		
Total	17	2.3661			

Therefore, the new performance index is accurate and can be used as an index for monitoring, predicting, and controlling the cutting speed performance measure as well as identifying the wire rupture limit.

4.4.2.2 Surface quality analysis

This section presents the analysis of the effects of the spark energy and pulse frequency parameters on surface quality of Ti6Al4V using coated and brass wire electrodes. **Figure 4.77** and **4.78** show the influence of the spark energy parameters on surface roughness using coated and brass wire electrodes respectively. These figures indicate that an increase of discharge power (*IP*) and/or discharge duration (*Ton*) results in increased surface roughness. As the discharge energy increases, the thermal energy concentration on the workpiece increases, which results in large craters, hence the surface roughness increases. The same conclusion can be drawn from the analytical relationship between surface roughness and discharge energy (**Equation 2.15**). **Figure 4.79** and **4.80** display the influence of cycle frequency on surface roughness at different spark energy levels

using coated and brass wire electrodes respectively. It is clear from these figures that pulse frequency has a small effect on surface roughness. Surface roughness increases with increasing pulse frequency at the same spark energy level. In addition, according to **Figure 4.77 – 4.80**, it is hard to analyze the effect of spark energy and pulse frequency together on surface roughness.

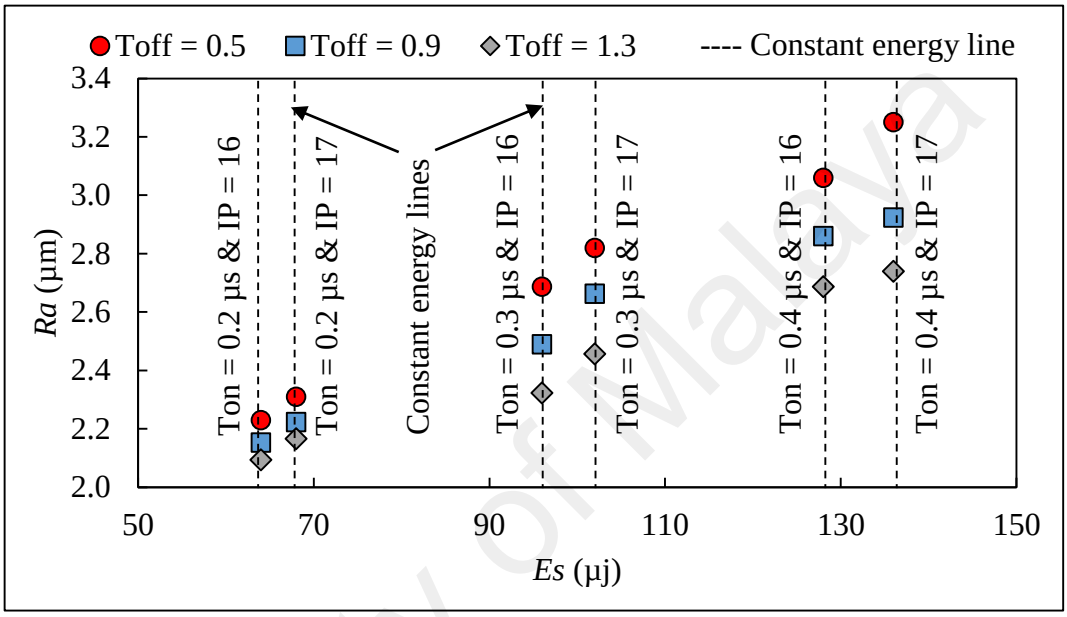

Figure 4.77: Influence of spark energy on surface roughness using coated wire

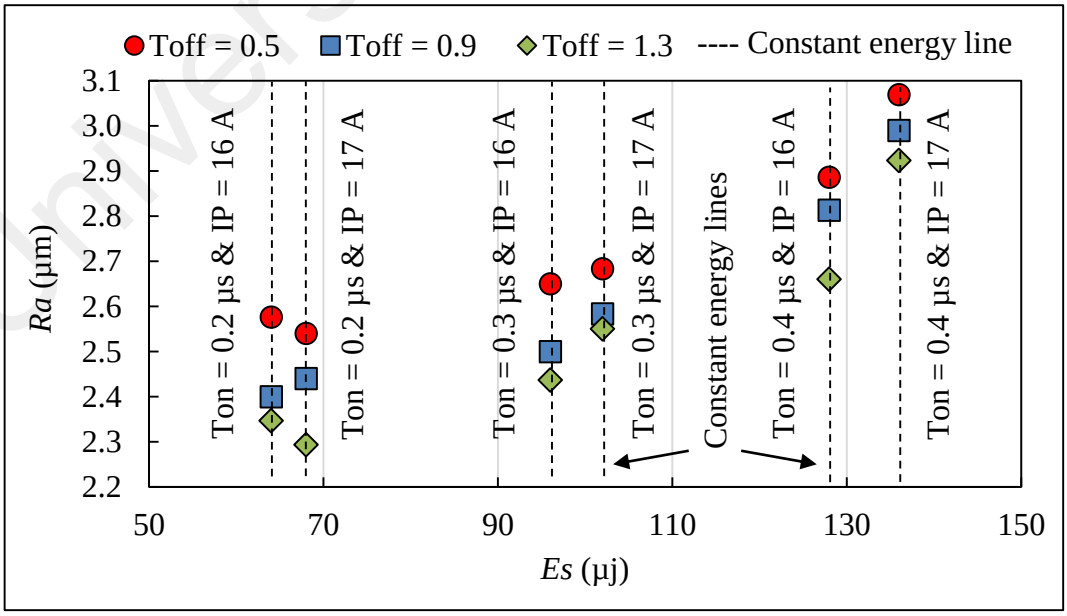

Figure 4.78: Influence of spark energy on surface roughness using brass wire

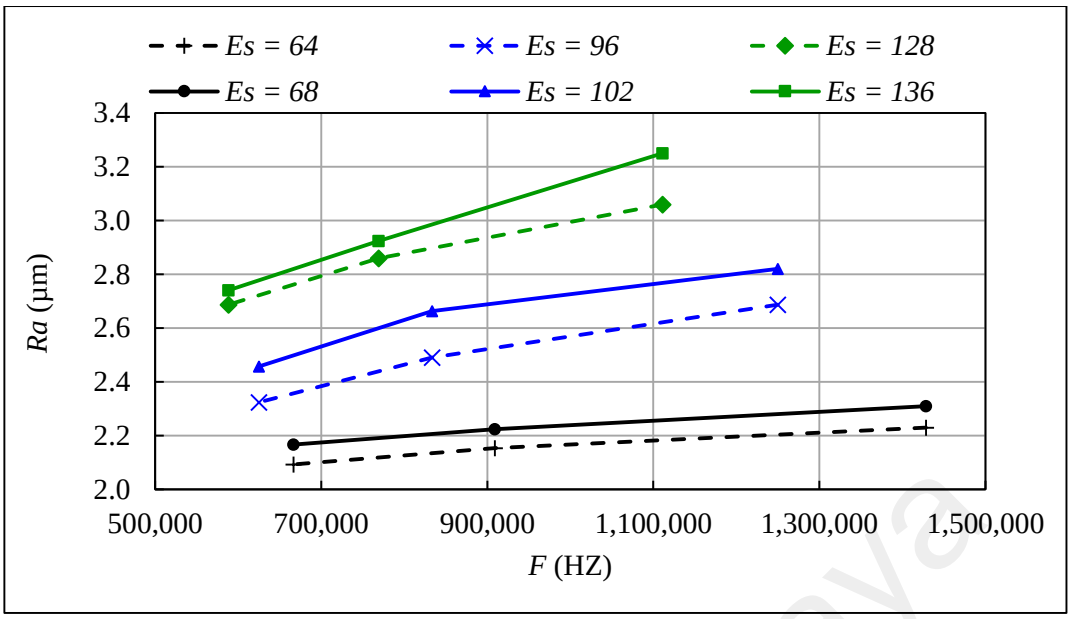

Figure 4.79: Influence of cycle frequency on surface roughness using coated wire

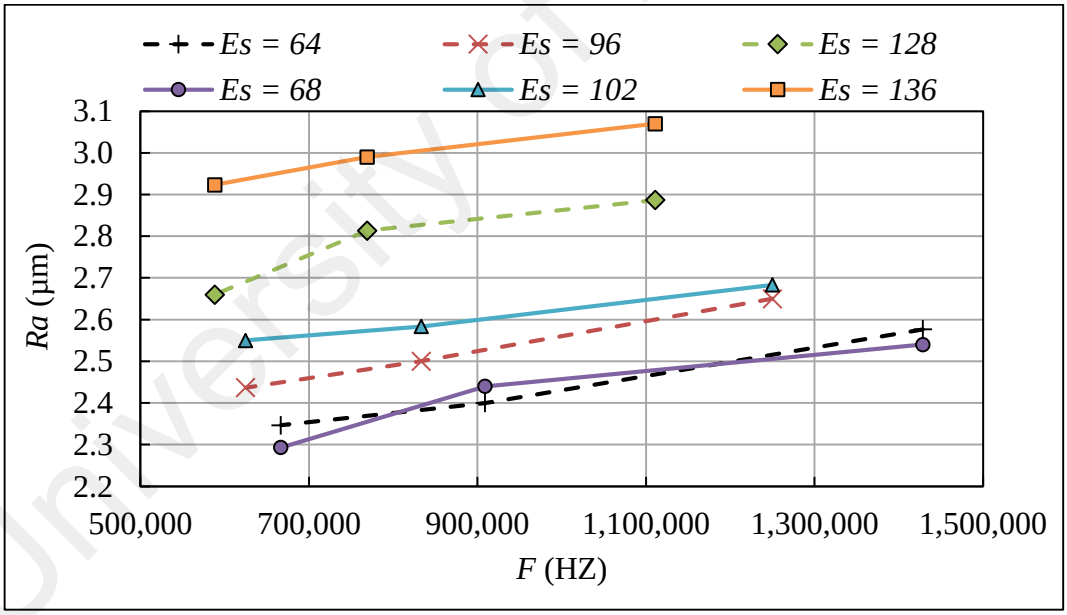

Figure 4.80: Influence of cycle frequency on surface roughness using brass wire

Figure 4.81 and **4.82** show the relation between surface roughness and the proposed performance index using coated and brass wire electrodes respectively. Surface roughness increases linearly with increasing the proposed performance index. When the electrical process parameters (*IP, Ton, and Toff*) change, the proposed performance index changes accordingly. Moreover, the analytical relationship between surface roughness

and the proposed performance index has a high coefficient of determination, (R^2 = 0.951 using coated wire and 0.832 using brass wire), high adjusted coefficient of determination, (R^2=0.958 using coated wire and 0.822 using brass wire), and low p-value ($p < 0.05$) as per **Table 4.11** and **4.12** (ANOVA), hence the performance index has significant effect on surface roughness. By using regression on the recorded data, the prediction models for surface roughness using coated and brass wire are expressed as follows:

$$\boldsymbol{Ra = 1.9599 + 0.0002(Es \times DF)} \quad \text{Using coated wire} \quad \textbf{4.20}$$

$$\boldsymbol{Ra = 2.26 + 0.000134\ (Es \times DF)} \quad \text{Using brass wire} \quad \textbf{4.21}$$

In **Equation 4.20** and **4.21**, surface roughness increases with increasing performance index.

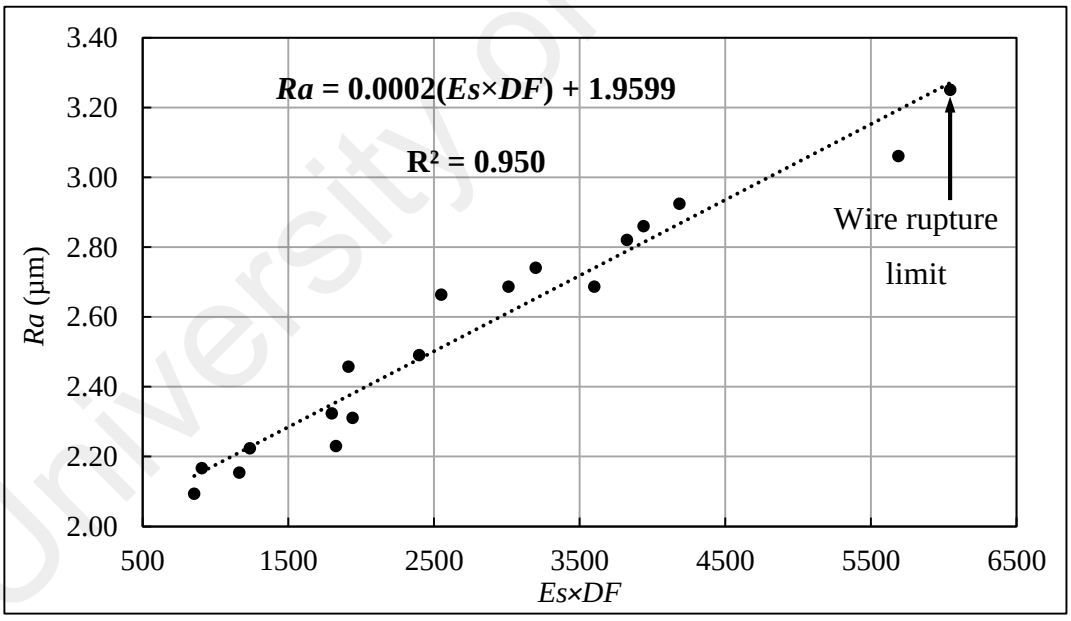

Figure 4.81: Experimental influence of weighted spark energy on the surface roughness using coated wire.

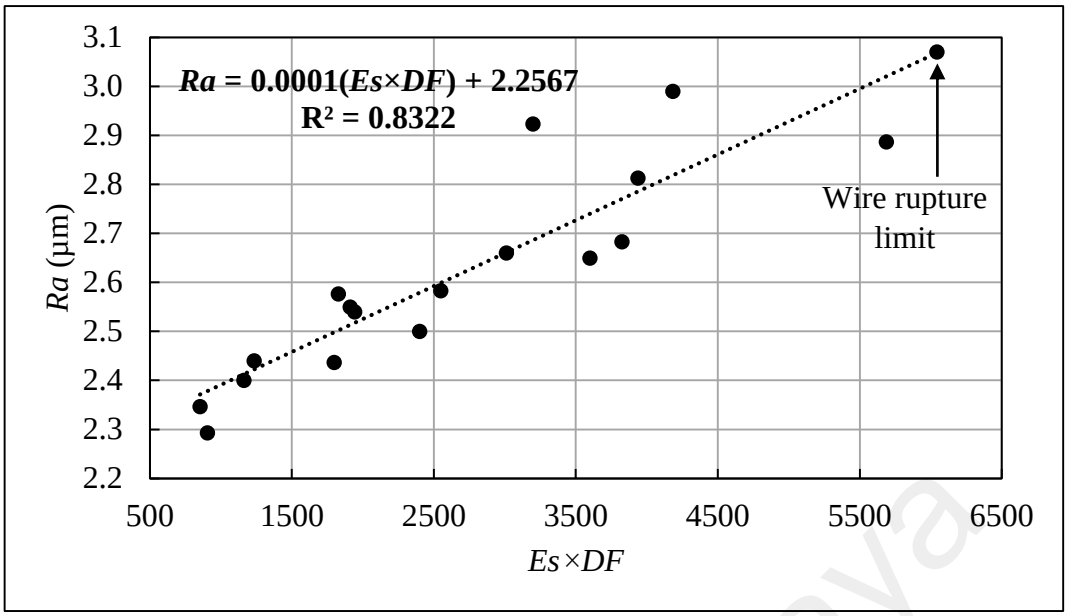

Figure 4.82: Experimental influence of weighted spark energy on the surface roughness using brass wire.

Table 4.11: ANOVA table for surface roughness using coated wire

Source	DF	Sum of Squares	Mean Square	F-ratio	P-value
Es×DF	1	1.8872	1.8872	309.03	0.000
Residual error	16	0.0977	0.0061		
Total	17	1.9849			

Table 4.12: ANOVA table for surface roughness using brass wire

Source	DF	Sum of Squares	Mean Square	F-ratio	P-value
Es×DF	1	0.72340	0.72340	79.33	0.000
Residual error	16	0.14590	0.00912		
Total	17	0.86930			

Figure 4.83 (a) and **(b)** show the SEM of two surfaces at two different levels of the proposed performance index of Ti6Al4V using coated wire electrode. These two surfaces represent two extreme cases of process conditions under the highest performance index (**Figure 4.83 (a)**) and the lowest performance index (**Figure 4.83 (b)**). Bigger craters and

more surface cracks due to larger amounts of molten work-material at each spark erosion can be identified on WEDM surfaces (**Figure 4.83 (a)**). On the other hand, crater size and number of cracks reduce drastically on surfaces machined with a low performance index, as shown in **Figure 4.83 (b)**. Thus, the proposed performance index is accurate and can be used for monitoring, predicting, and controlling surface roughness performance measures using spark energy and pulse frequency simultaneously.

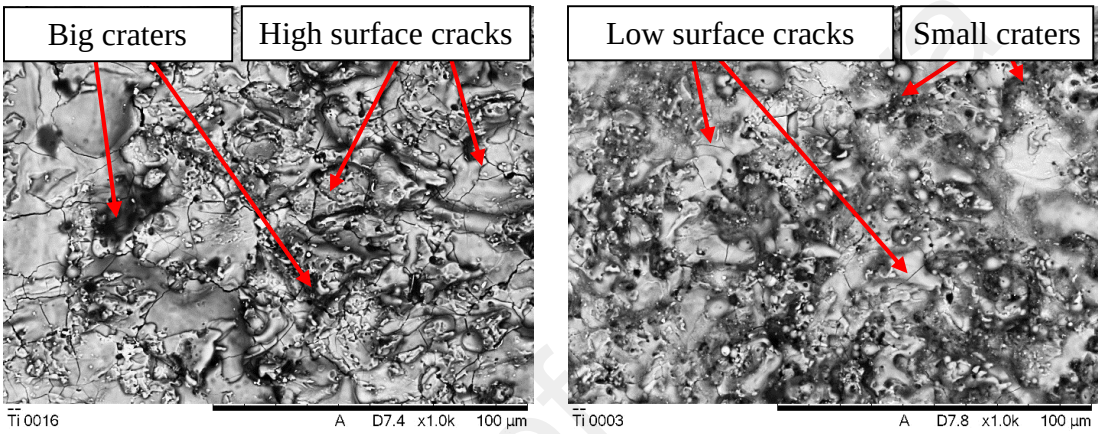

(a) **(b)**

Figure 4.83: SEM micrograph at (a) High levels of spark energy and duty percent (b) Low level of spark energy and duty percent

4.4.2.3 White layer thickness analysis

This section introduces the analysis of the effects of spark energy and pulse frequency parameters on white layer thickness of Ti6Al4V using coated and brass wire electrodes. The pulse duration has more prominent influence on white layer thickness than discharge current (**Figure 4.84** and **4.85**). However, white layer thickness increases as pulse off time decreases at the same energy level (the constant energy line is represented by a dashed line in **Figure 4.84** and **4.85**). **Figure 4.86** and **4.87** indicate the influence of cycle frequency on white layer thickness at different spark energy levels. White layer thickness increases with increasing pulse frequency. This is because the increase in pulse frequency increases the heat generated on the workpiece surface, hence the white layer thickness

increases. Moreover, according to **Figure 4.84 – 4.78**, it is difficult to study the dependence of white layer thickness on spark energy and pulse frequency simultaneously. Therefore, a new performance index is proposed to study the effect of pulse frequency with spark energy simultaneously on the white layer thickness.

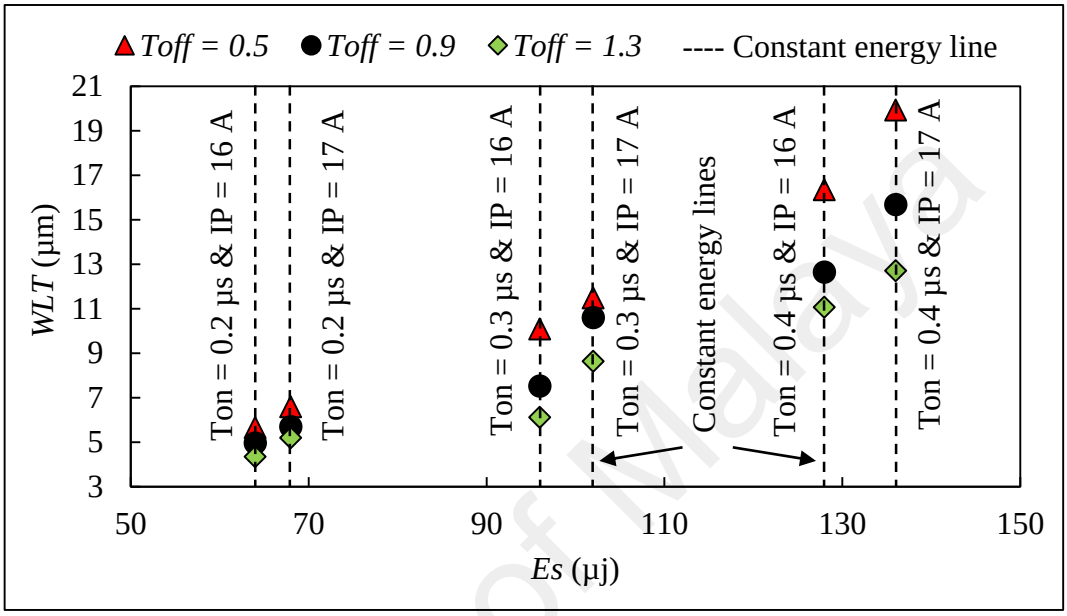

Figure 4.84: Influence of spark energy parameters on white layer thickness using coated wire

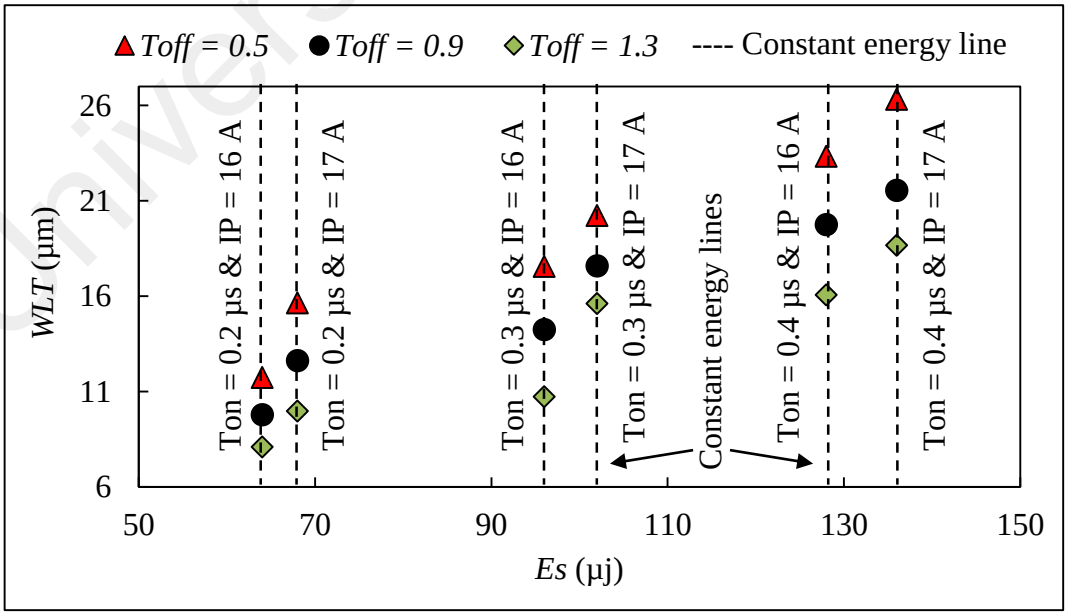

Figure 4.85: Influence of spark energy parameters on white layer thickness using brass wire

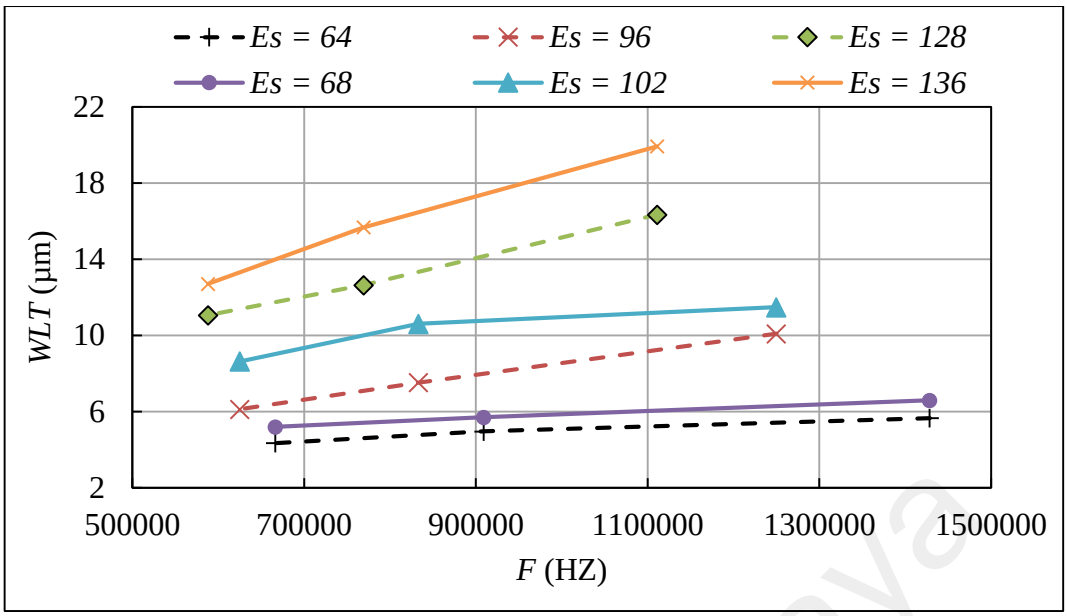

Figure 4.86: Influence of cycle frequency on white layer thickness using coated wire

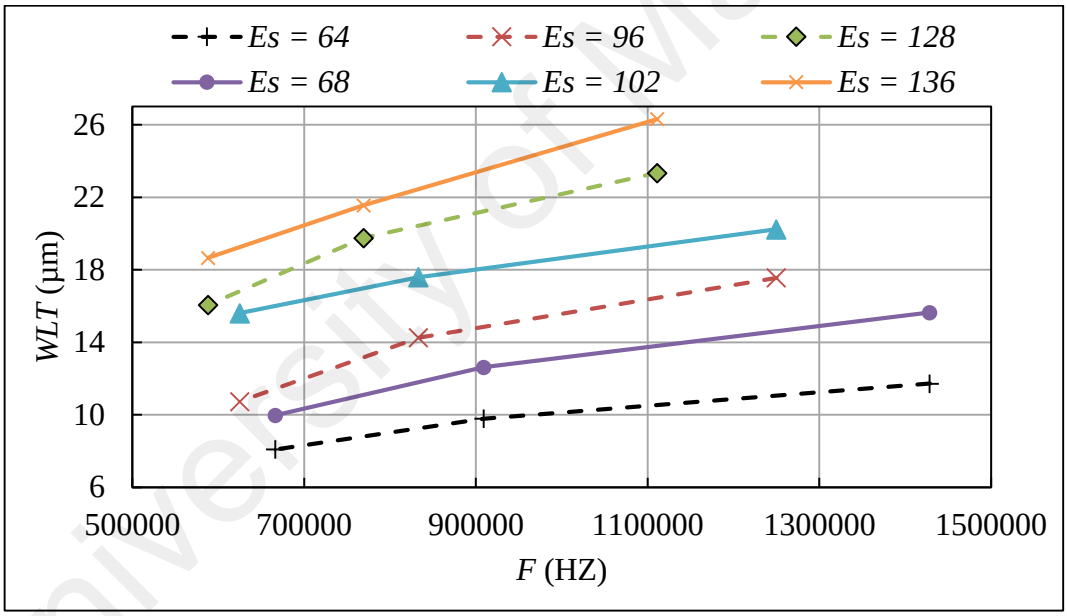

Figure 4.87: Influence of cycle frequency on white layer thickness using brass wire.

Figure 4.88 and **4.89** show the relation between white layer thickness and the proposed performance index for both coated and brass wire electrodes respectively. The white layer thickness increases linearly with increasing the proposed performance index. When the spark energy and frequency parameters (*IP*, *Ton*, and *Toff*) change, the proposed performance index changes accordingly, leading to a change in white layer thickness. Moreover, the effect of performance index on white layer thickness is introduced

statistically in the ANOVA tables (**Table 4.13** and **4.14**). According to ANOVA, at 95% confidence level ($p < 0.05$) the performance index has significant effect on white layer thickness. The empirical equations based on the regression technique are presented as follows:

$$\boldsymbol{WLT = 1.9531 + 0.0028\ (Es \times DF)} \qquad \text{Using coated wire} \qquad \textbf{4.22}$$

$$\boldsymbol{WLT = 7.36 + 0.00314\ (Es \times DF)} \qquad \text{Using brass wire} \qquad \textbf{4.23}$$

Equations **4.22** and **4.23** indicates that white layer thickness increases with increasing performance index. The analytical relationship between white layer thickness and proposed performance index has a high coefficient of determination ($R^2 = 0.924$ using coated wire and 0.912 using brass wire) and high adjusted coefficient of determination (R^2 (adj.) = 91.9% using coated wire and 90.6% using brass wire).

The samples of metallographic investigation show there is a recast layer (white layer) at low and high discharge energies (**Figure 4.90**). **Figure 4.90** shows the SEM of the edge for two samples at extreme performance index of Ti6Al4V using coated wire electrode. **Figure 4.90 (a)** shows the white layer thickness at high performance index, while **Figure 4.90 (b)** shows the white layer thickness at low performance index. In principle, increasing discharge energy increases the performance index, hence increasing recast layer thickness (**Figure 4.90**). Therefore, the proposed performance index is accurate and can be used for monitoring, predicting, and controlling the white layer thickness performance measure as well as avoiding wire rupture using spark energy and pulse frequency simultaneously.

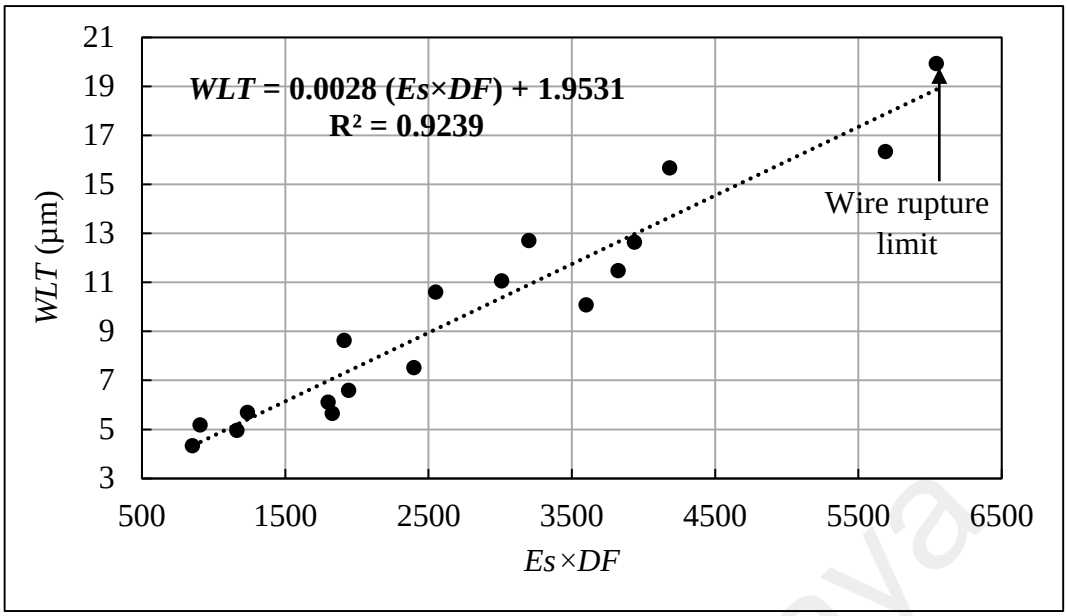

Figure 4.88: Experimental influence of weighted spark energy on the white layer thickness using coated wire

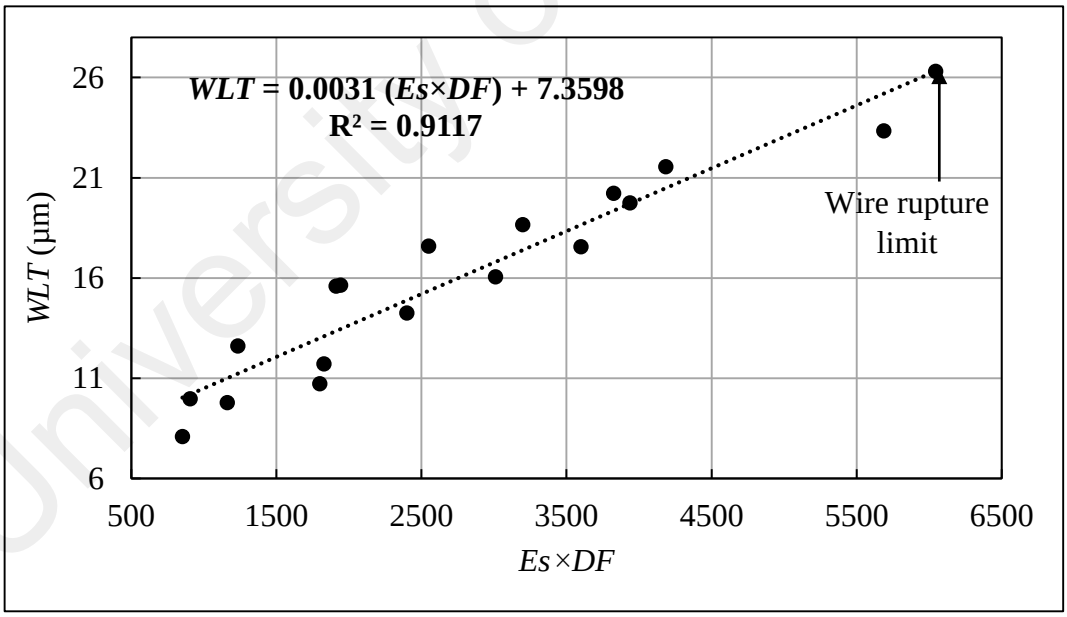

Figure 4.89: Experimental influence of weighted spark energy on the white layer thickness using brass wire

Table 4.13: ANOVA table for white layer thickness using coated wire

Source	DF	Sum of Squares	Mean Square	F-ratio	P-value
Es*×*DF	1	314.53	314.53	194.21	0.000
Residual error	16	25.91	1.62		
Total	17	340.45			

Table 4.14: ANOVA table for white layer thickness using brass wire

Source	DF	Sum of Squares	Mean Square	F-ratio	P-value
Es*×*DF	1	394.92	394.92	165.23	0.000
Residual error	16	38.24	2.39		
Total	17	433.16			

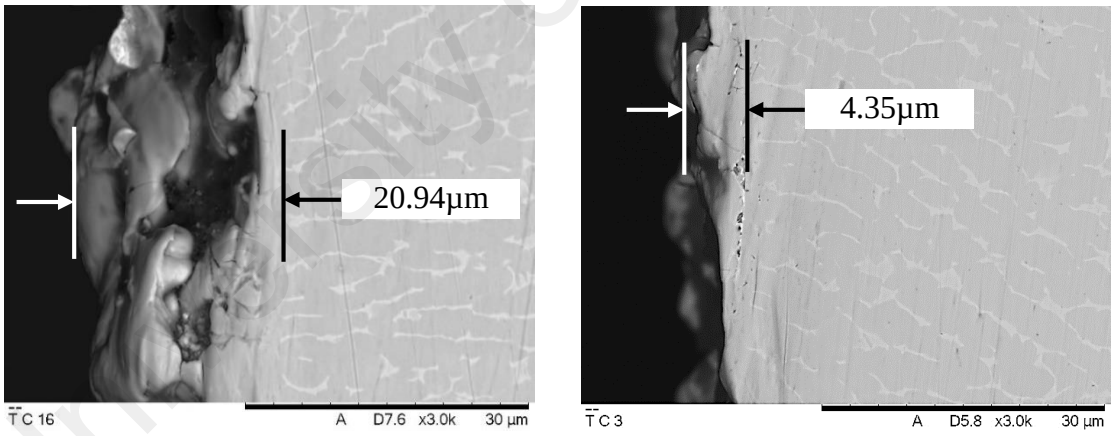

(a) **(b)**

Figure 4.90: SEM micrograph of the edge at (a) high levels of spark energy and pulse frequency (d) low levels of spark energy and pulse frequency

4.5 Conclusion

This study investigates the effect of cutting parameters (*IP*, *Ton*, *Toff*, *WS*, and *WT*) on the machining performance measures (*CS*, *Ra*, *WLT*, and *WL*) of Ti6Al4V and AISI1050 carbon steel workpieces using brass and coated wire electrodes. Two data analysis techniques (Taguchi and ANFIS) were used to achieve high productivity and best surface quality, from which similar conclusions were drawn. The peak current, pulse width, and pulse off time are the most significant parameters affecting cutting speed, surface roughness, white layer thickness, and wire rupture. Wire tension and wire speed have minor effect on cutting speed, surface roughness, and white layer thickness but they have pronounced effect on wire rupture. ANFIS was successfully used to develop an empirical model for modeling the relation between the predictor variables (*IP*, *Ton*, *Toff*, *WS*, and *WT*) and the performance parameters (*CS*, *Ra*, *WLT*, and *WL*). The training dataset for each ANFIS model is built using 18 measured values under different cutting conditions. Four values were used as testing data to verify the models where the average errors were very small for all models. These results indicate that ANFIS model with gbellmf is accurate and can be used to predict *CS*, *Ra*, *WLT*, and *WL* in WEDM. The ANFIS models results are also compared with the Taguchi model results. As anticipated, the ANFIS models provide efficient prediction because they generally offer the ability to model more complex nonlinearities and interactions. In addition, by analyzing the results in WEDM using the conceptual ANFIS approach, the following can be concluded:

- ANFIS was used to introduce technological knowledge base for the selection of machining parameters to achieve high productivity at highest possible surface quality for sustainable production and lowering process cost.
- High pulse width (0.4 µs), high peak current (17 A), and low pulse off time are recommended to obtain high productivity for the definite test range.

- Low pulse on time (0.2µs), low peak current (16A), high pulse off time (1.3 µs), high wire speed (11m/min), and high wire tension (10.5N) lead to a smaller surface roughness values, white layer thickness, and wire loss for the specific test range.
- Using coated wire electrode is better than using brass wire for smaller higher cutting speed and for smaller surface roughness and white layer thickness.
- High thermally conductive metals (AISI 1050 carbon steel) typically have a smaller WLT and less micro-cracking than those of a less conductive material (Ti6Al4V) in WEDM.
- High wire speed and low wire tension lead to smaller surface crater of the wire electrode hence it is recommended to prevent the wire rupture.

Based on the above analytical and experimental investigations, the machining performance of WEDM is directly dependent on spark energy parameters (*IP*, *Vd*, and *Ton*) and pulse frequency parameters (*Ton* and *Toff*). But, it is difficult to study the dependence of cutting speed, surface roughness, and white layer thickness on spark energy and pulse frequency simultaneously. Therefore, a new performance index is proposed to study the effect of pulse frequency with spark energy simultaneously on the machining performance measures. Based on the theoretical analysis and experimental results, the proposed performance index ($Es \times DF$) much more conveniently correlates the performance parameters (*CS*, *Ra* and *WLT*) with the spark energy and pulse frequency parameters in the WEDM process. By applying the proposed performance index ($Es \times DF$), it appears that using a lower spark setting with higher pulse cycle settings will reduce chip size and produce better flushing. This could lead to faster cutting with good surface finish and less wire rupture.

CHAPTER 5: PROPOSE A NEW PRODUCTION ECONOMIC INDEX TO IDENTIFY THE MOST SUITABLE WIRE FOR HIGHER PERFORMANCE CONSIDERING THE ECOLOGICAL AND ECONOMIC ASPECTS

5.1 Introduction

According to the previous analysis, the proposed performance index can be used to identify the performance outcomes based on the spark energy and pulse frequency for each wire electrode. Nonetheless, it cannot be used to identify the most feasible wire electrode from ecological (energy and wire consumption) and economic (energy and wire consumption costs) perspectives. Since the beginning of EDM technology, EDM manufacturers have created databases of the most common wires commercially available for stable machining. Although EDMs are equipped with cutting condition tables for each wire, it is still a difficult task to decide which wires are feasible for a particular operation according to technical limitations and what the most suitable and economic wire among them is. It is very hard to select an appropriate wire that adheres to the machining requirements as well as minimizes the machine tool energy, consumable utilization, and machining cost. Therefore, a new production economic index to identify the most feasible wire electrode for higher WEDM performance is proposed and introduced in this section keeping in view the ecological and economic aspects.

5.2 WEDM ecological and economic analysis

A model for ecological assessment is conceptualized in **Figure 5.1**. This figure illustrates the flow of energy consumption, wire electrode consumption, wire and workpiece recycling, and contaminated dielectric. During the machine tool utilization phase, the spark generator, workpiece motion system, wire electrode feeding system, flushing pump (also known as injection pump), filtration pump, and recycling system all consume electricity. During WEDM, deionized water is constantly being contaminated with metal particles produced during the WEDM process and water filters/resins are used

to treat this waste. The wire is continually fed throughout the WEDM process and cannot be reused on quality grounds, hence representing a significant source of wire consumption in WEDM.

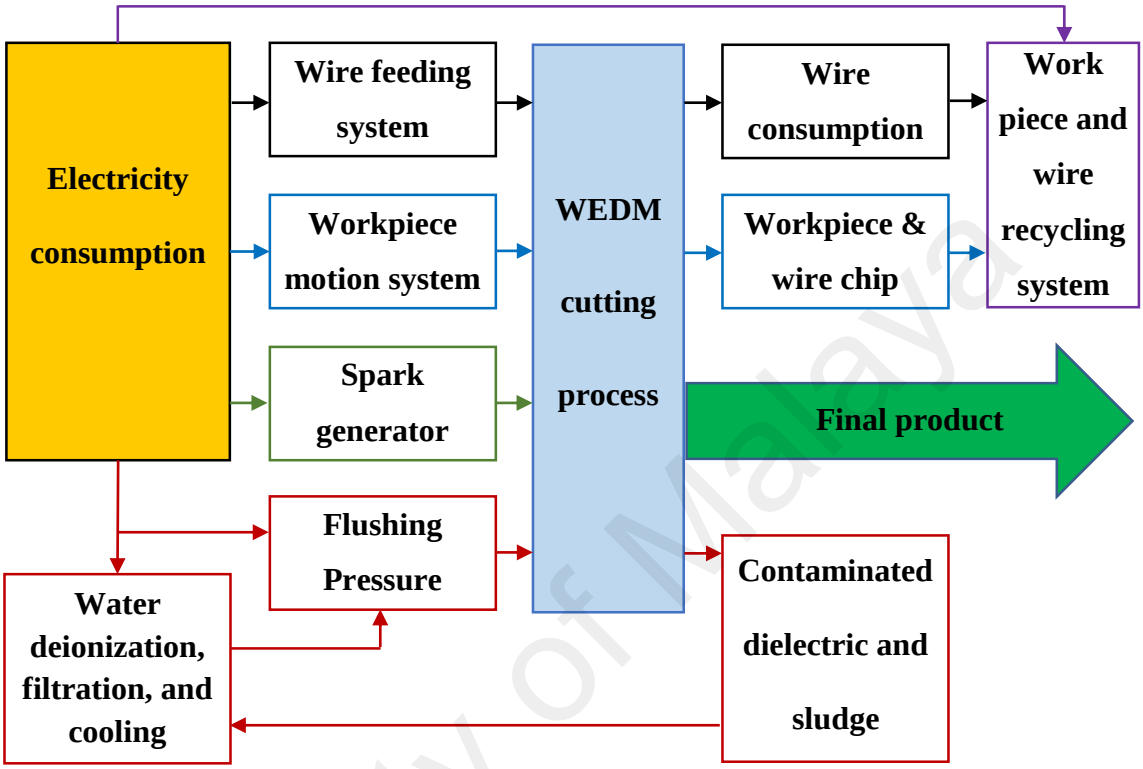

Figure 5.1: Electricity consumption and waste generation

5.2.1 Energy consumption and cost

The component-wise power distribution during the various phases of a machining process with a WEDM machine tool system is shown in **Figure 5.2** (Tönshoff et al., 1996). It can be seen there are two types of components in the power distribution diagram. First, there are process components related to power consumption, such as the injection pump and spark generation unit. Second, there are process components independent of power consumption, such as the filling pump, filter pump, auxiliary pump, and cooler.

The power consumed by the injection pump and spark generation unit depends upon the process, workpiece material, wire type and diameter, and cutting quality requirement. However, in this research, the power consumption of the injection pump is fixed because

the injection pressure is fixed for all wire electrodes under consideration. The other category of components (filling pump, filter pump, auxiliary pump, cooler) are not affected by the process requirements. Hence, the spark generation unit needs to be taken into account to calculate the electricity consumption during WEDM.

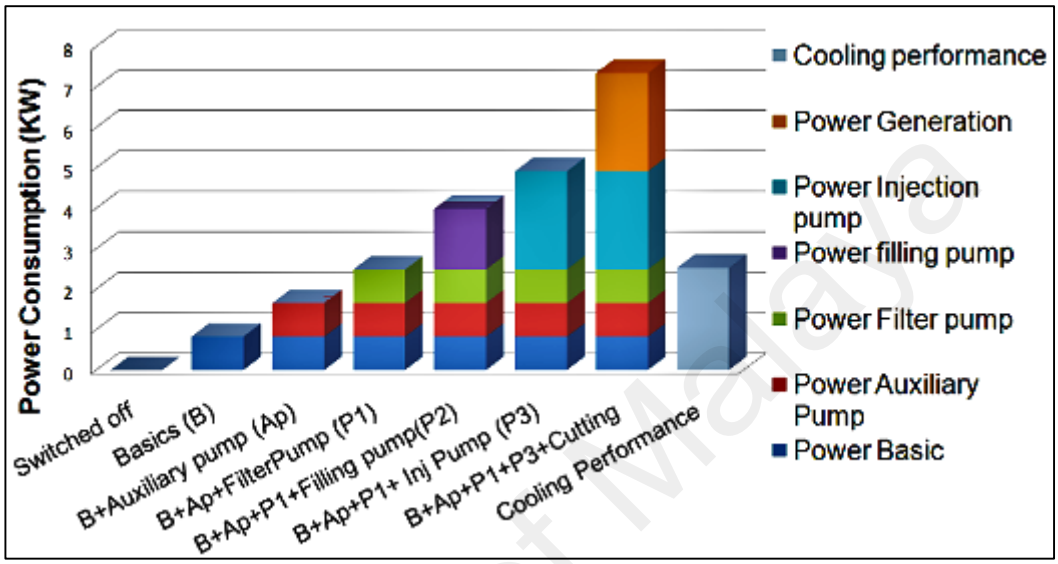

Figure 5.2: Power consumption along the time horizon in WEDM (Tönshoff et al., 1996)

The electricity cost is taken as 0.44 RM/kWh, and the energy consumed for generating electrical sparks can be calculated from **Equation 5.1**

$$E = IP \times V \times h \qquad \textbf{5.1}$$

where *IP* is the peak current in ambers, *V* is the spark gap voltage in volts, and *h* is the machining time in hours.

Hence the energy consumption cost can be calculated from **Equation 5.2**.

$$Ce = E \times 0.44 \qquad \textbf{5.2}$$

Where *Ce* is the energy cost in Malaysian Ringgit (RM).

5.2.2 Wire consumption and cost

One of the biggest costs involved in running a WEDM machine is the wire cost. However, there are a number of different ways to save cost on the EDM wire and get the best use out of the wire from start to finish. Wire electrode price is affected by raw material cost and copper concentration is the greatest determining factor in wire pricing. When comparing the cost of different wires, it is critical to take into consideration wire performance. Savings made by using a low-cost wire may be worthless if there is trouble with wire breakage, threading, or dirt build-up requiring down time to clean the wire path. A coated EDM wire can help increase cutting speed by as much as 10-30%, depending on cutting conditions. Coatings can be from a variety of different materials, the most common of which is Zinc. These wires are not perfect for every application, but in a shop where machine time is an issue or cutting conditions are poor, coated wires can help achieve more production. Coated EDM wires usually have a higher price but when needed; they are a very popular option. The costs of coated and brass wires are 65 RM/kg and 30 RM/kg respectively, although the wire cost also depends on spool size. This cost data was used for roughly comparing different wire materials.

In WEDM, wire speed can be used to calculate the consumed mass, as the wire is used only once due to quality concerns. The wire consumption is calculated with **Equation 5.3.**

$$WC = WS \times t \times Wm \qquad \textbf{5.3}$$

where *WC* is the wire consumption (kg), *WS* is the wire speed (m/min), *t* is the machining time (min), and *Wm* is the wire mass per meter (kg/m). The wire mass per meter was calculated by weighting 10 meters of the original wire electrode using a precise balancer.

The wire consumption cost can be calculated with **Equation 5.4.**

$$Cw = WC \times WP \qquad 5.4$$

Where *Cw* is the wire consumption cost in Malaysian Ringgit (RM) and *WP* is the wire price per kilogram (RM/kg).

5.3 Selected experimental parameters and results

In this study, brass and coated-wire electrodes were employed for machining titanium alloy grade 5 (Ti6Al4V). The machining parameters, including peak current, pulse width, and charging time were selected for this study based on the analysis in section (4.4) to develop a new performance criterion and identify the most suitable wire type for higher machining performance. A total of 18 data sets were selected in this study for coated and brass-wire electrodes, as demonstrated in **Table 5.1** and **5.2** respectively.

Table 5.1: Performance outcomes measured at different machining parameters with the coated wire

No.	Parameters				Performance factors					Performance outcomes		
	IP A	*Ton* µs	*Toff* µs	*WS* m/min	*Es*×*DF* Index	*Ce* RM	*Cw* RM	*Ct* RM	$\frac{Es \times DF}{Ct}$	*CS* mm/min	*Ra* µm	*WLT* µm
1	16	0.2	0.5	3	1829	0.0331	0.7086	0.7417	2465	1.42	2.23	5.66
2			0.9	7	1164	0.0346	1.7265	1.7611	661	1.36	2.15	4.96
3			1.3	11	853	0.0380	2.9764	3.0144	283	1.24	2.09	4.35
4		0.3	0.5	7	3600	0.0209	1.0426	1.0635	3385	2.25	2.69	10.09
5			0.9	11	2400	0.0267	2.0953	2.1221	1131	1.76	2.49	7.53
6			1.3	3	1800	0.0304	0.6504	0.6809	2644	1.54	2.32	6.12
7		0.4	0.5	3	5689	0.0137	0.2927	0.3064	18570	3.43	3.06	16.35
8			0.9	7	3938	0.0165	0.8219	0.8383	4698	2.85	2.86	12.65
9			1.3	11	3012	0.0189	1.4842	1.5031	2004	2.48	2.69	11.06
10	17	0.2	0.5	11	1943	0.0303	2.2398	2.2702	856	1.64	2.31	6.60
11			0.9	3	1236	0.0345	0.6955	0.7301	1694	1.44	2.22	5.71
12			1.3	7	907	0.0355	1.6691	1.7047	532	1.40	2.17	5.20
13		0.3	0.5	11	3825	0.0196	1.4453	1.4649	2611	2.55	2.82	11.48
14			0.9	3	2550	0.0216	0.4352	0.4568	5582	2.31	2.66	10.61
15			1.3	7	1913	0.0256	1.2012	1.2268	1559	1.95	2.46	8.63
16		0.4	0.5	7	6044	0.0130	0.6084	0.6214	9728	3.85	3.25	19.94
17			0.9	11	4185	0.0154	1.1361	1.1514	3634	3.24	2.92	15.68
18			1.3	3	3200	0.0187	0.3774	0.3961	8078	2.66	2.74	12.71

Table 5.2: Performance outcomes measured at different machining parameters with the brass wire

No.	Parameters				Performance factors					Performance outcomes		
	IP (A)	*Ton* (µs)	*Toff* (µs)	*WS* m/min	*Es*×*DF* Index	*Ce* (RM)	*Cw* (RM)	*Ct* (RM)	$\frac{Es \times DF}{Ct}$	*CS* mm/min	*Ra* (µm)	*WLT* (µm)
1	16	0.2	0.5	3	1829	0.0339	0.3379	0.3719	4918	1.38	2.58	11.73
2			0.9	7	1164	0.0424	0.9856	1.0280	1132	1.11	2.40	9.79
3			1.3	11	853	0.0552	2.0165	2.0717	412	0.85	2.35	8.09
4		0.3	0.5	7	3600	0.0289	0.6705	0.6994	5147	1.63	2.65	17.56
5			0.9	11	2400	0.0342	1.2481	1.2822	1872	1.37	2.50	14.26
6			1.3	3	1800	0.0428	0.4263	0.4691	3838	1.10	2.44	10.73
7		0.4	0.5	3	5689	0.0230	0.2295	0.2526	22524	2.04	2.89	23.34
8			0.9	7	3938	0.0265	0.6162	0.6428	6128	1.77	2.81	19.75
9			1.3	11	3012	0.0307	1.1227	1.1535	2611	1.53	2.66	16.07
10	17	0.2	0.5	11	1943	0.0342	1.1740	1.2081	1608	1.46	2.54	15.64
11			0.9	3	1236	0.0430	0.4030	0.4460	2772	1.16	2.44	12.62
12			1.3	7	907	0.0556	1.2164	1.2721	713	0.90	2.29	9.98
13		0.3	0.5	11	3825	0.0287	0.9851	1.0137	3773	1.74	2.68	20.23
14			0.9	3	2550	0.0325	0.3042	0.3367	7575	1.54	2.58	17.60
15			1.3	7	1913	0.0387	0.8455	0.8842	2163	1.29	2.55	15.61
16		0.4	0.5	7	6044	0.0229	0.5003	0.5232	11553	2.18	3.07	26.32
17			0.9	11	4185	0.0266	0.9150	0.9416	4444	1.87	3.02	21.56
18			1.3	3	3200	0.0293	0.2744	0.3037	10536	1.70	2.76	18.66

5.4 Analysis and discussion

The performance index proposed in section 4.4 correlates spark energy and pulse frequency with the machining performance measures (cutting speed, surface roughness, and white layer thickness) in using coated and brass-wire electrodes. According to the analytical and experimental investigations in section 4.4, the machining performance of WEDM is directly dependent on spark energy parameters (*IP*, *Vd*, and *Ton*) and duty factor, or pulse frequency parameters (*Ton* and *Toff*). The theoretical analysis and experimental results present good agreement and high potential for use in future research to control and predict WEDM conditions. By applying the proposed performance index ($Es \times DF$), it appears that using a lower spark setting with higher pulse cycle setting will reduce chip size and produce better flushing. This could lead to faster cutting with good surface finish and less wire rupture. Moreover, the performance index gives a good indication of the wire rupture limit.

However, based on the preceding analysis, this performance index cannot be used to identify the most suitable wire electrode for higher cutting rate and better surface quality considering economic and ecological aspects. Therefore, a new production economic index was proposed to select the most feasible wire electrode considering the economic and ecological aspects with the weighted energy performance index to attain higher machining performance with the lowest possible energy and wire consumption and cost. This can be done by dividing the proposed performance index by the total machining cost ($Es \times DF/Ct$).

5.4.1 Cutting speed analysis

Figure 4.75 and **4.76** display the change in cutting speed at different performance index levels using coated (**Figure 4.75**) and brass (**Figure 4.76**) wire electrodes. According to these two figures, cutting speed increases linearly with increasing performance index (*Es*×*DF*). At the same performance index level, the cutting speed values when using the coated wire are higher than when using brass wire. Hence, for higher cutting rate, it is recommended to use the coated-wire electrode to cut Ti5Al4V work material in WEDM. However, this performance index cannot be used to identify which wire is more economic and environmentally friendly. Therefore, a new cutting speed performance criterion (*Es*×*DF/Ct*) was developed to include energy and wire consumption and cost to identify the most suitable wire electrode for WEDM.

Figure 5.3 and **5.4** display the change in cutting speed at different new performance criteria levels using coated (**Figure 5.3**) and brass (**Figure 5.4**) wire electrodes. According to these figures, cutting speed increases with the increase in the new performance criterion for both wire electrodes. Moreover, the machining conditions of point (16) are not the best in terms of the economic aspect for both wire electrodes. However, the conditions of point (7) are economic and yield considerable cutting speed without wire rupture for both wire electrodes. The new performance criterion at point (7) for brass wire is around 22,500 (**Figure 5.4**) and for the coated wire electrode it is around 18,500 (**Figure 5.3**). Hence, the brass wire electrode is more feasible and economic than the coated-wire electrode for the cutting speed range of 1 to 2 mm/min but for the 2 to 3.5 mm/min range, the coated wire is more feasible when using the machining conditions of experiment (7). Therefore, based on the required cutting rate, the new production economic index can be used to identify the most economic and energy saving wire electrode.

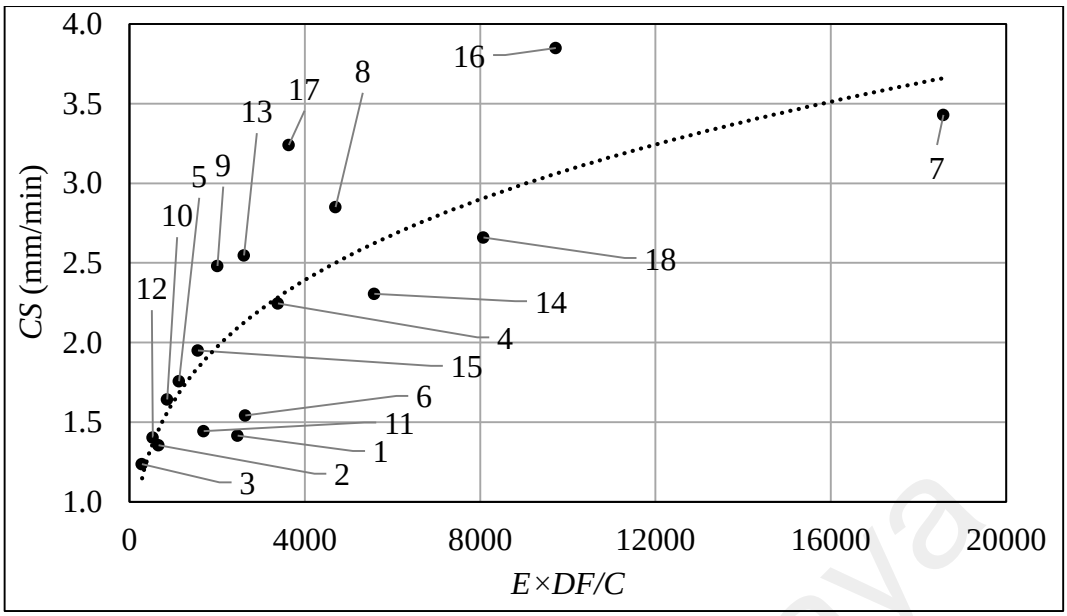

Figure 5.3: Experimental influence of the new performance criterion on cutting speed using the coated wire.

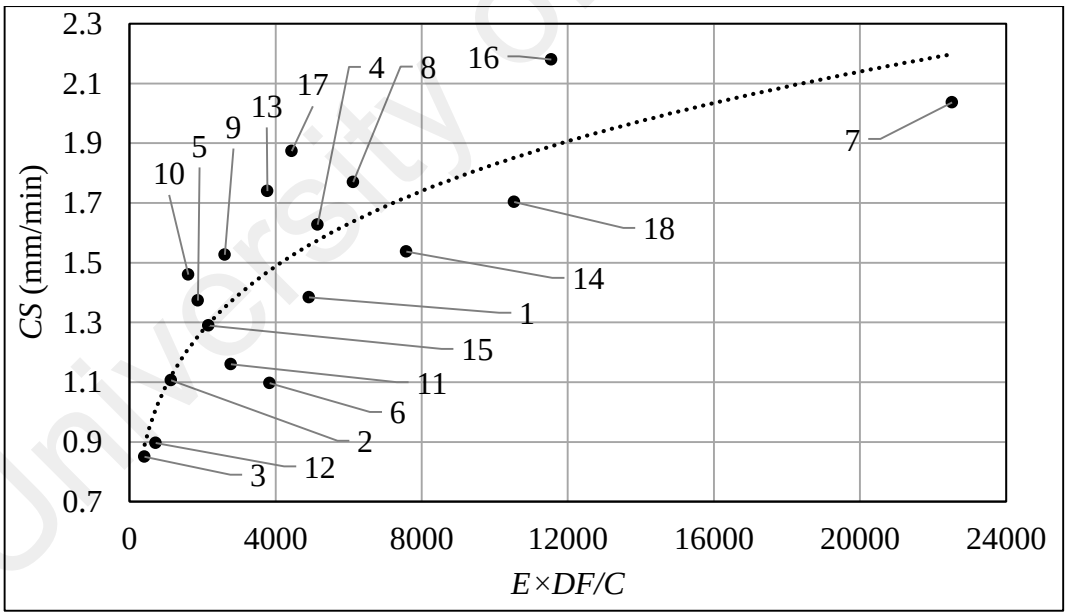

Figure 5.4: Experimental influence of the new performance criterion on cutting speed using the brass wire.

5.4.2 Surface roughness analysis

Figure 4.81 and **4.82** display the relation between surface roughness and the proposed performance index using coated (**Figure 4.81**) and brass (**Figure 4.82**) wire electrodes. Surface roughness increases linearly with increasing performance index. **Figure 5.5** shows the SEMs of two surfaces at the same level (point 15) of the proposed performance index using coated and brass wire electrodes, respectively. The crater and surface crack sizes on both surfaces are very similar. In addition, very small changes in surface roughness values between both samples were observed, with 2.46 and 2.55 µm for the coated and brass wire electrodes respectively. Hence, wire electrode type has no effect on surface roughness based on the performance index. It is clear from the analysis that the performance index cannot be used to identify the most suitable wire type considering energy and wire consumption and cost. To include the effects of the ecological and economic aspects on surface roughness, the proposed performance index is divided by the total cost of energy and wire consumption ($Es \times DF/Ct$)..

Figure 5.6 and **5.7** show the relations between surface roughness and the new performance criterion with coated (**Figure 5.6**) and brass (**Figure 5.7**) wire electrodes. Surface roughness increases with increasing performance criterion for both wires. In the surface roughness range of 2 to 2.7 µm, both wires are feasible based on the energy consumption and economic criteria. However, for the surface roughness range of 2.7 to 3.2 µm, the brass wire is more economic and feasible than the coated-wire electrode. This is because at all points, the brass wire electrode has higher performance criterion values than the coated wire, for instance at point (18) the performance criterion is around 10,500 (**Figure 5.7**) but for the coated wire it is around 8,000 (**Figure 5.6**). The same conclusion can be drawn regarding points (7) and (16). Hence, at specific surface roughness values, the newly proposed production economic index can be used to identify the most economic type of wire electrode.

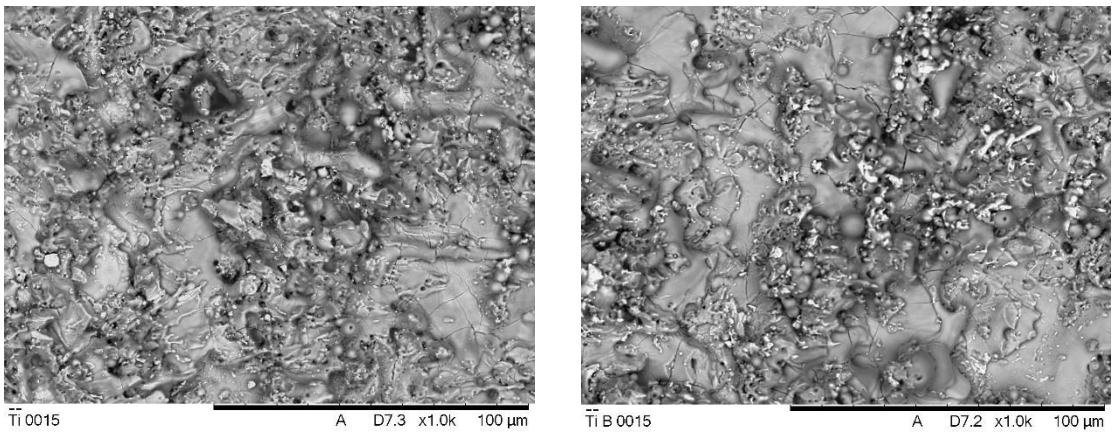

(a) **(b)**

Figure 5.5: SEM micrographs of the surface at the same performance index level (point 15) using (a) the coated wire, and (b) the brass wire electrode

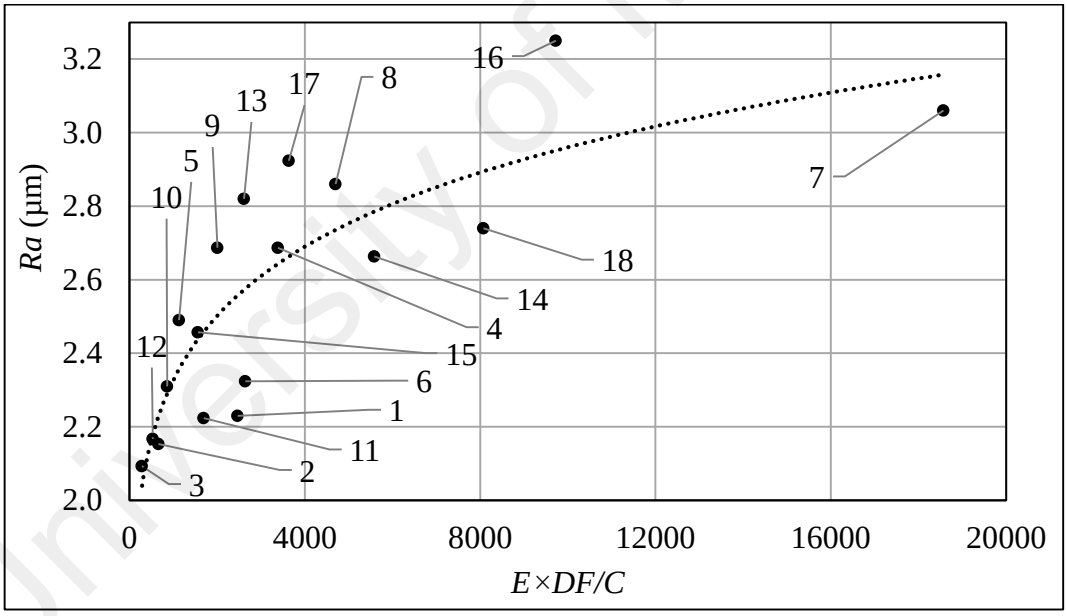

Figure 5.6: Experimental influence of the new performance criterion on surface roughness using the coated wire.

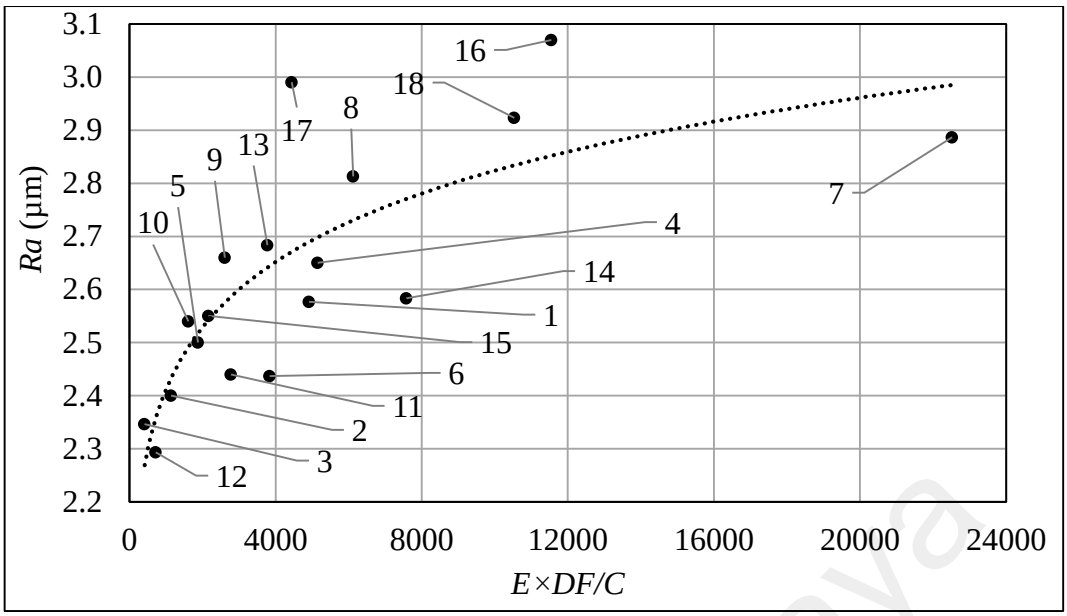

Figure 5.7: Experimental influence of the new performance criterion on surface roughness using the brass wire.

5.4.3 White layer thickness analysis

Figure 4.88 and **4.89** show the relation between white layer thickness and the proposed performance index using the coated wire (**Figure 4.88**) and brass wire electrode (**Figure 4.89**). The white layer thickness increases with increasing proposed performance index. At the same performance index, the white layer thickness values for using the coated wire electrode are higher than using the brass wire electrode. **Figure 5.8** displays the SEM of the edge of two samples (experiment no. 7) at the same performance index value. It is clear from this figure that the white layer thickness of sample (7) when using the coated-wire electrode is 16.35 µm (**Figure 5.8 (a)**) and for the same condition using the brass wire electrode it equals 23.34 µm (**Figure 5.8 (b)**). Therefore, the coated wire is more convenient for a thinner white layer based on the performance index analysis. However, the coated-wire electrode is costlier than the brass wire electrode. Hence, it is important to consider machining cost together with the performance index to identify the most feasible wire electrode type.

This section provides an analysis of the effects of the spark energy, pulse frequency, and total machining cost (energy and wire consumption costs) parameters on white layer thickness. A new performance criterion was developed to consider the effect of energy and wire costs on white layer thickness. **Figure 5.9** and **5.10** present the relation between white layer thickness and the proposed performance criterion for both coated (**Figure 5.9**) and brass (**Figure 5.10**) wire electrodes. White layer thickness increases with increasing proposed performance criterion for both wire electrodes. When the spark energy, pulse frequency, and total machining cost change, the proposed performance criterion changes accordingly, leading to a change in white layer thickness. The coated-wire electrode is more economic and feasible than the brass wire electrode for all white layer thickness ranges, as shown in **Figure 5.9** and **5.10**. For thinner white layers ranging from 5 to 10 µm, the coated wire is feasible based on the energy consumption and economic criteria and the most suitable cutting conditions are at point (4). However, for white layer thickness ranging from 10 to 20 µm, the coated wire is also more economic and feasible than the brass wire electrode and the best machining conditions are at point (7). Therefore, the coated wire is the best choice for machining Ti6Al4V in terms of thinner white layer and low cost.

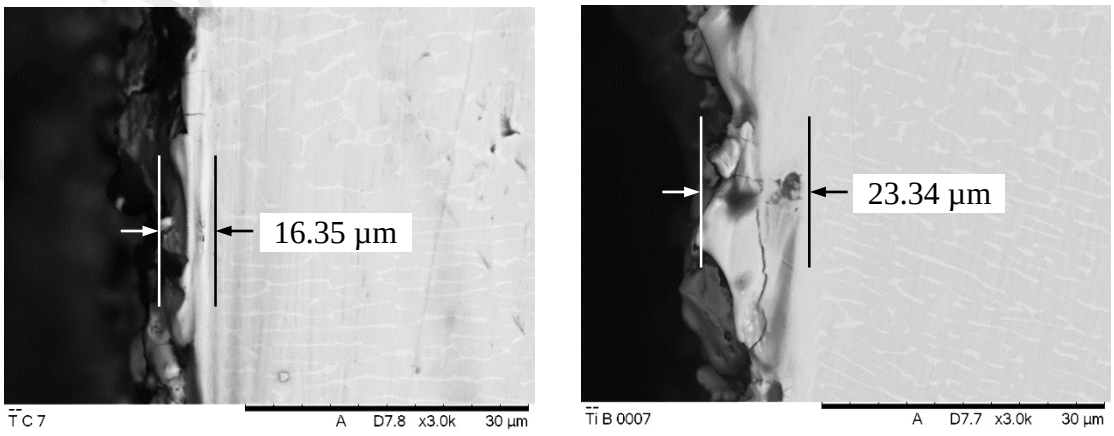

(a) **(b)**

Figure 5.8: SEM micrographs at the same performance index level (point 7) using (a) the coated wire and (b) the brass wire electrode

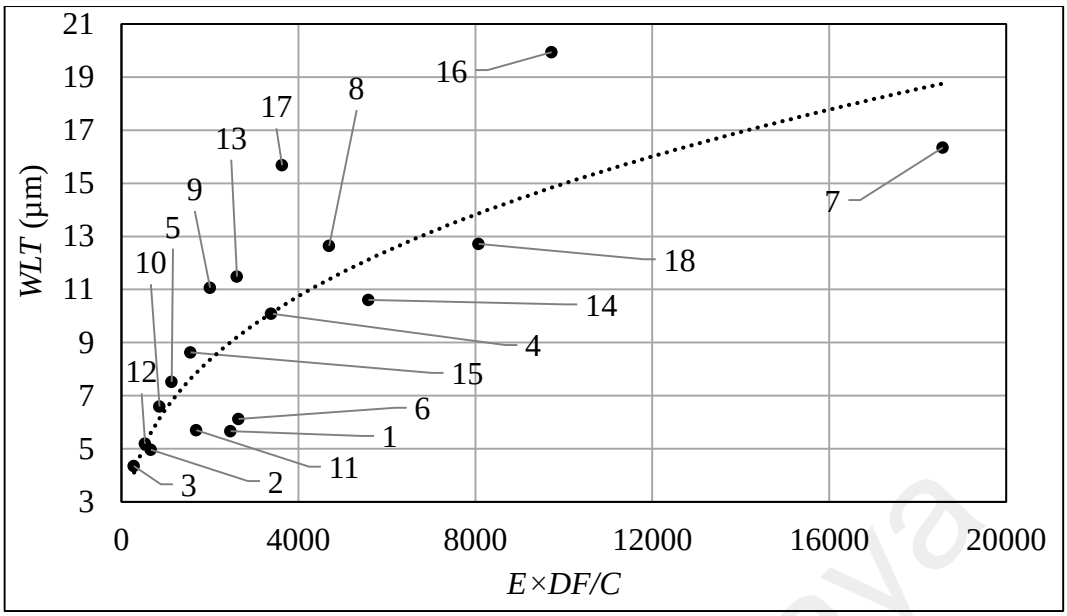

Figure 5.9: Experimental influence of the new performance criterion on white layer thickness using the coated wire.

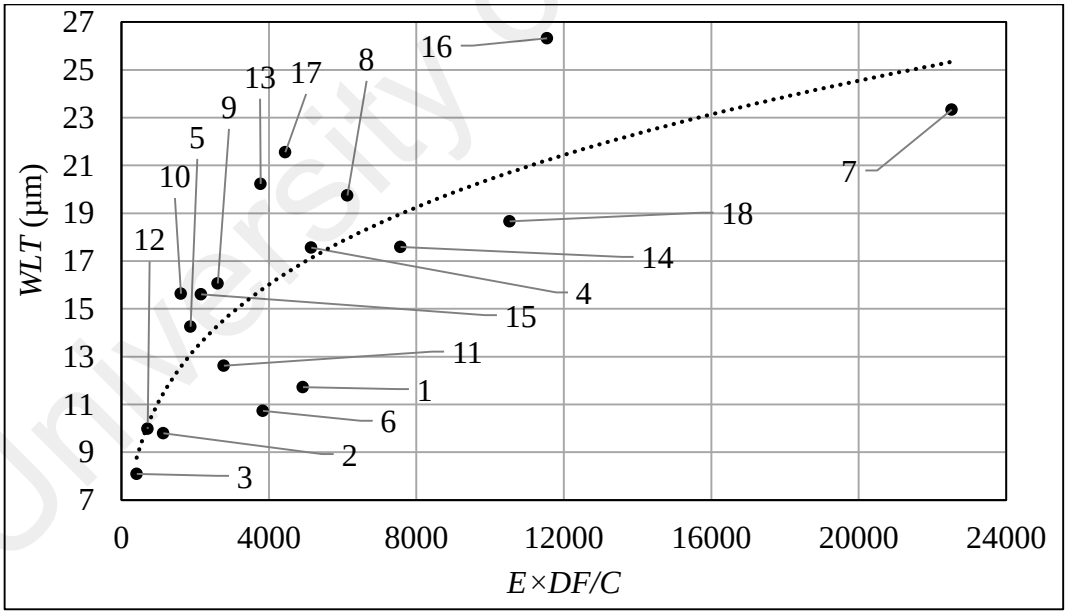

Figure 5.10: Experimental influence of the new performance criterion on white layer thickness using the brass wire.

Based on the proposed performance index and the developed production economic index, finding the optimum wire for any application entails reaching an acceptable compromise between the above-mentioned properties (wire rupture limit and electrical conductivity), since they are frequently conflicting. For example, high conductivity wires often have a low wire rupture limit. Hence, the challenge faced by WEDM manufacturers is to continuously push the envelope in the area of developing EDM wire electrodes that have high electrical conductivity and high tensile strength, are environmental friendly, and can reduce energy and wire consumption during WEDM. Therefore, the following section presents a new wire electrode design proposed to enhance machining performance considering the ecological and economic aspects.

5.5 Proposing a new electrode wire design for use in WEDM

This section introduces the basis for the design of a new composite wire electrode and the features of conductivity and good sparking ability are matched with an increase in accuracy. To attain superior accuracy, a high tensile strength core is chosen regardless of its electrical conductivity. In this way, the load applicable on the wire can be increased to establish more precise machining. Coating is added to provide the wire with sufficient electrical conductivity and finally, the wire is coated with a superficial layer to facilitate good sparking ability (Sarhan, Hamdi, & Maher, 2016). The following sections discuss the layers constituting this composite wire electrode in detail.

5.5.1 Wire electrode design

The design of this new wire electrode was especially developed for the WEDM process for better machining performance, more energy savings, and less wire rupture. The new design includes a high-strength steel core coated with pure copper, which is finally coated with Zn/Al alloy. The steel core serves to increase the applicable tensile load, hence reducing wire breakage and increasing cutting accuracy. The intermediate copper coating layer provides the wire with sufficient electrical conductivity to increase cutting speed and the Zn/Al alloy in the outer coating layer is for good flushability and sparking ability to enhance the surface quality as shown in **Figure 5.11**.

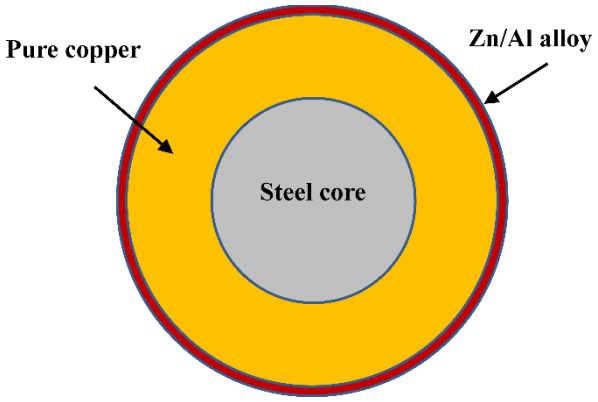

Figure 5.11: Cross section of the developed wire electrode

5.5.2 High tensile strength core

Figure 5.12 presents an Ashby diagram of the materials available in the wire and their electrical resistivity is plotted against their tensile strength. This figure signifies that it is impossible to match high tensile strength and good electrical conductivity in one material. Hence, a composite wire with a high tensile strength core coated with a layer with high electrical conductivity is developed. Therefore, the electrical conductivity and tensile strength are separated. A pearlitic steel core (0.6% C) was chosen for its high tensile strength at room temperature (4000 MPa or higher at 23°C) (Kruth et al., 2004).

At elevated wire temperatures during machining, the tensile strength of the pearlitic wire core is slightly lower while the strain is higher (**Figure 5.13**), which helps the wire elongate for a long time before cutting. At 150°C, which is often referred to as the establishment temperature of the wire, the tensile strength is still 3500 MPa. The strength of pearlitic steel is higher than any known wire electrode material (**Table 5.3:** . In comparison to Molybdenum wire, the tensile strength is double over the entire temperature range of interest (23-150°C) (Snoeys & Dekeyser, 1988).

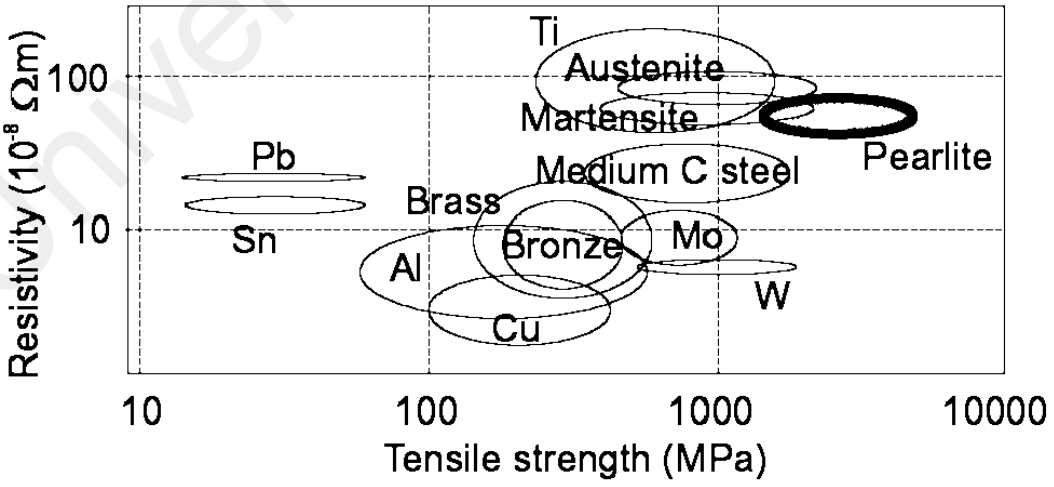

Figure 5.12: Resistivity vs. tensile strength Ashby chart of available wire materials (Kruth et al., 2004)

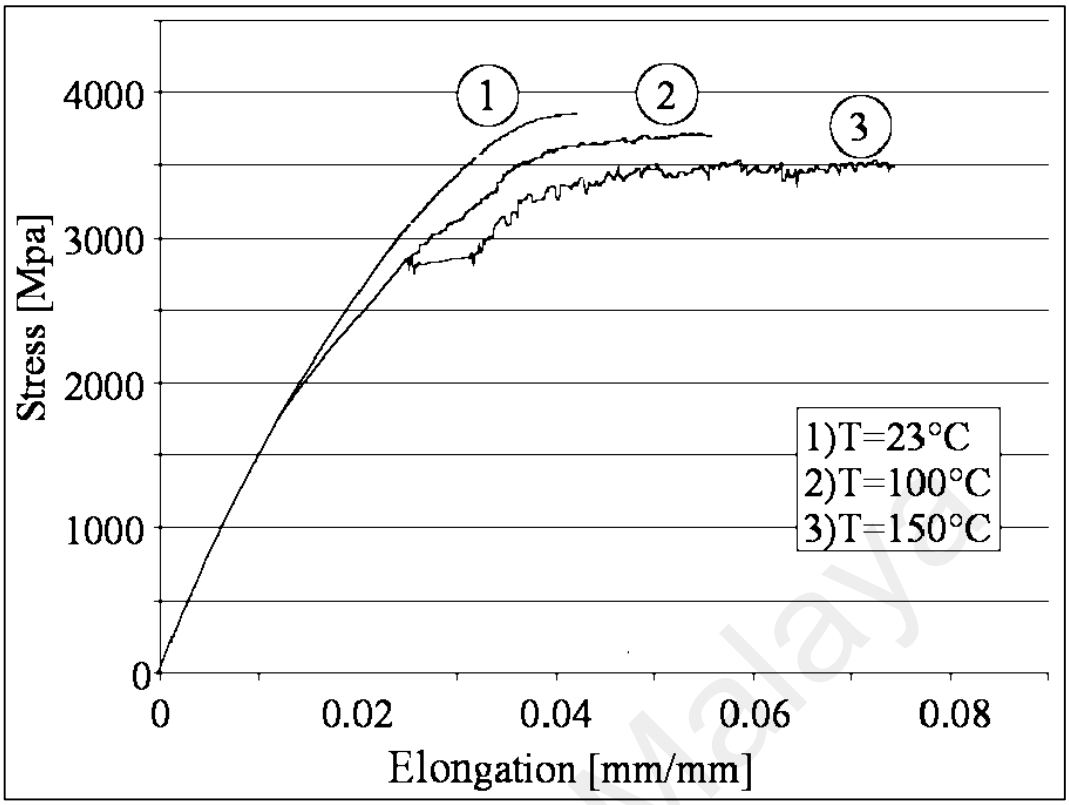

Figure 5.13: Stress-strain diagram of pearlitic steel at different temperatures.

Table 5.3: Tensile strength (MPa) of pearlitic steel wire and most common EDM wire electrode at different temperatures (Snoeys & Dekeyser, 1988)

Wire material	23° C	100° C	150° C
Pearlitic steel	3850	3690	3490
Hard brass CuZn37	1035	835	700
Molybdenum	1930	1820	1750

5.5.3 Intermediate layer with high electrical conductivity

The conductivity of a wire electrode can be increased by applying a conductive layer in between the core and the outer coating. The conductive layer will be electrically in parallel to the core. Good wire conductivity allows the application of high energies. Cutting speed mainly depends on the electrical conductivity of the wire electrode. **Table 5.4** compares the peak current of steel, brass, and copper wires. The lower peak current

of steel wire is due to the lower current resistance and higher impedance of the wire at higher frequencies due to the skin effect in the magnetic steel core. In WEDM, the basic frequency of the current signal is as high as 100 kHz for modern machines and still rising with the introduction of newer machines. At this frequency, the skin effect forces the current to the outer side of the steel core. For nonmagnetic materials, such as brass, copper or tungsten and molybdenum, the skin effect is not significantly present (Benny Schacht, Kruth, Lauwers, & Vanherck, 2004). Pure copper was chosen as a material with high electrical conductivity. Hence, the intermediate copper layer applied, since the current forced out of the core is given a conductive path, compensates the drop in steel core conductivity.

Table 5.4: Peak current for wires with changing electrical conductivity

Material	**Conductivity (%ICAS)**	**Cross section diameter**	
		100 µm	**250 µm**
Copper	100	300 A	455 A
Brass	26	275 A	432 A
Pearlitic steel	10	235 A	403 A
Pearlitic steel with copper intermediate layer	30	271 A	430 A

5.5.4 High sparking and flushing ability

The good sparking properties of Zinc-Aluminum alloy improve the sparking and flushing ability, leading to enhanced cutting rate and surface quality. A coating must be designed to provide the wire with good machining performance from the point of view of cutting rate. Many authors have reported the good sparking properties of zinc and its alloys, as discussed in the literature chapter.

5.6 Conclusion

Based on the analytical and experimental investigations above, it is concluded that the machining performance of WEDM is directly dependent on the spark energy, duty factor, and total machining cost parameters. The experimental results present good agreement and high potential for use in future research to control and select the most feasible wire electrode with the best WEDM machining conditions. The proposed production economic index ($Es \times DF/Ct$) much more conveniently correlates the performance parameters (*CS*, *Ra* and *WLT*) with the spark energy, duty factor, and machining cost parameters in the WEDM process. By applying the proposed production economic index, it appears that using a lower spark setting and higher pulse cycle setting with a brass wire electrode can decrease the surface roughness and white layer thickness and produce more economic cutting speed. This could lead to faster cutting, good surface finish, and less wire rupture.

Moreover, a new electrode wire was designed for use in WEDM comprising a high tensile strength core coated with a high electrical conductivity intermediate layer and outer-coated superficial layer. The core contains pearlitic steel materials with 0.6 carbon content to provide the wire high tensile strength for less rupture. The intermediate layer is made from pure copper to increase the electrical conductivity of the wire for high cutting rate. The outer-coated layer is made of Al/Zn alloy to provide the wire with high flushability and sparking ability to improve machined surface quality and increase the cutting rate.

CHAPTER 6: CONCLUSIONS

6.1 Conclusions and recommendations

This study investigated the effects of cutting parameters on the machining performance outcomes of Titanium alloy grade 5 (Ti6Al4V) and AISI1050 carbon steel workpieces using conventional brass and most recently coated-wire electrodes in the wire electrical discharge machining process (WEDM). The cutting parameters include peak current (*IP*), pulse on time (*Ton*), pulse off time (*Toff*), wire speed (*WS*), and wire tension (*WT*) and the machining performance outcomes include cutting speed (*CS*), surface roughness (*Ra*), white layer thickness (*WLT*), and wire rupture (*WL*).

Two data analysis techniques, namely the Taguchi approach and adaptive neuro-fuzzy inference system (ANFIS) were employed to achieve high productivity and the best surface quality, from which similar conclusions were drawn. Peak current, pulse on time, and pulse off time are the most significant parameters affecting cutting speed, surface roughness, white layer thickness, and wire rupture. Wire tension and wire speed have a minor effect on cutting speed, surface roughness, and white layer thickness, but they have a pronounced effect on wire rupture.

ANFIS was successfully used to develop an empirical model for modeling the relation between the predictor variables (*IP*, *Ton*, *Toff*, *WS*, and *WT*) and the performance outcomes (*CS*, *Ra*, *WLT*, and *WL*). The training dataset for each ANFIS model was built using 18 values measured under different cutting conditions. Four values were used as testing data to verify the models, and the average errors were very small for all models. These results indicate that the ANFIS model with gbellmf is accurate and can be used to predict *CS*, *Ra*, *WLT*, and *WL* in WEDM. The ANFIS model results were also compared with the Taguchi model results. As anticipated, the ANFIS models made efficient predictions because they generally offer the ability to model more complex nonlinearities

and interactions. In addition, by analyzing the results using the conceptual ANFIS approach, the following can be concluded:

- ANFIS was used to introduce a technological knowledge base for the selection of machining parameters to achieve high productivity and the highest possible surface quality for sustainable production and lower process cost.
- High pulse on time (0.4 µs), high peak current (17 A), and low pulse off time (0.5 µs) are recommended to attain high productivity for a definite test range.
- Low pulse on time (0.2 µs), low peak current (16 A), high pulse off time (1.3 µs), high wire speed (11 m/min), and high wire tension (10.5 N) lead to lower surface roughness, white layer thickness, and wire rupture for the specific test range.
- Using a coated-wire electrode is preferable to using a brass wire to achieve higher cutting speed, smaller surface roughness and a thinner white layer.
- Metals with high thermal conductivity (AISI 1050 carbon steel) typically exhibit a thinner white layer and less micro cracking than less conductive materials (Ti6Al4V) in WEDM.
- High wire speed and low wire tension lead to smaller wire electrode surface craters, hence these are recommended to prevent wire rupture.

According to the analytical and experimental investigations carried out, the machining performance of CNC-WEDM is directly dependent on spark energy parameters (*IP*, *Vd*, and *Ton*) and duty factor, or pulse frequency parameters (*Ton* and *Toff*). However, it is very difficult to study the effects of spark energy and pulse frequency simultaneously on machining performance. For this reason, a new, simple performance index was proposed to study the effects of spark energy in conjunction with pulse frequency at different duty

factors on machining characteristics to achieve superior machining performance with WEDM.

The proposed performance index (*Es*×*DF*) much more conveniently correlates the performance parameters (*CS*, *Ra* and *WLT*) with the spark energy and duty factor parameters in the WEDM process. The theoretical analysis and experimental results present good agreement and high potential for use in future research to control and predict WEDM machining conditions using the proposed performance index. With applying the proposed performance index, it appears that using a lower spark setting and higher pulse cycle setting can reduce chip size and facilitate better flushing. This could lead to faster cutting with good surface finish and less wire rupture. Moreover, the new performance index gives a good indication of the wire rupture limit.

However, the performance index cannot be used to identify the most feasible wire electrode from ecological (energy and wire consumption) and economic (machining costs) perspectives. Although WEDM machine tools are equipped with cutting condition tables for each wire electrode, it is still very hard to select an appropriate wire that abides by the machining requirements as well as minimizes the machine tool energy, consumable utilization, and machining cost. Therefore, a new production economic index was developed and introduced to identify the most feasible wire electrode for higher WEDM performance in terms of ecological and economic aspects.

The proposed production economic index criterion (*Es*×*DF*/*Ct*) can much more easily correlate the performance parameters (*CS*, *Ra* and *WLT*) with the spark energy, duty factor, and machining cost parameters in the WEDM process. By applying the developed production economic index, using a brass wire electrode is more feasible and economic than a coated-wire electrode in the cutting speed range of 1 to 2 mm/min, but for the 2 to 3.5 mm/min range, the coated wire is more feasible. In the surface roughness

range of 2 to 2.7 µm, both wires are feasible in terms of the energy consumption and economic criteria; however, in the surface roughness range of 2.7 to 3.2 µm, the brass wire is more economic and feasible than the coated-wire electrode. For all white layer thickness ranges (from 5 to 20 µm), the coated wire is more feasible in terms of the energy consumption and economic criteria.

With respect to the proposed performance index and the developed production economic index, finding the optimum wire for any application means reaching an acceptable compromise among the above-mentioned properties (wire rupture limit and electrical conductivity), since they are frequently conflicting. For example, high conductivity wires often have low wire rupture limits. Therefore, a new wire electrode design to enhance machining performance considering the ecological and economic aspects was proposed.

This new design provides an electrode wire comprised of a core and two coated layers. The core made of pearlitic steel materials with 0.6 carbon content gives the wire high tensile strength, the intermediate layer made of pure copper increases the electrical conductivity, and the outer coating layer made of Al/Zn alloy provides the wire with high flushability and sparking ability. Thus, the wire electrode facilitates superior machining performance and enhances product quality. It can save machining time, improve machining of sharp edges and corners, and surface quality, and increase the cutting rate. Besides, the new wire electrode can help reduce energy consumption and wire rupture, and is environmentally friendly and more economical than other wires.

6.2 Future works

Future works will address the following topics:

- Manufacturing the wire electrode design proposed.
- Investigating the effects of the new wire electrode on machining performance outcomes using the Taguchi technique and ANFIS modeling.
- Comparing the new wire and competitor wires on the market using the proposed performance index.
- Identifying the feasibility of the new wire electrode for high machining performance considering the ecological and economical aspects.

REFERENCES

Altpeter, F., & Perez, R. (2004). Relevant topics in wire electrical discharge machining control. *Journal of Materials Processing Technology*, *149*(1–3), 147-151. doi:http://dx.doi.org/10.1016/j.jmatprotec.2003.10.033

Antar, M. T., Soo, S. L., Aspinwall, D. K., Jones, D., & Perez, R. (2011). Productivity and Workpiece Surface Integrity When WEDM Aerospace Alloys Using Coated Wires. *Procedia Engineering*, *19*(0), 3-8. doi:http://dx.doi.org/10.1016/j.proeng.2011.11.071

Aoyama, S. (2001). Development of high performance wire electrode for wire electric discharge machining. *J Japan Soc Electrical Machining Engrs*, *35*, 46-51.

Aoyama, S., Kuroda, H., Seya, O., Kimura, T., & Sato, T. (2008). Development and applications of high-strenth-high conductivity copper alloy wire formed by continuous casting and hot rolling. *Hitachi Cable Review*(2), 102-102.

Aoyama, S., Tamura, K., Sato, T., Kimura, T., Sawahata, K., & Nagai, T. (1999). High-performance coated wire electrodes for high-speed cutting and accurate machining. *Hitachi Cable Review*, *18*, 75-80.

Baker, H. (1992). *ASM Metals Handbook: Alloy Phase Diagrames* (Vol. 3): ASM International.

Banzai, M., & Shibata, Y. (1990). US 4,968,867.

Barthel, B., Groos, H., & Hermanni, H. (1998). US 5,762,726.

Barthel, B., Groos, H., Hermanni, H., & Tauber, K. (1998). WO Patent 1,998,009,764.

Barthel, B., & Neuser, B. (2003). US 6566622 B1.

Barzani, M. M., Sarhan, A. A. D., Singh, R., Maher, I., & Farahany, S. (2015). *Investigation into effect of silicon morphology on surface roughness while machining Al-Si-Cu-Mg alloy*. Paper presented at the Malaysian International Tribology Conference 2015, Penang, Malaysia.

Baumann, I., & Barthel, B. (2002). US 6,348,667 B2.

Baumann, I., & Nöthe, T. (2011). US 2011/0290531 A1.

Blanc, P., Ly, M., & Sanchez, G. (2013). US 8,378,247 B2.

Brandes, E. A., Brook, G. B., & Smithells, C. J. (1998). *Smithells metals reference book* (7th ed / edited by E.A. Brandes and G.B. Brook. ed.). Oxford ; Boston: Butterworth-Heinemann.

Briffod, J.-P. (1993a). US 5,196,665 A.

Briffod, J.-p. (1993b). EP 0,521,569.

Briffod, J.-P., Martin, R., Pfau, J., Bommeli, B., & Schnellmann, D. (1982). US 4,341,939.

Briffod, J. (1990). US 4,977,303.

Briffod, J. P. (1999). US 5,858,136.

Burakowski, T., & Wierzchoń, T. (1999). *Surface engineering of metals : principles, equipment, technologies*. Boca Raton, Fla.: CRC Press.

Çaydaş, U., Hasçalık, A., & Ekici, S. (2009). An adaptive neuro-fuzzy inference system (ANFIS) model for wire-EDM. *Expert Systems with Applications, 36*(3, Part 2), 6135-6139. doi:http://dx.doi.org/10.1016/j.eswa.2008.07.019

Cheng, X., Yang, X. H., Huang, Y. M., Zheng, G. M., & Li, L. (2014). Helical surface creation by wire electrical discharge machining for micro tools. *Robotics and Computer-Integrated Manufacturing, 30*(3), 287-294. doi:http://dx.doi.org/10.1016/j.rcim.2013.10.010

Cheremisinoff, N. P. (1996). *Materials selection deskbook*. Noyes Publications Westwood, New Jersey, U.S.A.

Chiriotti, N., Pinaya, R. P., & Fluekiger, R. (2002). US 6495788 B1.

Convers, D., Balleys, F., & Pfau, J. (1981). US 4,287,404.

Cut, X.-X., Masuzawa, A., & Fujino, M. (1991). Study on Flushing for EDM (1st Report) -Proposal of 2D Small Vibration Method and Scan-Flushing Method-. *J Japan Soc Electrical Machining Engrs, 26*, 1-12.

Cut, X.-X., Masuzawa, T., & Taniguchi, N. (1993). Study on Flushing for EDM (2nd Report) -Analysis and simulation of the effect of jet flushing for EDM-. *J Japan Soc Electrical Machining Engrs, 27*, 10-22.

Dauw, D. F., & Albert, L. (1992). About the Evolution of Wire Tool Performance in Wire EDM. *CIRP Annals - Manufacturing Technology, 41*(1), 221-225. doi:http://dx.doi.org/10.1016/S0007-8506(07)61190-1

Dauw, D. F., & Beltrami, I. (1994). High-Precision Wire-EDM by Online Wire Positioning Control. *CIRP Annals - Manufacturing Technology, 43*(1), 193-197. doi:http://dx.doi.org/10.1016/S0007-8506(07)62194-5

Davis, J. R. (1998). *Metals handbook desk edition* (2 ed.): ASM International Handbook Committee.

Deiss, C. (2009). *Eco machine Study on Energy Consumption of wire and wire Erosion Machine* (Master), RWTH Aachen University, German.

Dekeyser, W., Snoeys, R., & Jennes, M. (1988). Expert system for wire cutting EDM, based on pulse classification and thermal modeling. *Robotics and Computer-Integrated Manufacturing, 4*(1–2), 219-224. doi:http://dx.doi.org/10.1016/0736-5845(88)90080-4

Dhanik, S., Xirouchakis, P., & Perez, R. (2011). A System for Resource Efficient Process Planning for Wire EDM. In J. Hesselbach & C. Herrmann (Eds.), *Glocalized Solutions for Sustainability in Manufacturing: Proceedings of the 18th CIRP International Conference on Life Cycle Engineering, Technische Universität Braunschweig, Braunschweig, Germany, May 2nd - 4th, 2011* (pp. 219-224). Berlin, Heidelberg: Springer Berlin Heidelberg.

El-Hofy, H. (2005). *Advanced machining processes*. New York, USA: McGraw-Hill.

Ezaki, S., Hasegawa, H., & Seto, H. (1991). US 5028756 A.

Ferreira, J. (2007). A study of die helical thread cavity surface finish made by Cu-W electrodes with planetary EDM. *The International Journal of Advanced Manufacturing Technology*, *34*(11-12), 1120-1132. doi:http://dx.doi.org/10.1007/s00170-006-0687-z

Fowle, F. F. (1933). US 1,896,613.

Fuller, R. (1995). *Neural fuzzy systems*. Berlin/Heildelberg: Åbo Akademis tryckeri, Åbo, ESF Series A:443.

Garg, R. (2010). *Effect of process parameters on performance measures of wire electrical discharge machining.* (Ph.D.), National institute of technology, kurukshetra.

Gedeon, M. (2011). Strip Vs wire. *Technical Tidbits*, *3*(11).

Ghodsiyeh, D., Golshan, A., & Shirvanehdeh, J. A. (2013). Review on Current Research Trends in Wire Electrical Discharge Machining (WEDM). *Indian Journal of Science and Technology*, *6*(2), 154-168.

Gonnissen, D., & Van Vooren, W. (2001). WO Patent 2,001,089,750.

Gonnissen, D., & Vooren, W. V. (2005). US 6,875,943 B2.

Gostimirovic, M., Kovac, P., Sekulic, M., & Skoric, B. (2012). Influence of discharge energy on machining characteristics in EDM. *Journal of Mechanical Science and Technology*, *26*(1), 173-179. doi:http://dx.doi.org/10.1007/s12206-011-0922-x

Groos, H. (1988). US 4766280 A.

Groos, H., Barthel, B., Noethe, T., & Dietrich, C. (2004a). US 6,781,081 B2.

Groos, H., Barthel, B., Noethe, T., & Dietrich, C. (2004b). US 6794597 B2.

Groos, H., & Hermanni, H. (1990). US 4,935,594.

Hermanni, H. (1990). US 4924050.

Herreroa, A., Azcaratea, S., Reesb, A., Gehringerc, A., Schothc, A., & Sanchezd, J. A. (2008). Influence of force components on thin Wire EDM. *Multi-Material Micro Manufacture*.

Hewidy, M., El-Taweel, T., & El-Safty, M. (2005). Modelling the machining parameters of wire electrical discharge machining of Inconel 601 using RSM. *Journal of Materials Processing Technology, 169*(2), 328-336.

Ho, K. H., Newman, S. T., Rahimifard, S., & Allen, R. D. (2004). State of the art in wire electrical discharge machining (WEDM). *International Journal of Machine Tools and Manufacture*, *44*(12–13), 1247-1259. doi:http://dx.doi.org/10.1016/j.ijmachtools.2004.04.017

Huang, Y., Ming, W., Guo, J., Zhang, Z., Liu, G., Li, M., & Zhang, G. (2013). Optimization of cutting conditions of YG15 on rough and finish cutting in WEDM based on statistical analyses. *The International Journal of Advanced Manufacturing Technology, 69*(5-8), 993-1008. doi:10.1007/s00170-013-5037-3

Inoue, K. (1983). US 4418263 A.

Inoue, K. (1985). US 4508604 A.

Intech, E. (1995). EDM Wire: A reference to understanding, selecting and using wire on wire-cut EDM machines. *USA*.

Iwata, Y., Obara, H., Ohsumi, T., & Matsuda, Y. (1995). Simulation of Wire EDM (1st Report) -Simulating Procedure and Examples-. *J Japan Soc Electrical Machining Engrs*, *29*, 40-48.

Izquierdo, B., Sánchez, J. A., Plaza, S., Pombo, I., & Ortega, N. (2009). A numerical model of the EDM process considering the effect of multiple discharges. *International Journal of Machine Tools and Manufacture, 49*(3–4), 220-229. doi:http://dx.doi.org/10.1016/j.ijmachtools.2008.11.003

Jahan, M. (2013). Micro-Electrical Discharge Machining. In J. P. Davim (Ed.), *Nontraditional Machining Processes*: Springer London.

Jameson, E. C. (2001). *Electrical Discharge Machining*. Dearborn, Michigan: Society of Manufacturing Engineers.

Jang, J.-S. R., Sun, C.-T., & Mizutani, E. (1997). *Neuro-fuzzy and soft computing : a computational approach to learning and machine intelligence*. U.S.A.: Prentice Hall, Inc.

Jangra, K., Grover, S., & Aggarwal, A. (2011). Simultaneous optimization of material removal rate and surface roughness for WEDM of WC-Co composite using grey relational analysis along with Taguchi method. *International Journal of Industrial Engineering Computations, 2*(3), 479-490.

Kaneko, H., & Onoue, M. (1984). US4424432 A.

Kanlayasiri, K., & Boonmung, S. (2007). Effects of wire-EDM machining variables on surface roughness of newly developed DC 53 die steel: Design of experiments and regression model. *Journal of Materials Processing Technology, 192–193*(0), 459-464. doi:http://dx.doi.org/10.1016/j.jmatprotec.2007.04.085

Kapoor, J., Singh, S., & Khamba, J. S. (2010). *Recent developments in wire electrodes for high performance WEDM*. Paper presented at the Proceedings of the World Congress on Engineering, London.

Kapoor, J., Singh, S., & Khamba, J. S. (2012). Effect of cryogenic treated brass wire electrode on material removal rate in wire electrical discharge machining. *Journal of Mechanical Engineering Science, 226*(11), 2750-2758. doi:10.1177/0954406212438804

Kapoor, J., Singh, S., & Khamba, J. S. (2012). High-performance wire electrodes for wire electrical-discharge machining - a review. *Proceedings of the Institution of Mechanical Engineers, Part B: Journal of Engineering Manufacture, 226*(11), 1757-1773. doi:10.1177/0954405412460354

Kern, R. (2007). Improving wire EDM productivity. *EDM Today*, 10-14.

Kern, R. (2008). EDM wire selection. *EDM Today*, 12-16.

Kern, R. (2013). The art and science of making EDM wire. Retrieved from http://www.edmtodaymagazine.com/

Kern, R. (2013). EDM wire primer. Retrieved from http://www.edmtodaymagazine.com/

Kinoshita, N., Fukui, M., & Gamo, G. (1982). Control of wire-EDM preventing electrode from breaking. *CIRP Annals - Manufacturing Technology, 31*(1), 111-114. doi:http://dx.doi.org/10.1016/S0007-8506(07)63279-X

Kondo, I., & Nishimoto, K. (1985). Precisely Process of Wire Electrode EDM. *J Japan Soc Electrical Machining Engrs, 19*, 12-27.

Koshy, P., & Menzies, I. (2010). US 2010/0012628 A1.

Kozak, J., Rajurkar, K. P., & Chandarana, N. (2004). Machining of low electrical conductive materials by wire electrical discharge machining (WEDM). *Journal of Materials Processing Technology, 149*, 266-271.

Kruth, J. P., Lauwers, B., Schacht, B., & van Humbeeck, J. (2004). Composite Wires with High Tensile Core for Wire EDM. *CIRP Annals - Manufacturing Technology, 53*(1), 171-174. doi:http://dx.doi.org/10.1016/S0007-8506(07)60671-4

Kruth, J. P., Van Humbeeck, J., & Stevens, L. (1995). *Micro structural investigation and metallographic analysis of the white layer of a surface machined by electro discharge machining*. Paper presented at the Proceedings of international symposium for electromachining isem 11.

Kumar, K., & Agarwal, S. (2012). Multi-objective parametric optimization on machining with wire electric discharge machining. *The International Journal of Advanced Manufacturing Technology, 62*(5-8), 617-633. doi:http://dx.doi.org/10.1007/s00170-011-3833-1

Kuriakose, S., & Shunmugam, M. S. (2004). Characteristics of wire-electro discharge machined Ti6Al4V surface. *Materials Letters, 58*(17–18), 2231-2237. doi:http://dx.doi.org/10.1016/j.matlet.2004.01.037

Kuroda, H., Aoyama, S., Kimura, T., Sawahata, K., & Sato, T. (2003). Development of high performance coated wire electrodes for high-speed cutting and accurate machining. *Hitachi Cable Review, 22*, 51-56.

Lacourcelle, L. (1998). US 5,721,414.

Lee, C.-S., Heo, E.-Y., Kim, J.-M., Choi, I.-H., & Kim, D.-W. (2015). Electrode wear estimation model for EDM drilling. *Robotics and Computer-Integrated Manufacturing*(0). doi:http://dx.doi.org/10.1016/j.rcim.2015.02.001

Lee, J.-C. (2006). US 2006/0138091 A1.

Lee, J.-C. (2008). US 2008/0245773 A1.

Levy, G. N., & Maggi, F. (1990). WED Machinability Comparison of Different Steel Grades. *CIRP Annals - Manufacturing Technology, 39*(1), 183-185. doi:http://dx.doi.org/10.1016/S0007-8506(07)61031-2

Li, H., Chen, C. L. P., Huang, H. P. (2001). *Fuzzy neural intelligent systems: Mathematical foundation and the applications in engineering*. Boca Raton, Florida, USA: CRC Press LLC.

Li, L., Guo, Y. B., Wei, X. T., & Li, W. (2013). Surface Integrity Characteristics in Wire-EDM of Inconel 718 at Different Discharge Energy. *Procedia CIRP, 6*(0), 220-225. doi:http://dx.doi.org/10.1016/j.procir.2013.03.046

Liao, Y. S., & Yu, Y. P. (2004). Study of specific discharge energy in WEDM and its application. *International Journal of Machine Tools and Manufacture, 44*(12–13), 1373-1380. doi:http://dx.doi.org/10.1016/j.ijmachtools.2004.04.008

Lin, C.-T., Chung, I. F., & Huang, S.-Y. (2001). Improvement of machining accuracy by fuzzy logic at corner parts for wire-EDM. *Fuzzy Sets and Systems, 122*(3), 499-511. doi:http://dx.doi.org/10.1016/S0165-0114(00)00034-8

Lin, P., & Liao, T.-T. (2009). An effective-wire-radius compensation scheme for enhancing the precision of wire-cut electrical discharge machines. *The International Journal of Advanced Manufacturing Technology, 40*(3-4), 324-331. doi:10.1007/s00170-007-1333-0

Luo, Y. F. (1999). Rupture failure and mechanical strength of the electrode wire used in wire EDM. *Journal of Materials Processing Technology, 94*(2–3), 208-215. doi:http://dx.doi.org/10.1016/S0924-0136(99)00107-7

Ly, M. (2010). US 7,687,738 B2.

Ly, M., & Sanchez, G. (2012). US 8,338,735 B2.

Maher, I. (2008). *Surface Roughness Prediction in End-Milling Process.* (MSC), Assiut University, Assiut University. Retrieved from http://drepository.asu.edu.eg/xmlui/handle/123456789/83027

Maher, I., Eltaib, M. E. H., & El-Zahry, R. M. (2006, 12-14/December). *Surface roughness prediction in end milling using multiple regression and adaptive neuro-fuzzy inference system.* Paper presented at the International Conference on Mechanical Engineering Advanced Technology For Industrial Production (MEATIP4), Assiut University, Egypt.

Maher, I., Eltaib, M. E. H., Sarhan, A. A. D., & El-Zahry, R. M. (2014). Investigation of the effect of machining parameters on the surface quality of machined brass (60/40) in CNC end milling-ANFIS modeling. *The International Journal of Advanced Manufacturing Technology, 74*(1-4), 531-537. doi:http://dx.doi.org/10.1007/s00170-014-6016-z

Maher, I., Eltaib, M. E. H., Sarhan, A. A. D., & El-Zahry, R. M. (2015). Cutting force-based adaptive neuro-fuzzy approach for accurate surface roughness prediction in end milling operation for intelligent machining. *The International Journal of Advanced Manufacturing Technology, 76*(5-8), 1459-1467. doi:http://dx.doi.org/10.1007/s00170-014-6379-1

Maher, I., Ling, L. H., Sarhan, A. A. D., & Hamdi, M. (2015). Improve wire EDM performance at different machining parameters - ANFIS modeling. *IFAC-PapersOnLine, 48*(1), 105-110. doi:10.1016/j.ifacol.2015.05.109

Maher, I., Sarhan, A. A. D., Barzani, M. M., & Hamdi, M. (2015). Increasing the productivity of the wire-cut electrical discharge machine associated with sustainable production. *Journal of Cleaner Production, 108*, 247-255. doi:10.1016/j.jclepro.2015.06.047

Maher, I., Sarhan, A. A. D., & Hamdi, M. (2015). Review of improvements in wire electrode properties for longer working time and utilization in wire EDM machining. *The International Journal of Advanced Manufacturing Technology, 76*(1-4), 329-351. doi:http://dx.doi.org/10.1007/s00170-014-6243-3

Maher, I., Sarhan, A. A. D., & Marashi, H. (2016). Effect of Electrical Discharge Energy on White Layer Thickness of WEDM Process *Reference Module in Materials Science and Materials Engineering*: Elsevier.

Maher, I., Sarhan, A. A. D., Marashi, H., Barzani, M. M., & Hamdi, M. (2015). *White layer thickness prediction in WEDM-ANFIS modelling.* Paper presented at the Malaysian International Tribology Conference 2015, Penang, Malaysia.

Maher, I., Sarhan, A. A. D., Marashi, H., Barzani, M. M., & Hamdi, M. (2016). White layer thickness prediction in Wire-EDM using CuZn coated wire electrode - ANFIS modeling. *Transactions of the IMF*. doi:10.1080/00202967.2016.1180847

Makino, Y., Obara, H., Ohsumi, T., & Niwa, S. (1995). Single discharging force and machining volume of Wire EDM. *J Japan Soc Electrical Machining Engrs, 30*, 1-10.

Marashi, H., Sarhan, A. A. D., Maher, I., & Sayuti, M. (2016). Various Techniques to Improve EDM Capabilities: A Review *Reference Module in Materials Science and Materials Engineering*: Elsevier.

Marashi, H., Sarhan, A. A. D., Maher, I., Sayuti, M., & Hamdi, M. (2015). *Enhanced surface roughness of AISI D2 steel machined using nano-powder mixed electrical discharge machining.* Paper presented at the Malaysian International Tribology Conference 2015, Penang, Malaysia.

McGeough, J. A. (1988). Electrodischarge machining *Advanced methods of machining*. New York, USA: Springer.

Menzies, I., & Koshy, P. (2008). Assessment of abrasion-assisted material removal in wire EDM. *CIRP Annals - Manufacturing Technology, 57*(1), 195-198. doi:http://dx.doi.org/10.1016/j.cirp.2008.03.135

Mohri, N., Fukuzawa, Y., Tani, T., & Sata, T. (2002). Some considerations to machining characteristics of insulating ceramics-towards practical use in industry. *CIRP Annals - Manufacturing Technology, 51*(1), 161-164. doi:http://dx.doi.org/10.1016/S0007-8506(07)61490-5

Montgomery, D. C., & Runger, G. C. (2003). *Applied Statistics and Probability for Engineers* (3 ed.). John Wiley & Sons, Inc.

Motoki, M., & summer, K. (1978). Recent EDM. *J Japan Soc Electrical Machining Engrs, 11*, 2-20.

Moulton, D. B. (1999). *Wire EDM the fundamentals*: EDM network, Sugar Grove, IL, USA.

Mujahid, M., & Conrad, R. (1991). EP 0275580 B1.

Mukherjee, K. K. (1998). US 5,808,262.

Myers, R. H., & Anderson-Cook, C. M. (2009). *Response surface methodology: process and product optimization using designed experiments* (Vol. 705): John Wiley & Sons.

Nakai, Y., Kishida, H., Ookubo, N., Nanjo, K., Murayoshi, Y., Numano, M., & Otsuka, Y. (2001). US6291790 B1.

Nakai, Y., Yamada, K., Miyazaki, K., Inazawa, S., Ezaki, S., & Kume, T. (2001). US 6,300,587 B1.

Negrerie, M., Leterrible, P., & Voirin, A. (1993). EP 0526361 A1.

Newton, T. R., Melkote, S. N., Watkins, T. R., Trejo, R. M., & Reister, L. (2009). Investigation of the effect of process parameters on the formation and characteristics of recast layer in wire-EDM of Inconel 718. *Materials Science and Engineering: A, 513–514*(0), 208-215. doi:http://dx.doi.org/10.1016/j.msea.2009.01.061

Nourbakhsh, F., Rajurkar, K. P., Malshe, A. P., & Cao, J. (2013). Wire Electro-Discharge Machining of Titanium Alloy. *Procedia CIRP*, *5*(0), 13-18. doi:http://dx.doi.org/10.1016/j.procir.2013.01.003

Obara, H. (1989). The analysis of wire break down limitation on wire EDM (1st report; analysis of water flow in cut groove). *J Japan Soc Electrical Machining Engrs, 22*, 10-22.

Obara, H., Abe, M., & Ohsumi, T. (1997). Prevention of wire breakage on Wire EDM - 1st report: comparison of spark gap detecting signals on Wire EDM-. *J Japan Soc Electrical Machining Engrs, 31*, 11-17.

Obara, H., Ohsumi, T., Masahashi, Y., Miyanishi, S., & Hatano, M. (2002). Fundamental study of accuracy of Wire EDM (6th report) -study of EDM conditions and servo feed function of finish cut-. *J Japan Soc Electrical Machining Engrs, 36*, 15-23.

Obara, H., Yamada, M., Ohsumi, T., & Hatano, M. (2002). Prevention of wire breakage during Wire EDM (3rd report) -discharge location and discharge voltage in case of high current discharge-. *J Japan Soc Electrical Machining Engrs, 36*, 24-30.

Okada, A., Oue, S., Uno, Y., SHOUJI, T., Fukushima, T., & Terada, O. (2007). Development of New CuW Electrode for High-Performance EDM. *J Japan Soc Electrical Machining Engrs, 41*, 69-76.

Okada, A., Uno, Y., Nakazawa, M., & Yamauchi, T. (2010). Evaluations of spark distribution and wire vibration in wire EDM by high-speed observation. *CIRP Annals - Manufacturing Technology*, *59*(1), 231-234. doi:http://dx.doi.org/10.1016/j.cirp.2010.03.073

Okada, A., Yamauchi, T., Arizono, K., Shimizu, T., & Uno, Y. (2008). Development of Coat Wire Electrode for High Performance WEDM (2nd Report) -Fundamental WEDM Characteristices of Φ50μm Coating Wire-. *J Japan Soc Electrical Machining Engrs, 42*, 12-19.

Okada, A., Yamauchi, T., Arizono, K., & Uno, Y. (2008). Effect of Surface Quality of Brass Coating Wire on Wire EDM Characteristics. *Journal of Advanced Mechanical Design, Systems, and Manufacturing, 2*(4), 735-741.

Okada, A., Yamauchi, T., Higashi, M., Shimizu, T., & Uno, Y. (2009). Development of Coated Wire Electrode for High-Performance WEDM (3rd Report)- Effects of wire surface unevenness on wire EDM characteristics -. *J Japan Soc Electrical Machining Engrs, 43*, 179-186.

Okada, A., Yamauchi, T., Nakazawa, M., Shimizu, T., & Uno, Y. (2011). Development of Coated Wire Electrode for High-Performance WEDM (4th Report)- Effects of high-resistance layer on wire electrode on WEDM characteristics. *J Japan Soc Electrical Machining Engrs, 45*, 64-70.

Otsuka, Y., Nakai, Y., Numano, M., Maruyama, T., Ohkubo, N., & Kishida, H. (2001). Development of high-speed electrode wire for wire electro-discharge machining. *SEI Tech Rev, 51*, 133–136.

Patil, N., & Brahmankar, P. K. (2010). Determination of material removal rate in wire electro-discharge machining of metal matrix composites using dimensional analysis. *The International Journal of Advanced Manufacturing Technology, 51*(5-8), 599-610. doi:http://dx.doi.org/10.1007/s00170-010-2633-3

Patil, N. G., & Brahmankar, P. K. (2009). Some studies into wire electro-discharge machining of alumina particulate-reinforced aluminum matrix composites. *The International Journal of Advanced Manufacturing Technology, 48*(5), 537-555. doi:10.1007/s00170-009-2291-5

Paul, C. P., Kumar, A., Bhargava, P., & Kukreja, L. M. (2013). *Nontraditional machining processes- Research advances* (J. P. Davim Ed.): Springer-Verlag London.

Pérez Delgado, Y., De Baets, P., Bonny, K., Carretero Olalla, V., Vleugels, J., Lawers, B., & Staia, M. H. (2013). Influence of wire-EDM on high temperature sliding wear behavior of WC10Co(Cr/V) cemented carbide. *International Journal of Refractory Metals and Hard Materials, 41*(0), 198-209. doi:http://dx.doi.org/10.1016/j.ijrmhm.2013.03.013

Portt, J. (1992). *Introduction to Wire EDM*. Michigan, USA.: John Portt.

Prohaszka, J., Mamalis, A. G., & Vaxevanidis, N. M. (1997). The effect of electrode material on machinability in wire electro-discharge machining. *Journal of Materials Processing Technology, 69*(1–3), 233-237. doi:http://dx.doi.org/10.1016/S0924-0136(97)00024-1

Puri, A. B., & Bhattacharyya, B. (2003). Modelling and analysis of the wire-tool vibration in wire-cut EDM. *Journal of Materials Processing Technology, 141*(3), 295-301. doi:http://dx.doi.org/10.1016/S0924-0136(03)00280-2

Rajurkar, K. P., Wang, W. M., & Lindsay, R. P. (1991). On-line monitor and control for wire breakage in WEDM. *CIRP Annals - Manufacturing Technology, 40*(1), 219-222. doi:http://dx.doi.org/10.1016/S0007-8506(07)61972-6

Ramasawmy, H., Blunt, L., & Rajurkar, K. P. (2005). Investigation of the relationship between the white layer thickness and 3D surface texture parameters in the die sinking EDM process. *Precision Engineering, 29*(4), 479-490. doi:http://dx.doi.org/10.1016/j.precisioneng.2005.02.001

Roy, R. K. (2001). *Design of experments using Taguchi approach*. New York, USA: John Wiley & Sons, Inc.

Saha, P., Singha, A., Pal, S., & Saha, P. (2008). Soft computing models based prediction of cutting speed and surface roughness in wire electro-discharge machining of tungsten carbide cobalt composite. *The International Journal of Advanced Manufacturing Technology, 39*(1-2), 74-84. doi:http://dx.doi.org/10.1007/s00170-007-1200-z

Salah, N. B., Ghanem, F., & Atig, K. B. (2006). Numerical study of thermal aspects of electric discharge machining process. *International Journal of Machine Tools and Manufacture, 46*(7–8), 908-911. doi:http://dx.doi.org/10.1016/j.ijmachtools.2005.04.022

Salonitis, K., Stournaras, A., Stavropoulos, P., & Chryssolouris, G. (2009). Thermal modeling of the material removal rate and surface roughness for die-sinking EDM. *The International Journal of Advanced Manufacturing Technology, 40*(3-4), 316-323. doi:http://dx.doi.org/10.1007/s00170-007-1327-y

Sánchez, J. A., & Ortega, N. (2009). *Machine tools for high performance machining*: Springer London.

Sarhan, A. A. D., Hamdi, M., & Maher, I. (2016). PI 2,016,700,115.

Schacht, B. (2004). *Composite wire electrodes and alternative dielectric for wire electrical discharge machining.* (PhD), University of Katholieke, Leuven, Belgium.

Schacht, B., Kruth, J.-P., Lauwers, B., & Vanherck, P. (2004). The skin-effect in ferromagnetic electrodes for wire-EDM. *The International Journal of Advanced Manufacturing Technology, 23*(11-12), 794-799.

Schuler, G. H. (1998). *Metal forming handbook*. New York: Springer-Verlag Berlin Heidelberg.

Seong, K. (1999). WO Patent 1,999,006,183.

Seong, K. C. (2002). US 6,482,535 B2.

Singh, A., & Ghosh, A. (1999). A thermo-electric model of material removal during electric discharge machining. *International Journal of Machine Tools and Manufacture, 39*(4), 669-682. doi:http://dx.doi.org/10.1016/S0890-6955(98)00047-9

Singh, S., Maheshwari, S., & Pandey, P. C. (2004). Some investigations into the electric discharge machining of hardened tool steel using different electrode materials. *Journal of Materials Processing Technology, 149*(1–3), 272-277. doi:http://dx.doi.org/10.1016/j.jmatprotec.2003.11.046

Snoeys, R., & Dekeyser, W. (1988). Knowledge-based system for wire-EDM. *The International Journal of Advanced Manufacturing Technology, 3*(3), 83-96. doi:10.1007/bf02601592

Sommer, C., & Sommer, S. (2005). *Complete EDM Handbook*: Advance Pub.

Sommer, C., & Sommer, S. (2013). *Complete EDM Handbook*. Texas, USA: Reliable EDM.

Su, C.-T. (2013). *Quality Engineering: Off-Line Methods and Applications*: CRC Press.

Tarng, Y. S., Ma, S. C., & Chung, L. K. (1995). Determination of optimal cutting parameters in wire electrical discharge machining. *International Journal of Machine Tools and Manufacture, 35*(12), 1693-1701. doi:http://dx.doi.org/10.1016/0890-6955(95)00019-T

Tomalin, D. (2011). US 8,067,689 B2.

Tomalin, D. S. (1999). US 5,945,010.

Tomalin, D. S. (2007). US 2007/0295695 A1.

Tominaga, H., Takayama, T., Ogura, Y., & Yamaguchi, T. (1987). US 4,686,153.

Tomlinson, W. J., & Adkin, J. R. (1992). Microstructure and properties of electrodischarge machined surfaces. *Surface Engineering, 8*(4), 283-288. doi:http://dx.doi.org/10.1179/sur.1992.8.4.283

Tomura, S., & Kunieda, M. (2009). Analysis of electromagnetic force in wire-EDM. *Precision Engineering, 33*(3), 255-262. doi:http://dx.doi.org/10.1016/j.precisioneng.2008.07.004

Tönshoff, H. K., Egger, R., & Klocke, F. (1996). Environmental and Safety Aspects of Electrophysical and Electrochemical Processes. *CIRP Annals - Manufacturing Technology, 45*(2), 553-568. doi:http://dx.doi.org/10.1016/S0007-8506(07)60510-1

Uhlmann, E., & Roehner, M. (2008). Investigations on reduction of tool electrode wear in micro-EDM using novel electrode materials. *CIRP Journal of Manufacturing Science and Technology, 1*(2), 92-96. doi:http://dx.doi.org/10.1016/j.cirpj.2008.09.011

van Luttervelt, C. A. (1989). On the Selection of Manufacturing Methods Illustrated by an Overview of Separation Techniques for Sheet Materials. *CIRP Annals - Manufacturing Technology, 38*(2), 587-607. doi:http://dx.doi.org/10.1016/S0007-8506(07)61127-5

Walder, G., & Balleys, F. (1999). US 5882490 A.

Wang, J., & Ravani, B. (2003). Computer aided contouring operation for traveling wire electric discharge machining (EDM). *Computer-Aided Design, 35*(10), 925-934. doi:http://dx.doi.org/10.1016/S0010-4485(02)00207-5

Weng, F. T., & Her, M. G. (2002). Study of the batch production of micro parts using the EDM process. *The International Journal of Advanced Manufacturing Technology, 19*(4), 266-270. doi:10.1007/s001700200033

Wright, R. N. (2010). *Wire Technology: Process Engineering and Metallurgy* (1 ed.): Butterworth-Heinemann.

Yamauchi, T., Okada, A., Morita, M., Shimizu, T., & Uno, Y. (2005). Development of coating wire electrode for high performance WEDM (1st report) -fundamental WEDM characteristics of coating wire-. *J Japan Soc Electrical Machining Engrs, 39*, 28-35.

Yan, M.-T., & Huang, P.-H. (2004). Accuracy improvement of wire-EDM by real-time wire tension control. *International Journal of Machine Tools and Manufacture, 44*(7–8), 807-814. doi:http://dx.doi.org/10.1016/j.ijmachtools.2004.01.019

Yan, M. T., Fang, G. R., Liu, Y. T., & Li, J. R. (2013). Fabrication of Polycrystalline Diamond Wheels by Micro Wire-EDM using a Novel Pulse Generator. *Procedia CIRP, 6*(0), 203-208. doi:http://dx.doi.org/10.1016/j.procir.2013.03.013

Yeh, C.-C., Wu, K.-L., Lee, J.-W., & Yan, B.-H. (2013). Study on surface characteristics using phosphorous dielectric on wire electrical discharge machining of polycrystalline silicon. *The International Journal of Advanced Manufacturing Technology, 69*(1-4), 71-80. doi:10.1007/s00170-013-4995-9

Yeo, S. H., Tan, H. C., & New, A. K. (1998). Assessment of waste streams in electric-discharge machining for environmental impact analysis. *Proceedings of the Institution of Mechanical Engineers, Part B: Journal of Engineering Manufacture, 212*(5), 393-401. doi:10.1243/0954405981515996

Zalnezhad, E., Sarhan, A. A. D., & Hamdi, M. (2013). Investigating the effects of hard anodizing parameters on surface hardness of hard anodized aerospace AL7075-T6 alloy using fuzzy logic approach for fretting fatigue application. *The International Journal of Advanced Manufacturing Technology, 68*(1-4), 453-464. doi:10.1007/s00170-013-4743-1

LIST OF PUBLICATIONS AND PAPERS PRESENTED

1. Maher, I., Sarhan, A. A. D., & Hamdi, M. (2015). Review of improvements in wire electrode properties for longer working time and utilization in wire EDM machining. The International Journal of Advanced Manufacturing Technology, 76, 329-351. doi: http://dx.doi.org/10.1007/s00170-014-6243-3, "Published" (ISI-cited Publication)
2. Maher, I., Sarhan, A. A. D., Barzani, M. M., & Hamdi, M. (2015). Increasing the productivity of the wire-cut electrical discharge machine associated with sustainable production. Journal of Cleaner Production, 108, 247-255. doi: http://dx.doi.org/10.1016/j.jclepro.2015.06.047, "Published" (ISI-cited Publication)
3. Maher, I., Sarhan, A. A. D., Marashi, H., Barzani, M. M., & Hamdi, M. (2016). White layer thickness prediction in Wire-EDM using CuZn coated wire electrode - ANFIS modeling. Transactions of the IMF. "Accepted", (ISI-Cited Publication).
4. Maher, I., Ling, L. H., Sarhan, A. A. D., & Hamdi, M. (2015). Improve wire EDM performance at different machining parameters - ANFIS modeling. Paper presented at the MATHMOD 2015 - 8th Vienna International Conference on Mathematical Modelling, Vienna University of Technology, Vienna, Austria. Doi: http://dx.doi.org/10.1016/j.ifacol.2015.05.109, "Published" Elsevier Publication.
5. Maher, I., Sarhan, A. A. D., Marashi, H., Barzani, M. M., & Hamdi, M. (2015). White layer thickness prediction in WEDM-ANFIS modelling. Paper presented at the Malaysian International Tribology Conference 2015, Penang, Malaysia. "Published" Google book Publication.

6. Maher, I., Sarhan, A. A. D. (2016). Proposing a new performance index to identify the effect of spark energy and pulse frequency at different duty factors in CNC-WEDM. Measurement. “Under review”, (ISI-Cited Publication).
7. Maher, I., Sarhan, A. A. D. (2016). Identify the optimum spark energy and pulse frequency values to achieve higher productivity in WEDM. Journal of mechanical science and technology. “Under review”, (ISI-Cited Publication).
8. Maher, I., Sarhan, A. A. D. (2016). Performance criteria to identify most suitable type of wire electrode for higher EDM performance considering the ecological and economic aspects. Machine tools and manufacture. “Under review”, (ISI-Cited Publication).
9. Maher, I., Sarhan, A. A. D., Marashi, H. (2016). Wire rupture optimization in wire electrical discharge machining using Taguchi approach. International Conference on Innovative Engineering Materials (ICIEM2016), Nanyang Technological University, Singapore. “Under review”

CHAPTERS IN A BOOK

1. Maher, I., Sarhan, A. A. D., Marashi, H., (2016). Effect of Electrical Discharge Energy on White Layer Thickness of WEDM Process, in: Reference Module in Materials Science and Materials Engineering, Elsevier, 2016. “Published”

PATENTS

1. Sarhan, A. A. D., Hamdi, M., & Maher, I. (2016). An electrode wire for use in wire electrical discharge machining. (PI 2,016,700,115)

APPENDIX

Appendix A: Taguchi analysis tables

Table A.1 S/N ratios of machining performance measures using brass wire

No.	S/N ratios (AISI 1050 Steel)				S/N ratios (Ti6Al4V)			
	CS	**Ra**	**WLT**	**WL**	**CS**	**Ra**	**WLT**	**WL**
1	-6.87	-5.21	-20.63	-20.63	2.81	-8.26	-18.83	-8.03
2	-2.30	-7.34	-19.32	-19.32	0.87	-7.61	-17.84	-9.43
3	-4.44	-6.73	-14.66	-14.66	-1.52	-7.44	-17.02	-7.91
4	-2.08	-8.22	-18.39	-18.39	4.23	-7.59	-19.62	-11.70
5	3.23	-10.05	-22.01	-22.01	2.68	-7.97	-18.35	-11.38
6	-1.69	-9.46	-18.38	-18.38	0.79	-7.74	-17.77	-11.68
7	-2.01	-9.83	-23.01	-23.01	6.16	-8.49	-21.83	-15.05
8	6.27	-10.48	-20.16	-20.16	4.95	-8.99	-20.90	-12.50
9	1.62	-9.97	-23.55	-23.55	3.67	-8.06	-20.08	-14.30
10	-4.98	-7.46	-19.39	-19.39	3.27	-7.64	-23.90	-13.93
11	-2.05	-8.40	-23.46	-23.46	1.11	-7.75	-22.02	-14.66
12	-2.75	-7.34	-21.34	-21.34	-1.11	-7.22	-19.99	-11.55
13	3.10	-10.73	-20.82	-20.82	4.76	-8.58	-26.13	-16.06
14	4.99	-9.60	-24.44	-24.44	3.61	-8.06	-24.92	-18.39
15	0.69	-9.63	-24.52	-24.52	2.21	-8.15	-23.88	-14.04
16	7.81	-11.56	-23.76	-23.76	6.76	-9.31	-28.41	-25.32
17	7.38	-11.08	-24.36	-24.36	5.42	-9.55	-26.68	-15.26
18	6.89	-9.88	-23.75	-23.75	4.60	-9.34	-25.43	-18.90

Table A.2 S/N ratios of machining performance measures using coated wire

No.	S/N ratios (AISI 1050 Steel)				S/N ratios (Ti6Al4V)			
	CS	**Ra**	**WLT**	**WL**	**CS**	**Ra**	**WLT**	**WL**
1	0.45	-6.97	-14.81	-16.65	3.00	-6.97	-15.11	-9.58
2	3.65	-9.33	-20.41	-15.67	2.64	-6.66	-14.16	-7.03
3	-0.68	-8.37	-18.40	-16.72	1.81	-6.42	-12.88	-6.56
4	10.52	-10.44	-23.87	-19.13	7.01	-8.59	-20.15	-7.53
5	6.15	-9.77	-24.09	-20.18	4.77	-7.93	-17.54	-8.60
6	2.25	-10.37	-20.86	-20.30	3.67	-7.32	-15.77	-12.21
7	10.60	-11.42	-21.21	-24.36	10.69	-9.72	-24.27	-13.46
8	8.99	-10.66	-25.90	-21.80	9.08	-9.13	-22.05	-11.67
9	4.84	-10.16	-25.24	-19.26	7.86	-8.59	-20.88	-10.91
10	8.87	-9.49	-21.86	-20.69	4.30	-7.27	-16.45	-9.01
11	4.85	-9.99	-21.78	-21.19	3.17	-6.94	-15.16	-9.57
12	0.86	-8.80	-22.15	-16.85	2.93	-6.73	-14.33	-8.02
13	11.28	-10.51	-22.21	-23.52	8.12	-9.01	-21.23	-6.81
14	7.71	-10.23	-23.53	-23.95	7.25	-8.51	-20.54	-12.55
15	3.98	-9.96	-20.78	-20.00	5.80	-7.81	-18.74	-11.37
16	8.72	-10.19	-23.09	-23.30	11.70	-10.24	-26.00	-18.67
17	10.18	-11.48	-24.80	-23.30	10.20	-9.32	-23.95	-17.97
18	6.05	-11.47	-25.54	-23.73	8.49	-8.76	-22.10	-21.50

Table A.3 Response table for S/N ratios using brass wire with AISI 1050 steel

Response table for S/N ratios of Cutting speed (Larger is better)					
Level	***IP***	***Ton***	***Toff***	***WS***	***WT***
1	-0.91903	-3.89993	-0.83964	-0.21914	-0.12359
2	2.34057	1.37336	2.91981	1.02568	1.27320
3		4.65888	0.05214	1.32577	0.98270
Delta	3.25959	8.55881	3.75945	1.54490	1.39678
Rank	3	1	2	4	5
Response table for S/N ratios of Surface roughness (Smaller is better)					
1	-8.589	-7.082	-8.836	-8.754	-8.730
2	-9.520	-9.615	-9.493	-9.195	-9.097
3		-10.467	-8.835	-9.215	-9.337
Delta	0.931	3.385	0.658	0.461	0.607
Rank	2	1	3	5	4
Response table for S/N ratios of White layer thickness (Smaller is better)					
1	-20.01	-19.80	-21.00	-22.48	-22.28
2	-22.87	-21.43	-22.29	-21.71	-21.25
3		-23.10	-21.03	-20.13	-20.80
Delta	2.86	3.30	1.29	2.35	1.48
Rank	2	1	5	3	4
Response table for S/N ratios of Wire loss (Smaller is better)					
1	-12.077	-6.503	-12.842	-12.835	-16.822
2	-16.341	-15.488	-15.540	-14.221	-11.952
3		-20.635	-14.245	-15.571	-13.852
Delta	4.264	14.132	2.697	2.736	4.870
Rank	3	1	5	4	2

Table A.4 Response table for S/N ratios using brass wire with Ti6Al4V

Response table for S/N ratios of Cutting speed (Larger is better)					
Level	***IP***	***Ton***	***Toff***	***WS***	***WT***
1	2.7370	0.9053	4.6655	3.2407	3.1804
2	3.4032	3.0440	3.1066	2.9938	2.9837
3		5.2610	1.4383	2.9759	3.0462
Delta	0.6662	4.3556	3.2272	0.2648	0.1968
Rank	3	1	2	4	5
Response table for S/N ratios of Surface roughness (Smaller is better)					
1	-8.016	-7.654	-8.311	-8.226	-8.273
2	-8.400	-8.013	-8.323	-8.200	-8.145
3		-8.957	-7.990	-8.198	-8.206
Delta	0.385	1.303	0.332	0.028	0.127
Rank	2	1	3	5	4
Response table for S/N ratios of White layer thickness (Smaller is better)					
1	-19.14	-19.93	-23.12	-21.85	-21.80
2	-24.60	-21.78	-21.79	-21.60	-21.77
3		-23.89	-20.70	-22.15	-22.03
Delta	5.46	3.96	2.42	0.55	0.25
Rank	1	2	3	4	5
Response table for S/N ratios of Wire loss (Smaller is better)					
1	-11.33	-10.92	-15.02	-13.00	-14.45
2	-16.46	-13.88	-13.60	-13.73	-14.09
3		-16.89	-13.06	-14.96	-13.14
Delta	5.13	5.97	1.95	1.96	1.31
Rank	2	1	4	3	5

Table A.5 Response table for S/N ratios using coated wire with AISI 1050 steel

Response table for S/N ratios of Cutting speed (Larger is better)					
Level	**IP**	**Ton**	**Toff**	**WS**	**WT**
1	5.196	3.000	8.405	5.804	5.317
2	6.944	6.980	6.923	6.430	6.119
3		8.230	2.882	5.976	6.775
Delta	1.749	5.230	5.523	0.626	1.458
Rank	3	2	1	5	4
Response table for S/N ratios of Surface roughness (Smaller is better)					
1	-9.721	-8.824	-9.835	-9.832	-10.074
2	-10.234	-10.213	-10.244	-10.216	-9.898
3		-10.896	-9.853	-9.885	-9.962
Delta	0.513	2.071	0.409	0.384	0.176
Rank	2	1	3	4	5
Response table for S/N ratios of White layer thickness (Smaller is better)					
1	-21.64	-19.90	-21.18	-21.88	-21.29
2	-22.86	-22.55	-23.42	-22.60	-22.70
3		-24.30	-22.16	-22.27	-22.77
Delta	1.21	4.40	2.24	0.72	1.48
Rank	4	1	2	5	3
Response table for S/N ratios of Wire loss (Smaller is better)					
1	-19.34	-17.96	-21.27	-19.92	-21.70
2	-21.84	-21.18	-21.02	-20.72	-19.46
3		-22.62	-19.47	-21.12	-20.61
Delta	2.49	4.66	1.80	1.20	2.24
Rank	2	1	4	5	3

Table A.6 Response table for S/N ratios using coated wire with Ti6Al4V

Response table for S/N ratios of Cutting speed (Larger is better)					
Level	**IP**	**Ton**	**Toff**	**WS**	**WT**
1	5.614	2.975	7.469	6.172	6.044
2	6.884	6.101	6.184	6.273	6.527
3		9.671	5.094	6.303	6.176
Delta	1.270	6.696	2.375	0.130	0.483
Rank	3	1	2	5	4
Response table for S/N ratios of Surface roughness (Smaller is better)					
1	-7.925	-6.833	-8.632	-8.035	-8.036
2	-8.287	-8.193	-8.081	-8.133	-8.192
3		-9.292	-7.604	-8.150	-8.089
Delta	0.362	2.459	1.028	0.115	0.156
Rank	3	1	2	5	4
Response table for S/N ratios of White layer thickness (Smaller is better)					
1	-18.09	-14.68	-20.53	-19.00	-18.83
2	-19.83	-19.00	-18.90	-18.94	-19.24
3		-23.21	-17.45	-18.95	-18.82
Delta	1.74	8.52	3.08	0.06	0.42
Rank	3	1	2	5	4
Response table for S/N ratios of Wire loss (Smaller is better)					
1	-9.729	-8.295	-10.845	-11.156	-13.145
2	-12.830	-9.845	-11.234	-10.904	-10.715
3		-15.697	-11.759	-11.778	-9.977
Delta	3.101	7.402	0.914	0.874	3.168
Rank	3	1	4	5	2